R-02-02

Strategy for a Rock Mechanics Site Descriptive Model

Development and testing of the theoretical approach

Isabelle Staub, Anders Fredriksson, Nils Outters
Golder Associates AB

May 2002

Svensk Kärnbränslehantering AB
Swedish Nuclear Fuel
and Waste Management Co
Box 5864
SE-102 40 Stockholm Sweden
Tel 08-459 84 00
+46 8 459 84 00
Fax 08-661 57 19
+46 8 661 57 19

ISSN 1402-3091
SKB Rapport R-02-02

Strategy for a Rock Mechanics Site Descriptive Model

Development and testing of the theoretical approach

Isabelle Staub, Anders Fredriksson, Nils Outters
Golder Associates AB

May 2002

Abstract

In the purpose of studying the possibilities of a Deep Repository for spent fuel, the Swedish Nuclear and Fuel Management Company (SKB) is currently planning for Site Investigations. Data collected from these Site Investigations are interpreted and analysed to achieve the full Site Description, which is built up of models from all the disciplines that are considered of importance for the Site Description. One of these models is the Rock Mechanical Descriptive Model, which would be developed for any site in hard crystalline rock, and is a combination and evaluation of the characterisation of rock mass by means of empirical relationships and a theoretical approach based on numerical modelling. The present report describes the theoretical approach.

The characterisation of the mechanical properties of the rock mass, viewed as a unit consisting of intact rock and fractures, is achieved by numerical simulations with following input parameters: initial stresses, fracture geometry, distribution of rock mechanical properties, such as deformation and strength parameters, for the intact rock and for the fractures. The numerical modelling was performed with the two-dimensional code UDEC, and the rock block models were generated from 2D trace sections extracted from the 3D Discrete Fracture Network (DFN) model. Assumptions and uncertainties related to the set-up of the model are considered. The numerical model was set-up to simulate a plain strain-loading test. Different boundary conditions were applied on the model for simulating stress conditions (I) in the undisturbed rock mass, and (II) at the proximity of a tunnel. In order to assess the reliability of the model sensitivity analyses have been conducted on some rock block models for defining the dependency of mechanical properties to in situ stresses, the influence of boundary conditions, rock material and joint constitutive models used to simulate the behaviour of intact rock and fractures, domain size and anisotropy. To deal with spatial variability and data uncertainties of the modelling results, and in order to minimise the number of numerical models to run, Monte Carlo simulations are used. The methodology was tested in Sweden on a limited set of data coming from the Äspö Hard Rock Laboratory. The mechanical properties of the rock mass were determined in two scales, (I) in a 550 m block in which “ordinary rock units” and “deformation zone units” are identified, and (II) in a box located at depth from –380 to –500 m, and divided in 30·30·30 m cubes.

Summary

In the purpose of studying the possibilities of a Deep Repository for spent fuel, the Swedish Nuclear and Fuel Management Company (SKB) is currently planning for Site Investigations. These Site Investigations are planned to provide the wide knowledge that is necessary to evaluate the reliability of the site for a final waste disposal /Andersson et al, 2002/.

Data collected from these Site Investigations are interpreted and analysed to achieve the full Site Description, which is built up of models from all the disciplines that are considered of importance for the Site Description. These models are related to geology, rock mechanics, thermal properties, hydrogeology, hydrogeochemistry, transport properties and surface ecosystems.

One of these models is the Rock Mechanical Descriptive Model, which would be developed for any site in hard crystalline rock. The rock mass mechanical properties cannot be directly measured during Site Investigations, but must be estimated. The characterisation of rock mass mechanical properties in the Site is the basis for predicting the short- and long-term stability of the rock mass, in consideration to excavations that are to be done when planning the final disposal, and to long-term alteration of rocks. The Rock Mechanical Descriptive Model shall describe the initial stresses and the distribution of rock mechanical properties such as deformation and strength properties for the intact rock, for the fractures, for the deformation zones, and for the rock mass viewed as a unit consisting of intact rock and fractures. The evaluation of these properties can be achieved through the application of empirical relationships or by a theoretical approach based on numerical modelling. Both methodologies imply some assumptions and uncertainties that need to be considered. The comprehensive Rock Mechanical Descriptive Model is a combination and evaluation of both approaches (Figure 1-2).

The basis of the theoretical approach is to determine the mechanical properties by numerical modelling and using known parameters of the rock, *i.e.* fracture geometry, and mechanical properties for the intact rock and for the fractures. The first task was to develop the methodology to use for modelling the rock mass behaviour. Then this methodology was applied in a “Test Case” on a limited set of real input data.

The methodology was developed in the purpose of characterising the mechanical properties of the rock mass, in any of the potential site. The reliability of the modelling is dependent onto the type/quality of input data, the numerical code chosen for numerical simulations, and the interpretation of the outcome (section 2). The input data must consider the fracture geometry, as well as mechanical properties of intact rock and fractures. The non-site related procedure developed for the characterisation of the rock mass is presented in a flow-chart (Figure 2-1).

Fracture geometry is often really complex and presents a non-linear spatial variability. This issue was handled by numerical stochastic modelling. Statistical data on fractures were used as input to simulate a three-dimensional Discrete Fracture Network (DFN) in the FracMan software. The numerical modelling was achieved by using the two-dimensional code UDEC, and the rock block models were generated from 2D trace sections extracted from the 3D DFN model.

The numerical model was set-up to simulate a plain strain-loading test. Vertical and horizontal displacements, and vertical stresses were monitored during loading and used for the interpretation of deformation and strength properties (section 3.2). Different boundary conditions were applied on the model for simulating stress conditions (I) in the undisturbed rock mass, and (II) at the proximity of a tunnel (Figure 3-5).

The reliability of the numerical modelling is grounded by the way the model is built up in the code. The validity of the model was checked by running some benchmark tests. Moreover, sensitivity analyses have been conducted on some rock block models for studying the dependency of mechanical properties to in situ stresses, the influence of boundary conditions, rock material and joint constitutive models used to simulate the behaviour of intact rock and fractures, domain size and anisotropy (section 3.3). 2D and 3D numerical simulations were also carried out on a simplified model for determining the influence of evaluating the mechanical properties of the rock mass in 2D (Figure 3-26).

Some modifications to the model were required for the modelling of deformation zones, which are mainly related to the modification of the fracture network, and the alteration of mechanical properties of intact rock and fractures in and at the proximity of these zones (section 3.4).

The data uncertainty and spatial variability of the material parameters for intact rock and fractures are expressed by the measured mean value and standard deviation, assuming a normal distribution. To deal with spatial variability and data uncertainties of the modelling results, and in order to minimise the number of numerical simulations, Monte Carlo simulations are used (section 3.5).

The methodology was tested on a limited set of data coming from the Äspö Hard Rock Laboratory. The mechanical properties of the rock mass were determined in two scales, (I) in a 550 m block in which “ordinary rock units” and “deformation zone units” are identified, and (II) in a box located at depth from –380 to –500 m, and divided in 30·30·30 m cubes (section 4).

Input data for the fracture network were mainly provided by tunnel mapping, input data for mechanical properties of intact rock and fractures were coming from results of laboratory tests conducted on core samples from 3 boreholes (section 5).

First, one model was run on one defined rock type to assess the influence of variation of input parameters on the outcome of the model, and refine the input parameters as interpreted from laboratory tests (section 6). The mechanical properties of the rock mass were evaluated for rock block models constituted of a homogeneous rock type. However, the cubes in the detailed model and “rock type” units in the large volume present a geology composed of a combination of these different rock types. The determination of the mechanical properties of such mixture of rocks was achieved by means of Monte Carlo simulations from results obtained on homogeneous models. Special models were run for the determination of mechanical properties in deformation zones (section 7).

The outcome of the Test Case are discussed and analysed in /Hudson (ed.), 2002/, as part of the Rock Mechanical Site Descriptive Model.

Sammanfattning

För att studera möjligheterna att bygga ett djupförlagt lager för använt kärnbränsle planerar Svensk Kärnbränslehantering AB för närvarande platsundersökningar. Dessa platsundersökningar utformas för att ge den breda kunskap som är nödvändig för utvärdering av säkerheten hos ett lager för använt kärnbränsle på aktuell plats /Andersson et al, 2002/.

Insamlad data från dessa platsundersökningar tolkas och analyseras för att ge en samlad platsbeskrivning. Denna beskrivning är uppbyggd av modeller från de olika ämnesområden som har betydelse för beskrivning av platsen. Dessa modeller behandlar geologi, bergmekanik, termiska egenskaper, hydrogeologi, hydrogeokemi, transportegenskaper och ytnära ekosystem.

En av dessa modeller är den beskrivande bergmekaniska modellen som kommer att tas fram för aktuella platser i hårt kristallint berg. Bergmassans mekaniska egenskaper kan inte direkt mätas vid platsundersökningen utan måste uppskattas. Karaktäriseringen av bergmassans mekaniska egenskaper på en plats är basen för analys av bergmassans kort- respektive långtidsstabilitet kring de tunnlar och bergrum som måste byggas. Den beskrivande bergmekaniska modellen skall beskriva initialspänningarna i bergmassan, fördelningen av mekaniska egenskaper såsom deformations- och hållfasthetsegenskaper hos det intakta berget, sprickor, sprickzoner och bergmassan sedd som en enhet bestående av intakt berg och sprickor. Utvärderingen av dessa egenskaper kan ske genom att använda empiriska samband eller genom ett teoretiskt angreppssätt byggt på numerisk modellering. Båda angreppssätten innefattar antaganden och osäkerheter som måste beaktas. Den slutgiltiga beskrivande bergmekaniska modellen är en kombination och värdering av båda angreppssätten (figur 1-2).

Utgångspunkten för det teoretiska angreppssättet är att bestämma de mekaniska egenskaperna genom numerisk modellering utgående från kända parametrar hos berget så som sprickgeometri, mekaniska egenskaper hos det intakta berget och hos sprickorna. I föreliggande projekt var första uppgiften att utveckla den metodik som skall användas för modellering av bergmassans uppförande enligt det teoretiska angreppssättet. Därefter skall metodiken användas på ett ”Test fall” bestående av en begränsad uppsättning av verkliga indata från undersökningarna vid Äspölaboratoriet.

Metodiken utvecklades med syftet att kunna karaktärisera de mekaniska egenskaperna hos en bergmassa. Tillförlitligheten hos modelleringen beror på typ och kvalité hos indata, den använda koden för numerisk simulering och utvärderingen av resultatet (avsnitt 2). Indata måste beakta sprickgeometrin såväl som de mekaniska egenskaperna hos intakt berg som hos sprickor. Den utvecklade icke platsspecifika metodiken för karaktärisering av en bergmassa presenteras i ett flödesschema (figur 2-1).

Sprickgeometrin är ofta mycket komplex och uppvisar icke linjär rumslig variation. Dessa fakta hanteras genom stokastisk numerisk modellering. Statistiska data på sprickor används som indata till en tre-dimensionell diskret spricknätsmodell (DFN) som genereras med programvaran FracMan. Den numeriska modelleringen genomförs med den två-dimensionella koden UDEC där bergblocken genereras utgående från två-dimensionella sprickspår som extraheras från den tre-dimensionella DFN-modellen.

Den numeriska modellen utformades för att simulera ett belastningsförsök under plant töjningstillstånd (plain strain). Vertikala och horisontala deformationer samt vertikalspänningar avlästes under belastningens påförande. De avlästa värdena används för att utvärdera deformations- och hållfasthetsegenskaper (avsnitt 3.2). Olika randvillkor påförs modellen för att simulera spänningsförhållandena (I) i den ostörda bergmassan och (II) i närheten av en tunnel (figur 3-5).

Tillförlitligheten hos den numeriska modellen beror på hur modellen har implementerats i den numeriska koden. Modellerna validerades genom att analysera ett antal kända belastningsfall (benchmark tests). Dessutom genomfördes ett antal sensitivitets tester där utfallet av mekaniska egenskaper hos några blockmodeller studerades beroendet på in situ spänningarna, randvillkor, använda materialmodeller för intakt berg och sprickor, modellstorlek samt anisotropi (avsnitt 3.3). Jämförande simuleringar utfördes på en förenklad modell i 2D respektive 3D för att bestämma inverkan av att utvärdera de mekaniska egenskaperna för bergmassan enbart genom 2D simuleringar (figur 3-26).

För modellering av deformationszoner krävdes en del modifieringar av metodiken. Modifieringarna var i huvudsak knutna till utseendet hos spricknätverket och förändring av de mekaniska egenskaperna hos det intakta berget och sprickorna i och i närheten av zoner (avsnitt 3.4).

Osäkerheten i data och den rumsliga variationen hos materialparametrarna för intakt berg och hos sprickorna uttrycktes med hjälp av uppmätt medelvärde och standardavvikelse samt genom att anta att datan är normalfördelad. För att hantera den rumsliga variationen och osäkerheten i modelleringsresultatet samt för att minimera antalet numeriska simuleringar utfördes Monte Carlo simuleringar (avsnitt 3.5).

Den framtagna metodiken testades på en begränsad del av data från undersökningarna vid Äspölaboratoriet. De mekaniska egenskaperna hos bergmassan bestämdes i två skalor, (I) i en 550 m blockskala där vanliga bergenheter och deformationszoner har identifierats och (II) i ett block på djupet –380 till –500 m som delats in i kuber med sidorna 30·30·30 m (avsnitt 4).

Indata till spricknätverksmodellen erhölls i huvudsak från tunnelkartering och indata till de mekaniska egenskaperna hos det intakta berget och sprickorna kom från laboratorieundersökningar på kärnor från tre borrhål (avsnitt 5).

Till att börja med analyserades en modell av den dominerande bergartstypen för att studera inverkan av variation hos indataparametrar på resultatet från modellen samt förfining av utvärdering av laboratorieförsöken (avsnitt 6). De mekaniska egenskaperna för bergmassan utvärderades för bergblock bestående av en enda bergart. Blocken i den detaljerade modellen och bergenheterna i den storskaliga modellen består dock av flera olika bergarter. De mekaniska egenskaperna hos block uppbyggda av en blandning av olika bergarter bestämdes genom Monte Carlo simulering utgående från resultaten erhållna på homogena block bestående av en enda bergart. Speciella modelleringar utfördes för att bestämma egenskaperna hos deformationszoner (avsnitt 7).

Resultatet från ”Test fallet” diskuteras och analyseras i /Hudson (ed.), 2002/ som en del i utveckling av den beskrivande bergmekaniska modellen.

Contents

Symbols and abbreviations

a	material constant (H-B failure criterion)
a_{jn}	joint aperture at zero normal stress [m]
a_n	initial value of joint normal stiffness [MPa/m]
a_s	initial value of joint shear stiffness [MPa/m]
A_i	C-Y model constant parameter
B	B-B model material parameter
B_i	C-Y model constant parameter
B-B	Barton-Bandis joint model
c_m	cohesion of the rock mass [MPa]
c_{pl}	cohesion of rock fracture at low normal stresses /Patton, 1966/ [MPa]
c_{ph}	cohesion of rock fracture at high normal stresses /Patton, 1966/ [MPa]
c	cohesion of intact rock [MPa]
c_p	peak cohesion of rock fracture [MPa]
c_r	residual cohesion of rock fracture [MPa]
C_i	C-Y model constant parameter
C_1	empirical constants associated to a load cycle
C_2	empirical constants associated to a load cycle
C_{10}	constant of proportionality
C_{21}	constant of proportionality
C-Y	Continuously Yielding joint model
d	diameter of the intact rock sample [m]
D	density [kg/m^3]
D_i	constant parameter, rock fractures
e_n	joint normal stiffness exponent
e_s	joint shear stiffness exponent
E	Young's modulus of the intact rock [GPa]
$E_{\%50}$	tangent Young's modulus of the intact rock [GPa]
E_{ini}	initial Young's modulus of the intact rock [GPa]
E_m	Young's modulus of the rock mass [GPa]
F	stress factor
G	shear modulus of the intact rock

GSI	Geological Strength Index
H-B	Hoek-Brown failure criterion
i	effective dilatancy angle of rock fractures [°]
jr	material parameter for joint roughness [m]
JCS	joint Compression Strength [MPa]
JCS_n	joint Compression Strength, natural scale [MPa]
JCS_0	joint Compression Strength, laboratory scale [MPa]
JCS_{100}	joint Compression Strength, 100 mm sample [MPa]
JRC	joint Roughness Coefficient
JRC_{mob}	mobilised Joint Roughness Coefficient
JRC_n	joint Roughness Coefficient, natural scale
JRC_{peak}	peak Joint Roughness Coefficient
JRC_0	joint Roughness Coefficient, laboratory scale
JRC_{100}	joint Roughness Coefficient, 100 mm sample
k	material constant, intact rock
K	bulk modulus [GPa]
K_n	joint normal stiffness at expected normal stress [MPa/m]
K_{ni}	initial joint normal stiffness for each loading cycle [MPa/m]
K_s	joint shear stiffness at expected normal stress [MPa/m]
L_n	joint length, natural scale [m]
L_x	length of monitoring profile along x-axis [m]
L_y	length of monitoring profile along y-axis [m]
L_0	joint length, laboratory scale [m]
m_b	material constant
m_i	material constant
M-C	Mohr-Coulomb failure criterion
Max K_n	maximum value of joint normal stiffness [MPa/m]
Max K_s	maximum value of joint shear stiffness [MPa/m]
N	number of fractures [m^{-1}]
P_{10}	linear fracture intensity [m^{-1}]
P_{21}	fracture intensity per unit area [m/m^2]
P_{32}	volumetric fracture intensity [m^2/m^3]
Q	rock mass quality index
r_e	factor to restore elastic stiffness
r	Schmidt hammer rebound number on wet fracture surfaces
R	Schmidt hammer rebound number on sawn unweathered fracture surfaces

RMR	Rock Mass Rating
RMR_{89}	Rock Mass Rating, updated in 1989
s	material constant
S-S	Strain-softening rock material model
u_n	normal displacement [mm]
u_{nc}	current normal displacement [mm]
u_{nl}	maximum closure for a completed load cycle [mm]
u_{npc}	accumulated irrecoverable closure [mm]
u_s	shear displacement [mm]
$u_{s,\,peak}$	peak shear displacement [mm]
u_s^p	plastic shear displacement [mm]
u_x	displacement along x-axis [mm]
u_y	displacement along y-axis [mm]
α	tilt angle [°]
$\Delta\sigma_n$	incremental normal stress due to the stiffness [MPa]
$\Delta\sigma_v$	increment in vertical stress [MPa]
$\Delta\sigma_y$	increment in stress along y-axis [MPa]
$\Delta\tau$	shear stress increment [MPa]
Δu_n	normal displacement increment [mm]
Δu_s	shear displacement increment [mm]
Δu_s^p	plastic shear displacement increment [mm]
ϕ	friction angle [°]
ϕ_b	fracture basic friction angle [°]
ϕ_{bp}	fracture peak friction angle, Barton-Choubey failure criterion [°]
ϕ_{br}	fracture residual friction angle, Barton-Choubey failure criterion [°]
ϕ_i	fracture intrinsic friction angle [°]
ϕ_m	fracture effective friction angle [°]
$\phi_m^{(i)}$	fracture initial friction angle [°]
ϕ_p	fracture peak friction angle [°]
ϕ_{pl}	fracture friction angle at low normal stresses, Patton criterion [°]
ϕ_{ph}	fracture friction angle at high normal stresses, Patton criterion [°]
ϕ_r	fracture residual friction angle [°]
ϕ_{rm}	friction angle of the rock mass [°]
γ	unit weigth of the rock [kN/m^3]

ν	Poisson's ratio of the intact rock
$\nu_{\%50}$	tangent Poisson's ratio of the intact rock
ν_{ini}	initial Poisson's ratio of the intact rock
ν_m	Poisson's ratio of the rock mass
σ_c	uniaxial compressive strength of the intact rock [MPa]
σ_{cd}	uniaxial compressive strength of a sample of diameter d [MPa]
σ_{cm}	uniaxial compressive strength of the rock mass [MPa]
σ_h	intermediate horizontal in situ stress [MPa]
σ_H	maximum horizontal in situ stress [MPa]
σ_n	normal stress [MPa]
σ_{n0}	effective normal stress generated by gravitational force [MPa]
σ_{tj}	tensile strength of fracture [MPa]
σ_{ti}	tensile strength of intact rock [MPa]
σ_v	vertical stress [MPa]
σ_y	stress along y-axis [MPa]
σ_1	maximum stress [MPa]
σ_{1C}	compressive strength of intact rock from triaxial test [MPa]
σ_{1F}	maximum stress at failure [MPa]
σ_2	intermediate stress [MPa]
σ_3	minimum stress [MPa]
τ	shear strength [MPa]
τ_l	limiting shear stress [MPa]
τ_m	bounding strength [MPa]
τ_p	peak shear strength [MPa]
τ_r	residual shear strength [MPa]
υ_{irr}	irrecoverable closure [mm]
υ_m	current maximum allowable closure [mm]
υ_{mi}	maximum allowable closure for load cycle i [mm]
ψ	dilation angle of the intact rock [°]

1 Introduction

The Swedish Nuclear and Fuel Waste Management Company (SKB) is responsible for managing Sweden's nuclear waste and site for its final disposal. SKB is currently planning to carry out Site Investigations for the Deep Repository for spent fuel. Site investigations are comprehensive investigations of the bedrock and the surface ecosystem from the ground surface and in boreholes. In this phase, detailed studies are also made on how the available generic design of a KBS-3 Deep Repository could be sited, how transports can take place, as well as what the environmental consequences will be during construction and operation and following closure of the repository. The investigations are planned to be carried out at three Sites with granitic rock in Sweden. As one of the tasks in the planning process a study has been carried out on how to develop a Rock Mechanical Descriptive Model for any Site in hard crystalline rock /Andersson et al, 2002/.

1.1 The Site Descriptive Model

1.1.1 Background

The Site Description is the major product from the Site Investigation. Based on the Site Description a design will be carried out. Finally a Safety Assessment will be carried out for the actual design at the actual Site.

The parameters that are of importance for the Site Description were first identified by a study on siting factors for a deep repository for spent fuel /Andersson et al, 1997/. The importance of these parameters were described more in detail in the study on "What requirements does the repository have on the host rock" /Andersson et al, 2000/. The investigation methods to collect these parameters, and how a Site Investigation programme is planned to be outlined in principle is described in /SKB, 2001b/.

1.1.2 Components of the Site Model

The full Site Description is built up of models from all the disciplines that SKB consider of importance for the Site Description. These models are:

- Geology
- Rock mechanics
- Thermal properties (of the rock)
- Hydrogeology
- Hydrogeochemistry
- Transport properties
- Surface ecosystems

The Geological Model forms a base for the other models, and it is a general ambition that the models should be mutually consistent. This also implies that developing the Site Descriptive Models will rest on substantial interaction between the different disciplines above.

1.2 Purpose of the Rock Mechanical Descriptive Model

The mechanical stability in the crust is normally good, especially in old geological formations such as for example the Baltic shield. The crystalline rock is built of minerals, forming the rock type, for example granite. The rock is intersected by fractures in various scales, from microcracks of the size less than a mineral grain up to large fractured zones. The total system of rock types and fractures is referred to as the Rock Mass. The properties of the rock mass control the strength.

The rock mass is subjected to a state of stress. Stress is defined as a second-order tensor quantity requiring six independent values for its specification at a point in a solid. The stress field can be described with vertical and horizontal components. The vertical stress is mainly gravitational and can to a large extent be explained as the product of the depth and the unit weight of the overlying rock mass. The horizontal stress is both a result of the unit weight of the overlying rock mass and the tectonic forces acting at the actual site, and is therefore more difficult to predict than the vertical stress. In addition, discontinuities in various scales can have a local influence on the in situ state of stress /Martin et al, 2001/.

The rock mass is a mechanical system that is normally in static equilibrium under the prevailing loads. Disturbances of this equilibrium may be caused by load changes, for example due to excavation of cavities in the rock, or to changes in mechanical properties by alteration. If the loading exceeds the strength, the rock mass will fail. Failure may lead to instability if the deformations are large enough. However, failure as such does not necessary entail instability as small deformations, without consequences for performance and safety, may restore equilibrium to the system. In the SKB report "What requirements does the repository have on the host rock" /Andersson et al, 2000/ it is identified that the major rock mechanical aspect to consider for the Deep Repository is the risk for spalling during construction. Even if extensive spalling may not have an effect on the long time safety, it has a significant influence on the constructability mainly because of the possible hazard for workers, and thus for time and costs for the construction.

1.2.1 Model requirements

The purpose of the Rock Mechanical Descriptive Model is described in /SKB, 2001a/. The parameters included in this model shall serve as a basis for design and safety assessment, and for the analyses performed during these steps. The model shall describe the initial stresses and the distribution of rock mechanical properties such as deformation and strength properties for the intact rock, for fractures and for zones of weakness in the rock volume, these three being taken separately, and of the rock mass viewed as a unit consisting of intact rock and fractures. The model shall also describe the rock quality with regard to constructability. The investigated volume shall for this reason cover at least the possible location for the repository, which may be a surface of 2–4 km^2. The disposal area is the largest part, but there are many other openings to be built as well.

The Rock Mechanical Descriptive Model must meet the following requirements /Andersson et al, 2002/:

- Ensure that the necessary variables and parameters have been included.
- Allow full transparency of data gathering, management, interpretations, analysis and the presentation of results.
- Provide interpreted rock mechanics data (properties and stresses) for the entire model.
- Have the capability to illustrate a spatial variation of the parameters in the model.
- Handle uncertainty due to sparse data, irregular distribution of data and interpretative issues.

1.2.2 Relevant scales

Rock mechanical considerations for a deep KBS-3 repository are looked up at three different scales, see Figure 1-1.

1. The repository scale, including the entire rock mass around the repository and up to the surface.
2. The tunnel scale, in practice capturing the mechanical processes that may be expected around any underground opening. These processes are normally limited within 1.5–2 times the diameter of the opening. Of special concern for a KBS-3 repository are the volume closest to the deposition tunnels and the deposition holes for vertical placement in the floor.
3. The local scale, the volume closest to any opening where the mechanical effects are as largest. Of special concern for a KBS-3 repository is the volume within less than one diameter from the deposition holes (D = 1.75 m).

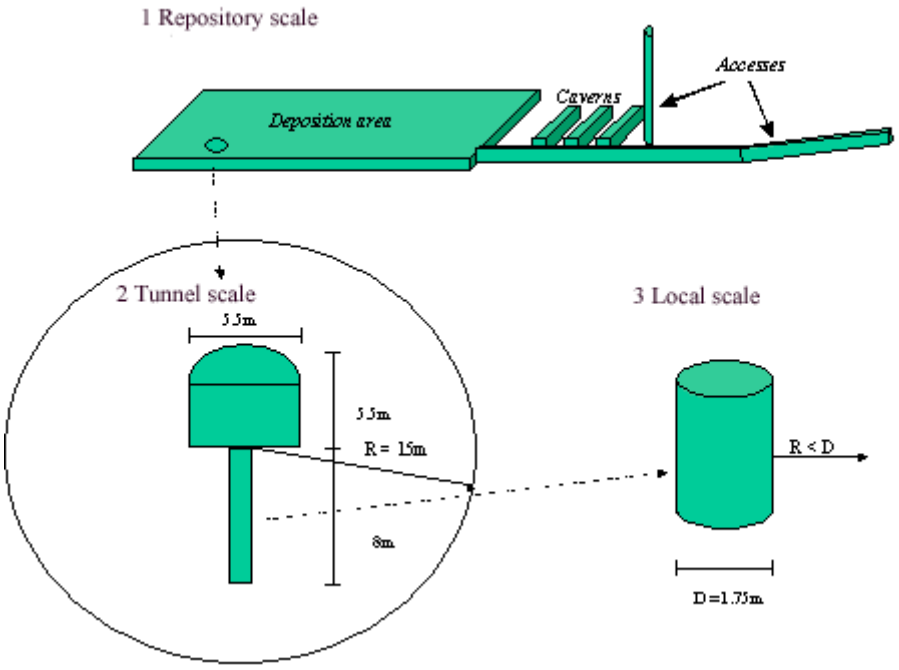

Figure 1-1. *Illustration of the various scales of importance for the rock mechanical considerations for siting and constructing of a KBS-3 repository /Andersson et al, 2002/.*

Some of the caverns that are planned for auxiliary systems may have dimensions up to 15–18 m in span or height. It is however estimated that "the tunnel scale" as defined in this section captures the key questions for constructability for the bulk of the tunnels (the deposition tunnels) with a minimum resolution of 30 by 30 m in the model. This scale is most likely also sufficient to cover rock mechanical aspects in "the repository scale" as well. For detailed scale analyses, a higher resolution is required.

The density of measurement points during the site investigations would not allow a very accurate description of the variability in the detailed scale, such a characterisation can only be done underground. However, typical data are measured in a small scale (like bore cores), whereas the main modelling focus during site investigation is properties in tunnel scale. This means that methods need to be developed to handle the upscaling of a few detailed measurements into rock mass properties at tunnel scale.

1.3 Overview of the modelling approach

The Site Descriptive Model is in essence a prediction, in this case of rock mechanical conditions. The model should address the needs as specified in the previous section.

Furthermore, a guiding principle in developing the model strategy is that the opinion on "what are the relevant questions for rock mechanical modelling" may vary by time.

1.3.1 What shall be described?

Determination of what to describe in the model may be obtained by answering the following questions:

- What are the properties and their attributes to be predicted?
- What principles shall be applied to deal with uncertainties?
- What are the possible property ranges for the prediction?

Listing of parameters

The SKB selection of parameters to be explored during the site investigation rests on several assessments of what is required to be determined for the use of safety assessment and design. The general objectives of the rock mechanical analysis support of the design activity during the site investigation phase are outlined in /SKB, 2000/. When the site investigations are finished, the activity design shall have:

- presented one site-adapted deep repository facility among several analysed and proven its feasibility,
- identified facility-specific technical risks, and
- developed detailed design premises for the detailed investigation phase.

The site-specific properties in the Site Descriptive Model need to make such analyses possible. The general site investigation programme /SKB, 2001a/ lists relevant rock mechanics parameters /Table 5-2 in SKB, 2001a/. Out of these general tables, a more specific table, Table 1-1, is set up.

Table 1-1 provides the identified first order parameters that shall be considered during rock mechanical modelling. An initial estimation of the acceptable range for values is also given in this table. However, these estimates may need re-evaluation when applied as a general methodology during the site investigations.

Table 1-1 also indicates which scale is needed for describing the parameter. This scale should be consistent with the intended use of the parameter. Accordingly, the scale in focus is "the tunnel scale", *i.e.* around 30 m.

During the investigation programme, the main focus of the parameters is on the rock mass properties, whereas the intact rock and fracture properties are rather used as input for determining the rock mass properties.

Table 1-1. Listing of first order mechanical rock parameters to be predicted by the Rock Mechanical Model, with initial suggestion on acceptable uncertainty values (builds on table 5.2 in /SKB, 2001a/).

Rock mass **Parameter (generally a function of space)**	**Scale**	**Units**	**Acceptable estimation[1]**
Orientation of in situ principal stresses	tunnel scale (30 m)	degrees, azimuth/dip	± 20º (if anisotropic otherwise less strict)
Magnitude of in situ principal stresses	tunnel scale (30 m)	MPa	± 20% but high precision is required for judging whether σ_1 < 60 MPa
Rock mass modulus, E_m	tunnel scale (30 m)	GPa	± 15% if 15 MPa< E_m< 45 MPa less than 10% if E_m> 45 MPa
Rock mass strength (H-B, M-C failure criteria)	tunnel scale (30 m)	various	Conclusions whether there is risk for substantial rock failure (e.g. spalling) should be accurate. Such evaluations may e.g. be made using the diagram 5-1 in /Andersson et al, 2000/
Rock Quality Designation (RQD)	tunnel scale (30 m)	%	± 20%

1.3.2 Modelling components

The components of the Rock Mechanical Descriptive Model as well as the proposed flow chart to achieve a complete model are illustrated in Figure 1-2. The two important components are the Mechanical Characterisation Model and the in situ Rock Stress Model.

To set up the Mechanical Characterisation Model two approaches are used:

- A theoretical approach — which is a description and characterisation based on measured data (usually on the small scale) from the field (boreholes) or laboratory (analyses of borehole cores) and the properties typically used in analyses. The development of the methodology is based on numerical simulations that apply the theoretical relationships.
- An empirical approach — which includes evaluation based on the geological description, using existing rock mass classification system schemes, empirical links and experiences from similar areas.

The ground data for both approaches is the Geometrical Model of the target area. The development of this model is mostly influenced by the interpretation of regional and local structure geology, as well as rock types. The combination of these structural features and different rock types design geometrical blocks and units in the Site Investigation volume. Hence, the Geometrical Model presents a visualisation of the "deformation zone units2 and "ordinary rock units".

These two approaches are at the end combined to a final Mechanical Characterisation model. Together with the in situ rock stress model the complete Descriptive Rock Mechanics Model is formed.

The theoretical approach is presented in this document, the empirical approach in /Röshoff et al, 2002/ and the in situ Rock Stress Model in /Hakami et al, 2002/.

As a subset of this development project, a Test Case has been carried out in which the different modelling techniques have been applied to a limited set of real field data, and where the modelling results have been compared with the full presently existing understanding/description of the site, see /Hudson ed. 2002/.

The first part of this document reports the set-up of the theoretical approach as defined for the purpose of the project, and the sensitivity analysis performed on parameters (sections 2 and 3). The methodology as described in those sections of the report is non site-dependent.

Then, the theoretical approach is applied on a specific area on Äspö, Sweden (sections 4 to 7). The study is based on a specific and controlled amount of data.

At last, discussions on parameters, results and conclusions on the relevance of the methodology for the Site Investigation are presented in sections 8 and 9.

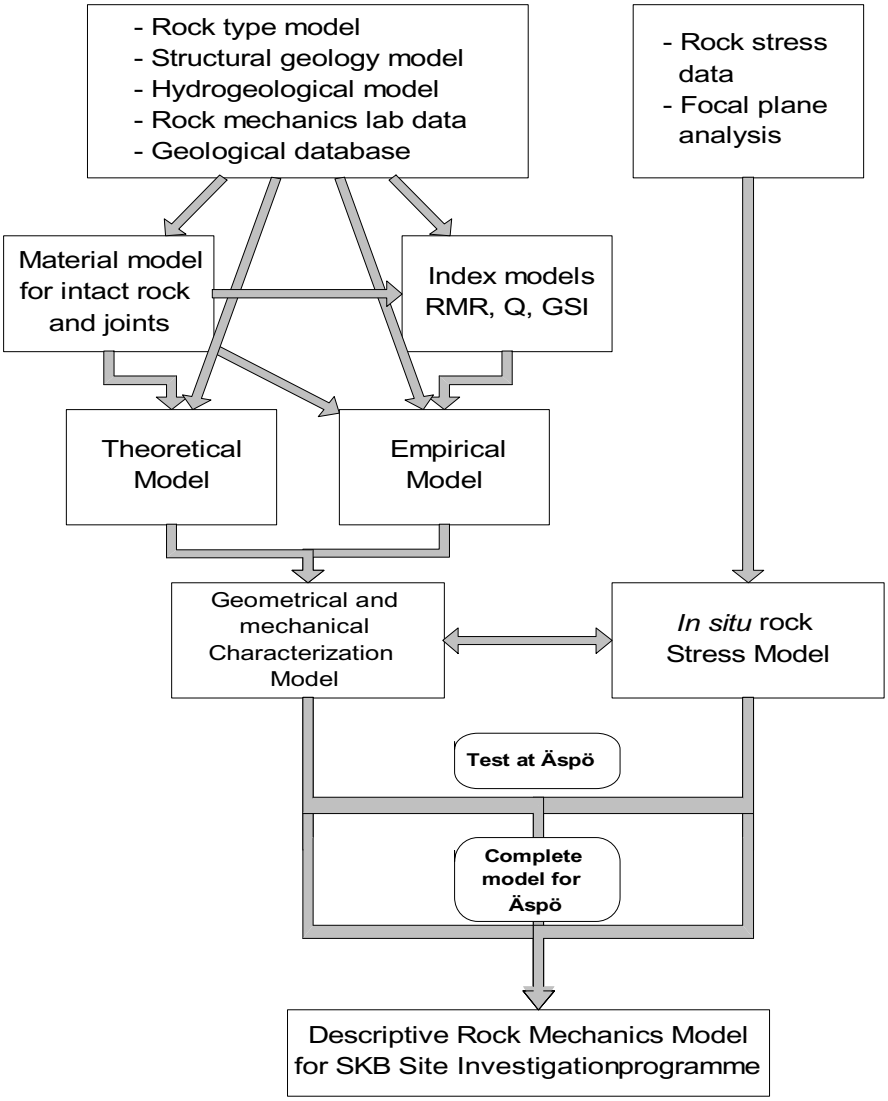

Figure 1-2. *Input data and flowchart for the Descriptive Rock mechanics Model (modified from /Andersson et al, 2002/).*

2 Overview of the methodology

Deformation properties and rock mass strength are not only dependent on the intact rock, but also on the fracture network (number and orientation of fracture sets, intensity, mineralisation,…) and the presence of deformation zones. Therefore, characterisation of both the intact rock and of the fractures is required to define the mechanical behaviour of the rock mass. Therefore, the intact rock and the rock fractures were apprehended separately.

2.1 Introduction

A general mechanical model for rock masses must consider the following items:

- mechanical behaviour of intact rock,
- mechanical behaviour of fractures, and
- geometry of fractures.

The theoretical approach includes these three items.

The mechanical behaviour of the intact rock can be identified from conventional laboratory tests on small samples. Constitutive laws for intact rock are presented in section 3.1.2. Estimation of the mechanical behaviour of fractures can be achieved in the laboratory through direct shear tests on fractures under various loading conditions. Constitutive laws for fractures are presented in section 3.1.3.

The geometry of the rock fractures can be described in statistical terms and generated by simulations. A literature review concerning statistical representation of the fracture geometry and models to generate fracture geometry is presented in Appendix A.

In order to consider the three items (mechanical behaviour of intact rock and fractures, and fracture geometry) an analytical or numerical model is needed. The model will give the rock mass response under different loading conditions. A literature review concerning models for fractured rock masses is presented in Appendix B.

2.2 Methodology

Based on the literature reviews presented in Appendix A and B a methodology was chosen for the theoretical approach. The methodology is presented as a flow chart in Figure 2-1 and described in the following paragraphs of this section. The description of the methodology in the flow chart is non-site related and can be applied in any site for this type of characterisation.

The methodology is based on Discrete Element Method for the modelling of behaviour of rock masses. The rock mass is modelled as a discontinuous geometry in which contacts between blocks are fractures. The input parameters required for the model are the fracture geometry, and the mechanical properties of fractures and intact rock. The theory behind this methodology is presented in appendix B.

A Discrete Fracture Network (DFN) model was chosen to simulate the fracture network. For a given fracture density, the number of fractures generated in a 3D DFN model is highly variable depending on the size distribution of the fractures, and of the truncation value for the minimum fracture size. The parameter of size considered in this context is related to length of fractures, and expressed as the equivalent radius of a circular fracture. Nevertheless, a DFN model based on real fracture data for a 30·30·30 m cube can contain from 1000 to more than 15000 fractures. It is at the moment technically difficult to do 3D simulations with a realistic network of discrete disc-shaped fractures. However it was determined fully possible to realise the modelling of the mechanical behaviour of a fractured rock mass in two dimensions considering rock sections of different directions. For this purpose, the 2D numerical code UDEC was selected as calculation tool.

The computations of the mechanical properties of the rock mass are based on multiple stochastic realisations. Multiple realisations reflect the variability and possible distribution of input parameters to the model and permit a statistical analysis of the results. Each simulation is treated independently in UDEC. The influence of variability of one parameter is obtained by running UDEC several times and scanning the values this parameter can reasonably take, all other parameters being constant.

2.2.1 DFN model

A Discrete Fracture Network model is developed from specific relationships between characteristics such as fracture shape, size (expressed as the equivalent radius of a circular fracture), orientation of fracture sets, and termination. The values and statistical law distribution of these characteristics are evaluated from analysis of core logging and outcrops mapping. Each model consists of a particular combination of the parameters (see Appendix A).

The DFN model provides the ground data for the simulation of fractures in the UDEC model.

2.2.2 FracMan® DFN modelling

FracMan® is the software used to generate fractures in three dimensions (3D) within a given rock volume. The definition of input parameters and the theoretical background of DFN models as developed in FracMan® are presented in /Dershowitz et al, 1998/.

The size of the modelling volume can be modified according to the size of the required DFN model.

To take into account the variability of the input parameters, the DFN model is generated several times by means of Monte Carlo simulations, and the fracture population statistics analysed for each simulated model.

2.2.3 Generation of 2D fracture trace sections

The three-dimensional Discrete Fracture Network (DFN) generated by FracMan® must be transferred to two-dimensional fracture trace sections to fit UDEC. Since the boundary conditions of the UDEC model are preferably set to normal loading only (no shear conditions), fracture traces are obtained in planes aligned with the in situ principal stresses at the investigated site.

Three different fracture trace planes of size 30·30 metres aligned with the in situ principal stress field are identified. These planes cut the DFN model in its centre. The DFN model size must be set large enough to avoid any truncation of the fracture traces at the boundaries of the trace planes: the edges of the trace planes are always located within the volume of the 3D DFN models.

2.2.4 Rock material mechanical properties from laboratory tests

The mechanical properties of the different types of rock material are obtained from laboratory tests, such as uniaxial and triaxial compression tests, and Brazil tests, see section 3.1.2.

2.2.5 Fracture mechanical properties from laboratory tests

The mechanical properties of the different fracture sets considered are obtained from laboratory tests, such as normal load tests, shear tests and tilt tests, see section 3.1.3.

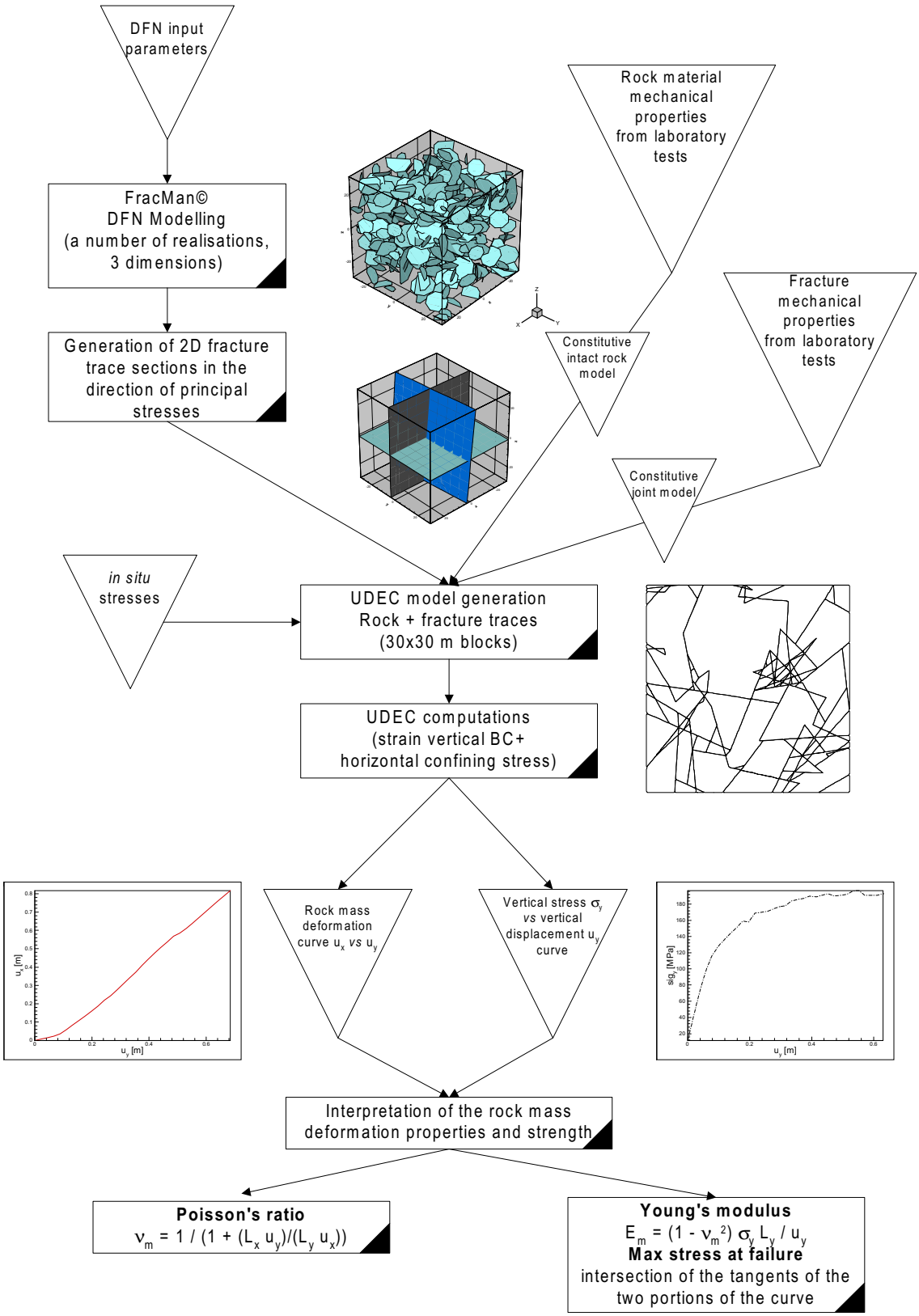

Figure 2-1. *Flowchart for the theoretical approach.*

2.2.6 UDEC model generation

A model size of 30·30 m was considered the most suitable in accordance to design and characterisation purposes, see section 1.2.2.

The UDEC block model is built in different steps that are the following. First, the intact rock is modelled as a single rock block of the size of the model. Then, the fracture traces are integrated in the model. Due to numerical coding in UDEC, parts of fractures that terminate in the rock after intersection with another fracture, and fractures that are isolated in the rock mass, are removed from the model during the meshing and the generation of the blocks.

When the block model is generated, mechanical properties as previously determined from laboratory tests (sections 2.2.4 and 2.2.5) are assigned to the intact rock and fractures. Then, suitable constitutive models that will simulate the behaviour of the material must be chosen.

2.2.7 Constitutive models for intact rock and fractures

Different constitutive models are available in UDEC that are used to model the behaviour of the intact rock and of the fractures.

The models that have been chosen for this project are:

- The Mohr-Coulomb plasticity model for the intact rock,
- The Barton-Bandis model for rock fractures (and occasionally for numerical reasons the Continuously Yielding model).

The influence of the constitutive models used in this project was also studied, see sections 3.3.1 and 3.3.6.

2.2.8 In situ stresses

The in situ stress conditions are reproduced in the UDEC model by means of the IN SITU command, with consideration to the actual intensity of stresses. The State of Stress is considered in 3D in the model, as in situ stresses in the out-of-plane direction must be taken into account to avoid failure in this plane. Orientations of in situ stresses are also considered by means of the 2D trace sections extracted from the DFN model in the directions of the 3 initial principal stresses (see section 2.2.3). The stress magnitude and orientation are provided by the in situ Rock Stress Model /Hakami et al, 2002/.

2.2.9 Boundary conditions

Stress and velocity boundary conditions are applied to the block model.

Stress boundary conditions

Stress boundary conditions are applied first during consolidation under in situ stresses, and confining stresses are applied during the computation of the plain strain test. The vertical boundaries of the model are free to move during consolidation under in situ stresses.

The prescribed consolidating stresses are in equilibrium with the in situ stresses in the section plane (x and y direction).

Since the block model tested in UDEC is similar to a plain strain-loading test, confining stresses are applied on the vertical boundaries of the model.

The state of equilibrium of the model is checked after applying the stress boundary conditions, and before to start loading.

Velocity boundary conditions

The boundary conditions as previously described are modified after consolidation, in order to begin the computations of the plain strain-loading test. Two types of velocity boundary conditions are applied to the model: zero velocity and constant velocity boundary.

Zero velocity boundaries are applied to disable displacements in one or two directions. A constant velocity boundary simulates the loading on the rock block model under testing.

Two different set-ups for stress and velocity conditions were used.

- Zero velocity on the left vertical side (simulating that horizontal deformation is set to zero on this side), and on the bottom side (simulating that vertical deformation is set to zero on this boundary). Confining stresses are applied on the right vertical side, and constant boundary velocity on the top boundary.

- Zero velocity on the bottom boundary (simulating that vertical deformation is set to zero on this boundary), confining stresses are applied on both vertical sides, and constant boundary velocity is applied on the top boundary.

Argumentation for the validity of the boundary conditions is presented in section 3.2.1 and 3.3.2.

2.2.10 UDEC computations

The mechanical testing is simulated by a vertical loading applied on top of the model by means of a constant velocity displacement obtained by a constant boundary velocity applied during a specified number of computational cycles (see section 2.2.9). Even if the stress boundary conditions are such that the model is in an initial force-equilibrium state before alteration, the equilibrium state is checked before performing vertical loading.

The vertical loading is applied to the model beyond the elastic behaviour of the components of the model (rock material and fractures) so that the estimation of the rock mass strength can be assessed.

The following parameters are monitored during the plain strain-loading test (see Figure 3-7):

- Vertical displacement along a horizontal profile located within the top loading block,
- Vertical stress along a horizontal profile located within the top loading block, and
- Horizontal displacements along one vertical profile at the right boundary of the model, or along two vertical profiles, depending of the model set-up.

The monitoring profiles consist of 25 monitoring points that are equally distributed along a reference line. The value at a computing node is attributed to the nearest monitoring point on the reference lines. The mean value of the monitored variable on the 25 points is then calculated at each loading step.

2.2.11 Rock mass deformation properties and strength

The deformation properties of the rock mass are evaluated from two curves drawn by respectively plotting of: (1) horizontal displacement, u_x, *vs.* vertical displacement, u_y, and (2) vertical stress, σ_y, *vs.* vertical displacement, u_y.

The first curve is used to evaluate the Poisson's ratio of the rock mass. The deformation modulus and the rock strength are determined from the second curve (see sections 3.2.2 and 3.2.3).

3 Description of the methodology

This chapter focuses on the methodology developed in the theoretical approach, and also tackles the sensitivity and statistical analyses that have been conducted in order to determine the validity of the model.

The methodology as described hereunder can then be applied on any site.

3.1 Input data to the theoretical approach

3.1.1 Geometry of fractures

The term "fractures" is used to refer to any mechanical breaks in a rock mass, which implies any kind of discontinuity such as joints, fissures, faults and cracks. Then, specific attention is paid to deformation zones as defined by SKB /Andersson et al, 2000/.

The main issue is to characterise features that are three-dimensional but present limited, often two-dimensional, exposure on outcrops, in boreholes and tunnels.

Three different approaches have been developed to simulate fracture networks that are Stochastic Continuum (SC), Channel Network (CN) and Discrete Fracture Network (DFN). The choice of model depends on the purpose of the study, namely the modelling of transport or the visualisation of the geology. In the frame of this project, realistic simulation of the fracture network in the area of investigation represents the main interest, and as regard to this, DFN models have been used.

Different conceptual models are applied to build DFN models, and each is developed on specific relationships between characteristics such as location of fracture sets, termination, and fracture shape. Each model consists of a particular combination of the fracture system characteristics. The choice of the conceptual model is dependent on the general pattern of the natural fracture network and the aim of the modelling: characterisation and visualisation of the fracture network in a rock mass, definition of a specific pattern along deformation zone, reconstruction of a pattern based on fracturing history, *etc*.

The fracture pattern for each developed DFN model is characterised by the following parameters: orientation of the fracture sets, volumetric intensity of each fracture set, expressed as the area of fractures/volume, size distribution of fractures in each set. The size distribution of fractures, as defined for a DFN model, is evaluated from trace lengths obtained from outcrop and lineament mapping, and is expressed as the equivalent radius of a circular fracture. The validity of the radius size distribution obtained is checked by simulating a DFN model and extracting sampling planes with orientation consistent to the "sampling windows" in the field. The distribution of trace lengths on these planes is compared to the distribution of trace lengths mapped on site. The radius size distribution is adjusted if necessary until it fits the measured data.

The relation between "raw" fracture data and input data for a DFN model is illustrated in Table 3-1.

Table 3-1. "Raw" fracture data and derived input fracture data for a DFN model.

"raw" fracture data	Source	DFN input data
Fracture orientation (strike, dip)	Boreholes, outcrops, tunnels	Fracture sets Orientation of fractures in each set
Trace length	Tunnels, outcrops, lineaments	Size distribution
Termination	Tunnels, outcrops, lineaments	Choice of the model, hierarchy of the sets
Fracture intensity(*)	Boreholes, scanlines (P_{10}), outcrops (P_{21}).	Fracture intensity (P_{32})

(*) The expressions of P_{10}, P_{21} and P_{32} are explained in section 5.2.1.

As the DFN model is developed for rock mechanical purposes, all fractures, conductive and non-conductive, over the truncation size are included in the analysis.

The background of the DFN approach, the definition of the conceptual models and their field of applicability are presented in appendix A.

3.1.2 Mechanical properties of intact rock

The mechanical properties of the different types of rock materials considered are obtained from laboratory tests. The evaluation of these properties from laboratory test results is done according to theoretical constitutive laws describing the behaviour of the material.

This section is a short description of the theoretical expressions of use for determining the mechanical properties required for the modelling. Complementary data are presented in appendix C.

Deformation properties

The deformation properties of the intact rock can be expressed by two parameters, the Young's modulus, E, and Poisson's ratio, ν. These parameters are determined from uniaxial compression tests /ISRM, 1999/. UDEC uses the elastic constants K (bulk modulus) and G (shear modulus) as input parameters. These are related to E and ν by the following equations:

$$K = \frac{E}{3(1-2\nu)} \tag{3.1}$$

$$G = \frac{E}{2(1+\nu)} \tag{3.2}$$

Strength properties

Based on the results of uniaxial, triaxial and Brazil tests the strength of the intact rock /ISRM, 1983/ can be plotted in a σ_1-σ_3 diagram as shown in Figure 3-1, where σ_1 and σ_3 represent the maximum and minimum stresses at failure. The strength envelope can be either fitted by the Hoek-Brown (H-B) failure criterion, expressed as:

$$\sigma_1 = \sigma_3 + \sigma_c \cdot \left(m_b \cdot \sigma_3 / \sigma_c + s \right)^a \tag{3.3}$$

or by the Mohr-Coulomb (M-C) failure criterion /Hoek and Brown, 1997/ expressed as:

$$\sigma_1 = \sigma_3 \cdot \left(1+\sin\phi\right) \Big/ \left(1-\sin\phi\right) + 2 \cdot c \cdot \cos\phi \Big/ \left(1-\sin\phi\right) \tag{3.4}$$

where c and ϕ represent the cohesion and friction angle of the material. The parameters m_b, s and a are material constants and σ_c is the uniaxial strength of the intact rock. For intact rock, the material constant s is set to 1.0 and *a* to 0.5.

Using the H-B criterion, we can obtain a curve fitted to the experimental data by selecting an appropriate value for the parameter m_b in equation (3.3), see Figure 3-1.

Similarly using the M-C criterion, c and ϕ can be obtained by linear regression of the test results, see Figure 3-1.

The greatest difference between the two failure criteria is at low compression stresses and tensile stresses. The influence of the strength failure criterion on strength properties has been studied and the results are presented in section 3.3.1.

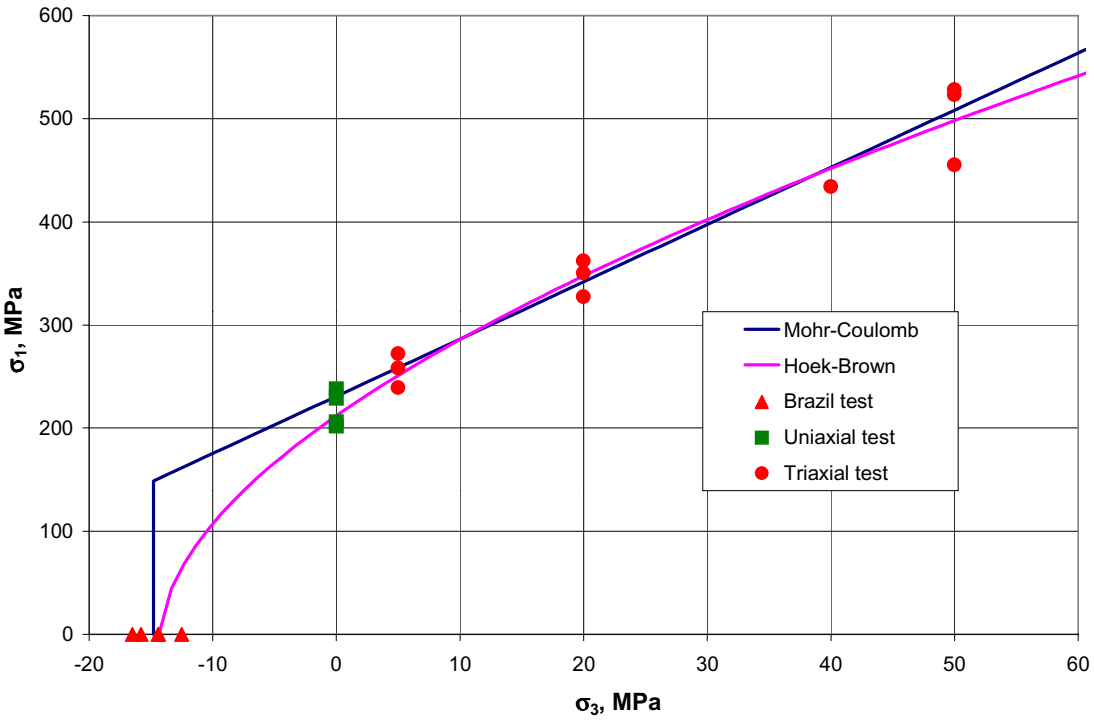

Figure 3-1. *Strength envelopes for the intact rock, using M-C and H-B failure criteria.*

3.1.3 Mechanical properties of fractures

Numerical modelling of practical problems with fractures may take fractures through rather complex load paths. In UDEC two constitutive joint models are available for modelling rather complex load paths. The models are the Continuously Yielding joint model and the Barton-Bandis joint model. The theoretical background of these models is described in the following sections as they are implemented in UDEC.

The term “joints” is used when referring to the constitutive models and input parameters, as it is the term used in the UDEC manual.

Continuously Yielding joint model

The Continuously Yielding joint model proposed by /Cundall and Hart, 1984/ is intended to simulate the internal mechanism of progressive damage of fractures under shear. The essential features of the Continuously Yielding model include the following:

- The curve of shear stress/shear displacement is always tending toward a target, shear strength of the rock fracture.
- The target shear strength decreases continuously as a function of accumulated plastic displacement.
- The dilation angle is the difference between the apparent friction angle and the residual friction angle.

The model is described as follows. The response to normal loading is expressed incrementally as:

$$\Delta\sigma_n = K_n \cdot \Delta u_n \tag{3.5}$$

where $\Delta\sigma_n$ is the increment in normal stress, Δu_n the increment in normal displacement, and the normal stiffness, K_n, is given by:

$$K_n = a_n \cdot \sigma_n^{e_n} \tag{3.6}$$

representing the observed increase of stiffness with normal stress. a_n, initial joint normal stiffness, and e_n, exponent of joint normal stiffness, are model parameters. In general, zero tensile strength is assumed.

For shear loading, the model displays irreversible, non-linear behaviour. The shear stress increment, $\Delta\tau$, is calculated as:

$$\Delta\tau = F \cdot K_s \cdot \Delta u_s \tag{3.7}$$

where Δu_s is the increment in shear displacement, and the shear stiffness, K_s, can also be taken as a function of normal stress as:

$$K_s = a_s \cdot \sigma_n^{e_s} \tag{3.8}$$

where a_s, initial joint shear stiffness, and e_s, exponent of joint shear stiffness, are model parameters. The tangent modulus, $\Delta\tau$, is governed in equation (3.7) by the factor F, which depends on the distance from the actual stress curve to the "target" or bounding strength curve, τ_m, as:

$$F = \frac{\left(1 - \tau / \tau_m\right)}{1 - r_e} \tag{3.9}$$

The factor r_e, which is initially zero, is intended to restore the elastic stiffness immediately after a load reversal – that is, r_e is set to τ/τ_m and therefore F is equal to 1. The bounding strength is given by:

$$\tau_m = \sigma_n \cdot \tan(\phi_m) \cdot \mathrm{sgn}(\Delta u_s) \tag{3.10}$$

The parameter ϕ_m can be understood as the friction angle that would apply if the joint were to dilate at the maximum dilation angle. As damage accumulates, this angle is continuously reduced according to the following equation:

$$\Delta\phi_m = -\left/_{jr}\right.\left(\phi_m - \phi_b\right)\cdot\Delta u_s^p \tag{3.11}$$

where the plastic displacement increment, Δu_s^p, is defined as:

$$\Delta u_s^p = \left(1-F\right)\cdot\left|\Delta u_s\right|, \tag{3.12}$$

ϕ_b is the basic friction angle of the rock surface, and jr is a material parameter (with dimension of length) which expresses the joint roughness.

The parameter jr controls the rate at which ϕ_m decreases with plastic shear displacement. A small value of jr causes ϕ_m to decrease rapidly; a large value of jr leads to a slower reduction of ϕ_m and therefore to a larger peak stress. The peak is reached when the bounding strength equals the shear stress. The incremental relation for ϕ_m is equivalent to:

$$\phi_m = \left(\phi_m^{(i)} - \phi_b\right)\cdot\exp\left(\left.-u_s^p\right/_{jr}\right) + \phi_b \tag{3.13}$$

where $\phi_m^{(i)}$ is the initial value of ϕ_m and represents the in situ state of the joint. The plastic displacement, u_s^p, always increases.

The effective dilatancy angle is calculated as:

$$i = \tan^{-1}\left(\left|\tau\right|/\sigma_n\right) - \phi_b \tag{3.14}$$

i.e. dilation takes place whenever the stress is above the residual strength level, and is obtained from the actual friction angle.

The model parameters associated with the Continuously Yielding model are summarised in Table 3-2.

Table 3-2. Parameters associated with the Continuously Yielding joint model /from UDEC, 2000a/.

Parameter	Description
a_n	Joint normal stiffness, initial value, MPa/m
e_n	Joint normal stiffness exponent
a_s	Joint shear stiffness, initial value, MPa/m
e_s	Joint shear stiffness exponent
jr	Joint roughness parameter, m
$\phi_m^{(i)}$	Joint initial friction angle, º
ϕ_b	Basic joint friction angle, º

Barton-Bandis joint model

Series of empirical relations have been developed by N. Barton and S. Bandis to describe the effects of surface roughness on discontinuity deformation and strength.

These relations are known collectively as the Barton-Bandis joint model. A complete explanation of these relations can be obtained from /Barton, 1982; Bandis et al, 1985/. In summary, the Barton-Bandis joint model encompasses the following features /UDEC, 2000b/.

Joint normal behaviour

The joint normal behaviour for the Barton-Bandis model encompasses:

- hyperbolic stress-displacement path,
- hysteresis due to successive load/unload cycles,
- normal stiffness increase due to successive load/unload cycles,
- normal stiffness change due to surface mismatch caused by shear displacement.

The equation that controls the normal stress-displacement path for the Barton-Bandis model is (see Figure 3-2):

$$\sigma_n = -\frac{u_{nc} \cdot K_{ni}}{1 - u_{nc} / \upsilon_{mi}} \tag{3.15}$$

where u_{nc} is the current normal displacement (mm),

K_{ni} is the initial normal stiffness, dependent to loading cycle (MPa/mm),

and

υ_{mi} is the maximum allowable closure (mm) for load cycle i.

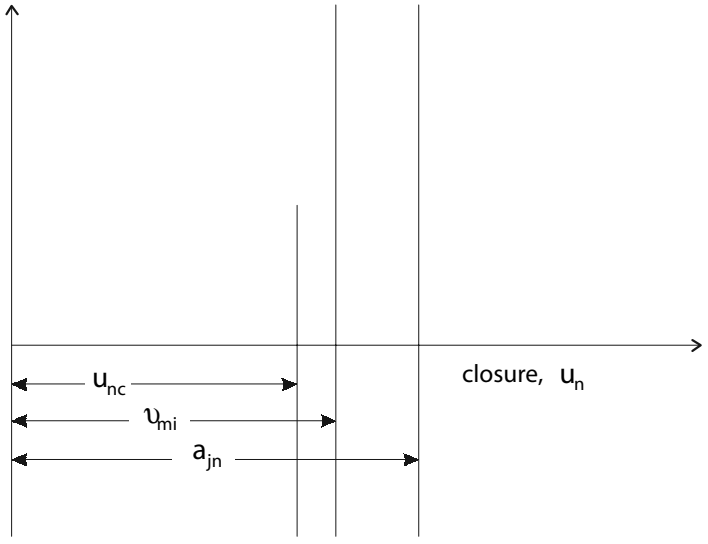

Figure 3-2. *Normal stress-displacement curve /UDEC, 2000b/.*

The initial joint normal stiffness (K_{ni}), which changes with load cycle number, is calculated by:

$$K_{ni} = 0.0178 \cdot \frac{JCS_0}{a_{jn}} + 1.748 \cdot JRC_0 - 7.155 \tag{3.16}$$

where JCS_0 is the laboratory-scale joint wall compression strength,

a_{jn} is the joint aperture at zero normal stress, and

JRC_0 is the laboratory-scale roughness coefficient.

The maximum allowable closure (υ_{mi}) for load cycle *i* is given by:

$$\upsilon_{mi} = A_i + B_i \cdot JRC_0 + C_i \cdot \left(\frac{JSC_0}{a_{jn}} \right)^{D_i} \tag{3.17}$$

where A_i, B_i, C_i and D_i are constants associated with the load cycle number.

To calculate the path for an unload cycle following a load cycle, a new υ_{mi} and K_{ni} are calculated. K_{ni} is calculated from equation (3.16) using a new aperture value, a_{jn}, which is reduced by the irrecoverable closure, υ_{irr}. The current maximum allowable closure, υ_m, is recalculated from equation (3.17), also using a_{jn} reduced by υ_{irr}. The irrecoverable closure, υ_{irr}, is calculated from equation (3.18):

$$\upsilon_{irr} = \left[C_1 - C_2 \cdot \left[\frac{JCS_0}{a_{jn}} \right] \right] \cdot \frac{u_{nl}}{100} \tag{3.18}$$

where u_{nl} is the maximum closure for a completed load cycle, and

C_1, C_2 are empirical constants for the current cycle.

To maintain displacement continuity, υ_{irr} is added to the sum of the previous irrecoverable closures and subtracted from the current closure. For the next load cycle, K_{ni} remains constant, and a new υ_m is calculated using equation (3.17) and the constants for the next load cycle. If a partial unload was done, the hyperbolic curve is shifted on the deformation axis, and υ_{mi} is modified to provide load continuity.

Successive load/unload cycles will continue to stiffen the joint normal behaviour, see Figure 3-3. The empirical constants derived by Barton and Bandis do not change after cycle 4, but the aperture will continue to decrease. The load cycle number will not increase beyond 10, and the load and unload curves will become identical. To maintain numerical stability, the stiffness of the model is limited to the joint normal stiffness at expected normal loads, K_n, which is specified as input to UDEC. A linear stiffness function is substituted into the stress displacement calculations when the stiffness of the Barton-Bandis model exceeds K_n.

To represent an undisturbed joint in a rock mass, all joints are numerically cycled three times from zero normal stress to 60% of the joint wall compressive strength. Therefore, each joint starts at normal load cycle 4 and shear cycle 1.

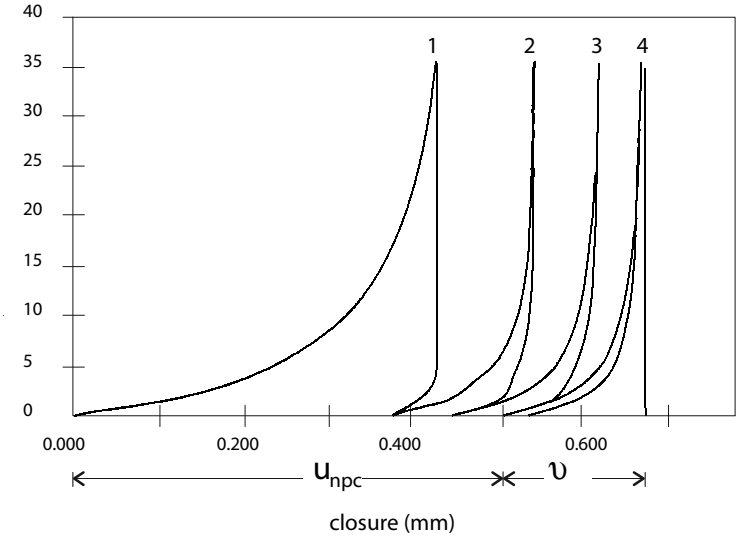

Figure 3-3. *Joints numerically cycled to load cycle 4 at start of execution /UDEC, 2000b/.*

Joint shear behaviour

The joint shear behaviour for the Barton-Bandis model encompasses the following features:

- dilation as a function of normal stress and shear displacement,
- joint damage due to post-peak shear, and
- reduced secondary peak shear upon post-peak shear reversal.

The shear resistance of a joint is calculated using the concept of mobilised roughness /Barton, 1982/. The mobilised roughness coefficient, JRC_{mob}, is a function of the joint properties: length, normal load, current shear displacement, and shear displacement history. The relation between normalised shear displacement ($u_s/u_{s,\,peak}$) and the normalised mobilised roughness coefficient (JRC_{mob}/JRC_{peak}) is shown in Figure 3-4.

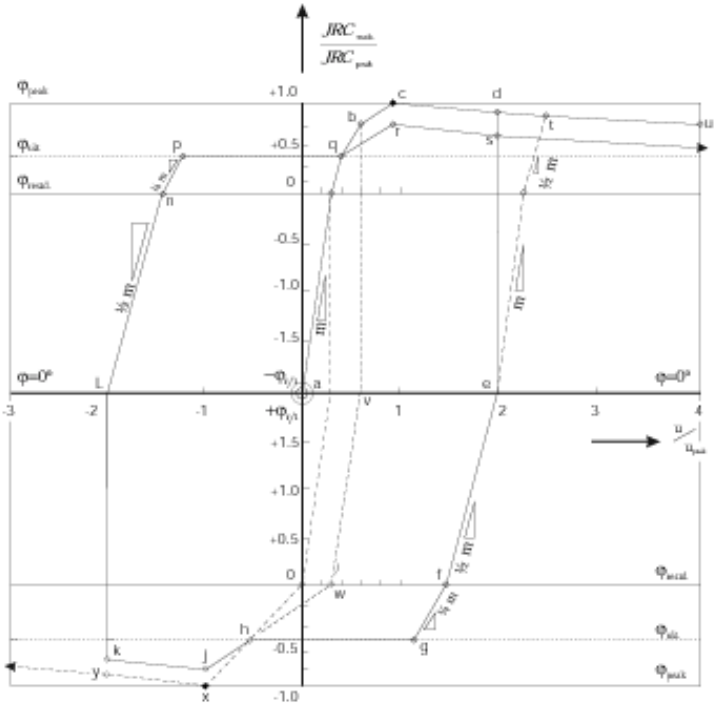

Figure 3-4. *Model for simulating the effects of displacement on shear strength of joints /Barton, 1982/.*

To implement the shear stress model, a limiting shear stress, τ_l, is calculated from the full-scale roughness coefficient, JRC_n, the joint wall compressive strength, JCS_n, and the peak shear displacement, $u_{s,\,peak}$:

$$JRC_n = JRC_0 \cdot \left(\frac{L_n}{L_0} \right)^{-0.02 \cdot JRC_0} \tag{3.19}$$

$$JCS_n = JCS_0 \cdot \left(\frac{L_n}{L_0} \right)^{-0.03 \cdot JRC_0} \tag{3.20}$$

$$u_{s,peak} = \frac{L_n}{500} \cdot \left(\frac{L_n}{L_0} \right)^{0.33} \tag{3.21}$$

where L_0 is the laboratory-scale joint length,

L_n is the field-scale joint length,

JCS_0 is the laboratory-scale joint wall compression strength, and

JRC_0 is the laboratory-scale roughness coefficient.

The mobilised joint roughness coefficient, JRC_{mob}, is calculated according to:

$$JRC_{mob} = B \cdot JRC_n \tag{3.22}$$

where B is a function of shear displacement, $u_s / u_{s,\,peak}$.

The limiting shear stress, τ_l, is calculated by:

$$\tau_l = \sigma_n \cdot \tan\left(JRC_{mob} \cdot \log_{10}\left({JCS_n}/{\sigma_n} \right) + \phi_r \right) \tag{3.23}$$

where ϕ_r is the residual friction angle, and

σ_n the current normal stress.

The shear stress approaches the limiting shear stress incrementally by multiplying the shear displacement increment, $\Delta u_{s,}$ by the shear stiffness, K_s. The stiffness is defined as one of two initial linear segments of the load path, depending on shear displacement. The incremental shear stress, $\Delta\tau$, is calculated from the following expression:

$$\Delta\tau = \Delta u_s \cdot K_s \tag{3.24}$$

where

$$K_s = \sigma_n \cdot \tan\left(\frac{0.75 \cdot \phi_r}{0.2 \cdot u_{s,peak}} \right) \cdot L_n \qquad \text{for } (u_s/\, u_{s,\,peak}) < 0.20 \tag{3.25}$$

or

$$K_s = \sigma_n \cdot \tan\left(\frac{0.25 \cdot \phi_r}{0.1 \cdot u_{s,peak}} \right) \cdot L_n \qquad \text{for } (u_s/\, u_{s,\,peak}) > 0.20 \tag{3.26}$$

The mobilised dilation is also calculated from the mobilised roughness. The formulation calculates a normal dilation increment, Δu_n, based on the shear displacement increment, Δu_s, and the current normal stress, σ_n:

$$\Delta u_n = \Delta u_s \cdot \tan\left(0.5 \cdot JRC_{mob} \cdot \log_{10}\left({JCS_n}/{\sigma_n} \right) \right) \tag{3.27}$$

When successive shear cycles of forward and reverse shear occur, the mobilised roughness is reduced by 50% each time the peak shear displacement is passed.

The model parameters associated with the Barton-Bandis model are summarised in Table 3-3.

Table 3-3. Parameters associated with the Barton-Bandis model /from UDEC, 2000b/.

Parameter	Description
JRC_0	Lab-scale roughness coefficient
JCS_0	Lab-scale joint wall compressive strength, MPa
L_0	Lab-scale joint length, m
ϕ_r	Residual angle of friction, º
σ_c	Intact rock uniaxial compressive strength, MPa
K_n	Normal stiffness of joint at expected normal loads, MPa/m
K_s	Initial shear stiffness of joint at expected normal loads, MPa/m
a_{jn}	Joint aperture at zero normal stress, mm

The mechanical properties of fractures that are used as input in these models are evaluated from laboratory tests, see appendix C.

The influence of the constitutive model on the mechanical properties of rock fractures is handled in this project and the results are presented in section 3.3.6.

3.2 Set-up of the numerical model

3.2.1 Description of the model

The numerical model simulates a plain strain-loading test of the rock mass with constant confining stress. Different values of confining stresses were applied for the same set-up of parameters, simulating:

- the variation of in situ stresses with depth,
- at the same depth, the stress conditions (I) in the undisturbed rock mass, and (II) at the proximity of the tunnel, see Figure 3-5.

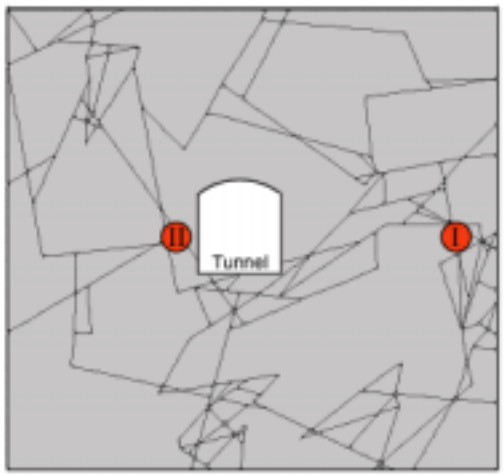

Figure 3-5. *Stress state in the rock mass in relation to an excavation.*

The rock mass is loaded by means of a top loading block that is pushed down with a constant velocity. Applying the vertical loading by means of a top block generated a better distribution of stresses and deformation for measurements in the model under testing. If not using a top block, several monitoring profiles in the 30 m rock blocks had been required. High mechanical properties are assigned to the loading block to make it stiff and non deformable (the deformation modulus is set about 1000 times higher than the deformation modulus of the intact rock). The interface between the loading block and the rock mass block is assumed to have no friction.

Actual in situ and confining stresses are applied to the model, see Figure 3-6a. The model is anisotropic in respect to the in situ stresses, and the values of stresses are assigned to the model in accordance to the orientation of the 2D trace sections towards the 3D stress field, and the depth of the simulated block. Two different models are then tested depending on the Stress State of the rock mass:

- (I) Plain strain loading test on the undisturbed rock mass, Figure 3-6c-I,
- (II) Unloading to reach a confining stress of 75% of the in situ horizontal stress, see Figure 3-6b. This is to simulate the conditions at the proximity of a tunnel. When the equilibrium of the model is reached, the plain strain-loading test starts (Figure 3-6c-II).

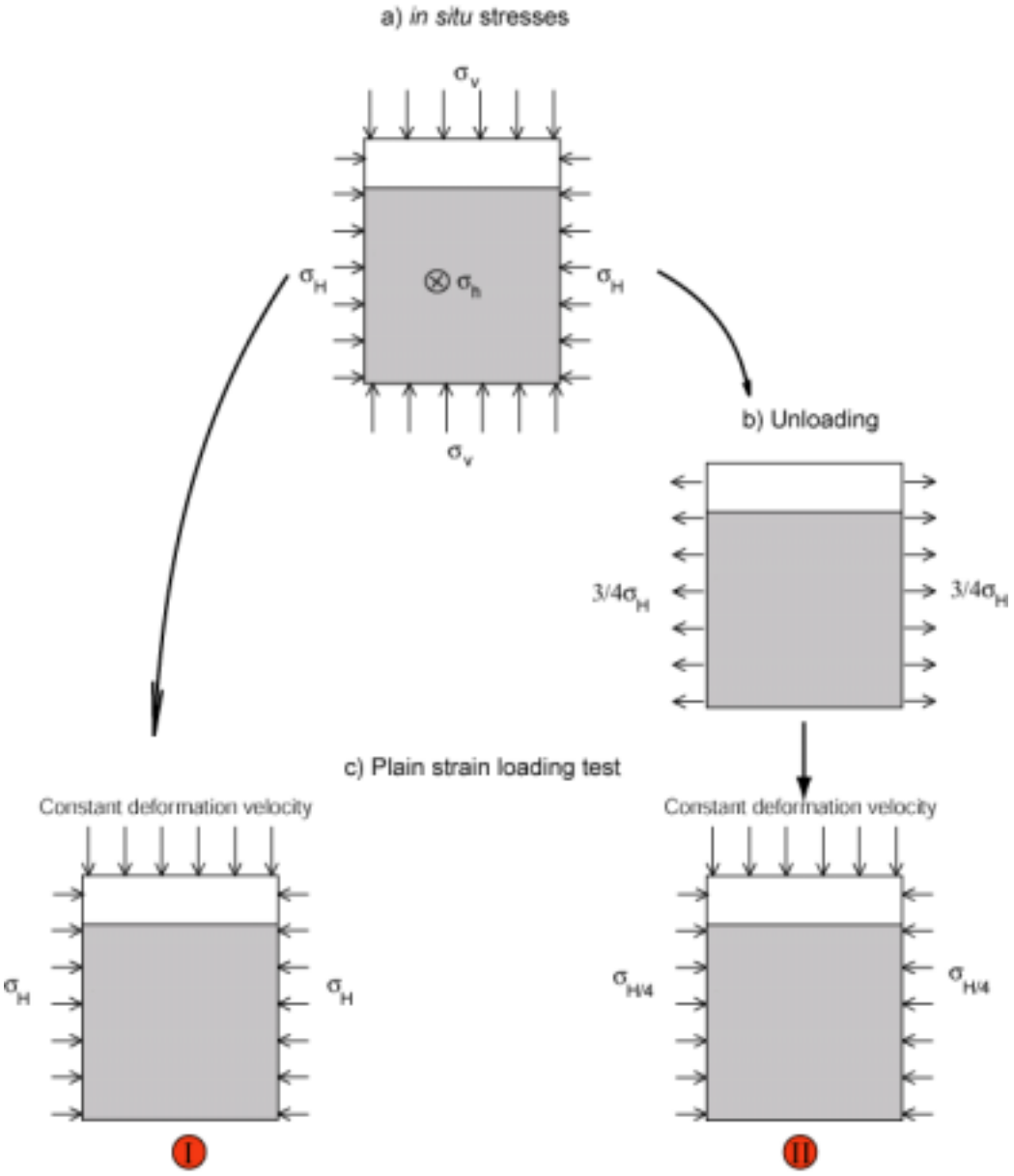

Figure 3-6. *Simulations of the Stress State (I) in the* in situ *rock mass, and (II) at the proximity of an excavation.*

In both cases, the loading is applied gradually to the model by alternation of loading/equilibrium cycles. The loading block is pushed down at constant velocity for a finite number of computational cycles resulting in a specific vertical deformation. Then the boundary velocity at the top is set to zero and state equilibrium is reached by cycling until the unbalance force is insignificant. The state of stress and vertical and horizontal deformations are then recorded before the next loading cycle starts. By applying this procedure, the deformation velocity has very little influence on the results.

The size chosen for the rock block model for characterisation purposes is 30·30 m, see section 1.2.2. As described in section 2.2.9, two different set-ups are used for applying confining stresses:

- Confining stresses are applied on both vertical sides, and one point is fixed on the bottom boundary, Figure 3-7a. This set-up simulates conditions valid for the characterisation of the undisturbed rock mass in in situ conditions.
- Confining stresses are applied on one vertical side, the other vertical side is fixed in the horizontal direction, and the bottom boundary is fixed in the vertical direction, Figure 3-7b. This set-up represents conditions around a tunnel. In this case, the rock mass will give some constraints on one side and the rock blocks are free to move on the free face towards the tunnel. As described in the previous paragraph, the confining stress is reduced to 75% of the horizontal in situ stress. Ideally it would be required to have zero confining stress on the free vertical side but this would lead to instability in the model and to numerical problems.

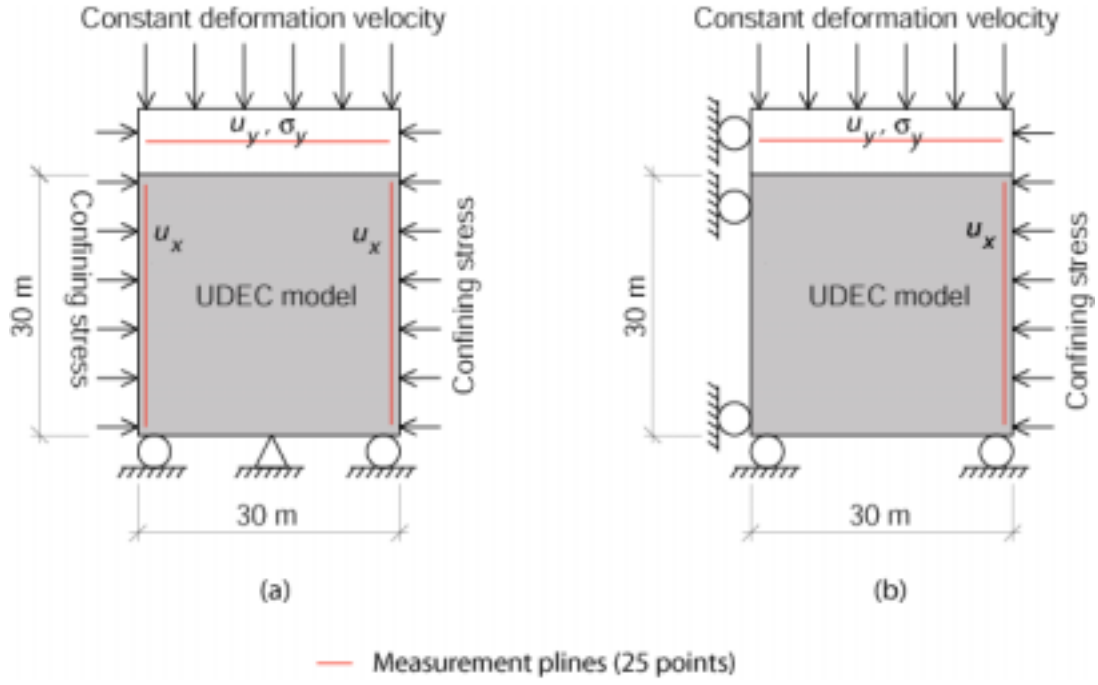

Figure 3-7. *The numerical UDEC models: (a) Confining stresses applied on both sides, and (b) Confining stresses applied on one vertical side.*

The influences of the boundary conditions and of the model size are investigated in more detail in sections 3.3.2 and 3.3.3.

3.2.2 Evaluation of the rock mass deformation properties from the model

During the numerical loading test the vertical stress, σ_v, and horizontal deformation, u_x, are recorded as a function of the vertical deformation, u_y. The recording process is described in section 2.2.10. The Poisson's ratio, ν_m, and the deformation modulus, E_m, of the rock mass are calculated according to the following equations:

$$\nu_m = \frac{1}{1 + \frac{(L_x \cdot u_y)}{(L_y \cdot u_x)}} \tag{3.28}$$

$$E_m = \frac{(1 - \nu_m^2) \cdot \Delta\sigma_y \cdot L_y}{u_y} \tag{3.29}$$

where L_x and L_y are the length over which u_x and u_y are monitored. Equations (3.28) and (3.29) are derived from Hooke´s law for plain strain loading. When evaluating the Poisson's ratio and the deformation modulus of the rock mass, u_x, u_y and σ_y are taken from the initial linear part of the recorded curves, see Figure 3-8.

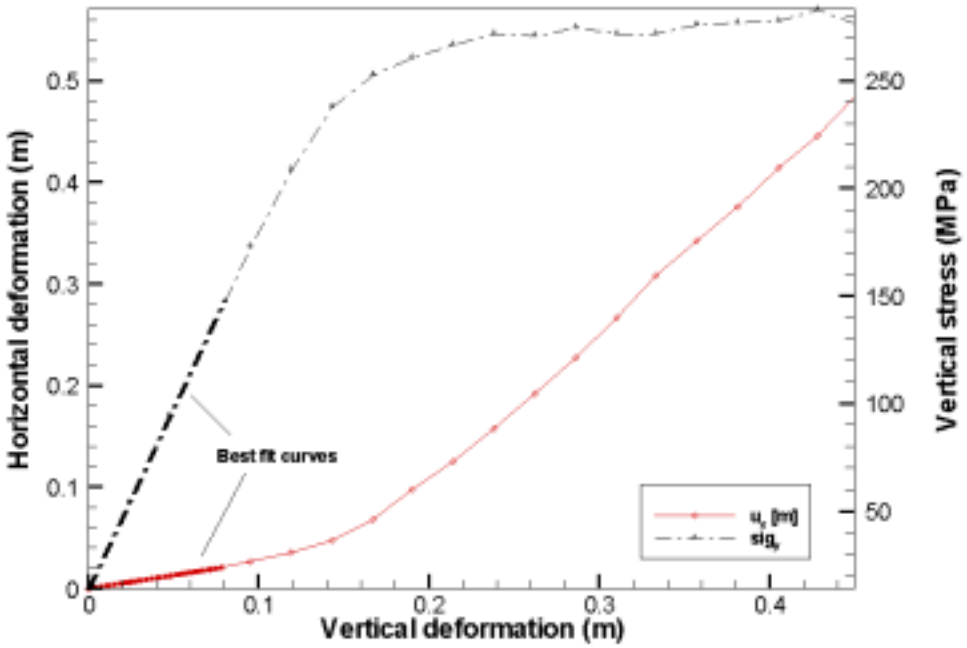

Figure 3-8. *Evaluation of deformation properties.*

3.2.3 Evaluation of the rock mass strength from the model

In geotechnical software a failure criterion is used to describe the rock mass strength. Two well-known failure criteria are the Hoek-Brown and Mohr-Coulomb criteria.

The generalised Hoek-Brown failure criterion for jointed rock masses is defined by equation (3.3). The values of the model constants should be determined by statistical analysis of sets of stresses (σ_1 and σ_3) at failure. The range of minor principal stress values, σ_3, over which these combination of stresses are given is critical in determining reliable values for the constants.

Most geotechnical softwares use the Mohr-Coulomb's failure criterion, in which the rock mass strength is defined by the cohesive strength, c_m, and the angle of friction, ϕ_{rm}.

The linear relationship between the major and minor principal stresses, respectively σ_1 and σ_3, for Mohr-Coulomb criterion is given by equation (3.4).

There is no direct correlation between equation (3.4) and the non-linear Hoek-Brown criterion defined by equation (3.3). Equation (3.4), describing the Mohr-Coulomb mode, can also be fitted to pairs of principal stresses at failure.

In order to keep down the number of numerical simulations the Mohr-Coulomb failure criterion has been used to evaluate the strength of the rock mass. A sensitivity analysis on the failure criterion used is presented in section 3.3.1.

The evaluated rock mass properties shall be valid for a 30·30 m rock volume around the deposition tunnels, see section 1.2.2. The confining stress around the tunnels will range from zero at the tunnel wall, to the horizontal initial stress at a distance of about five times the radius of the tunnel (about 15 m). To get an average it was decided to run two loading tests in the numerical model. The first test is first consolidated to the initial stresses and then loaded in vertical compression to failure. The second test is first consolidated to the initial stresses, then unloaded to a horizontal stress that is one quarter of the initial value (valid for a distance of about 0.2 times the radius of the tunnel from the tunnel wall) and then loaded in vertical compression to failure, see section 3.2.1. From these numerical loading tests two sets of principal stresses at failure, σ_{1a}, σ_{3a} and σ_{1b}, σ_{3b}, are obtained. σ_1 at failure is evaluated at the crossing point of two straight lines. These are regression lines (least square methods) of the two sections of the recorded curve, before and after breakpoint, see Figure 3-9.

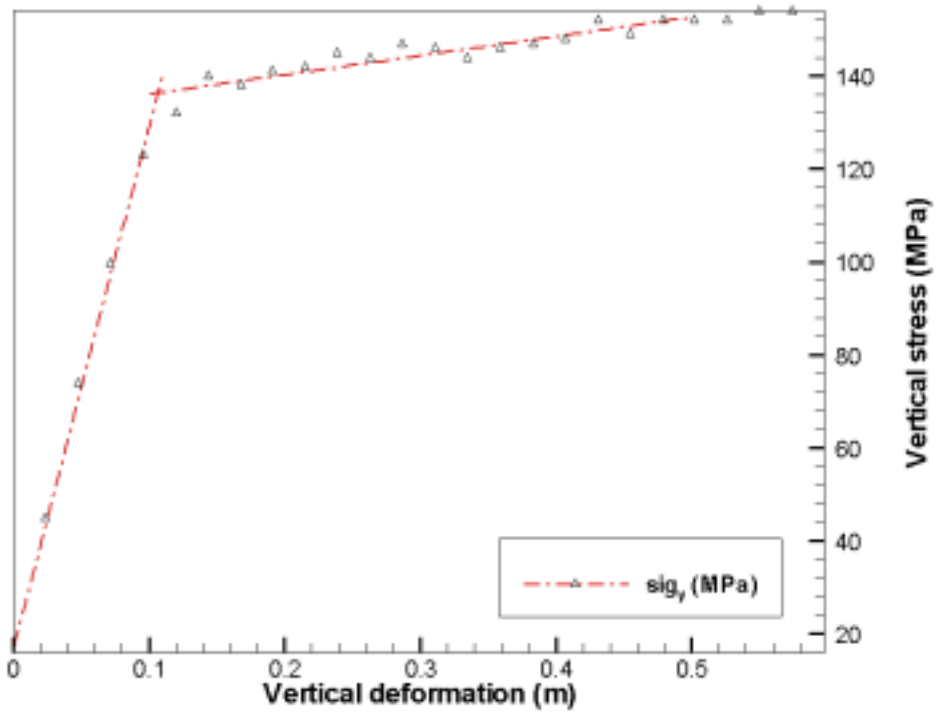

Figure 3-9. *Evaluation of the major principal stress at failure.*

With respect to the Mohr-Coulomb failure criterion, the cohesion, c_m, the friction angle, ϕ_{rm}, and the uniaxial strength, σ_{cm}, of the rock mass are calculated according to the following equations /Hoek and Brown, 1997/:

$$\phi_{rm} = \arcsin\left(k-1 \middle/ k+1\right) \tag{3.30}$$

$$\sigma_{cm} = \sigma_{1b} - k\sigma_{3b} \tag{3.31}$$

$$c_m = \sigma_{cm} \cdot \left(1-\sin\phi_{rm}\right) \middle/ 2\cos\phi_{rm} \tag{3.32}$$

$$\text{where } k = \left(\sigma_{1a}-\sigma_{1b}\right) \middle/ \left(\sigma_{3a}-\sigma_{3b}\right) \tag{3.33}$$

3.3 Sensitivity analysis on the model

3.3.1 Influence of the material model for the intact rock

Intact rock models

Three different failure criteria models for the intact rock have been tested, first the Mohr-Coulomb (M-C) failure criterion, second the Hoek-Brown (H-B) failure criterion, and third a Strain–Softening model (S-S) based on M-C. The mechanical properties of the intact rock, here a diorite, are determined from the uniaxial, triaxial and Brazil tests, see also appendix C, and are the input parameters to the different models. They are shown in Table 3-4 to Table 3-6.

The input parameters used for the Strain–Softening model are given according to Figure 3-10 to Figure 3-11. The variations of cohesion, friction angle and tensile strength with plastic strain are established in order to give a reduction of about 60% of the strength after the peak value.

Table 3-4. Input parameters to the M-C model.

E, GPa	ν	c, MPa	ϕ, °	ψ, °	σ_{ti}, MPa
73.0	0.27	31	49	0	–14.8

Table 3-5. Input parameters to the H-B model.

E, GPa	ν	σ_c, MPa	m_b
73.0	0.27	212	14.71

Table 3-6. Input parameters to the S-S model.

E, GPa	ν	c, MPa	ϕ, °	ψ, °	σ_{ti}, MPa
73.0	0.27	See Figure 3-10	See Figure 3-11	0	See Figure 3-12

With
- E Deformation modulus of the intact rock
- c Cohesion of the intact rock
- ν Poisson's ratio of the intact rock
- ϕ Friction angle of the intact rock
- ψ Dilation angle of the intact rock
- σ_{ti} Tensile strength of the intact rock
- σ_c Uniaxial compressive strength of the intact rock
- m_b Parameter constant, dependent onto the intact rock

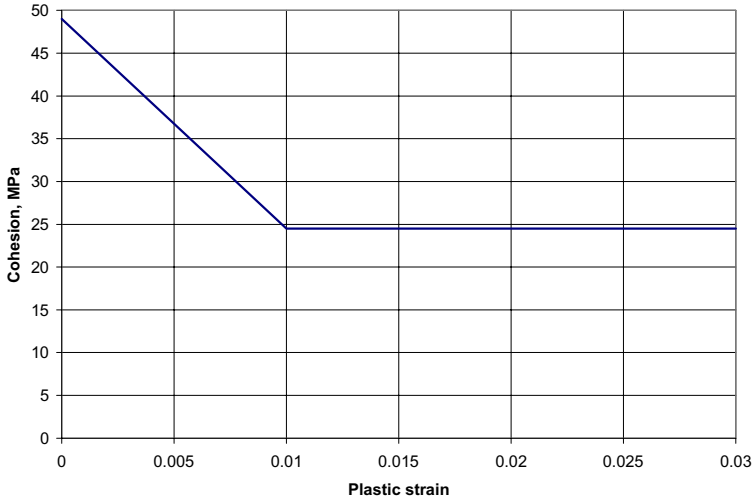

Figure 3-10. *Variation of cohesion with plastic strain.*

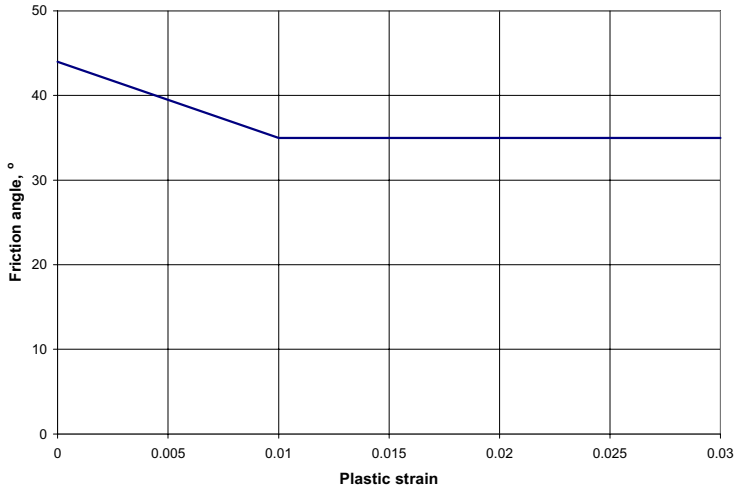

Figure 3-11. *Variation of friction angle with plastic strain.*

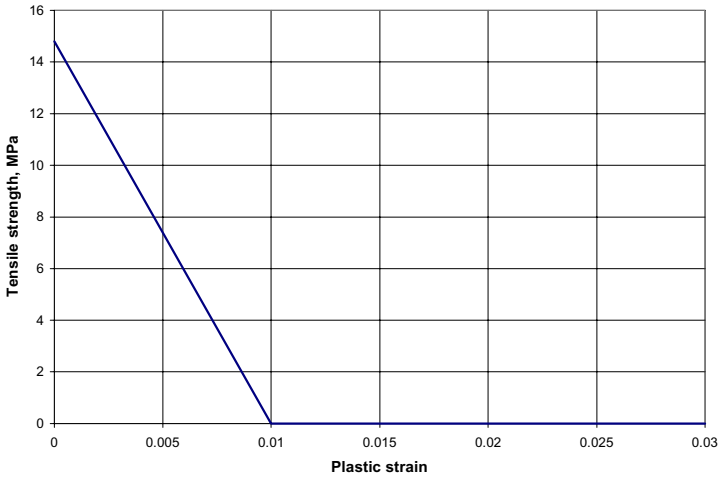

Figure 3-12. *Variation of tensile strength with plastic strain.*

In Figure 3-13 the simulated stress-deformation curves obtained by applying different material models are presented for a 30·30 meters block of intact rock, confined at 22.4 MPa. The mechanical properties are given in Table 3-7.

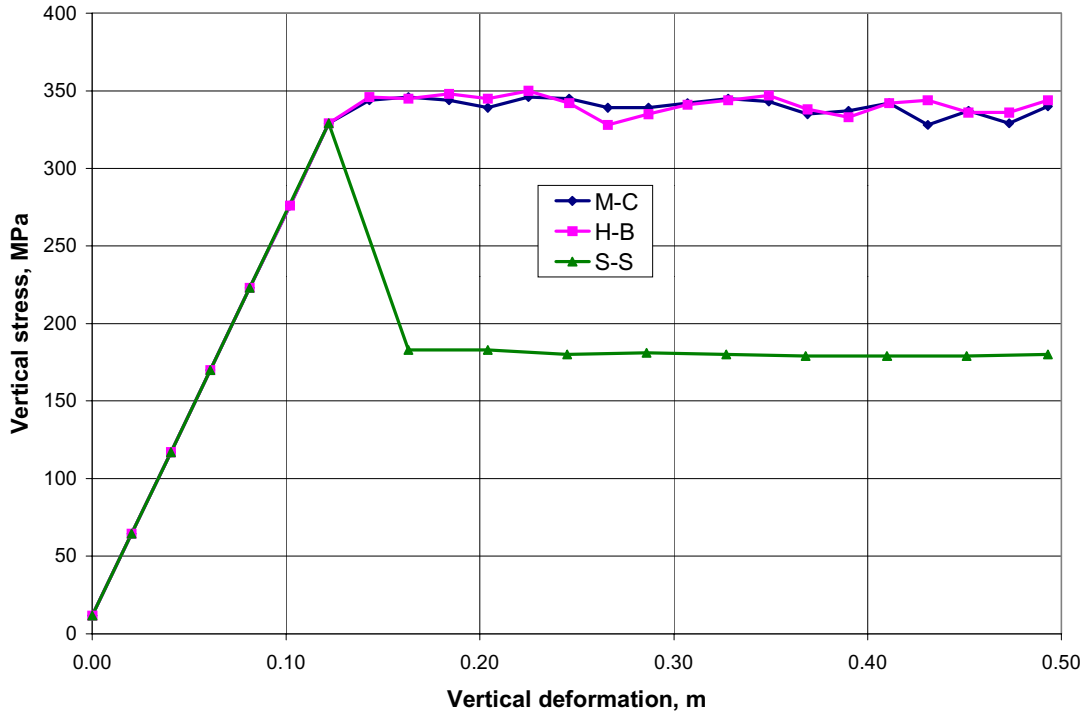

Figure 3-13. *Stress-deformation curves for intact rock, obtained for M-C, H-B and S-S models, confined at 22.4 MPa.*

Table 3-7. Evaluation of the deformation properties and stress at failure on the intact rock, for the different rock models.

Rock model	σ_3 [MPa]	ν_m	E_m [GPa]	σ_{1F} [MPa]
H-B	22.4	0.23	72.7	341.1
M-C	22.4	0.23	72.7	339.8
S-S	22.4	0.23	72.7	329.0

Fracture mechanical properties

For the tests on different material models for the intact rock, the Barton-Bandis joint model as implemented in UDEC is used. The fracture properties are set according to Table 3-8.

Table 3-8. Fracture properties applied when testing intact rock models.

K_n [(1)] (MPa/m)	K_s [(1)] (MPa/m)	ϕ_r (°)	σ_c (MPa)	JRC_0	JCS_0 (MPa)	L_0 (m)	a_{jn} (mm)
44e3	29.9e3	30.0	212	9.3	170	5.51e–2	0.58

(1) Values expected at σ_n=23 MPa

with
- K_n Joint normal stiffness at expected normal loads
- K_s Joint shear stiffness at expected normal loads
- ϕ_r Joint residual angle of friction
- σ_c Uniaxial compressive strength of the intact rock
- JRC_0 Joint Roughness Coefficient
- JCS_0 Joint Wall Compressive Strength
- L_0 Laboratory-scale joint length
- a_{jn} Joint aperture at zero normal stress

Rock mass behaviour

In Figure 3-14 the calculated stress-deformation curves for a fractured rock mass are shown for different confining stresses. The rock mass block is 30·30 meters and loaded with confining stresses on both vertical sides. The block is loaded with constant deformation velocity in the vertical direction. For each confining stress three curves are shown that represent the three different material models applied to simulate the behaviour of the intact rock. The differences between the models are quite insignificant up to the peak value. The S-S model shows a pronounced peak at all confining stress levels. At the highest confining stress the H-B and M-C models provide a higher stress at failure than the S-S model. The deformation properties and stresses at failure are presented in Table 3-9.

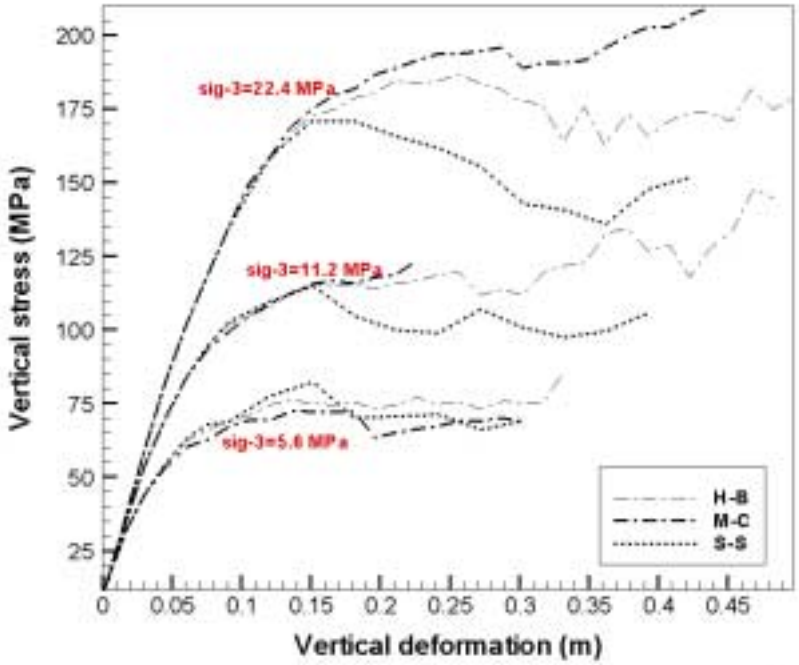

Figure 3-14. *Calculated stress-deformation curves for material model H-B, M-C and S-S at different confining stresses.*

Table 3-9. Evaluation of the deformation properties and stress at failure for the different rock models at different stress levels.

Rock model	σ_3 [MPa]	ν_m	E_m [GPa]	σ_{1F} [MPa]
H-B	22.4	0.20	45.0	170.6
	11.2	0.23	36.7	112.7
	5.6	0.26	30.0	73.3
M-C	22.4	0.27	41.7	179.2
	11.2	0.29	38.2	103.4
	5.6	0.39	27.2	66.8
S-S	22.4	0.21	43.0	171.0
	11.2	0.20	40.0	115.0
	5.6	0.26	30.3	82.6

Hoek and Brown envelopes for a fractured rock mass are fitted to the stresses at failure for each model. For the S-S model, the peak values are used and for the H-B and M-C model the stresses at failure are evaluated according to the procedure outlined in section 3.2.3. The H-B envelopes and the data points are shown in Figure 3-15. The same data points can be fitted to the Mohr-Coulomb envelopes, see Figure 3-16. The three models give almost the same results except at low stresses where the M-C model gives the lowest stress at failure and the S-S model the highest.

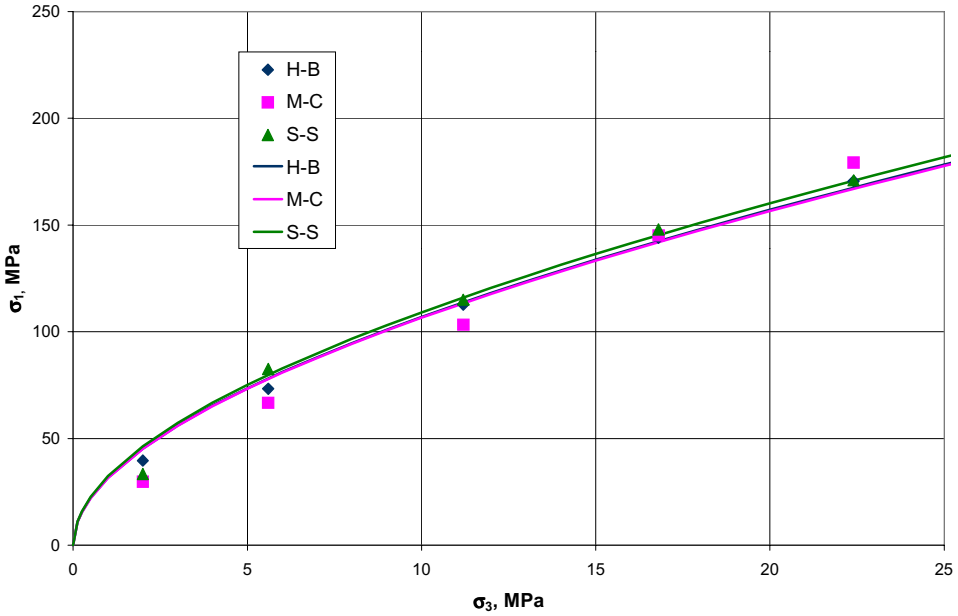

Figure 3-15. *Hoek and Brown failure envelopes.*

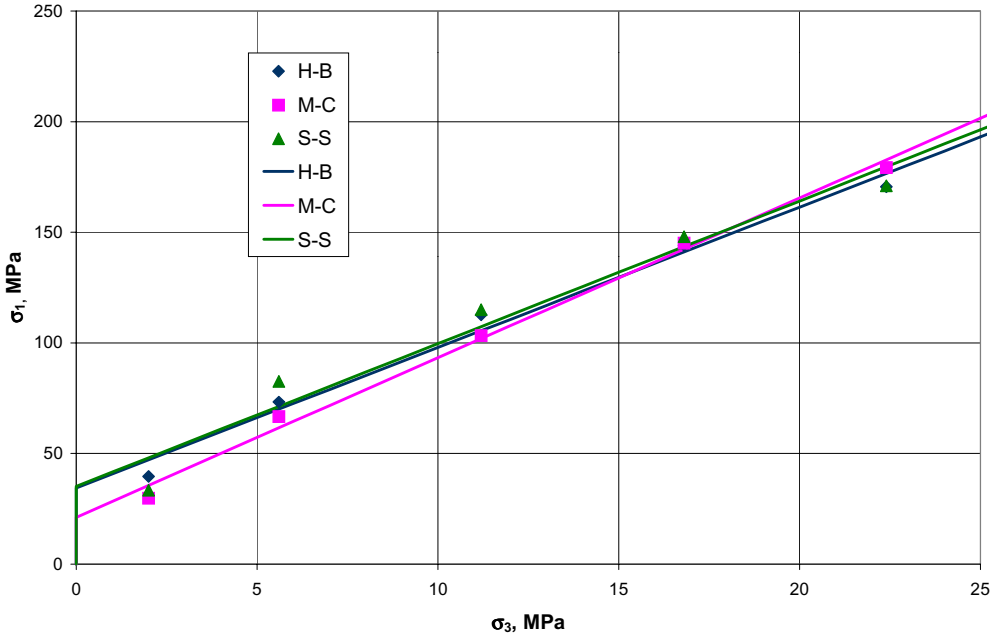

Figure 3-16. *Mohr-Coulomb envelopes.*

Considering the fair discrepancy of the results obtained on stresses at failure and envelopes on the tested diorite using the different intact rock models, and considering that the M-C model is much simpler to use than the H-B and S-S models in UDEC, the M-C model will be used further on to simulate the behaviour of the intact rock.

3.3.2 Influence of boundary conditions

The influence of both set-ups for boundary conditions, presented in section 3.2.1, on the mechanical properties of the rock mass is analysed in this section.

Two different set-ups were simulated, one run with confining stresses applied on the right vertical side only, the other one with confining stresses applied on both vertical sides, all other parameters remaining constant, see Figure 3-17.

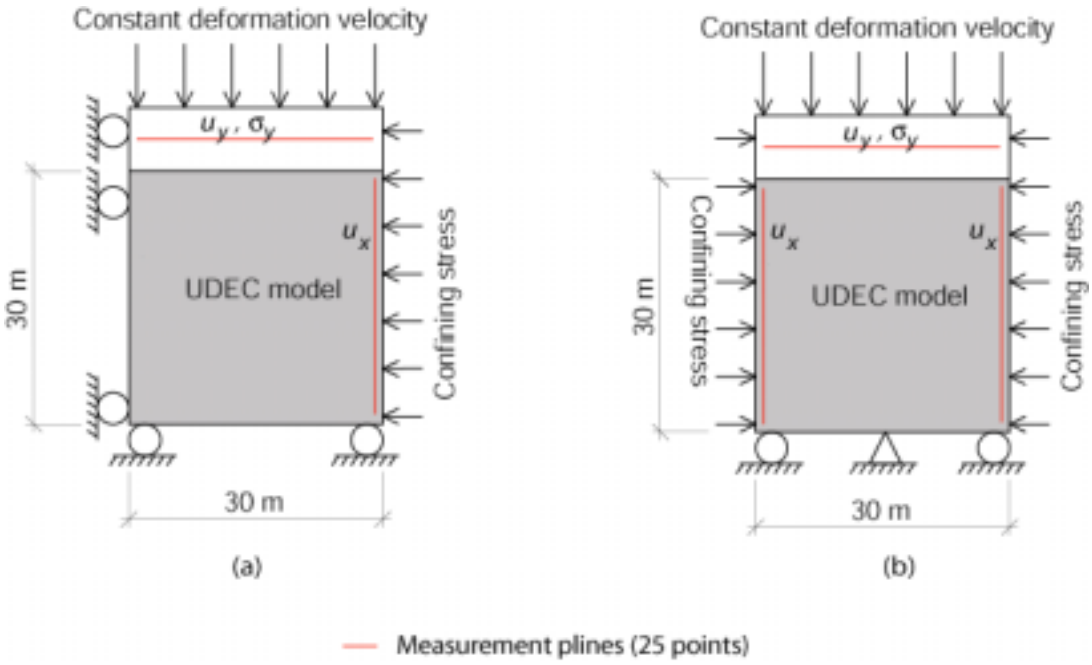

Figure 3-17. *Set-up of the boundary conditions for the same model size; a) loading on one vertical side and b) loading on both vertical sides.*

The modifications made on the model as illustrated in Figure 3-17a are presented in Figure 3-17b, and are the following:

- No assumptions of zero deformation on the left vertical boundary. Instead, this side is under confining stress as is the right vertical side.
- The same assumptions are applied on the bottom boundary (see section 3.2.1), but a grid point has been fixed to avoid free side sliding of the model when loading.

The models were run on granodiorite as intact rock, confining stresses at 22.4 MPa, Continuously Yielding model for the fractures, and M-C model for the intact rock.

Simulations with fracture traces extracted from the same trace section

The influence of the boundary conditions has been tested on two model sizes, 20·20 and 30·30 m. First, the fracture traces used as input in the different UDEC models were extracted from the same 2D fracture trace section, see Figure 3-18. This was meant to decrease sources of variation in relation to the geometry of the model.

The model loaded on both vertical sides is subjected to little more deformation than the model loaded on one vertical side, and provides a lower value of stress at failure, see Table 3-10. However, the variations are not so important, and almost insignificant in the case of the 30·30m model. Anyhow, the results are built on only one computation.

Table 3-10. Rock mass deformation properties and stresses at failure for different boundary conditions, same fracture section.

Model	E_m (GPa)	ν_m	σ_{1F}(MPa) for σ_3=22.4 MPa
20·20 – 1 side	45.5	0.28	202.6
20·20 – 2 sides	43.0	0.28	193.5
30·30 – 1 side	47.3	0.27	191.2
30·30 – 2 sides	47.3	0.27	189.4

Simulations based on sampled fracture networks

In order to assess the variability of the influence of boundary conditions, the input data for fracture traces have been taken randomly from different realisations of the DFN model on a vertical section of a given orientation, see section 2.2.3. The same model set-up as described above has been used, except for the generation of the rock blocks in UDEC. Ten 2D trace sections extracted from 10 simulations of the DFN model were used for both models, and both boundary conditions' set-up, leading to a total of 40 UDEC model runs. The results of the simulations are presented in Table 3-11.

Table 3-11. Rock mass deformation properties and stresses at failure for different boundary conditions, for sample fracture simulations.

Model	E_m (GPa)		ν_m		σ_{1F}(MPa) for σ_3=22.4 MPa	
	Mean	Std dev.	Mean	Std dev.	Mean	Std dev.
20·20 – 1 side	47.2	7.8	0.29	0.03	193.3	24.1
20·20 – 2 sides	45.8	8.6	0.29	0.03	185.3	26.2
30·30 – 1 side	41.3	5.6	0.29	0.02	166	26.2
30·30 – 2 sides	41.7	6.3	0.29	0.03	166.5	27.6

The 20·20 m model that is confined on both vertical sides is subjected to more deformation than the 20·20 m confined on one side, and provide lower values for stress at failure. Meanwhile, the values obtained on the 30·30 m model are almost the same in both cases, but fairly higher when confining stresses are applied on both vertical sides, see Table 3-11.

Conclusions

The boundary conditions seem to have very little influence on the rock mass deformation properties and stress at failure, especially when running the 30·30 m model.

More than the boundary conditions, the fracture pattern, which controls the generation of rock blocks in UDEC, seems to have a strong influence on the deformation properties of the simulated rock mass.

3.3.3 Influence of domain size

Simulations with fracture traces extracted from the same trace section

In order to determine the influence of the domain size on mechanical properties, models of different sizes were built. The chosen sizes were 20·20, 30·30, 40·40 and 60·60 m.

To enable comparisons in the best possible way, the fracture network in each model was built from the same fracture traces' file by increasing the simulation window from the centre of the section, see Figure 3-18.

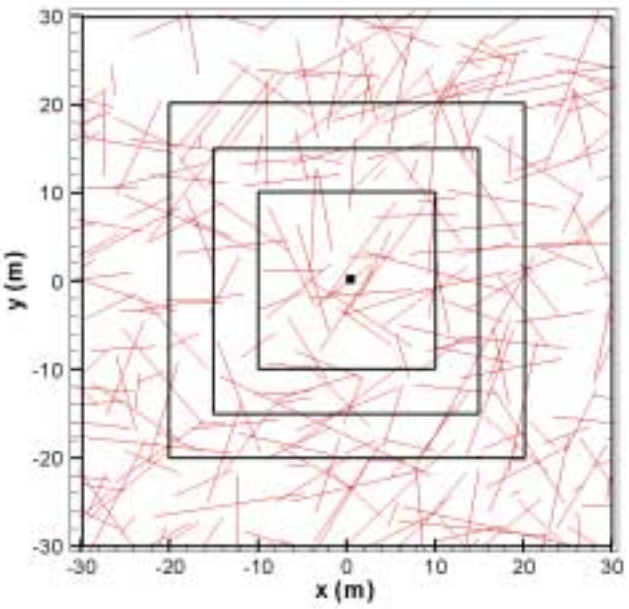

Figure 3-18. *Construction of the fracture pattern for the different models.*

The same set-up of parameters (initial stresses, confining stresses applied on both vertical sides, rock type: granodiorite) was applied for the intact rock and the fractures. The intact rock and rock fracture models used in UDEC were respectively a Mohr-Coulomb model and a Continuously Yielding model with constant normal and shear stiffness, and constant friction angle. Only confining stresses of 22.4 MPa were simulated. The set-up of the model is illustrated in Figure 3-17b. Four different models were run, and one simulation was run for each model size. The results are presented and compared in Table 3-12.

Table 3-12. Rock mass deformation properties and principal stresses at failure for different model sizes, confined on both vertical sides.

Model	E_m (GPa)	ν_m	σ_{1F}(MPa) for σ_3=22.4 MPa
20·20	43	0.28	193.5
30·30	47.3	0.27	189.4
40·40	47.2	0.26	168.7
60·60	44.3	0.26	167.3

The results of the simulations do not define any trend in the variation of mechanical properties in relation to the size of the model, see Table 3-12. Anyhow, these results are based on only one simulation for each model size.

Simulations based on sampled fracture networks

In order to get more results more simulations were run on the different model sizes. Ten two-dimensional fracture trace sections were extracted for each model size from ten realisations of the DFN model, according to the procedure described in section 2.2.3.

The three model sizes, 20·20, 30·30 and 40·40 meters, were then run ten times, for each fracture trace sections, all other parameters being constant. The statistical interpretation of the results of these simulations is presented in Table 3-13. No trend for the evaluation of mechanical properties for different model sizes can be established from these simulations.

Table 3-13. Rock mass deformation properties and principal stresses at failure for different model sizes, confining stresses applied on both vertical sides.

Model	E_m (GPa)		ν_m		σ_{1F} (MPa) for σ_3=22.4 MPa	
	Mean	Std dev.	Mean	Std dev.	Mean	Std dev.
20·20	45.8	8.6	0.29	0.03	185.3	26.2
30·30	41.7	6.3	0.29	0.03	166.5	27.6
40·40	51.1	4.5	0.25	0.01	176.9	12.9

The values presented in Table 3-12 are in the range of values expected according to the statistical distributions shown in Table 3-13.

Conclusions

It is not possible to define a trend of the rock mass mechanical properties in relation to the size of the model. For a specific geometry, the 30·30 m model provides the highest deformation modulus, but values for the stress at failure that can be considered as mean values compared to the other models (Table 3-12). Nevertheless, when looking at the sample simulations, the 30·30 m model generates the lowest mean values for the deformation modulus and stress at failure (Table 3-13).

As mentioned in the previous section, the fracture pattern in the model seems to have a strong influence on the deformation properties of the simulated rock mass. Even when using the same fracture trace section, different rock blocks are created that are related to the different window sampling size, and the geometry of the rock blocks will be of prime influence on the rock mass mechanical properties. Hence, the variation of deformation and strength properties as presented in Table 3-12 would be related to the fracture pattern built in relation to the domain size, and not directly to the model size.

3.3.4 Influence of the discarded joints

The fracture traces that terminate in the intact rock and do not intersect with any other fracture traces are discarded when "meshing" and generating the rock blocks in UDEC.

In the following, fracture traces defined as input from the DFN model are called actual fractures. The artificial segments designed to retain in the model actual fractures that are discarded by UDEC are called fictitious joints.

In order to determine the influence of discarded joints on the mechanical properties of the rock mass, a manual procedure has been applied that enables to artificially maintain actual fractures that are otherwise discarded by UDEC. The plots of actual fracture traces before meshing, and of the rock blocks as generated by UDEC were compared. The fracture traces that are discarded by UDEC when processing were identified and linearly extended until their intersections with actual fractures that remain in the model after "meshing" or until their intersections with the boundary of the model, see Figure 3-19. This procedure was applied on two different 2D fracture trace sections that had also been tested with the "usual" described set-up for modelling.

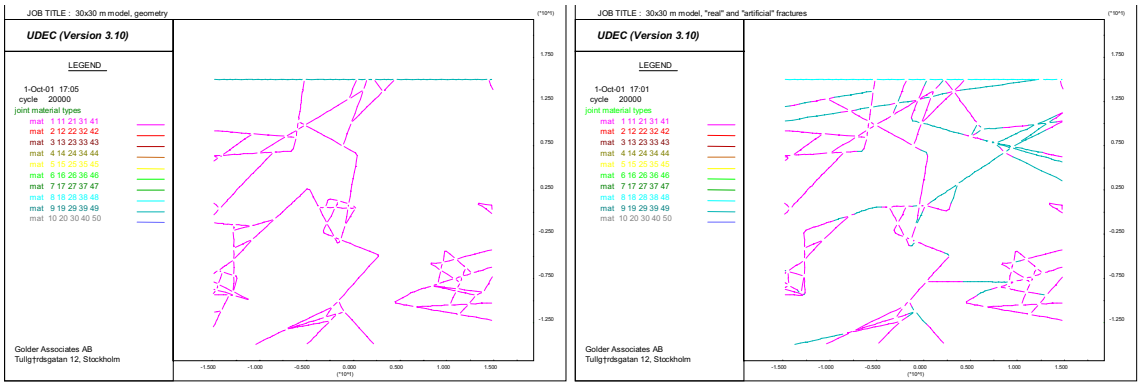

(a) (b)

Figure 3-19. *(a) Geometry of the model when some fracture traces are discarded by UDEC; (b) Modified model geometry: actual fractures are in purple, fictitious joints in blue.*

The rock joint model chosen is a Barton-Bandis model for actual fractures and a Coulomb slip model for the fictitious joints. The mechanical properties of the fictitious joints had been defined as to avoid their impact on the rock mass behaviour, see Table 3-14. To determine these properties, a test was run on the intact rock, then on the rock block where all fractures (actual and fictitious) were assumed to possess fictitious mechanical properties. Parameters of the model that influence on the behaviour of the rock model (normal, K_n, and shear, K_s, stiffness) were adjusted until the fractures did not have any impact on the deformation of the rock.

The mechanical properties assigned to the actual fractures are in accordance to properties used in the Test Case, see section 5.2.2, and are presented in Table 3-14.

Table 3-14. Mechanical properties assigned to the "real" and "artificial" fractures.

	K_n [(1)] (MPa/m)	K_s [(1)] (MPa/m)	c_p (MPa)	ϕ_p (°)	ϕ_r (°)	σ_{tj} (MPa)	σ_c (MPa)	JRC_0	JCS_0 (MPa)	L_0 (m)	a_{jn} (mm)
Actual fractures	44e3	29.9e3	–	–	30	–	218	9.3	170	5.5e–2	0.58
Fictitious joints	3e6	5e6	1e06	38	–	1e6	–	–	–	–	–

(1) Values expected at σ_n=23 MPa

with
- K_n Joint normal stiffness at the expected normal stress
- K_s Joint shear stiffness at the expected normal stress
- c_p Joint cohesion
- ϕ_p Joint angle of friction
- ϕ_r Joint residual angle of friction
- σ_{tj} Joint tensile strength
- σ_c Intact rock uniaxial compressive strength
- JRC_0 Lab-scale joint roughness coefficient
- JCS_0 Lab-scale joint compressive strength
- L_0 Lab-scale joint length
- a_{jn} Initial aperture at zero stress

The set-up used is a 30·30 m model, with confining stress applied on both vertical sides; the M-C model is used to simulate the intact rock.

Two different models were run: (1) actual fractures and fictitious joints are assigned their respective mechanical properties, as defined in Table 3-14; (2) both actual fractures and fictitious joints are assigned mechanical properties of actual fractures.

Models with actual fractures and fictitious joints

Only one rock block model was run with this set-up. The stress-deformation curves obtained by simulations of this model are illustrated in Figure 3-20 and the interpreted mechanical properties are presented in Table 3-15. The results obtained for the "usual" run are presented for comparison.

The modified rock model built on actual fractures and fictitious joints appear to be slightly stiffer than the model with discarded fractures ("usual" run), but the difference is fairly insignificant.

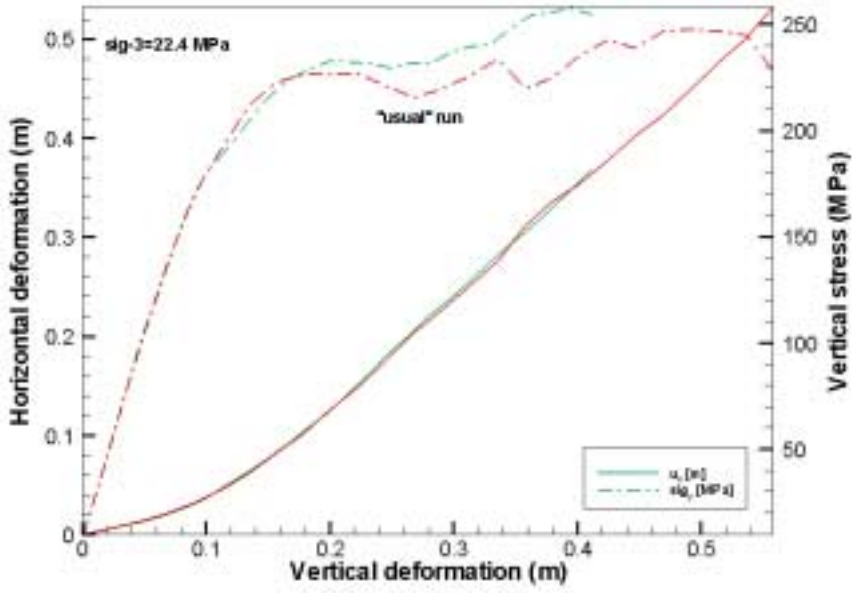

Figure 3-20. *Stress-deformation curves for one fracture network, section 01. The red lines correspond to simulations with discarded fractures ("usual" runs), the green lines to simulations where actual fractures and fictitious joints are used.*

Table 3-15. Rock mass mechanical properties, section 01, actual fractures and fictitious joints.

	Joint model	σ_3 [MPa]	ν_m	E_m [GPa]	σ_{1F} [MPa]
"usual" run	B-B	22.4	0.24	53.3	215.2
actual fract. and fictitious joints	B-B / M-C	22.4	0.23	53.5	215.8

Fictitious joints as actual fractures

In this case, mechanical properties of actual fractures (Table 3-14) were assigned to both actual fractures and fictitious joints. Two models were run for two different fracture traces' section and the stress-deformation curves are shown in Figure 3-21. The curves obtained for the "usual" run are also shown for comparison.

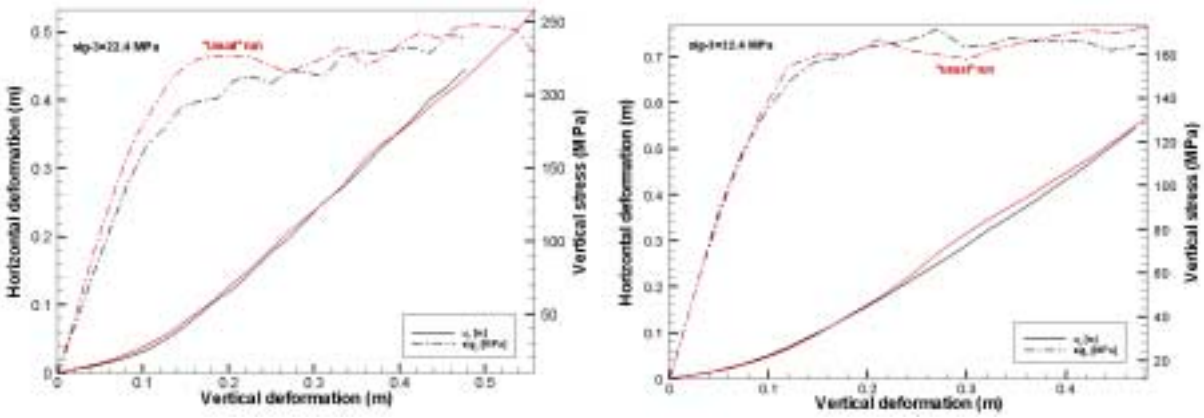

(a) (b)

Figure 3-21. *Stress-deformation curves for two geometrical models. (a) fracture section 01; (b) fracture section 19. The red lines correspond to simulations with discarded fractures ("usual" runs), the black lines to simulations where actual fractures and fictitious joints are assigned mechanical properties of actual fractures.*

The interpreted mechanical properties for both models are presented in Table 3-16.

The influence of the fictitious joints, modelled as actual fractures, on the mechanical properties of the rock mass is limited, but not of the same range for both models. The model built from trace section 01 becomes more deformable when run with actual fractures and fictitious joints modelled as actual fractures. Results from trace section 19 show that the model run with actual fractures and fictitious joints as actual fractures is slightly stiffer than the same model in "usual" run, see Table 3-16.

Table 3-16. Mechanical properties of the rock mass, for two different trace sections.

	section	Joint model	σ_3 [MPa]	ν_m	E_m [GPa]	σ_{1F} [MPa]
"usual" run	01	B-B	22.4	0.24	53.3	215.2
fictitious joints as actual		B-B	22.4	0.21	46.7	193.8
"usual" run	19	B-B	22.4	0.31	36.1	157.6
fictitious joints as actual		B-B	22.4	0.30	38.8	164.3

It seems that the geometry of the fracture network and of the rock blocks generated in UDEC is the main factor to influence on the mechanical properties when extending fractures and creating fictitious joints.

The influence of in situ stresses on the behaviour of the modified rock models was simulated by running the model built on trace section 19, assuming two different levels of confining stress, 22.4 MPa and 5.6 MPa, see Figure 3-22. The influence of the fictitious joints (modelled as actual fractures on this model) on the mechanical properties of the rock mass is almost insignificant when testing at 22.4 MPa confining stress, see Table 3-17. At the same stress level and for the same set-up, the model built on trace section 01 (see Table 3-16) showed a slight increase in the deformation modulus and decrease in stress at failure. At lower confining stresses, the modified network shows a lower Young's modulus but higher stress at failure than the "usual" run, see Table 3-17.

Table 3-17. Deformation properties and stress at failure, trace section 19, for the "usual" run and for fictitious joints modelled as actual fractures.

	Joint model	σ_3 [MPa]	ν_m	E_m [GPa]	σ_{1F} [MPa]
"usual" run	B-B	22.4	0.31	36.1	157.6
		5.6	0.41	25.9	61.4
fictitious joints as actual	B-B	22.4	0.30	38.8	164.3
		5.6	0.46	22.1	71.4

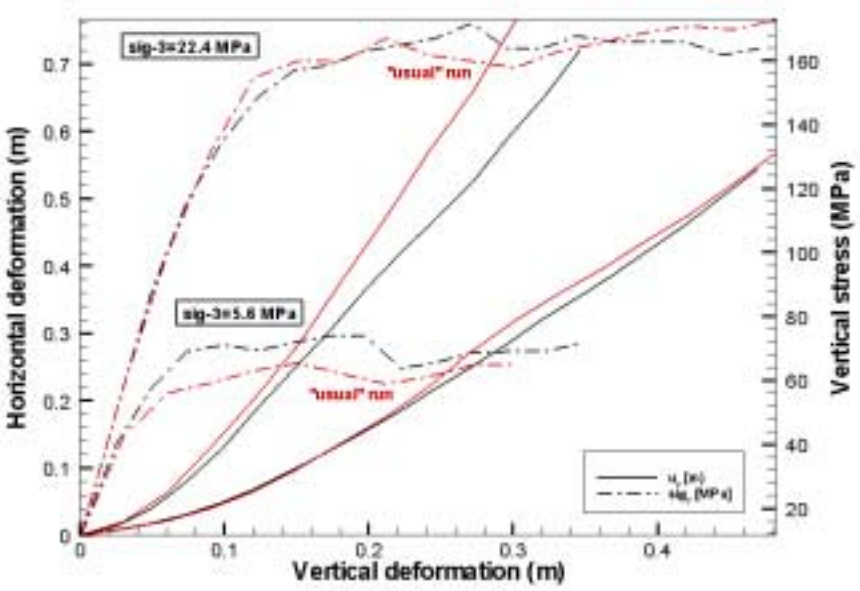

Figure 3-22. *Stress-deformation curves for one fracture network (trace section 19). The red lines correspond to simulations with discarded fractures ("usual" runs), the black lines to simulations where actual fractures and fictitious joints are assigned mechanical properties of actual fractures.*

Conclusions

As regard to the simulations that have been run, the impact of the discarded fractures on the deformation properties of the rock mass seems to be almost insignificant. The rock mass even appears to be slightly stiffer when running with actual fractures and fictitious joints. This could be due to numerical problems at contacts on the fractures, and particularly at the contact nodes between fictitious joints and actual fractures. Problems might be due to high stiffness contrast between actual fractures and fictitious joints. Moreover, assigning different properties to different parts of the same fracture is difficult to achieve in UDEC, as some fracture sections might be assigned wrong properties, and some segments seem not to possess any properties at all. This is due to the fact that "UDEC" can slightly translate fracture traces when meshing. The problems are particularly pronounced when using the B-B joint model. Hence, the rock model must be checked and modified until the mechanical properties have been properly assigned to all segments.

Assigning mechanical properties of actual fractures even to the fictitious joints did not reveal important modifications on the deformation properties. The variation of the deformation properties and rock mass strength might mostly depend on the fracture pattern and the way "artificially" extended fractures change the generation of rock blocks in UDEC.

Nevertheless, keeping the parts of fractures that terminate in the rock or isolated fractures would be required if studying and simulating fracture propagation.

The procedure of extending and keeping isolated fractures is highly time-consuming. Since the deformation properties and stress at failure were not significantly affected by the fact that fractures are discarded when processing, the models have all been run by applying "usual" UDEC procedure with discarded fractures.

3.3.5 2D simplification from the 3D model

The transfer of a three-dimensional fracture network into a two-dimensional trace network with the same overall mechanical properties is not trivial. For example, even if there are no block formed by the fractures in a three-dimensional fracture network, fracture traces in a two-dimensional cross-section may form blocks. The difference between the 3D and 2D model is likely to depend on the nature of the fracture network.

The number of fractures generated in a 3D DFN model is highly variable depending on the radius size distribution of the fractures, and of the truncation value for the minimum fracture radius size. Nevertheless, a real fracture network model for a 30·30·30 m cube can contain from 1000 to more than 10000 fractures. Applying the parameters defined for the DFN model in the Test Case, and only representing fractures with a radius larger than 0.5 m, leads to 15000 to 17000 fractures in a 30·30·30 m cube. It is at the moment unrealistic to do 3D simulations with real fracture networks, but some tests on simple fracture networks have been performed. In this part of the study, a simplified fracture network consisting of six fractures has been used, see Figure 3-23.

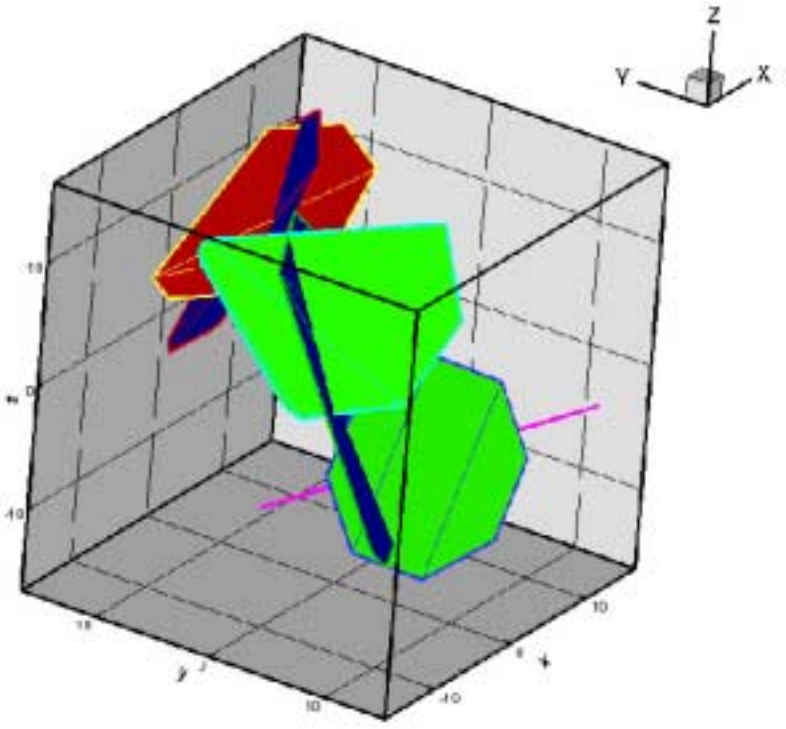

Figure 3-23. *The simplified fracture network used.*

This fracture network has been modelled in three-dimension with 3DEC, see Figure 3-24. The model block is 30·30·30 m. In order to construct the models (3D and 2D) the fractures need to be extended to the boundary of the block. This limits the number of fractures that can be handled in the three-dimensional model. In order to improve the quality of the comparison between 3D and 2D simulations, the two-dimensional sections were extracted from the 3DEC cube model, with the six fractures being extended to the limits of the cube. 19 two-dimensional vertical sections, taken by stepwise rotation of 10° of the vertical plane in the interval 0–180°, were extracted, the geometry of the perpendicular "reference" sections xz and yz is illustrated in Figure 3-25.

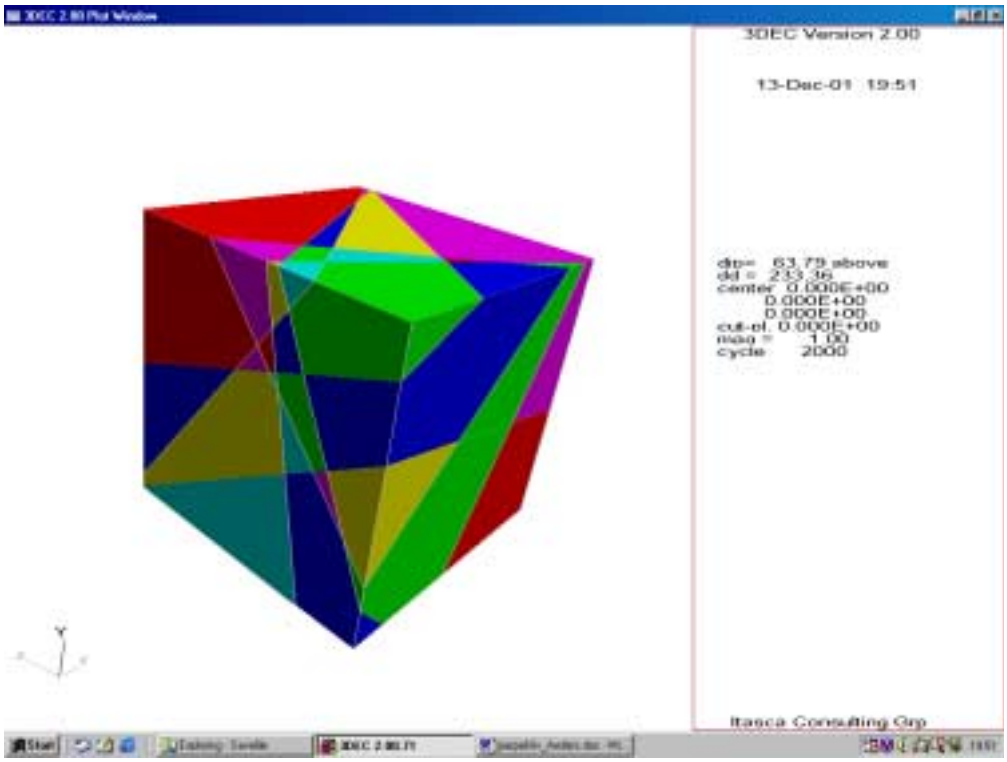

Figure 3-24. *The 3DEC model.*

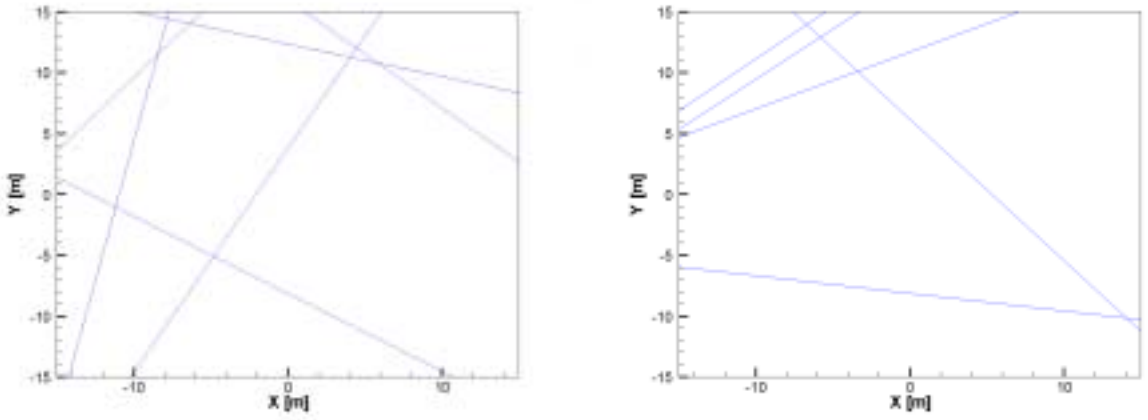

(a) (b)

Figure 3-25. *The two-dimensional UDEC models: (a) section xz, (b) section yz.*

The fracture planes, even the extended parts, were assigned properties of actual fractures, in UDEC as in 3DEC. The fractures have been modelled with a Coulomb model with constant shear and normal stiffness and the intact block with an elasto-plastic Mohr-Coulomb model. The input parameters for intact rock and fractures are given in Table 3-18. The model block has been loaded by compression in the vertical direction at constant velocity (10 mm/s) and the confining stresses have been constant and isotropic, at a value of 20 MPa.

The 3D tests have been performed by Itasca Geomekanik AB.

Table 3-18. Input parameters for intact rock and fractures.

Intact rock	E, GPa	ν	c, MPa	ϕ, °	ψ, °	σ_{ti}, MPa
Granodiorite	73.0	0.27	31	49	0	–14.8

with
- E Deformation modulus of the intact rock
- c Cohesion of the intact rock
- ν Poisson's ratio of the intact rock
- ϕ Friction angle of the intact rock
- ψ Dilation angle of the intact rock
- σ_{ti} Tensile strength of the intact rock

Fractures	K_n [(1)] (GPa/m)	K_s [(1)] (GPa/m)	c_p (MPa)	ϕ_p (°)	σ_{tj} (MPa)
actual fractures	44	29.9	–	30	–

(1) Values expected at σ_n=23 MPa

with
- K_n Joint normal stiffness at expected normal loads
- K_s Joint shear stiffness at expected normal loads
- c_p Joint cohesion
- ϕ_p Joint angle of friction
- σ_{tj} Joint tensile strength

In Figure 3-26 the calculated stress-deformation curves obtained for the 3D and the 19 two-dimensional models are compared. Evaluated deformation modulus, E_m, Poisson's ratio, ν_m, and maximum principal stress at failure, σ_{1F}, are sum up in Table 3-19. The deformation modulus has been evaluated in the stress interval 20–60 MPa for all cases.

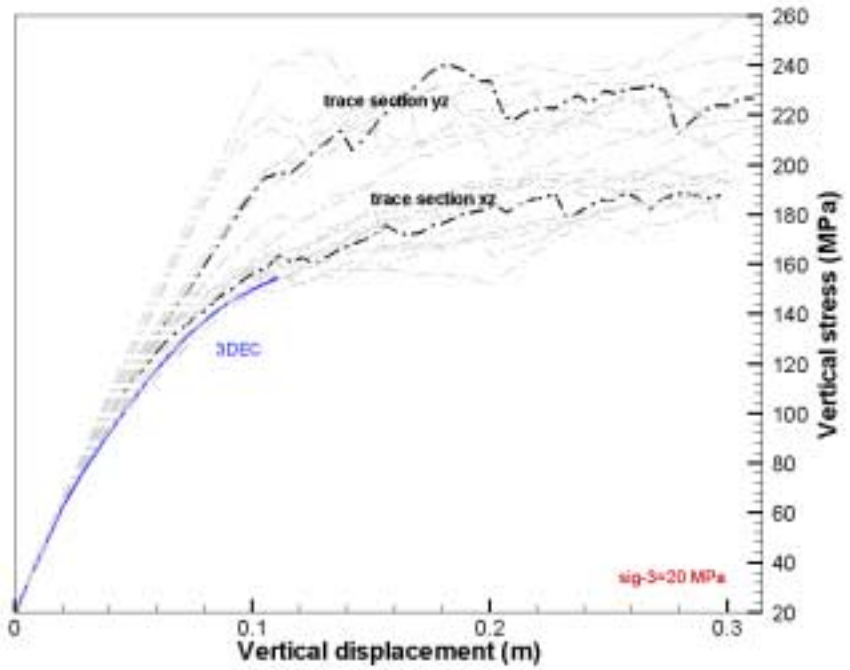

Figure 3-26. *Calculated vertical stress – vertical deformation curves. The 3DEC curve is for a triaxial loading situation and the UDEC curves for plain strain loading.*

Table 3-19. Evaluation of the deformation properties and stress at failure for the different rock models.

trace-file	σ_3 [MPa]	ν_m		E_m [GPa]		σ_{1F} [MPa]	
		mean	std dev.	mean	std dev.	mean	std dev.
3DEC		-	-	68.0	-	155*	-
2D-all		0.23	0.01	65.18	1.29	177.58	29.70
2D-all-MAX	20	0.24	-	67.3	-	231.05	-
2D-all-MIN		0.22	-	62.7	-	134.20	-
2D-xz		0.23	-	64.51	-	175.06	-
2D-yz		0.22	-	64.79	-	210.39	-

* σ_{1F} *for the 3DEC model is the vertical stress value reached when the simulation was stopped*

The three-dimensional model in 3DEC and the two-dimensional models in UDEC give a deformation modulus in the same order round 66–68 GPa. The UDEC models give on average slightly lower values. As can be seen on Figure 3-26, the principal stress at failure of the 3DEC model might not be reached, and the evaluation of the principal stress at failure require that the model would be run at higher vertical strains. However, the 3D model, in the actual conditions, could not be compress at higher vertical strains and the 3DEC simulations had to be stopped when the vertical displacement was up to 0.12 m. The principal stress at failure is on average higher for the two-dimensional models. Nevertheless, the range of principal stress at failure is extended for the two-dimensional models. The ratio of σ_{1F} for the 3D to σ_{1F} for the 2D models is in the range of 1 to 1.5.

Figure 3-26 shows that the results of the 3DEC model are similar to the softest two-dimensional models, both in deformation modulus and principal stress at failure, see Table 3-20. These 2D sections are in the axis of the most unfavourable stability

situation in 3D and the direction of most important deformation. Figure 3-27 illustrates the geometry for the softest sections in two-dimensions. The fact that the principal stress at failure of the 3D model is similar to the principal stress at failure of the weakest 2D sections is conforming to expectations.

Table 3-20. Deformation properties and stress at failure for the 3DEC model and the softest 2D models.

trace-file	σ_3 [MPa]	ν_m	E_m [GPa]	σ_{1F} [MPa]
3DEC		-	68.0	155*
2D-sec9	20	0.23	65.04	144.96
2D-sec13		0.23	63.80	134.22

* *σ_{1F} for the 3DEC model is the vertical stress value reached when the simulation was stopped*

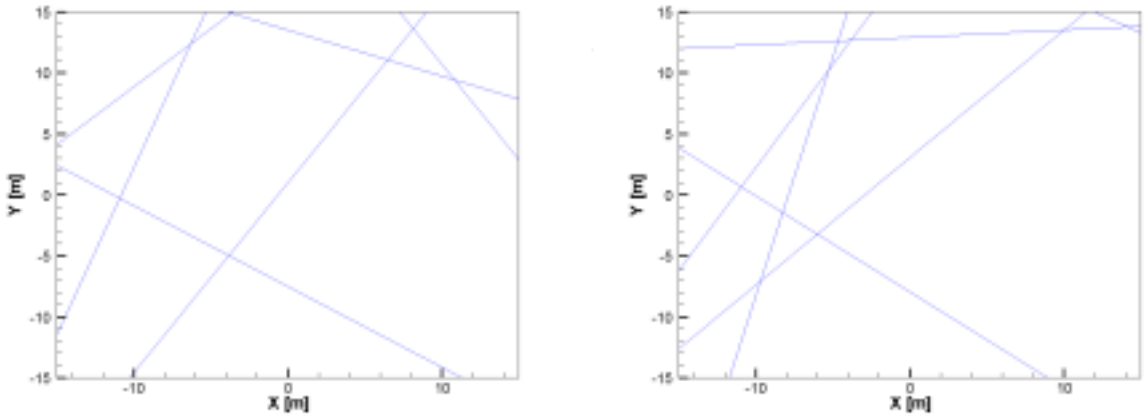

(a) (b)

Figure 3-27. *Geometry of the 2 softest two-dimensional models: (a) section 9, (b) section 13.*

Further studies must be performed to study the behaviour of the 3DEC model close to failure. With very few fracture planes in the model the differences between 3D and 2D simulations are probably large and ought to decrease with the number of fracture planes. Nevertheless, the simulations show that the discrepancy of results decrease when the two-dimensional sections are in the axis of the most unfavourable stability situation in the 3D model.

Conclusions

A 3D model based on a simplified fracture network presents a deformation modulus that is somewhat higher than for the 2D sections extracted from this model, and based on the same fracture system.

The rock mass strength of the 3D model is in the range of the one obtained for the 2D sections taken in the weakest directions. This illustrates that it is important to extract the 2D vertical sections in different directions in relation to the fracture system when

simulating with a 2D programme. The aim is to find out the weakest orientations that will better match the results of a 3D simulation.

3.3.6 Influence of the constitutive model for rock fractures

Different constitutive models for rock fractures have been tested: linear (Coulomb-slip model) and non linear (Continuously Yielding and Barton-Bandis models). The application of non-linear models enables the simulation of more complex fracture behaviour. The Continuously Yielding model is developed to simulate the internal mechanism of progressive damage of joints under shear. The Barton-Bandis integrates the surface roughness of fractures, and accounts also for damage of fractures under normal loading and shear displacement, see also section 3.1.3.

Both non-linear constitutive joint models were tested with the same model set-up. The input parameters for the constitutive models are presented in Table 3-21, and their evaluation is provided in appendix C.

Table 3-21. Input parameters for the constitutive joint models.

	a_n (MPa/m)	e_n	Max K_n (MPa/m)	a_s (MPa/m)	e_s	Max K_s (MPa/m)	$\phi_m^{(i)}$ (º)	ϕ_i (º)	jr (m)
C-Y model	10.4e3	0.46	44e3	5.7e3	0.53	30e3	35	40	0.002

with
- a_n Initial joint normal stiffness
- e_n Exponent of joint normal stiffness
- Max K_n Maximum value of joint normal stiffness
- a_s Initial joint shear stiffness
- e_s Exponent of joint shear stiffness
- Max K_s Maximum value of joint shear stiffness
- ϕ_i Joint intrinsic friction angle
- $\phi_m^{(i)}$ Joint initial friction angle
- jr Joint roughness parameter

	K_n (1) (MPa/m)	K_s (1) (MPa/m)	ϕ_r (º)	σ_c (MPa)	JRC_0	JCS_0 (MPa)	L_0 (m)	a_{jn} (mm)
B-B model	44e3	30e3	30	214	9.3	170	5.51e–2	0.58

(1) Values expected at σ_n=23 MPa

with
- K_n Joint normal stiffness at expected normal loads
- K_s Joint shear stiffness at expected normal loads
- ϕ_r Joint residual friction angle
- σ_c Uniaxial compressive strength of the intact rock
- JRC_0 Laboratory-scale Joint Roughness Coefficient
- JCS_0 Laboratory-scale Joint Wall Compressive Strength
- L_0 Laboratory-scale joint length
- a_{jn} Joint aperture at zero normal stress

Tests were run to visualise the influence of the non-linear constitutive joint models. Two 2D sections extracted from the DFN model were run applying respectively the Continuously Yielding and the Barton-Bandis models, all other parameters being constant. Confining stresses were applied on both sides, the intact rock was

granodiorite, the constitutive model for the intact rock Mohr-Coulomb, the in situ stress level is 22.4 MPa. The stress-deformation curves are presented in Figure 3-28 and the interpreted mechanical properties in Table 3-22. The curves show some discrepancy in the deformation of the rock mass when applying one or the other constitutive joint models on the same model (Figure 3-28). In both cases, the deformation under loading of the rock mass appears to be slightly greater when using the Continuously Yielding model, see Table 3-22.

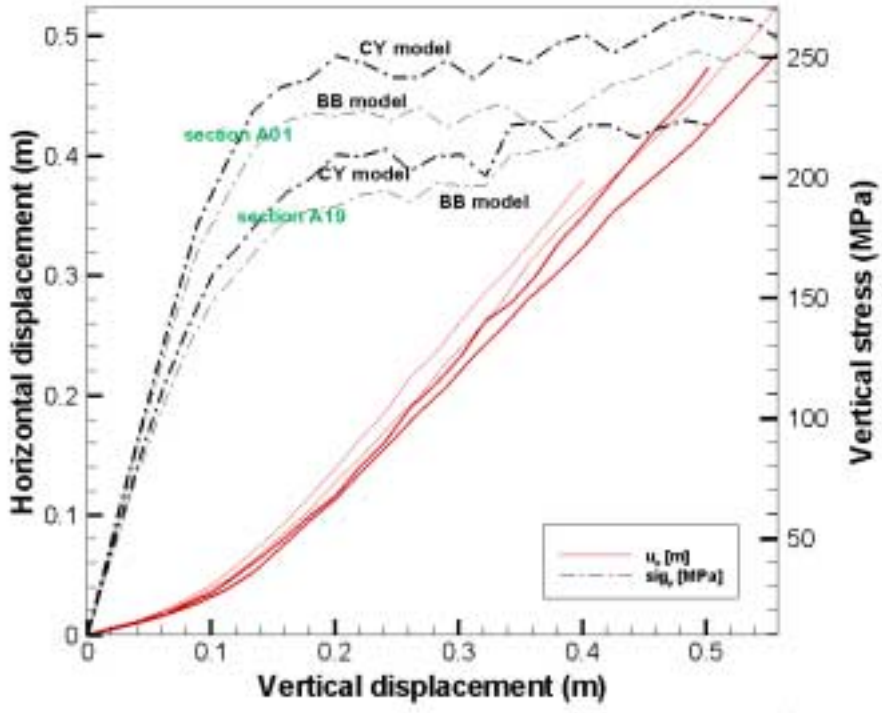

Figure 3-28. *Stress-deformation curves for 2 different joint models, tested on two different 2D sections.*

Table 3-22. Mechanical properties of the rock mass, for the Barton-Bandis and Continuously-Yielding constitutive joint models.

trace-file	Joint model	ν_m	E_m [GPa]	σ_{1F} [MPa]
A01	C-Y	0.21	56.3	236.5
A01	B-B	0.23	55.1	215.2
A19	C-Y	0.20	49.4	197.3
A19	B-B	0.23	47.5	178.4

Using the B-B joint model leads to lower deformation moduli and stress at failure for both fracture network models, but the differences in deformation properties are almost insignificant.

As the Barton-Bandis joint model is the only model to account for properties of the intact rock by integrating the uniaxial compressive strength, this is the one used along this work.

3.3.7 Influence of anisotropy

The anisotropy of the rock mass and its mechanical properties has been studied as regard to the in situ State of Stress. Anisotropy was accounted for by extracting three 2D fracture trace sections from the 3D DFN model. The orientations of these 3 planes were consistent to the directions of the principal in situ stresses, σ_1, σ_2 and σ_3.

The model set-up applied is the same for each section, but the values of confining stresses on the vertical boundaries are set according to the values of in situ stresses on the faces of the planes.

This study was carried out in the Test Case, and the results are presented in section 6.2.

3.4 Special set-up for the deformation zones

Intact rock and fracture networks are often altered in deformation zones and in their zone of influence. Mechanical properties of the intact rock are often diminished because of weathering and crushing. Fracture networks might differ from the background fracturing by means of different orientation of fracture sets and fracture intensity related to tectonic constraints.

The set-up as described in the previous sections is developed for the characterisation of the rock mass, but does not account for deformation zones. However, evaluation of the mechanical properties in deformation zones is an issue to be handled in the Rock Mechanical Descriptive Model. Hence, the model set-up should be modified for the modelling of deformation zones.

This section presents the assumptions related to the modelling of deformation zones, and the main modifications from the numerical model as previously described, see sections 3.1 to 3.3. Applications of this set-up for the determination of input data are illustrated in section 5.4 and results from simulations on deformation zones are presented in section 7.2.

3.4.1 List of assumptions related to the modelling of deformation zones

The methodology for modelling of deformation zones is based on the same principles as described in section 2, and so are assumptions regarding numerical and modelling issues, and quality of input data. The evaluation of mechanical properties of the rock mass in deformation zones is the same as presented in section 3.2. Nevertheless, some few more assumptions and modifications to the model were required in order to properly model and characterise the deformation zones, which are:

- The model size has been taken 10 times smaller than for the modelling of the rock mass, that means 3·3 meters. This set-up is adjusted to running models with higher fracture densities.
- The modelling plane is a section that is perpendicular to the deformation zones, so that the Young's modulus can be calculated. This implies that shear displacements can occur as the 2D model is not oriented along the 3 principal stress directions.

3.4.2 Geometry of fractures in the deformation zones

The fracture pattern in deformation zones and influence areas of these deformation zones is affected by the stresses and the deformation associated to these features. The parameters used in a DFN model for defining the rock mass fracturing characteristics, such as fracture orientation, fracture radius size distribution and intensity, must be modified in accordance to the actual pattern.

Specific input data are required to model the fracture pattern in the deformation zones. A DFN model focused on the characterisation of the fracturing in the deformation zones should be provided.

3.4.3 Mechanical properties assigned to the rock mass in the zones

Mechanical properties of intact rock and fractures can be altered in deformation zones, and the degree of alteration will depend on the localisation from the "core" of the zone. A detailed study and mapping of intact rock and fracture surfaces in the deformation zones enable the determination of the appropriate properties.

3.5 Distribution of the parameters – Monte Carlo simulations

The uncertainty of a model can be separated in conceptual uncertainty, data uncertainty and spatial variability.

The conceptual uncertainty originates from an incomplete understanding of the principal structure of the analysed systems and its interacting processes. This uncertainty is not discussed further in this section.

Data uncertainty concern uncertainty in the values of the parameters in a model. Data uncertainties may be caused by measuring errors, interpretation errors, or the uncertainty involved in extrapolation when the parameter varies in space.

Spatial variability concerns the variation in space of a parameter value. Spatial variability is not an uncertainty but is of course often a cause for data uncertainty.

The data uncertainty and spatial variability are often expressed in statistical terms as mean value, standard deviation and type of distribution. In our case the spatial variability can be separated into the spatial variability of the geometry of the fractures, the spatial variability of the rock type, and into the data uncertainty and spatial variability of the parameters describing the properties of the intact rock and the fractures.

The spatial variability of the fracture system is described by the DFN model.

The spatial variability of the rock type is described by the percentage of different rock types in a rock block.

The data uncertainty and the spatial variability of the material parameters for a specific rock type are expressed by the measured mean value and the standard deviation. A normal distribution is assumed.

A common way to get the statistical parameters for a model with many input parameters that can be expressed in statistical terms is to run Monte Carlo simulations. One set of parameters is randomly chosen according to the statistical distributions of the

parameters and the response of the model with these parameters is calculated. By running a lot of simulations and by treating the outcome in a statistical way the mean and the standard deviation of the outcome from the model can be estimated.

In order to minimise the number of numerical calculations with UDEC a simplified way of doing the Monte Carlo simulations has been used according to the following:

- The influence of the geometry of the fracture system is estimated by running UDEC calculations with 20 realisations of the fracture system with values of all other parameters equal to the mean value. The result is statistically treated.
- The influence of one specific parameter on the outcome from the model is calculated by keeping all other parameters constant. Using the calculated influence of the parameter on the outcome of the model in a simple Monte Carlo simulation in Excel, the influence of the specific parameter distribution can be added to the influence of all other parameters.
- By using the calculated distributions of the properties for each rock type and then combining the different rock types with respect to their measured percentage, the statistical parameters for the ”combination” can be estimated.

Monte Carlo simulations for ϕ_{rm}, c_m and σ_{cm}

The influence of the residual friction angle of fractures, ϕ_r, is calculated in UDEC, keeping all other parameters constant. If a linear influence of ϕ_r on the friction angle ϕ_{rm} and on the cohesion c_m of the rock mass is assumed the influence can be expressed by an equation of the form:

$$\phi_{rm} = \phi_{rm}\left(\phi_r = 30^o\right) - \text{const}_{\phi_{rm}} \cdot \left(30 - \phi_r\right) \tag{3.34}$$

$$c_m = c_m\left(\phi_r = 30^o\right) - \text{const}_{c_m} \cdot \left(30 - \phi_r\right) \tag{3.35}$$

The rock mass uniaxial compressive strength σ_{cm} can then be calculated according to the following equation:

$$\sigma_{cm} = \frac{2 \cdot c_m \cdot \cos\phi_{rm}}{1 - \sin\phi_{rm}} \tag{3.36}$$

The distributions of $\phi_{rm}(30°)$ and $c_m(30°)$, are obtained from the different UDEC simulations run for the 20 realisations with mean values of all parameters. The distribution of ϕ_r is known from the tilt tests.

The Monte Carlo simulation is straightforward where a sample of each of the three parameters' distributions, $\phi_{rm}(30°)$, $c_m(30°)$ and ϕ_r, is generated and then each of the formulas above, see equations (3.34) to (3.36), is used to generate a sample of ϕ_{rm}, c_m and σ_{cm}. This is repeated a number of times. The outcomes are then analysed and the statistical parameters for the distribution are calculated. The error between the input mean and the mean of the generated sample is less than 0.1% for each parameter.

Monte Carlo simulations for E_m for each rock type

The behaviour of the rock mass is a combination of the behaviour of the intact rock and the behaviour of the fractures. The principle relationship for the deformation modulus of a fractured rock mass can be written as:

$$\frac{1}{E_m} = \frac{1}{E} + \frac{N}{K_n} \tag{3.37}$$

where

E_m is the deformation modulus for rock mass [Pa]
E is the Young's modulus for intact rock [Pa]
N is the number of fractures [1/m]
K_n is the normal stiffness at expected normal stress [Pa/m]

The mean and standard deviation for E is known from laboratory tests and the UDEC simulations provide the distribution of E_m. During the UDEC simulations the deformation modulus, E, is kept at the average and therefore the influence of the fractures can be back calculated for all the UDEC simulations using the rewritten form of the equation (3.37) above:

$$\frac{N}{K_n} = \frac{1}{E_m} - \frac{1}{E} \tag{3.38}$$

The mean and standard deviation is calculated for the fracture influence, N/K_n.

Monte Carlo simulations are then performed using the known E distribution and the calculated N/K_n distribution. The deformation modulus of the rock mass, E_m, is calculated using equation (3.37). The outcomes are then analysed and the statistical parameters for the distribution of the deformation modulus are calculated.

Monte Carlo simulations for a whole rock block

Above is explained how the distributions of the properties for a single rock type are calculated. A combination of statistical distributions of mechanical parameters is used to combine the properties of single rock types to obtain the properties of rock blocks composed of different rock types.

The four different rock types that compose the rock block in the target area are characterised by their mechanical properties. The probability of occurrence for each property follows a normal distribution defined by its mean and standard deviation.

The probability of occurrence of a given value of a given parameter is combined with the probability to find this rock type. This process is done for the four different rock types. Thus the probability is calculated as the mean of the probability density functions (PDF) of mechanical parameters weighted with the probability of the existence of the four rock types.

In our case it can be assumed that the probability of finding a rock type within a rock block of the target area is independent of the rock block size. This can be discussed since the greenstone, for example, is found within large lenses in rock units and its proportion has been determined on the basis of a rock unit volume that is large compared to the blocks of the target area.

Figure 3-29 shows an example of the outcome from a generic Monte Carlo simulation using a combination of PDFs. f1(x) to f4(x) are the distributions for four different rock types, x being the mechanical parameter (E_m, c_m, ϕ_{rm}, σ_m) to be evaluated for the combination. Into brackets are the designed proportions of each rock type in a designed block, in this example the proportions are respectively 8%, 54%, 3% and 35%.

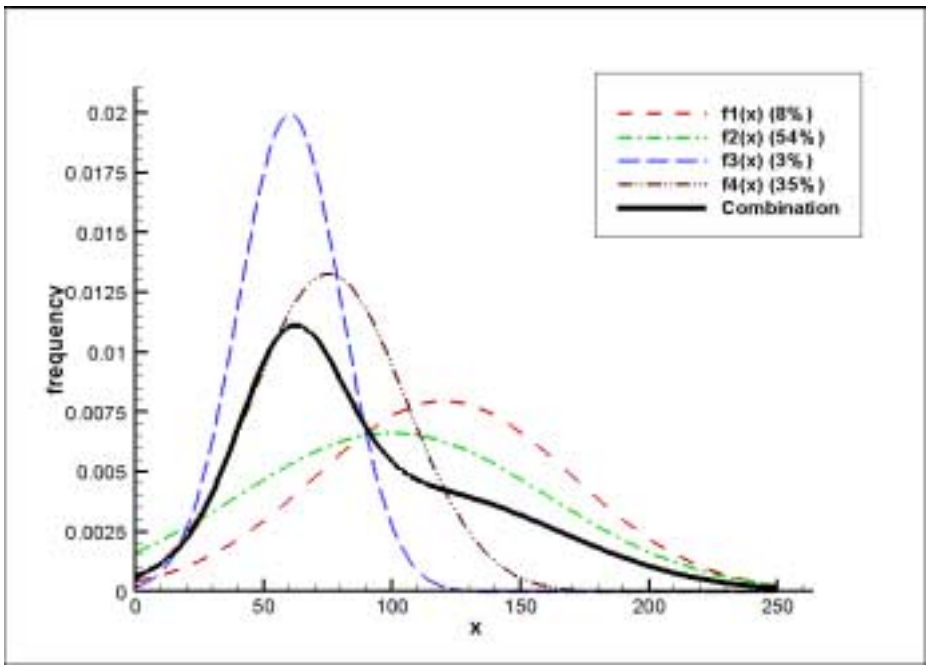

Figure 3-29. *Example of combination of distributions.*

4 The Test Case area

4.1 Presentation of the Test Case area

The area that has been chosen for the application of the methodology is situated on the Southeast corner of the Äspö island (Figure 4-1). Two models were designed:

- a large model, which is a cube of 550 m sides, going from the surface down to 1000 m depth. The geometrical model for the Test Case was developed from this model
- a detailed model, defined by a box located at depth from –380 to –500 m. This box is included in the large model (Figure 4-2).

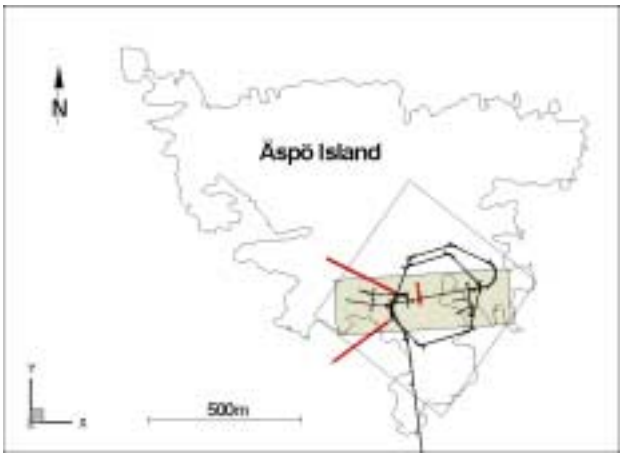

Figure 4-1. *Localisation of the large and detailed models on the Äspö island; visualisation of the boreholes and of the access tunnel (X: East, Y: North).*

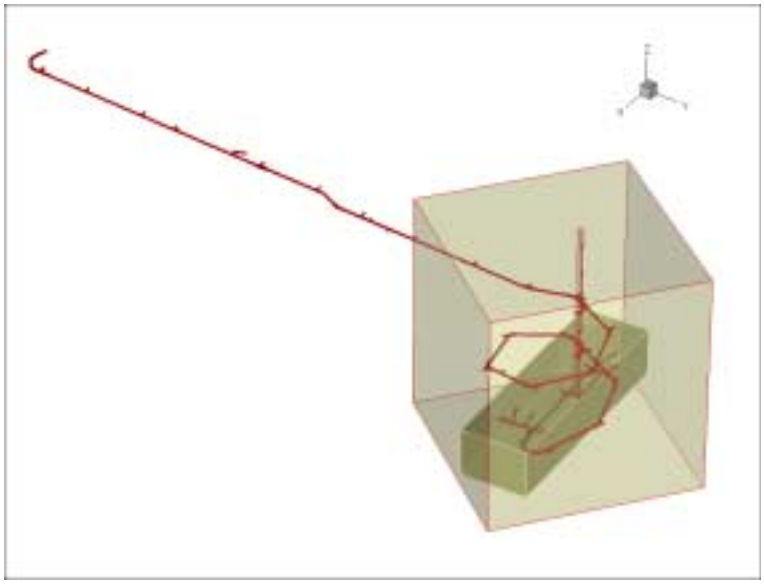

Figure 4-2. *3D view of the 2 models; visualisation of the access tunnel and of the shaft (X: East, Y: North).*

4.1.1 The large model

Structural geology in general, and the dimensions, geometry and geological characteristics of the deformation zones in particular, make up the framework for rock mechanics models, and are of influence for construction and design of underground facilities.

A model that covers the volume defined by the 550 m box has been developed for the purpose of this study in RVS (Rock Visualisation System tool, developed by SKB). This model gives an overview of the position and orientation of local deformation zones in the area (Figure 4-3). In order to take into account variations of width, local orientation and undulations, the zones were assigned some thickness. The width of the modelled zones is a function of the actual observed widths and interpreted undulations of the zone.

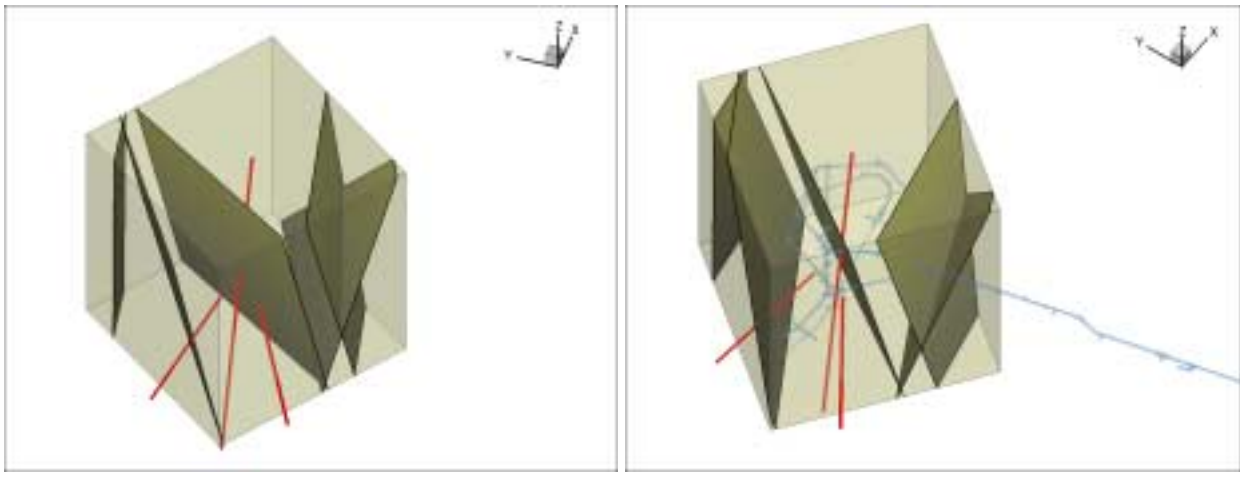

Figure 4-3. *Two 3D views of the 550 m model, with localisation of the deformation zones, the boreholes and the access tunnel (X: East, Y: North). NB: the deformation zones are represented as planes without width on this figure.*

Two different types of "rock units" were defined: (1) the "ordinary rock units" identifying the fractured rock mass, and (2) the "deformation zone units" identifying the deformation zones. According to this definition, the model is composed of 14 "rock units" blocks, of which six are "ordinary rock units" and eight are "deformation zone units" (Figure 4-4).

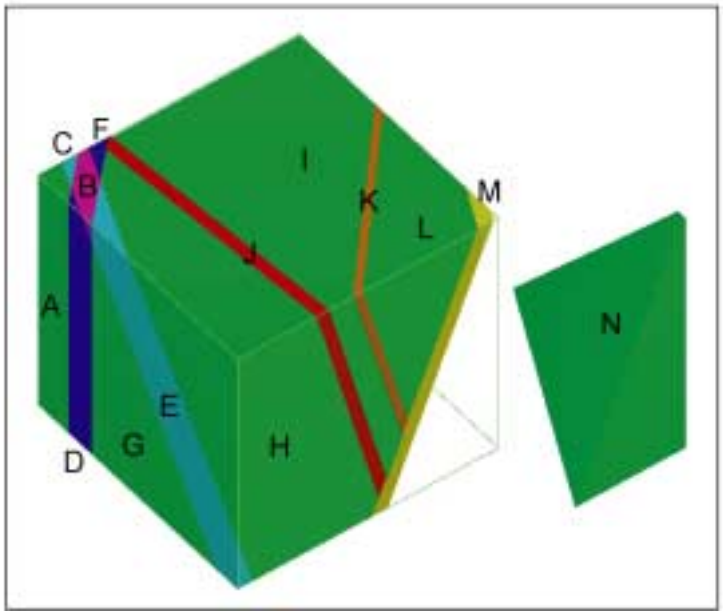

Figure 4-4. *Presentation of the different blocks or "rock units" in the RVS 550 m model. Deformation zones are here visualised with their actual width.*

4.1.2 The detailed model, or target area

The box is composed of 4 layers, and the cubes are numbered from 1 to 420 from the Northwest corner at the upper depth layer (Figure 4-5). In the following, the denotations refer to the cube numbers and the centre point co-ordinates of the cubes. A general view of the model illustrates that two of the three boreholes are on the side of the model (Figure 4-6), and data will mostly be provided by the subvertical borehole going through the middle of the model.

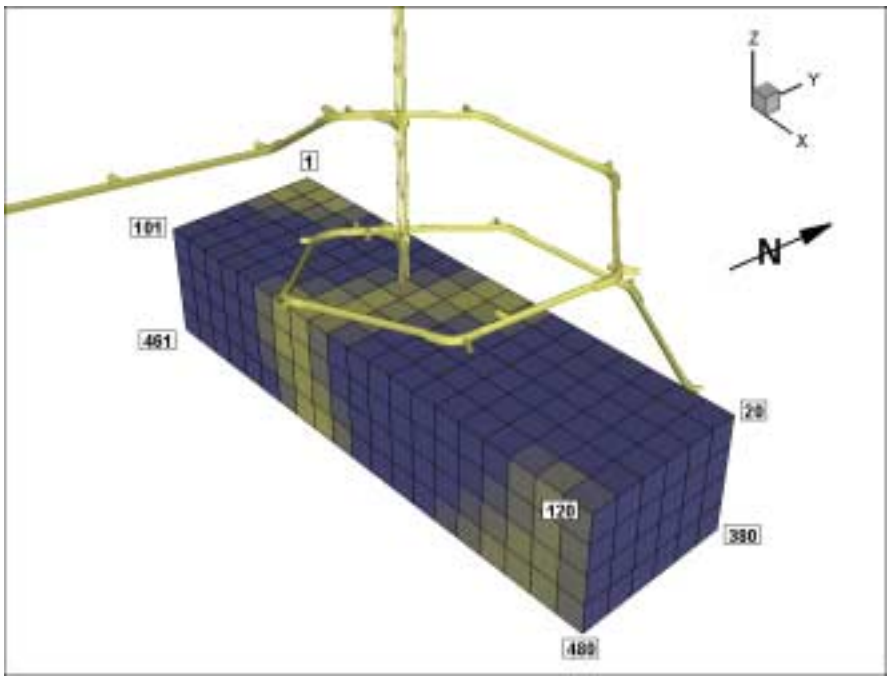

Figure 4-5. *Numbering of the detailed model (X: East, Y: North).*

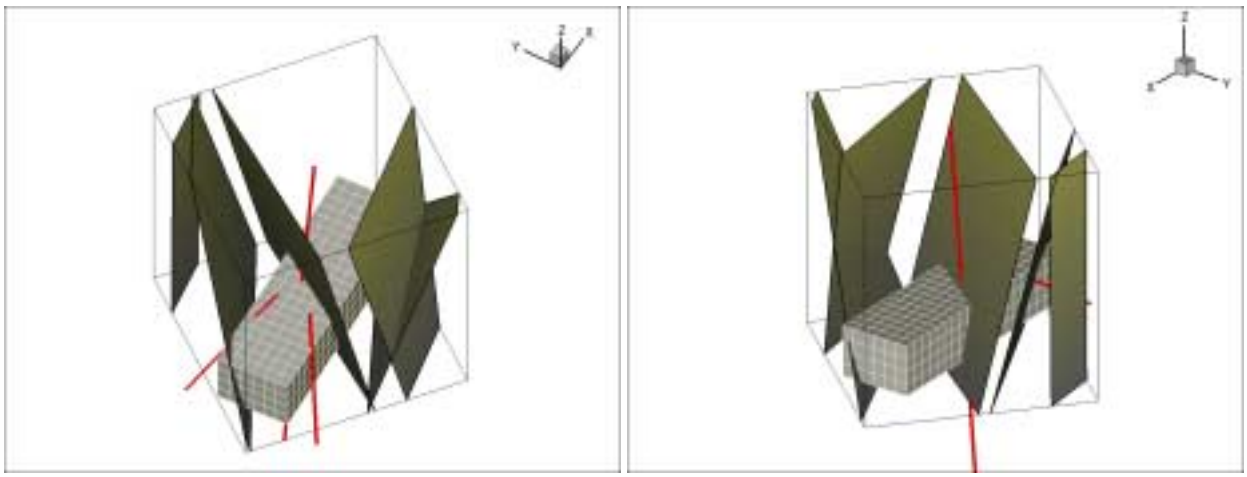

Figure 4-6. *Two 3D views of the detailed model, with localisation of the deformation zones and localisation of the boreholes (X: East, Y: North).*

In relation to the way width is assigned to deformation zones, see section 4.1.1, some cubes may contain more than one "rock unit" type. Indeed, the location and width of the actual deformation zone can vary in the area defined by the "deformation zone unit", see Figure 4-7. All cubes defined as "deformation zone unit" in the RVS model can be "ordinary rock unit" or "deformation zone".

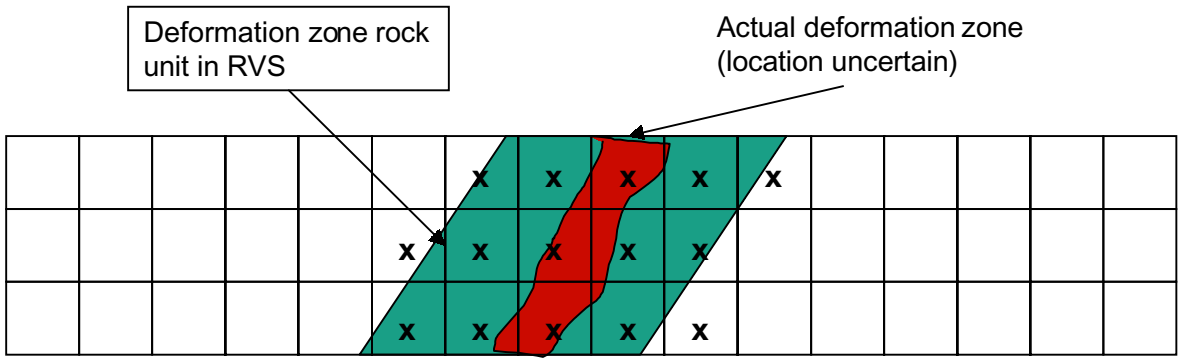

Figure 4-7. *Definition of "rock unit" types on a deformation zone.*

The predictions are made in each cube of the model and in case a cube contains more than one "rock unit" type, predictions are provided for each "rock unit" type.

4.2 Review of the input data

The sets of data used for the Test Case are taken out from SICADA, and are mainly coming from three boreholes, one subvertical, KAS02, that is almost 1000 m long, and two inclined boreholes, KA2598A and KA2511A, that are located on the western part of the model (Figure 4-6). One can notice that the subvertical borehole is almost at the middle point of both models, and that no borehole data at all are available on the eastern side of the models.

Data are also provided by geological surface mapping, laboratory tests and geophysical measurements. Table 4-1 presents the type of data that have been used for the development of the model and for the computations, and their sources.

Table 4-1. Review of the available and used input data, and their sources.

Input data	Origin
Geometrical model	Hudson (2002)
DFN model	Hermansson *et al.* (1998)
Greenstones model	Hudson (2002)
Rocktype	borehole core mapping, Sicada
Density of intact rock	Sundberg and Gabrielsson (1999), Nisca (1988)
RQD	borehole core mapping, Sicada
Fracture density	borehole core mapping, Sicada
E-modulus	Stille and Olsson (1989), Nordlund *et al.* (1999)
Poisson's ratio	Stille and Olsson (1989), Nordlund *et al.* (1999)
Triaxial compression tests	Nordlund *et al.* (1999)
Aperture	Lanaro (2001)
Normal load tests on fractures	Stille and Olsson (1989), Lanaro (2001)
Shear tests on fractures	Stille and Olsson (1989), Lanaro (2001)
Tilt tests	Makurat *et al.* (2002)
Joint wall strength	Makurat *et al.* (2002)
Shaft mapping (fracture orientation and rock type)	Sicada

5 Input data for the Test Case

5.1 Input data for intact rock

5.1.1 Rock type identification and distribution over the model volume

Mainly four rock types are identified in the area that are granodiorite, fine-grained granite (or aplite), Småland granite and greenstones.

According to the geometrical model /Hudson (ed.), 2002/, all "ordinary rock units" are considered to be of the same nature. Moreover, a rock unit is a volume that is assumed to possess the same properties within the whole volume, which means that the geology and the fracture network are assumed to be the same through the whole "ordinary rock unit".

The geology of the "ordinary rock units" must be defined. Data on rock type distribution in the rock mass with depth are provided by core mapping of the 3 boreholes KAS02, KA2511 and KA2598. The granite and granodiorite are the most dominant rock types and the rock mass consists of more than 80% of any of these two types. Figure 5-1 shows that the amount of the two rock types changes abruptly and that there might be a depth dependency of more granodiorite towards depth. The continuous length of the four rock types range between a couple of centimetres to more than 180 m.

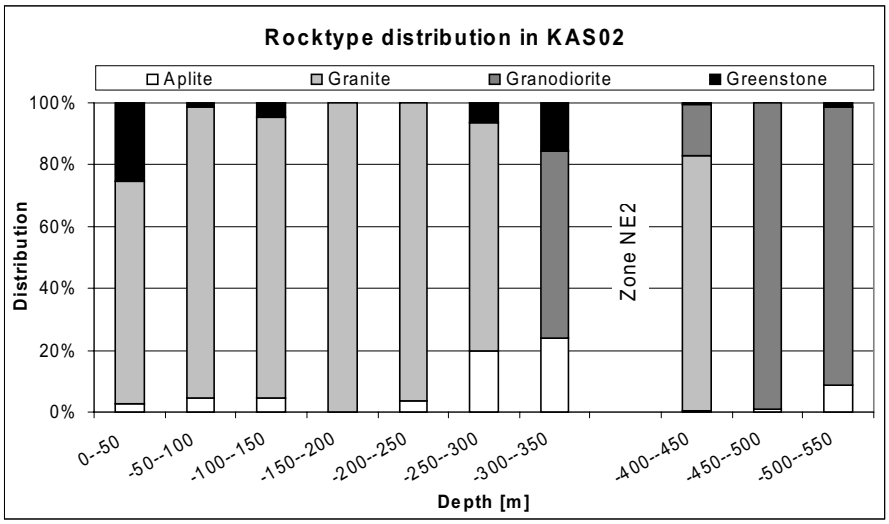

Figure 5-1. *Rock type distribution in KAS02.*

Nevertheless, the spatial variability is very difficult to assess, particularly when dealing with plutonic rocks that can occur as local lenses and dykes. As a consequence, a statistic analysis of the rock type distribution along the borehole inside the 550 m model has been performed to estimate the general rock type distribution in the "ordinary rock units".

To investigate if there are major differences between the rock type distribution in the different rock cubes, *i.e.* A to N, the boreholes are divided in sections that correspond to which rock block they intersect, see Table 5-1. The major difference is the amount of granite and granodiorite, but these two rock types always sum up to more than 80% of all rock types identified.

Since there are no strong evidence to reject this hypothesis, the distribution of rock types in all "ordinary rock units" is considered as the average distribution obtained in the three blocks and in the boreholes, that is corrected by weighting of the length of the boreholes, see Table 5-1.

Table 5-1. Distribution of rock types in boreholes in different rock blocks.

Block	Block H			Block I	Block G	
Bore hole	KA2511	KAS02	KA2598	KAS02	KA2598	**Total**
Length [m]	*178.3*	*152.1*	*298.4*	*350.3*	*22.0*	***1001.1***
aplite	6.3%	3.4%	12.0%	8.6%	0.0%	**8.2%**
granite	0.0%	26.9%	72.5%	74.3%	100.0%	**53.9%**
granodiorite	93.7%	68.3%	15.2%	9.4%	0.0%	**34.9%**
greenstone	0.0%	1.3%	0.3%	7.7%	0.0%	**3.0%**

Note: Total is the average rock type distribution corrected by weighting of the borehole lengths

The discussion above is based on the assumption that the three boreholes are representative for the rock unit and that the extension of the rock type volumes is equal in space.

5.1.2 Mechanical properties

The mechanical properties of each rock type have been evaluated from data provided by laboratory tests (Table 5-2) and the detailed process of evaluation and results are presented in appendix C.

Table 5-2. Test results available for the evaluation of the intact rock mechanical properties.

	/Stille and Olsson, 1989/				/Nordlund et al, 1999/
	Greenstone	Fine-grained Granite	Diorite	Granite	Diorite
Uniaxial compression test	X	X	X	X	X
Triaxial test					X
Brazilian test					X
Three-point bending test					X

Table 5-3, Table 5-4, Table 5-5 and Table 5-6 summarise the input parameters that have been calculated from the tests and that are required for the modelling task. To estimate cohesion, c, and friction angle, ϕ, of granite, greenstones and aplite, the friction angle has been set to 45° according to results obtained on granodiorite /Nordlund et al, 1999/, and the cohesion back-calculated according to the following equation:

$$c = \frac{\sigma_c \left(1 - \sin\phi\right)}{2\cos\phi} \qquad (5.1)$$

where σ_c is the uniaxial compression strength of the intact rock (see also appendix C).

The dilation angle has been assumed to be equal to zero for all rock types.

Table 5-3. Intact rock mechanical properties applied to the greenstones.

Intact rock: Greenstones		
	Mean value	Std Dev.
E, GPa	52.5	17.4
ν	0.22	–
c , MPa	23.8	–
σ_c, MPa	115	–
ϕ, ^{o}	45	–
σ_{ti}, MPa	8	–
D (g/cm^3)	2.96	–

Table 5-4. Intact rock mechanical properties applied to the granodiorite.

Intact rock: Granodiorite		
	Mean value	Std Dev.
E, GPa	73.0	2.9
ν	0.27	–
c , MPa	31.0	–
σ_c, MPa	214	–
ϕ, ^{o}	49	–
σ_{ti}, MPa	14.8	–
D (g/cm^3)	2.75	–

Table 5-5. Intact rock mechanical properties applied to the aplite.

Intact rock: aplite		
	Mean value	Std Dev.
E, GPa	65	4.3
ν	0.22	–
c , MPa	47.2	–
σ_c, MPa	228	–
ϕ, ^{o}	45	–
σ_{ti}, MPa	15	–
D (g/cm^3)	2.67	–

Table 5-6. Intact rock mechanical properties applied to the granite.

Intact rock: granite		
	Mean value	Std Dev.
E, GPa	62	0.5
ν	0.24	–
$_c$, MPa	37.7	–
σ_c, MPa	182	–
ϕ, ^{o}	45	–
σ_{ti}, MPa	12.8	–
D (g/cm^3)	2.64	–

With:
- E Young's modulus of the intact rock
- ν Poisson's ratio of the intact rock
- c Cohesion of the intact rock
- σ_c Uniaxial compressive strength of the intact rock (normalised to 50 mm samples)
- ϕ Friction angle of the intact rock
- σ_{ti} Tensile strength of the intact rock
- D Density of the intact rock

Regarding the granodiorite, significant discrepancies on mechanical properties were revealed when looking at the results from both studies (Table 5-7). As most of the test results, and especially triaxial tests, are provided by /Nordlund et al, 1999/ and in order to be consistent in the input data, the values that have been used are those provided by /Nordlund et al, 1999/.

Table 5-7. Discrepancy of data on the granodiorite.

Diorite	/Stille and Olsson, 1989/	/Nordlund et al, 1999/	Ratio
σ_c, MPa	169	214	1.27
E, GPa	60	73	1.22

5.2 Input data for fractures

5.2.1 Geometry of the fracture network

The fracture pattern in the "ordinary rock units" and in the "deformation zones units", see section 4.1.1, is considered separately, as the general configuration observed in the rock mass might be disturbed in the zone of influence of these major deformation zones.

According to the assumptions made by the geologists and presented in the geometrical model /Hudson (ed.), 2002/, the influence of deformation zones on the fracture pattern in "ordinary rock units" is included in the uncertainty thickness of the zone.

As a consequence, the same fracture pattern is assigned to all "ordinary rock units", and specific fracture patterns were built for each deformation zone, on the basis of lithological and structural information, see section 5.4.2.

The fracture pattern of the rock mass was simulated by a Discrete Fracture Network (DFN) model that is developed on the data from the Äspö ZEDEX tunnel section /Hermansson et al, 1998/. The study of fracture network in the prolonged part of the ZEDEX tunnel has been checked against previous DFN models developed in the Äspö area.

The data that are prevalent for the development of a DFN model for the rock mechanical model are the mean fracture orientation, the identification of different fracture sets that can mobilise different properties, the fracture density, fracture size distribution and terminations of fractures against others. The results of the analysis that have been used for this project are reported shortly in this report. For detailed explanations the reader is referred to /Hermansson et al, 1998/.

The analysis of fracture orientation enhanced three fracture sets, two subvertical (sets 1 and 2) and one subhorizontal (set 3), see Table 5-8. Studies based on fracture terminations reveal that they might be a geological explanation for the segmentation of the bedrock in the Äspö area, the set 1 being the oldest; then set 2 was formed thereafter and finally set 3. Nevertheless, other parameters such as mineral fillings and age fillings should be investigated.

Table 5-8. Orientation and termination of fracture sets /from Hermansson et al, 1998/.

		Set 1	Set 2	Set 3
Orientation	Trend (°)	348.2	46.4	142.8
	Plunge (°)	4.2	7.4	63.7
Terminations		–	25%	37%

Note: the orientation is given as dip direction and dip angle of the mean pole to the fracture plane.

The cumulative frequency curve of trace lengths shows that about 90% of fracture traces are shorter than 2 m, and about 10% are from 2 up to 20 m. These two populations of fractures were analysed separately for size distribution and fracture intensity. The analysis of size distribution, as defined in section 3.1.1, has been conducted on trace lengths of fractures, for each set separately. According to previous studies in Äspö, the fracture size distribution follows a lognormal distribution /see Hermansson et al, 1998/. The results of the analysis are presented in Table 5-9.

The fracture intensity in a FracMan DFN model is defined as the amount of fracture area per unit volume of rock, P_{32} (m^2/m^3). This parameter can not be assessed in the field but can be estimated on the basis of a linearly correlation with P_{21} (m/m^2), which is defined as the amount of fractures intersecting an outcrop surface, or with the P_{10} (m^{-1}), which is the fracture frequency along a scanline or a borehole. The correlation between the fracture intensity parameters is defined as /Dershowitz and Herda, 1992/:

$$P_{32} = C_{21} \cdot P_{21} \tag{5.2}$$

$$P_{32} = C_{10} \cdot P_{10} \tag{5.3}$$

C_{10} and C_{21} are constants of proportionality that depend on the orientation and radius size distribution of the fractures, and the orientation of outcrops (P_{21}) or scan lines/boreholes (P_{10}).

P_{21} and P_{10} are parameters that are dependent on orientation and shape of fractures as well as orientation and shape of the outcrop/scanline. P_{32} has here the advantage to be independent to the orientation and radius size distribution of fractures.

The determination of P_{32} for a given DFN model is determined as followed: a DFN model is generated on a "guessed" P_{32}. Sampling lines and/or surfaces are simulated in the model, and the P_{10} and /or P_{21} of the simulations are checked against the values of the actual data. The ratio of simulated/actual parameters leads to the definition of the constant of proportionality C_{10}/C_{21}, and to the determination of the actual P_{32}. The fracture intensity, P_{32}, determined for each fracture set is presented in Table 5-9.

Table 5-9. P_{32} and radius fracture size distribution /from Hermansson et al, 1998/.

		Set 1	Set 2	Set 3
P_{32} (m^2/m^3)	Small fractures	0.4	0.87	0.44
	Large fractures	**0.23**	**0.7**	**0.11**
Fracture size	Small fractures	0.25 / *0.25*	0.5 / *0.25*	0.25 / *0.25*
radius (m)	Large fractures	**4 / *2***	**5 / *1***	**4 / *2***

Note: for fracture size, the first number represents the mean value, the second the standard variation. Small fractures: trace shorter than 2m; large fractures: trace longer than 2m.

The stochastic fracture network in the rock mass was then simulated by a DFN model based on the combination of the previous distributions for fracture orientation, size, intensity. For the purpose of this project, the DFN model was generated in rock volumes of 50·50·50 m, in order to avoid truncations of fracture traces at the edges of the 30·30 m section planes (see section 2.2.3). As illustrated in Figure 7-2a numerous small fracture traces are generated by this model, which is consistent to the relative high frequency of small fracture traces.

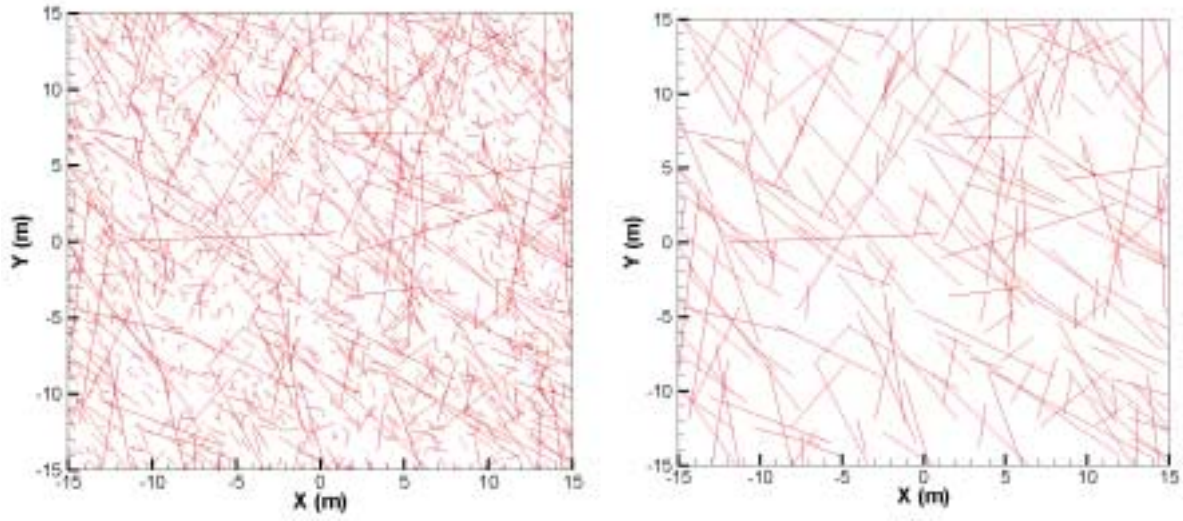

(a) (b)

Figure 5-2. *2D trace section from a DFN model (a) with all fractures, (b) with fractures larger than 2 m.*

Most of those small fracture traces are in the rock mass, and do not terminate against any other fracture traces. They would be discarded when "meshing" and generating rock blocks in UDEC, see section 3.3.4. For comparison the DFN model was simulated by discarding all fractures with a radius smaller than 1 m (Figure 5-2b), and the rock blocks models generated in UDEC compared. This analysis confirmed that most of the fractures smaller than 2 m are discarded when generating the model in UDEC. As a consequence and to reduce computation time, a censoring radius of 1 m was set for generating the DFN models used for extracting the 2D fracture trace sections. The fracture pattern obtained for a censored 2D section, and the rock block model created in UDEC from the same fracture trace file are illustrated in Figure 5-3.

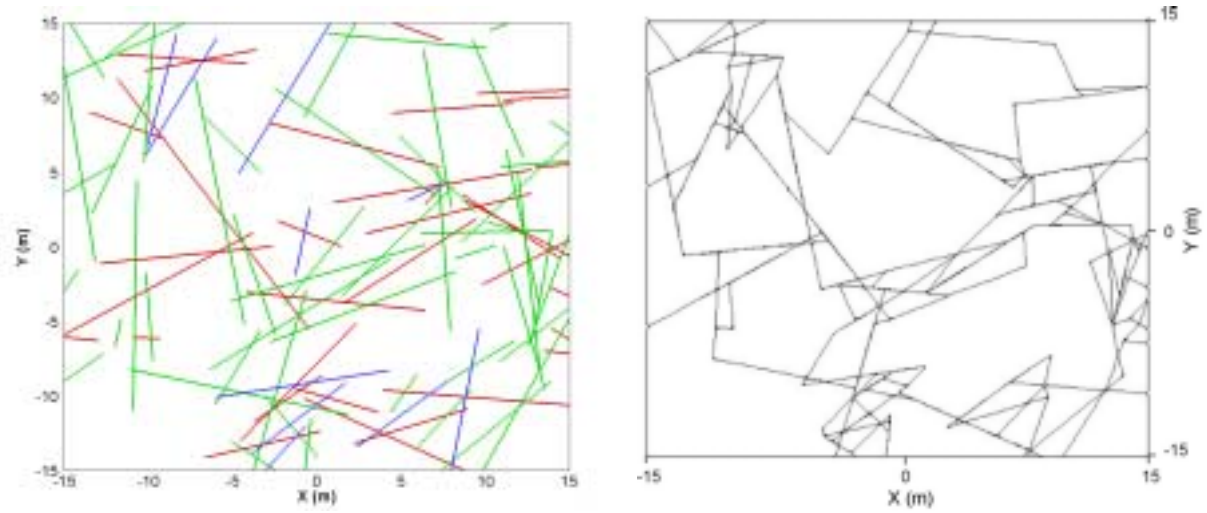

(a) (b)

Figure 5-3. *(a) Fracture traces for a 2D section, and (b) the resulting rock block model in UDEC.*

5.2.2 Fracture mechanical properties

The fracture mechanical properties have been evaluated from different laboratory tests, which data are provided in /Stille and Olsson, 1989/, in /Lanaro, 2001/, and by core logging /Makurat et al, 2002/, see Table 5-10. The evaluation of properties is presented in appendix C.

Table 5-10. Test results available for the evaluation of rock fractures mechanical properties.

	/Stille and Olsson, 1989/	/Lanaro, 2001/	/Makurat et al, 2002/
Normal load test	X	X	
Shear load test	X	X	
Aperture		X	
Tilt test			X
Schmidt hammer test			X

On basis of the results provided, two sets of parameters have been identified, one for the sub-vertical fracture sets and one for the sub-horizontal fracture set.

The mechanical properties and behaviour of the fractures evaluated from /Stille and Olsson, 1989; Lanaro, 2001/ show important discrepancy for both subhorizontal and subvertical sets of fractures, which is expressed by much higher values for shear and normal stiffness from Lanaro's data (Figure 5-4). The normal stiffness calculated from /Lanaro, 2001/ is really high compared to reference values for fractures. As a consequence, the mechanical properties used as input for modelling are those evaluated from /Stille and Olsson, 1989/.

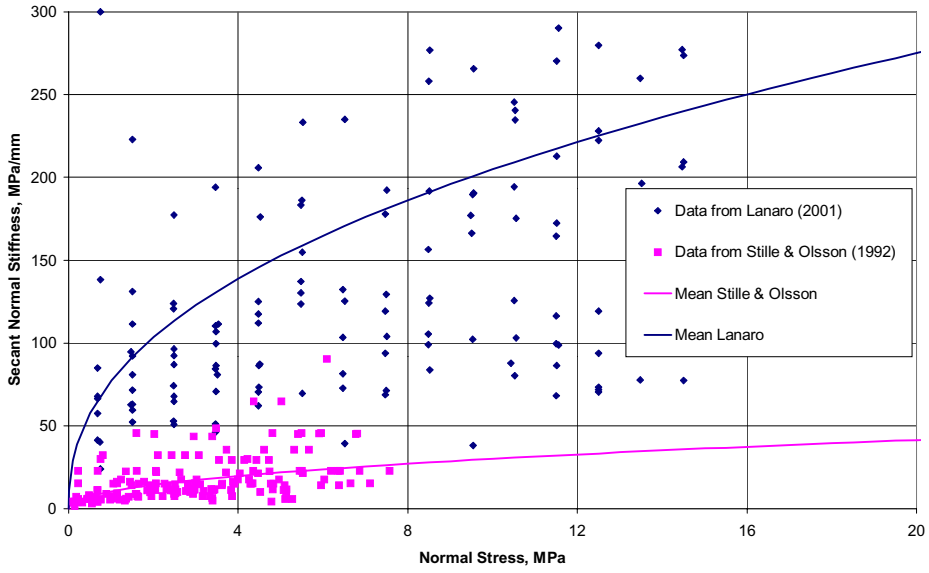

Figure 5-4. *Discrepancy of data from normal loading test on rock fractures.*

The mechanical properties evaluated for rock fractures are presented in Table 5-11. As explained in appendix C, there is no unique solution for the determination of values for JRC_0, JCS_0 and ϕ_r. The sensitivity analysis on these parameters is presented in section 6.3.

Table 5-11. Input parameters for the sets of fractures, assuming a fractured rock mass in the granodiorite, and the Barton-Bandis joint constitutive model.

	K_n [(1)] (MPa/m)	K_s [(1)] (MPa/m)	ϕ_r (°)	σ_c (MPa)	JRC_0	JCS_0 (MPa)	L_0 (m)	a_{jn} (mm)
Subvertical sets	61.5e3	35.5e3	25/30/35	214	4/9.3/ 12/16	40/110/ 170	5.51e–2	0.56
Subhorizontal set	21.9e3	15.7e3	25/30/35	214	4/9.3/ 12/16	40/110/ 170	6.1e–2	0.2

(1) Values expected at σ_n=23 MPa

with
- K_n Joint normal stiffness at expected normal loads
- K_s Joint shear stiffness at expected normal loads
- ϕ_r Residual joint angle of friction
- σ_c Intact rock uniaxial compressive strength (back calculated for 50 mm diameter samples)
- JRC_0 Lab-scale roughness coefficient
- JCS_0 Lab-scale joint wall compressive strength
- L_0 Lab-scale joint lengths
- a_{jn} Joint aperture at zero normal stress

5.3 Initial stresses

The values for initial principal stresses were provided by Itasca Geomekanik AB and are reported in /Hakami et al, 2002/. The values used for the modelling correspond to predictions made on the target area. According to the principal stress orientations and magnitude predictions, σ_1 is identified as the maximum horizontal stress or σ_H, and σ_3 as the minimum vertical stress or σ_v. σ_2 is referred as the intermediary horizontal stress or σ_h. The mean values for σ_1, σ_2 and σ_3 presented in Table 5-12, have been used to simulate the in situ stress state at each depth in the detailed model.

Table 5-12. Principal stress magnitudes /from Hakami et al, 2002/.

	σ_H (MPa)	σ_h (MPa)	σ_v (MPa)
Level 1 (–380/–410m)	19	10.7	10.2
Level 2 (–410/–440m)	20.2	11.5	10.7
Level 3 (–440/–470m)	21.3	12.3	11.2
Level 4 (–470/–500m)	22.4	13.1	11.7

Note: detailed description about data evaluation is provided in the aforementioned report

The mean principal stress orientations are considered consistent with depth and taken as follows:

Table 5-13. Principal stress orientation /from Hakami et al, 2002/.

	Strike (°)	Dip (°)
σ_H	136	0
σ_h	226	0
σ_v	0	90

5.4 Deformation zones

The information related to deformation zones is provided in the geometrical model's report /Hudson (ed.), 2002/. Some complementary data were obtained from surface mapping presented in /Munier, 1995; Tirén and Beckholmen, 1987/.

The application of the methodology on the deformation zones is considered to be an exercise, and the outcome of the modelling in term of values must be considered very carefully. Indeed, the models have been built mostly from interpolation on qualitative data, and guesswork based on engineering expertise.

Nevertheless, the outcome of the modelling are hereunder presented as a basis for discussion on the validity of the approach developed for the deformation zones.

5.4.1 List of assumptions related to the modelling of deformation zones

Specific assumptions and modifications from the "usual" set-up are required for the modelling of deformation zones. The list of assumptions, as presented in section 3.4, is completed for the Test Case by site-specific assumptions that are related to the type and quality of data provided for the Test Case.

The assumptions made for the modelling of deformation zones and in the frame of the Test Case are the following:

- The model size has been taken 10 times smaller than for the modelling of the rock mass, that means 3·3 meters. This set-up is necessary to run models with higher fracture densities.
- The fractures in the zones are considered of "infinite length" at the model size, for mainly two reasons. No quantitative data were available regarding the equivalent radius of the fracture sets in the zones. Then, if assuming that the mean equivalent radius is the same as the one determined for large fractures (larger than 2 m) in the rock mass (Table 5-9), there is very high probability that the fractures will go through the 3·3 m blocks.
- The modelling plane is a section that is perpendicular to the deformation zones, so that the Young's modulus can be calculated.
- Confining stresses were applied on both vertical sides.
- According to the quantity and quality of data used, the confidence level of all blocks identified as deformation zones is very low, and set to 3 ("guesswork").

5.4.2 Geometry

(for general information, see section 3.1.1)

The fracture network in each fracture zone has been modelled from qualitative information published in /Munier, 1995; Tirén and Beckholmen, 1987/, in the geometrical report /Hudson (ed.), 2002/, and from core logging. Statistical analysis of surficial fracture mapping are presented as stereoplots of fracture sets in the main deformation zones in Äspö /Munier, 1995/. The strike and dip of the fracture sets are not precisely quantified, but range of values can be determined from the plots. Only the orientation of fracture sets defined as parallel to the deformation zones could be defined with higher confidence.

Suitable density data related to each fracture set in each fracture zone were not available. Therefore, the density of fractures was estimated from the density observed in the boreholes KAS02 and KA2598A when going through the zone. The fracture density was not averaged on the all length of boreholes reported to cross the "RVS deformation zone units", but on parts of boreholes inside these "deformation zone units" in which fracture density was sensibly higher. This is valid for both deformation zones NE2 and EW1b. For the other deformation zones, some descriptive information was sometimes available in the aforementioned reports, such as "fracture density is high in the all zone". Fracture density values were estimated according to these descriptions. Even if it might be considered as a rough assumption, the properties assigned to EW-1a are the same as those defined for EW-1b, which means that we studied a "EW-1" zone.

Due to the lack of data, the same fracture density was set to all fracture sets in a fracture zone, but some standard deviation was given in the model when building the fracture network in UDEC. This is reflected as a range of fracture density's mean values presented in Table 5-14. The uncertainty in fracture orientation was handled in the same way.

Table 5-14. Fracture strike and dip, and fracture density for deformation zones.

Fracture zone	Strike	Dip	P_{10} [(1)]
NE-1	N230	30	
	N140	90	2–10
	N0	0	
NE-2	N130	0–10	3–6
	N35	0–15	
EW-1[(2)]	N90	0	
	N0	85–90	2.5–8
	N300	20–30	
EW-3	N70	80–90	
	N145	0–10	3–8
	N40–60	0–30	

[(1)] The range given is a range observed on the mean value.

[(2)] Include EW-1a and EW-1b

The modelling of a section perpendicular to NE-2 was not valid on the basis on the information available. Indeed, only two fracture sets are identified, one parallel to the zone and the other perpendicular to it. Taking a perpendicular section to the zone implies that only traces from the fractures parallel to the zones contribute to the model.

Due to lack of any other information, the DFN model developed for "ordinary rock units" (section 3.1.1) was then used to build the fracture geometry of NE-2, but the mechanical properties assigned to intact rock and fractures are those presented in section 5.4.4.

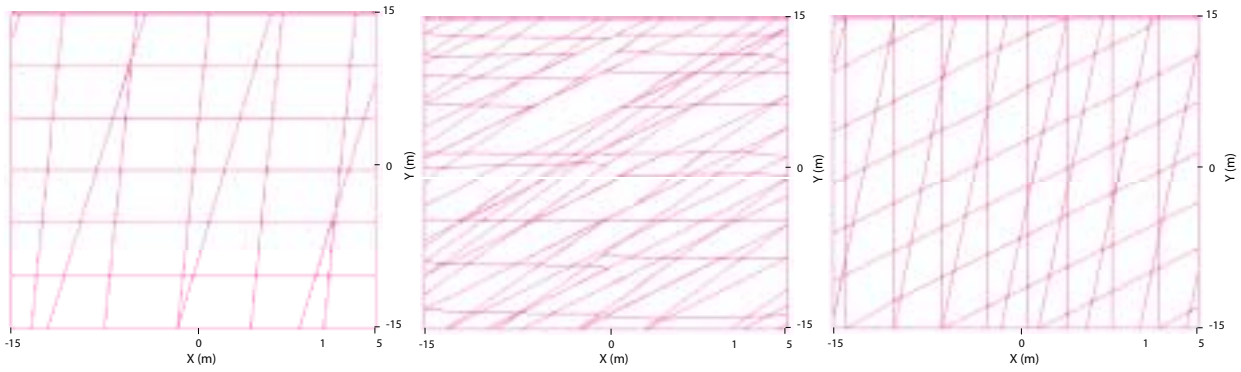

Figure 5-5. *Geometrical modelling of the deformation zones': a) EW-1; b) NE-1; c) EW-3.*

As shown in Figure 5-5 the geometry of the rock blocks in the UDEC model is highly related to the relative orientation of the fracture sets to the orientation of the section towards the zone. This is a factor that will strongly influence the behaviour of the model, and therefore the mechanical parameters of the rock mass in the deformation zones.

5.4.3 Rock type distribution

The geometrical model /Hudson (ed.), 2002/ provides qualitative and general description of the main rock types identified in the deformation zones. The rock type distribution for deformation zones NE2 and EW1b can also be checked against the core logging of the boreholes KAS02 and KA2598A. On basis of these data, the rock type distribution is provided as a percentage of the different rock type, see Table 5-15.

Table 5-15. Rock type distribution in the deformation zones, as a percentage.

	Granite	Granodiorite	Aplite	Greenstones
EW-3	0	100	0	0
NE-2	0	90	10	0
EW-1[(1)]	100	0	0	0
NE-1	0	90	10	0

[(1)] Includes EW-1a and EW-1b

5.4.4 Mechanical properties assigned to intact rock and fractures in the zones

According to /Gupta and Rao, 2001/, some relationships can be established between the weathering degree of a given rock type and the decrease in Young's modulus and strength of the same intact rock. With the assumption of a slight degree of alteration, the mechanical properties of intact rock in the zones have been reduced to 80% of the intact rock Young's modulus and strength in the deformation zones. With regards to the lack of information, the same reduction factor has been used for the simulations of all deformation zones. Table 5-16 and Table 5-17 list the parameters used in the deformation zones, for the granite and granodiorite.

Table 5-16. Mechanical properties applied to the granite in the deformation zones.

Intact rock: granite		
	Mean value	Std Dev.
E, GPa	49.6	0.4
ν	0.24	–
c , MPa	30.2	–
ϕ, ^{o}	45	–
σ_c, MPa	145.6	–
σ_{ti}, MPa	12.8	–
D (g/cm^3)	2.64	–

Table 5-17. Mechanical properties applied to the granodiorite in the deformation zones.

Intact rock: Granodiorite		
	Mean value	Std Dev.
E, GPa	58.4	2.32
ν	0.27	–
c , MPa	24.8	–
ϕ, ^{o}	49	–
σ_c, MPa	171.2	–
σ_{ti}, MPa	14.8	–
D (g/cm^3)	2.75	–

With:

E	Young's modulus of the intact rock
ν	Poisson's ratio of the intact rock
c	Cohesion of the intact rock
ϕ	Friction angle of the intact rock
σ_c	Uniaxial compressive strength of the intact rock (normalised for 50 mm samples)
σ_{ti}	Tensile strength of the intact rock
D	Density of the intact rock

The same mechanical properties were assigned for all fracture sets in all deformation zones, see Table 5-18. To overcome numerical problems arising when using the Barton-Bandis joint model for modelling the deformation zones, a Continuously Yielding model with constant normal, K_n, and shear, K_s, stiffness, and constant joint friction angle, ϕ_r, has been applied for modelling the behaviour of fractures. The definition of the residual friction angle is calibrated against tilt tests on fractures in the deformation zones crossed by boreholes KAS02 and KA2598A.

Table 5-18. Mechanical properties assigned to the fracture sets in the deformation zones.

	K_n [(1)] (MPa/m)	K_s [(1)] (MPa/m)	ϕ_r (°)	jr (m)
Fracture sets	44e3	29.9e3	20	0.002

[(1)] Values expected at σ_n=23 MPa

with

K_n	Joint normal stiffness at expected normal loads
K_s	Joint shear stiffness at expected normal loads
ϕ_r	Residual joint friction angle
jr	Joint roughness parameter

6 Modelling methodology applied to the Test Case

The modelling tests have been carried out according to the procedure described in section 3. Before to proceed with modelling, the assumptions done need to be listed.

Then, some complementary benchmark tests were carried out to test the input parameters against the material and joint constitutive models that have been chosen to perform the modelling task applied to the Test Case. For instance, a simple loading test was conducted on an intact rock block, with a Mohr-Coulomb model, in order to check the Young's modulus obtained by simulation and the value determined from laboratory tests.

Simple shear tests have been conducted to check the input parameters on fracture properties, using the Continuously Yielding and the Barton-Bandis joint models.

6.1 List of assumptions for the model

Introduction

When applying the theoretical model to the Test Case, a number of assumptions of different origins are required. Assumptions were made on the proposed geometrical model, on the mechanical properties of the rock material and fractures, on the numerical model used in UDEC and on the interpretation of the calculated rock mass properties. On one hand, assumptions can be required for the validity of a theory. This concerns a large spectrum of assumptions from the estimation of parameters by laboratory tests to the applicability of numerical modelling. On the other hand, assumptions are sometimes required due to the shortcoming of input data. The later type of uncertainty can be reduced when more data are made available.

Assumptions on the geometrical model

The following assumptions on the geometrical model have been made.

DFN model

- The orientations of the fractures follow the same distribution in the whole 550 m model and in the detailed model.
- The same radius size distribution is applied for fractures in the whole 550 m model and in the detailed model.
- The fracture location in space follows a Poisson' s distribution.
- The density of fracture is constant over a given 30·30·30 m cube, or within an "ordinary rock unit".
- The density of fracture in the 30 m cubes can be changed for area characterised by boreholes according to the local fracture frequency.

Rock units

- Assumptions have been made concerning the definition of "rock unit" types (see definition of the geometrical model, section 4.1).
- Assumptions have been made concerning the definition of deformation zones (see definition of the geometrical model, section 4.1).

Rock material mechanical properties

- The intact rock material mechanical properties are constant for a given rock type over a given 30 m cube volume.
- The mean value is used as input data.

Fracture mechanical properties

- Both vertical fracture sets are assigned the same mechanical properties.
- Mechanical properties are constant on the whole fracture plane.
- The same fracture mechanical properties have been assigned for all fractures in a set, in the different rock types.
- The mean value is used as input data.

Deformation zones

Most of the assumptions considered in this project are related to the lack of relevant fracture data in deformation zones, and should then be considered as particularly relevant for this application of the methodology.

- The fracture density can be estimated from core logging from boreholes. The section of borehole going through a deformation zone is isolated, and the fracture frequency (P_{10}) is calculated in this section.
- The fracture frequency is considered to be constant over the entire deformation zone.
- Normal and shear stiffness, and aperture assigned to fractures in "ordinary rock units" have been assigned to the fracture sets in the "deformation zone units". As the model on deformation zones could not be run with the B-B model, the fracture mechanical properties have been fitted in a C-Y model.
- The residual friction angle of fractures was arbitrarily reduced to 20°, taking into account the clayey filling.
- The mechanical properties for intact rock were modified on the basis of literature review (see section 5.4.4) and alteration data on the rock in the deformation zones provided by core logging.

Numerical model (UDEC)

- Simulations in 2D are made under plain strain loading conditions.
- A 2D section of rock mass is assumed to behave mechanically like in 3D. The systematic error induced by this assumption can be compensated by a scaling function still to be determined, see section 3.3.5.
- Since fracture traces that terminate in the rock or that are entirely located in the rock are deleted when blocks are generated in UDEC, their effect on deformation properties and rock strength is neglected (see section 3.3.4 for the validity of this assumption).
- There is no fracture propagation taking place in the rock blocks under extreme loading.
- Coupled hydro-mechanical effects on the fractures are neglected.
- The orientation of the principal stress is orthogonal to the sides of the model.
- The Barton – Bandis joint constitutive model is used to model the mechanical behaviour of the fractures.
- The Barton – Bandis model handle load reversal.
- The Continuously-Yielding joint constitutive model is used to model the mechanical behaviour of fractures in deformation zones.
- Scaling of fracture properties according to fracture length is automatically done by UDEC.
- The Mohr-Coulomb failure criterion is applied to blocks.
- Effective stress parameters. No pore pressure assumed.
- Assumptions on in situ stresses are consistent with Itasca's work /Hakami et al, 2002/: the orientation of in situ stress is kept constant with depth. The magnitude is kept constant at a specified depth level in the 30·30 m model.

Assumptions due to the shortcoming of input data

- Triaxial test data are available only for one rock type (diorite). The parameters for the other rock types are assumed on engineering experience basis.
- Orientation and density of fracture sets in the deformation zones have been defined from general stereoplots of the zones. Detailed surface mapping over the areas is required.

6.2 Influence of the variation of the input parameters

Before running the calculations for the different rock types, a sensitivity analysis of the input parameters has been conducted on a fractured rock mass in 100% of granodiorite.

The following variation of parameters was defined (Note: the parameters were changed one at a time):

- Influence of anisotropy: as mentioned in the section 2.2.3 of this report, three 2D sections of perpendicular orientation were extracted from the 3D fracture model. With all other parameters constant, simulations were run on those 2D sections, and the deformation properties of the rock mass were evaluated.

- Influence of the fracture sets: with respect to the mechanical properties evaluated from laboratory tests, 2 sets of fracture properties could be identified, one for the sub-vertical fractures, one for the sub-horizontal fractures. The influence of the differentiation of the fracture sets by their mechanical properties was determined by (1) running the model with different mechanical properties for each set, and (2) running the same model but assigning the same mechanical properties to all fracture sets.

- Influence of the mechanical properties of fractures: due to shortcoming of data, see appendix C, some of the model parameters can take a wide range of values. In order to determine the influence of these values on the deformation properties of the rock mass, different combinations of the parameters were simulated. The values used on the granodiorite rock mass block are the following:

  JCS_0: 40, 110, **170**
  JRC_0: 4, **9.3**, 12, 16
  ϕ_r: 25, **30**, 35

Values for the other input parameters of the model are set according to Table 5-11.

Note: when varying one parameter, for example JCS_0, the "standard values", marked in red, were set to the other parameters. This leads to 10 different combinations.

- Influence of the initial stresses: four different in situ stresses set-ups have been defined (see section 5.3), that simulate the increase of principal stresses with depth. While other parameters are constant, 4 simulations were run at the 4 stress values predicted for each depth level in the target area.

The same set of parameters for mechanical properties of the intact rock was used for all simulations, see Table 5-4.

The following conclusions can be drawn from these analyses:

- Influence of the anisotropy: the Young's modulus and Poisson's ratio were slightly affected by changes of section orientation. Some differences of 2.5% were obtained, which is an indication of the anisotropy of the rock mass. However, in accordance to the low discrepancy of obtained values, it was decided at first to run all the simulations on the same section. The section used in the following is a vertical section parallel to the major principal horizontal stress.

- Influence of the fracture sets: no significant influence of the set of parameters assigned to the horizontal set of fracture has been showed. This can be correlated to the relatively low frequency of fractures from this set, see Table 5-9 and Figure 5-2. Assigning different mechanical properties to different fracture sets is feasible but is heavy in programming. Therefore, all fracture sets were assigned the mechanical properties that had been defined for the sub-vertical sets of fractures.

- Influence of the mechanical properties of fractures: no significant influence of JRC_0 and JCS_0 could be found from these tests. However, the input value of the residual friction angle, ϕ_r, influences the deformation parameters of the rock mass. As a consequence, the standard parameters were used as input data for JCS_0 and JRC_0, respectively 170 and 9.3, and the influence of ϕ_r was investigated by running 3 different simulations for each model, all other parameters being unchanged, on the values 25, 30 and 35°.

- Influence of the initial stresses: the Young's modulus and compressive strength at failure increase with depth and as a function of the in situ stresses while the Poisson's ratio decrease. A variation in the range of 7 to 9% was calculated from the shallowest to the deepest level of the target area for these different parameters. Therefore, sensitivity analyses were run at the highest initial stress level, corresponding to the deepest level, and only standard cases were run at different depth levels.

6.3 Refined set-up of parameters for modelling

According to the information provided by the sensitivity analysis presented in the previous section, the mechanical properties for intact rock and fractures as defined previously in sections 5.1.2 and 5.2.2, were refined. The input parameters required in UDEC are presented in Table 6-1 for the intact rock and in Table 6-2 for the rock fractures. The set-up for the initial stresses is the same as presented in section 5.3.

Table 6-1. Input parameters for the intact rock, according to the Mohr-Coulomb material model

	D (kg/m^3)	K (MPa)	G (MPa)	c (MPa)	ϕ (°)	ψ (°)	σ_{ti} (MPa)
Småland granite	2.64	39e3	25e3	37.7	45	0	12.8
Aplite	2.67	38e3	26e3	47.2	45	0	15
Greenstones	2.96	31e3	21e3	23.8	45	0	8
Granodiorite	2.75	52e3	28e3	31	49	0	14.8

With
- D — Density of the intact rock
- K — Bulk modulus of the intact rock
- G — Shear modulus of the intact rock
- c — Cohesion of the intact rock
- ϕ — Friction angle of the intact rock
- ψ — Dilation angle of the intact rock
- σ_{ti} — Tensile strength of the intact rock

Table 6-2. Input parameters used for modelling the behaviour of rock fractures, according to the Barton-Bandis joint constitutive model.

	K_n [(1)] (MPa/m)	K_s [(1)] (MPa/m)	ϕ_r (°)	σ_c (MPa)	JRC_0	JCS_0 (MPa)	L_0 (m)	a_{jn} (mm)
Greenstones	44e3	29.9e3	25 30 35	115	12	92	5.51e–2	0.58
Granodiorite	44e3	29.9e3	25 30 35	214	9.3	170	5.51e–2	0.58
Småland granite	44e3	29.9e3	25 30 35	182	8.2	146	5.51e–2	0.58
Aplite	44e3	29.9e3	25 30 35	228	9.1	180	5.51e–2	0.58

Note: the same mechanical properties are assigned to all sets of fractures
(1) Values expected at σ_n=23 MPa

with
- K_n Joint normal stiffness at expected normal loads
- K_s Joint shear stiffness at expected normal loads
- ϕ_r Residual angle of friction
- σ_c Intact rock uniaxial compressive strength (back calculated for 50 mm diameter samples)
- JRC_0 Lab-scale roughness coefficient
- JCS_0 Lab-scale joint wall compressive strength
- L_0 Lab-scale joint lengths
- a_{jn} Joint aperture at zero normal stress

6.4 Comparison of modelling results with empirical relations for rock masses

One of the most widely used empirical failure criteria is the Hoek-Brown (H-B) criterion. The generalised form of the criterion for jointed rock masses is defined by:

$$\sigma_1 = \sigma_3 + \sigma_c \cdot \left(m_b \cdot \sigma_3 / \sigma_c + s \right)^a \tag{6.1}$$

Hoek et al, 1995, introduced the Geological Strength Index, GSI, to provide a system for estimating the rock mass strength for different geological conditions. Once the GSI has been estimated the strength parameters in the H-B failure criterion for hard rocks are calculated as follows:

$$m_b = m_i \cdot \exp\left(\frac{GSI - 100}{28} \right) \tag{6.2}$$

$$s = \exp\left(\frac{GSI - 100}{9} \right) \tag{6.3}$$

$$a = 0.5 \tag{6.4}$$

The deformation modulus of the rock mass can be estimated by:

$$E_m = 10^{GSI-10/40} \tag{6.5}$$

For a blocky well interlocked undisturbed rock mass consisting of cubical blocks formed by three intersecting fracture sets and with joint surfaces that are very rough, fresh unweathered, the Geological Strength Index, GSI is from 65 to 85 /Marinos and Hoek, 2000/. GSI can also be related to the commonly used rock mass classification systems, the rock mass quality index Q /Barton et al, 1974/ or the rock mass rating, RMR /Bieniawski, 1989/. Figure 6-1 shows the rock mass rating, RMR_{89}, along the three boreholes in the Test Case area. The ground water rating is set to 15 and the adjustment for joint orientation is set to zero. The GSI value can be estimated according to the following expression:

$$GSI = RMR_{89} - 5 \tag{6.6}$$

In this case GSI is in the interval 70–75.

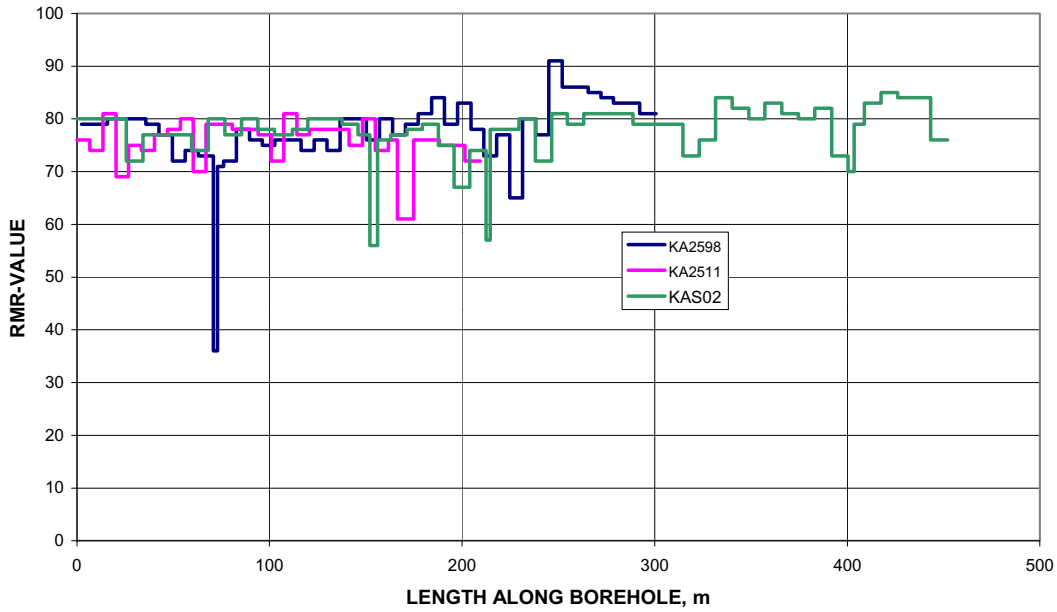

Figure 6-1. *Rock Mass Rating, RMR_{89}, along boreholes in the Test Case area.*

The triaxial tests on intact diorite samples have given the following results:

σ_c = 218 MPa, m_i = 15.

GSI = 65 gives:

m_b = 4.3 s = 0.020 a = 0.5 E_m = 23.7 GPa

GSI = 75 gives:

m_b = 6.14 s = 0.062 a = 0.5 E_m = 42.2 GPa

GSI = 85 gives:

m_b = 8.78 s = 0.189 a = 0.5 E_m = 75.0 GPa

The theoretical modelling results used for comparison are obtained on the diorite. The model was run for twenty realisations of the 2D fracture trace sections. The input parameters for the intact rock are presented in Table 6-1, and the mechanical properties of fractures in Table 6-2, assuming a residual friction angle of 30°. Each rock block model was run at three levels of confining stresses.

In Figure 6-2 the H-B envelopes are compared with the results from the theoretical approach for different fracture geometry at three levels of confining stresses. The Mohr-Coulomb envelope is obtained by linear regression of the theoretical modelling results. The calculated rock mass strength is in the same order as given by the empirical H-B relationships.

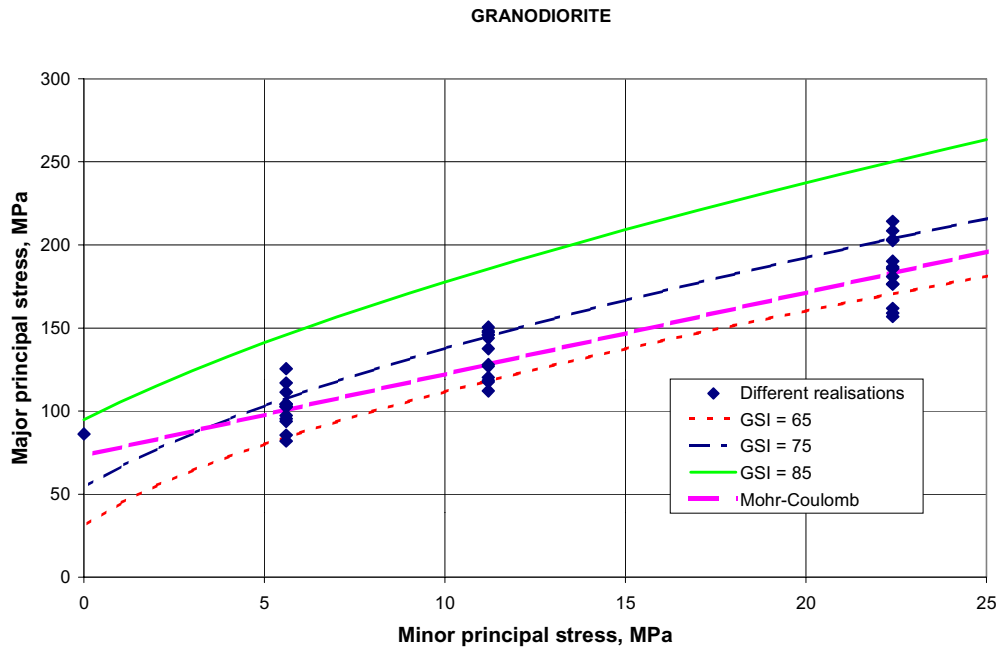

Figure 6-2. *H-B envelopes compared with results of the theoretical approach.*

In Figure 6-3 the deformation modulus, E_m, of the rock mass is compared to calculated results from the theoretical approach for different fracture geometry at three levels of confining stresses. The theoretical calculated values are in the same order as given by the empirical relationship /Hoek et al, 1995/. The calculated deformation modulus increases with the confining stress.

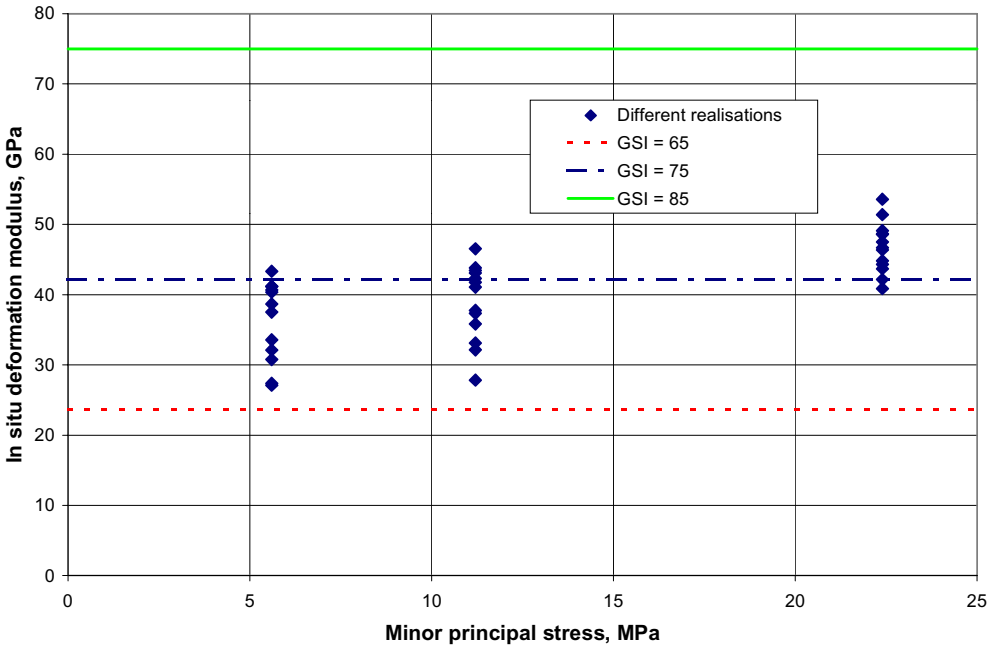

Figure 6-3. *The empirical estimated* in situ *deformation modulus compared with the results of the theoretical approach.*

6.5 Data uncertainty

With respect to these data, the simulations were first carried out on rock block models constituted of homogeneous rock types. For each rock type, at one depth level, simulations were run to check the influence of the rock fracture friction angle: 20 simulations were run on ϕ_r=30°, and then 1 simulation for respectively ϕ_r 25 and 35°. Then, for the same depth level, the same set-up of variation of parameters and number of simulations have been applied to conduct loading tests at a reduced horizontal stress (for a description of this test, see section 3.2.1).

Note: the 20 simulations run on the same set-up of parameters are related to 20 different simulations of the fracture pattern. The twenty 2D trace sections are obtained from 20 realisations of the 3D DFN model (see section 2.1.4). It should be noted that up to 30% of the simulations failed because of complex fracture patterns.

Data uncertainty resulting from all these simulations has been handled in different ways depending on the type of data.

The data uncertainty of the input parameters for the DFN model is managed through means and standard deviations of statistical functions. The influence of the spatial variability in the 3D model is estimated by running Monte Carlo simulations on the input parameters for the model. 20 different 3D models are then created, and the 2D trace sections files are extracted for each of these models. Then, 20 different rock block models are generated in UDEC and run, all other parameters remaining unchanged. The variability is then statistically determined from the results of the computations.

The data uncertainty related to input mechanical properties of intact rock and fractures is handled in two steps. First, all simulations are run by using the mean value for the parameters. The influence of one specific parameter, for example the friction angle of

fractures, is estimated by changing the value of this parameter, all other parameters being the same. Then, using the calculated influence of the parameter on the outcome of the mode in simplified Monte Carlo simulation, the influence of all parameters on the output data can be combined, see section 3.5.

The rock models in UDEC were always run assuming 100% of the same rock type. In order to estimate the discrepancies between the different rock types identified in the Test Case area, the simulations were realised 4 times, representing the four different rock types. However, the 30·30·30 m cubes are lithologically heterogeneous. The percentage of occurrence of each rock type in a cube can be estimated from borehole core mapping, see section 5.1.1. This distribution is used in a simplified Monte Carlo simulation to combine the output from the lithologically homogeneous models in a way to represent the probability of occurrence of the different rock types in the cubes, see section 3.5.

In addition to data uncertainty, it is necessary to describe the confidence in the model predictions. The confidence in a descriptive model is the total assembly of indications, motives and argument in support of the model. To have high confidence on the predictions does not imply that there is low uncertainty. However, if the uncertainty is poorly defined and founded, the confidence in the model will be low.

Three confidence levels were defined in the methodology that can be defined as followed:

- Confidence level 1 when predictions are supported by local data,
- Confidence level 2 when predictions are the result of interpolation and reasoning,
- Confidence level 3 when predictions are the result of guesswork.

According to the data made available for the Test Case, only two levels can be applied to this work. The confidence level is set to 1 for a rock block when a borehole or boreholes goes through it. The confidence level for all other blocks is set to 3.

7 Output data from the Test Case modelling

The outcome of the modelling is presented for each rock type in section 7.1 and for the deformation zones in section 7.2. In sections 7.3 and 7.4 these data are used and combined to evaluate the properties of the different blocks and cubes in the large and detailed geometrical models (see sections 4.1.1 and 4.1.2), taking into account the probability of occurrence of different rock types in the blocks and cubes, data uncertainty and spatial variability (see sections 6.5 and 3.5).

7.1 Rock mass properties for different rock types

The results of the calculations are summarised in Table 7-1 to Table 7-4. The mechanical properties of the fractured rock mass are presented for each rock type, assuming that the entire volume is constituted by the same rock. The results correspond to in situ stresses of depth level 4 (the deepest level in the target area), *i.e.* σ_H=22.4 MPa.

The rock mass deformation parameters and strength were evaluated according to the procedure described in sections 3.2.2 and 3.2.3. The value of the rock mass strength is valid for a specific interval of confining stress [5.6 MPa–22.4 MPa] and using the M-C failure criterion.

Table 7-1. Mechanical properties of a fractured rock mass in greenstones – depth level 4.

GREENSTONES	Mean value	Std Dev.
E_m, σ_H, GPa	34.3	9.3
ν_m, σ_H	0.24	0.02
E_m, $\sigma_{H/4}$, GPa	24.9	8.8
ν_m, $\sigma_{H/4}$	0.36	0.06
σ_{cm} , MPa	61.0	13.3
c_m, MPa	14.8	2.9
ϕ_{r_m}, ^{o}	38.0	2.7

Table 7-2. Mechanical properties of a fractured rock mass in granodiorite – depth level 4.

GRANODIORITE	Mean value	Std Dev.
E_m, σ_H, GPa	46.6	4.3
ν_m, σ_H	0.26	0.01
E_m, $\sigma_{H/4}$, GPa	36.0	5.9
ν_m, $\sigma_{H/4}$	0.37	0.04
σ_{cm} , MPa	73.3	16.4
c_m, MPa	16.4	3.3
ϕ_{r_m}, ^{o}	41.4	3.8

Table 7-3. Mechanical properties of a fractured rock mass in aplite – depth level 4.

APLITE	Mean value	Std Dev.
E_m, σ_H, GPa	41.1	4.1
ν_m, σ_H	0.23	0.02
E_m, $\sigma_{H/4}$, GPa	34.1	5.4
ν_m, $\sigma_{H/4}$	0.31	0.03
σ_{cm} , MPa	97.5	27.8
c_m, MPa	22.3	5.9
ϕ_{rm}, ^{o}	40.4	5.5

Table 7-4. Mechanical properties of a fractured rock mass in granite – depth level 4.

GRANITE	Mean value	Std Dev.
E_m, σ_H, GPa	40.3	3.0
ν_m, σ_H	0.24	0.02
E_m, $\sigma_{H/4}$, GPa	28.9	5.3
ν_m $\sigma_{H/4}$	0.39	0.04
σ_{cm} , MPa	95.0	37.4
c_m, MPa	22.5	8.2
ϕ_{rm}, ^{o}	38.6	4.5

with
- E_m Young's modulus of the rock mass
- ν_m Poisson's ratio of the rock mass
- σ_H Major horizontal stress
- σ_{cm} Compressive strength of the rock mass
- c_m Cohesion of the rock mass
- ϕ_{rm} Friction angle of the rock mass

The same type of tables are available for each rock type at the other depth levels, in this way taking into account the influence of stress dependency with depth on the mechanical properties of the rock mass. The comparison of properties for the same rock type but at different depth levels show an increase of the Young's modulus and of the rock mass strength with depth, see Table 7-5.

The same comparisons in the same range of values are made on the other rock types for the same depth levels.

Table 7-5. Young's modulus and rock mass strength at different depth levels, in the granodiorite.

GRANODIORITE	E_m, σ_H, GPa		σ_{cm} , MPa	
	Mean value	Std Dev.	Mean value	Std Dev.
Level 1 (–380/–410m)	43.3	4	50.3	11.2
Level 2 (–410/–440m)	44.4	4.1	57.6	12.9
Level 3 (–440/–470m)	45.5	4.2	64.8	14.5
Level 4 (–470/–500m)	46.6	4.3	73.3	16.4

7.2 Mechanical properties for deformation zones

The modelling results on deformation zones are presented in Table 7-6 to Table 7-9. The results are presented by deformation zone, assuming that the rock type distribution is the same in the entire zone (Table 5-15). The results correspond to in situ stresses of depth level 4 (the deepest level in the target area), *i.e.* σ_H=22.4 MPa.

The rock mass deformation parameters and strength were evaluated according to the procedure described in sections 3.2.2 and 3.2.3. The value of the rock mass strength is valid for a specific interval of confining stress [5.6 MPa–22.4 MPa] and using the M-C failure criterion.

Table 7-6. Mechanical properties for deformation zone EW-3, depth level 4.

EW-3	Mean value	Std Dev.
E_m, σ_H, GPa	15.54	1.86
ν_m, σ_H	0.08	0.007
E_m, $\sigma_{H/4}$, GPa	0.85	0.1
ν_m $\sigma_{H/4}$	0.45	0.05
σ_{cm} , MPa	0*	–
c_m, MPa	0	0
ϕ_{r_m}, ^{o}	26.8	3.21

Table 7-7. Mechanical properties for deformation zone NE-2, depth level 4.

NE-2	Mean value	Std Dev.
E_m, σ_H, GPa	35.43	4.35
ν_m, σ_H	0.31	0.026
E_m, $\sigma_{H/4}$, GPa	24.47	3
ν_m $\sigma_{H/4}$	0.42	0.04
σ_{cm} , MPa	56.1	20.44
c_m, MPa	13.41	4.7
ϕ_{r_m}, ^{o}	38.9	4.37

Table 7-8. Mechanical properties for deformation zone EW-1, depth level 4.

EW-1[(1)]	Mean value	Std Dev.
E_m, σ_H, GPa	13	1.56
ν_m, σ_H	0.35	0.03
E_m, $\sigma_{H/4}$, GPa	6.8	0.8
ν_m $\sigma_{H/4}$	0.58	0.063
σ_{cm} , MPa	47.4	17.31
c_m, MPa	11.8	4.14
ϕ_{r_m}, ^{o}	36.8	4.42

(1) Includes deformation zone EW-1a and EW-1b

Table 7-9. Mechanical properties for deformation zone NE-1, depth level 4.

NE-1	Mean value	Std Dev.
E_m, σ_H, GPa	4.5	0.4
ν_m, σ_H	0.11	0.009
E_m, $\sigma_{H/4}$, GPa	2.4	0.2
ν_m $\sigma_{H/4}$	0.34	0.037
σ_{cm} , MPa	0.5	0.2
c_m, MPa	0.2	0.07
ϕ_{r_m}, ^{o}	24.5	3

with E_m Young's modulus of the rock mass
ν_m Poisson's ratio of the rock mass
σ_H Major horizontal stress
σ_{cm} Compressive strength of the rock mass
c_m Cohesion of the rock mass
ϕ_{rm} Friction angle of the rock mass

7.3 Mechanical properties of the rock units in the 550 m model

According to the geometrical model /Hudson (ed.), 2002/, all "ordinary rock units" in the rock mass (rock unit type 1) have been assigned the same lithology, fracture network and mechanical properties for intact rock and fractures. Therefore, the same rock type distribution was applied to these blocks – A, G, H, I, L, and N, see Table 7-10. The values used were obtained by statistical analysis along the boreholes, and the procedure is described in section 5.1.1.

Table 7-10. Rock type distribution for the "ordinary rock units" (rock unit type 1).

	Granite	Granodiorite	Aplite	Greenstones
Distribution (%)	53.9	34.9	8.2	3

The rock type distribution in the "deformation zone units" was based on the information provided by the geologists, see section 5.4.3. A rough quantitative interpretation of the qualitative descriptions has been made in order to be able to assign mechanical properties to the material in the deformation zones (Table 7-11).

Table 7-11. Rock type distribution for "deformation zone units" (rock unit type 2).

	Granite	Granodiorite	Aplite	Greenstones	Block ID
EW-3	0	100	0	0	K
NE-2	0	90	10	0	J
EW-1	100	0	0	0	B, C, D, E, F
NE-1	0	90	10	0	M

The visualisation and localisation of the different "rock unit" types in the model are presented in Figure 4-4. The identification of the deformation zones in the models is presented in Figure 7-1.

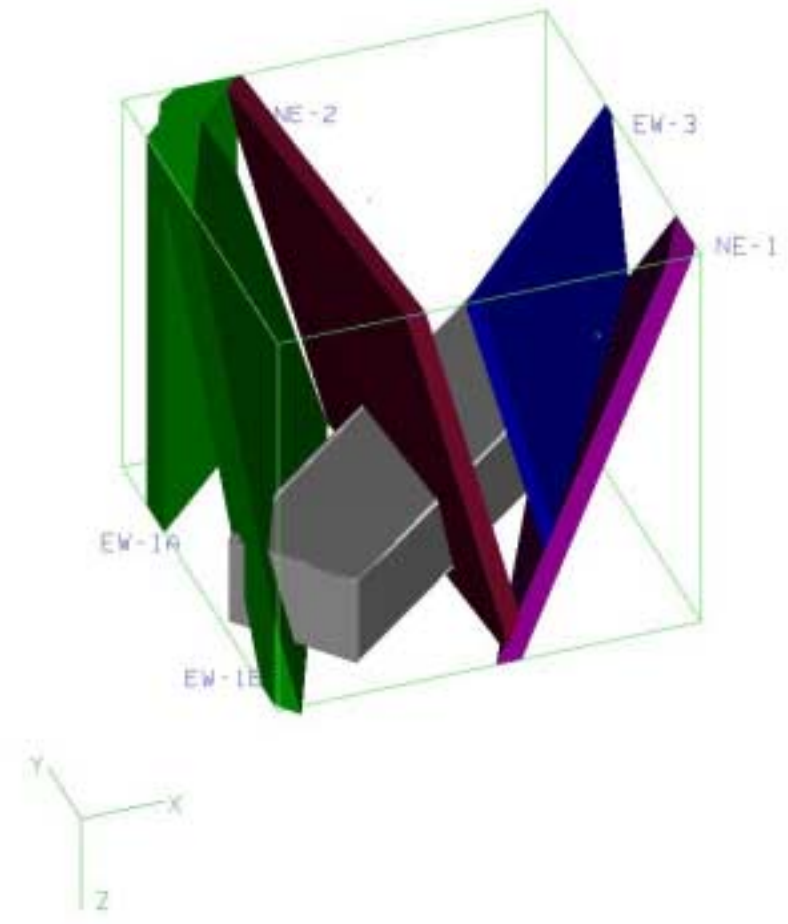

Figure 7-1. *Identification of the local deformation zones (X:East, Y: North). The grey box is the detailed model area.*

The estimated deformation properties of the different blocks are presented in Table 7-12 and the results of the strength properties in Table 7-13. The confidence levels have been assigned according to the definitions presented in section 6.5.

As illustrated in Figure 4-4, most of the blocks go from the surface to –550 m. This implies that the mechanical properties of the rock mass might change with depth and in relation to the increase in in situ stresses. The influence of depth and in situ stresses has been handled at the detailed model's scale, between –380 and –500 m, see section 7.1 and Table 7-5.

The mechanical properties of the blocks in the 550 m model were evaluated from properties presented in sections 7.1 and 7.2 by means of Monte Carlo simulations, see section 3.5. These mechanical properties are obtained for simulations run at a stress level corresponding to depth level 4, that means between –470 and –500 m. Hence, the interpretation of properties on the entire blocks, presented in Table 7-12 and Table 7-13, are based on properties established at depth of –470 to –500 m.

Using only these values for evaluating mechanical properties of the "rock units" might be a shortcoming of this methodology. An expectation might be to provide a relationship between variation of mechanical properties from the surface to –550 m depth. However the depth dependency of the deformation modulus is not a well-known relationship and its study was out of scope of this work, and would have required much more time and simulations.

Table 7-12. Deformation properties of the different blocks in the large model.

Block ID	Rock unit Type[(1)]	E_m (GPa)		ν_m		Confidence
		Mean	Std Dev.	Mean	Std Dev.	
A	1	42.46	5.08	0.25	0.02	3
B	2	13.01	1.56	0.35	0.03	3
C	2	13.01	1.56	0.35	0.03	3
D	2	13.01	1.56	0.35	0.03	3
E	2	13.01	1.56	0.35	0.03	3
F	2	13.01	1.56	0.35	0.03	3
G	1	42.46	5.08	0.25	0.02	1
H	1	42.46	5.08	0.25	0.02	1
I	1	42.46	5.08	0.25	0.02	1
J	2	35.43	4.35	0.31	0.026	3
K	2	15.54	1.86	0.08	0.007	3
L	1	42.46	5.08	0.25	0.02	3
M	2	4.5	0.4	0.11	0.009	3
N	1	42.46	5.08	0.25	0.02	3

(1) Rock unit type 1: "ordinary rock unit"; rock unit type 2: "deformation zone unit"

Table 7-13. Strength properties of the different rock units.

Block ID	Rock unit Type[(1)]	σ_{cm} (MPa)		c_m (MPa)		ϕ_{rm} (°)		Confidence
		Mean	Std Dev.	Mean	Std Dev.	Mean	Std Dev.	
A	1	86.9	32.57	20.2	7.30	39.7	4.50	3
B	2	47.4	17.31	11.8	4.14	36.8	4.42	3
C	2	47.4	17.31	11.8	4.14	36.8	4.42	3
D	2	47.4	17.31	11.8	4.14	36.8	4.42	3
E	2	47.4	17.31	11.8	4.14	36.8	4.42	3
F	2	47.4	17.31	11.8	4.14	36.8	4.42	3
G	1	86.9	32.57	20.2	7.30	39.7	4.50	1
H	1	86.9	32.57	20.2	7.30	39.7	4.50	1
I	1	86.9	32.57	20.2	7.30	39.7	4.50	1
J	2	56.1	20.44	13.41	4.7	38.9	4.37	3
K	2	0	–	0	0	26.8	3.21	3
L	1	86.9	32.57	20.2	7.30	39.7	4.50	3
M	2	0.5	0.2	0.2	0.07	24.5	3	3
N	1	86.9	32.57	20.2	7.30	39.7	4.50	3

(1) Rock unit type 1: "ordinary rock unit"; rock unit type 2: "deformation zone unit"

7.4 Mechanical properties of the rock units in the target area

The target area has been divided in 30·30·30 m cubes, distributed on four horizontal depth levels, see section 4.1.2. The localisation of the cubes is referred to by the centroid co-ordinates. A "rock unit" type is assigned to each cube and can be identified as rock mass or "ordinary rock unit" (rock unit type 1) or "deformation zone unit" (rock unit type 2). According to the geometrical model, some cubes can be identified as either "ordinary rock unit" or "deformation zone unit". In this case, predictions are presented for both "rock unit" types in the same cube, see section 4.1.2.

Cubes of type "deformation zone units" are those totally included or just crossed in the corner by the "deformation zone" representative volume, see Figure 7-2. All these cubes can also contain "ordinary rock units" and are assigned double predictions.

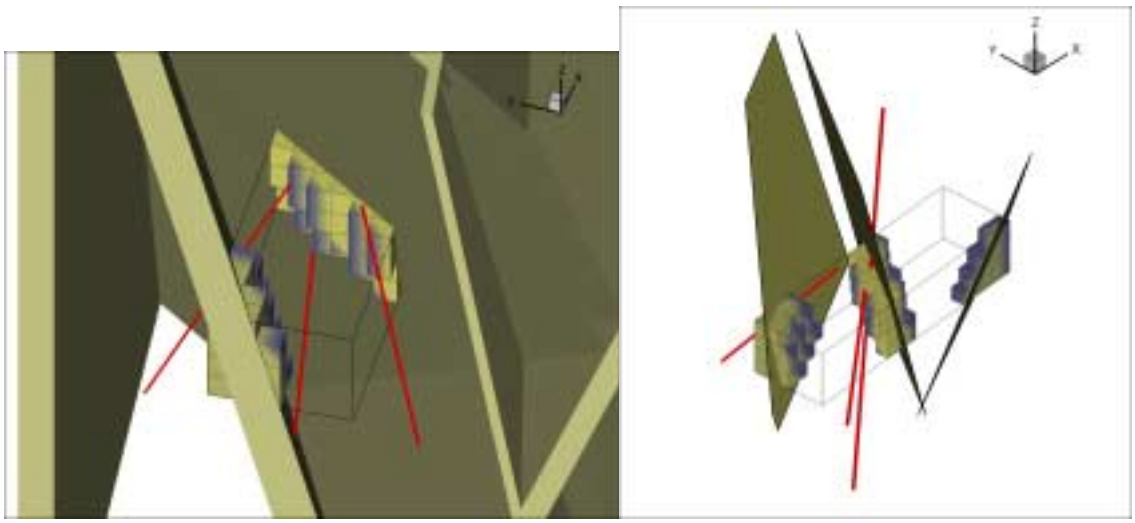

Figure 7-2. *3D views of the determination of the cubes intersected by deformation zones. A) Detail of the RVS model. B) Overview of the models with only "deformation zone unit" cubes enlighten. NB: deformation zones are then represented as planes with zero width.*

For the "ordinary rock unit", the nature of the intact rock has been defined from borehole core logging. When a borehole goes through a cube, the rock type distribution given by the core mapping inside the cube has been used, and given as a percentage of each rock type, see Table 7-14. For the other cubes, the statistical distribution as presented in section 3.1.1 is used for calculations, see Table 7-10.

For the "deformation zone unit", the rock type has been assigned on the basis of the geometrical model's report /Hudson (ed.), 2002/, and expressed as a percentage of each rock type (Table 7-14). The rock type distribution for "deformation zone units" is related to EW-1b for cubes 4 and 5, and to NE-2 for cubes 50, 170 and 290.

The predictions are presented in two sections depending on the degree of confidence on the data. Results for cubes of confidence level 1 are presented in section 7.4.1 and results for cubes of confidence level 3 in section 7.4.2.

The confidence levels were assigned according to the definitions in section 6.5. Figure 7-3 illustrates the 30 m cubes that will be assigned confidence 1, *i.e.* nine of the 420 cubes contained in the detailed model.

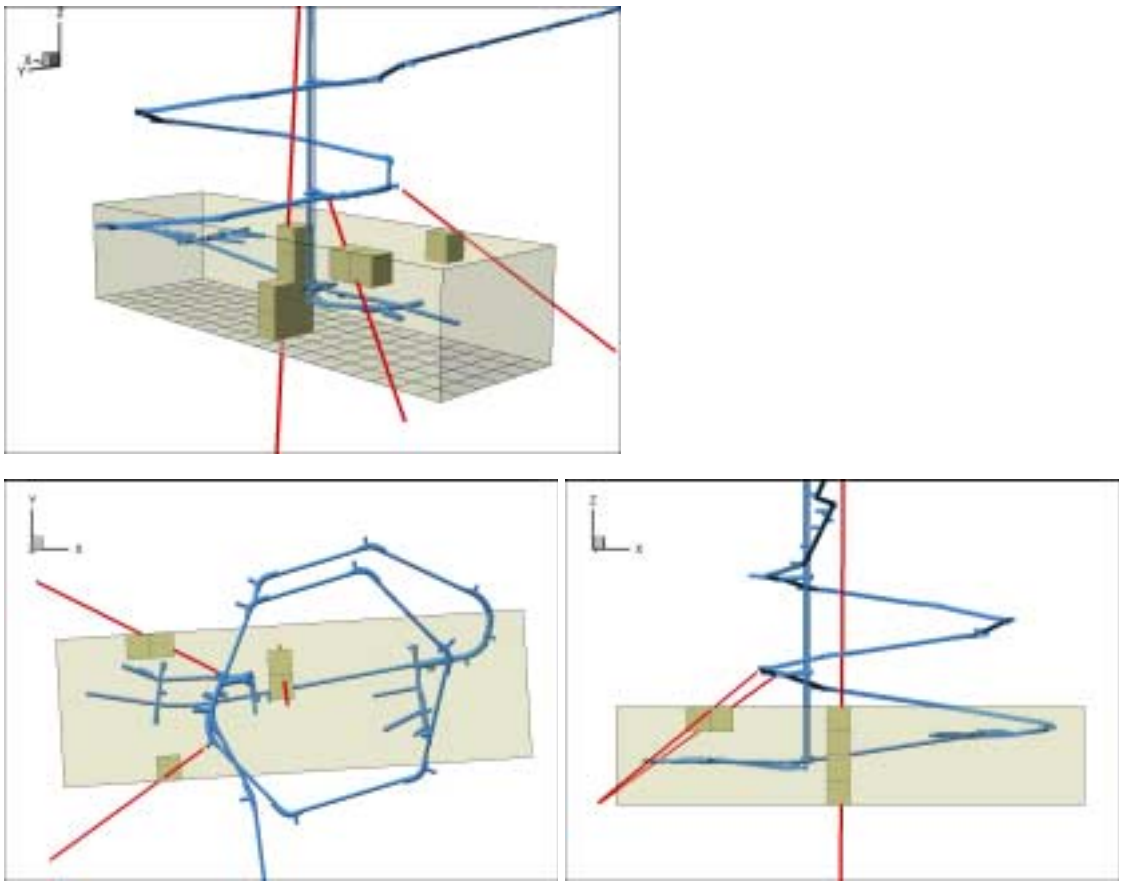

Figure 7-3. *3D perspective, top and profile views of the cubes of confidence 1 (X: East, Y: North).*

Figure 7-4 represents the spatial localisation of the 9 cubes of confidence level 1 on the four depth layers. All the other cubes are of confidence level 3.

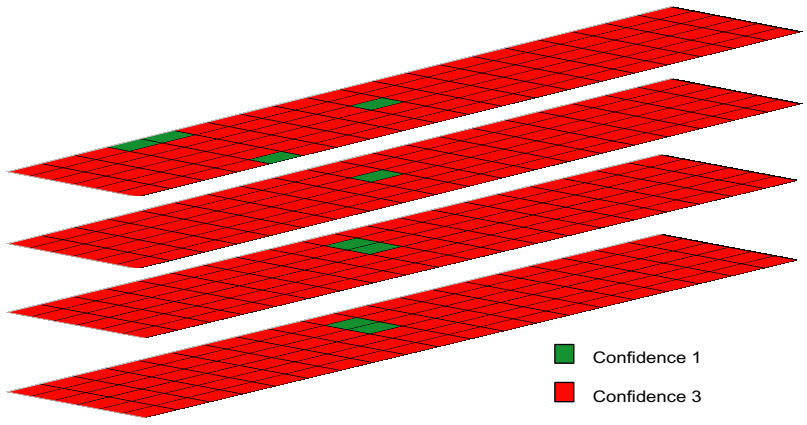

Figure 7-4. *Confidence levels for the cubes in the detailed model.*

7.4.1 Predictions for cubes of confidence level 1

Table 7-14 presents the rock type distribution in the different rock unit types for each cube of confidence 1.

Table 7-14. Rock type distribution in the cubes with confidence level 1.

Cube ID	Centrum co-ordinates (m)			Rock type distribution (%) Rock unit type 1[(1)]				Rock type distribution (%) Rock unit type 2[(1)]		
Nr	X	Y	Z	granite	diorite	aplite	greenstone	granite	diorite	aplite
4	1933.811	7333.952	–395	80.3	0	19.7	0	100	0	0
5	1963.755	7335.784	–395	80.3	0	19.7	0	100	0	0
50	2117.138	7285.053	–395	39.4	28.2	12.5	19.9	0	90	10
105	1972.912	7186.063	–395	0	88.3	11.7	0	–	–	–
170	2117.138	7285.053	–425	100	0	0	0	0	90	10
270	2115.307	7314.997	–455	22.5	75.9	1.7	0	0	90	10
290	2117.138	7285.053	–455	22.5	75.9	1.7	0	0	90	10
390	2115.307	7314.997	–485	0	100	0	0	–	–	–
410	2117.138	7285.053	–485	0	100	0	0	–	–	–

[(1)] 1: “ordinary rock unit”; 2: “deformation zone unit”

The localisation of the cubes in space is illustrated in Figure 7-5. Only the cubes with confidence 1 are numbered.

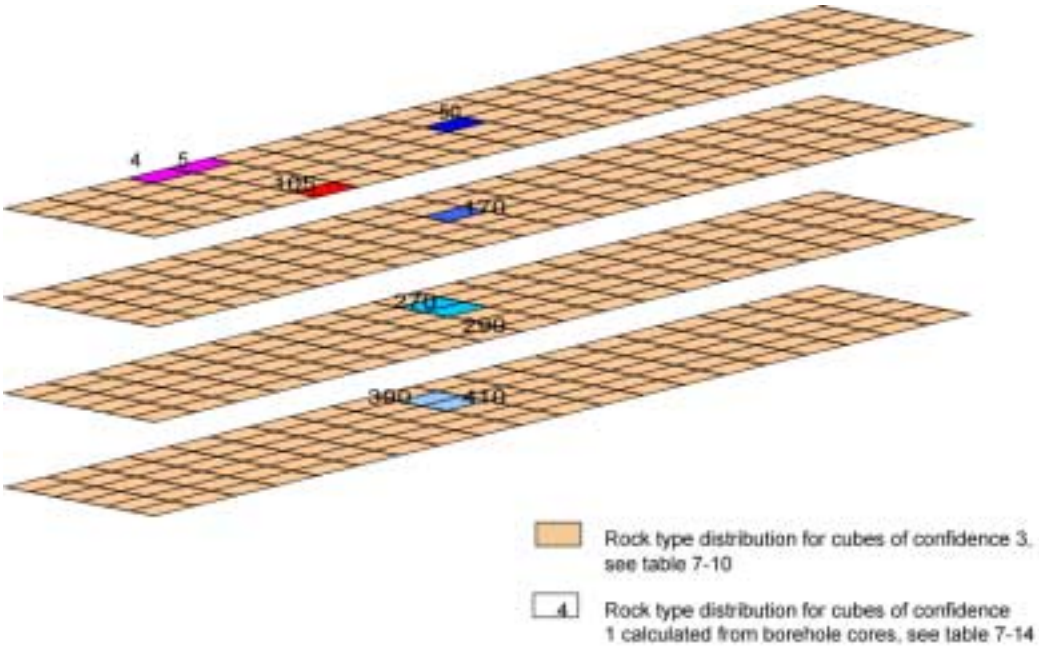

Figure 7-5. *Rock type distribution in the cubes of the detailed model.*

The simulations have been conducted according to the methodology presented in section 3 and with the parameters defined in sections 5 and 6. The mechanical properties of the cubes are the results of the combination of properties obtained for each rock type with respect to their probability of occurrence, see section 3.5. The results of the deformation properties of the different cubes with confidence level 1 are presented in Table 7-15 and Table 7-16, and the results of the strength properties in Table 7-17.

Table 7-15. Young's modulus for the cubes with confidence level 1.

		Centrum co-ordinates (m)			E_m (GPa)			
					σ_H [2]		$\sigma_{H/4}$	
Cube ID	Rock unit Type[1]	X	Y	Z	Mean	Std Dev.	Mean	Std Dev.
4	1	1933.811	7333.952	–395	38.8	3.61	15.95	3.37
	2				13.01	1.56	6.81	1.31
5	1	1963.755	7335.784	–395	38.8	3.61	15.95	3.37
	2				13.01	1.56	6.81	1.31
50	1	2117.138	7285.053	–395	39.22	6.13	18.15	6.15
	2				35.43	4.35	24.47	5.15
105	1	1972.912	7186.063	–395	42.57	4.38	24.13	4.26
170	1	2117.138	7285.053	–425	39.51	3.51	19.7	3.6
	2				35.43	4.35	24.47	5.15
270	1	2115.307	7314.997	–455	44.2	4.7	30.51	6.1
	2				35.43	4.35	24.47	5.15
290	1	2117.138	7285.053	–455	44.2	4.7	30.51	6.1
	2				35.43	4.35	24.47	5.15
390	1	2115.307	7314.997	–485	46.6	4.3	36	5.9
410	1	2117.138	7285.053	–485	46.6	4.3	36	5.9

[1] 1: "ordinary rock unit"; 2: "deformation zone unit"

[2] The values of σ_H are related to the depth level of each cube

Table 7-16. Poisson's ratio for the cubes with confidence level 1.

		Centrum co-ordinates (m)			ν_m			
					σ_H [2]		$\sigma_{H/4}$	
Cube ID	Rock unit Type[1]	X	Y	Z	Mean	Std Dev.	Mean	Std Dev.
4	1	1933.811	7333.952	–395	0.26	0.02	0.6	0.06
	2				0.35	0.03	0.58	0.08
5	1	1963.755	7335.784	–395	0.26	0.02	0.6	0.06
	2				0.35	0.03	0.58	0.08
50	1	2117.138	7285.053	–395	0.27	0.02	0.57	0.07
	2				0.31	0.02	0.42	0.06
105	1	1972.912	7186.063	–395	0.28	0.01	0.52	0.06
170	1	2117.138	7285.053	–425	0.25	0.02	0.54	0.06
	2				0.31	0.02	0.42	0.06
270	1	2115.307	7314.997	–455	0.26	0.02	0.43	0.05
	2				0.31	0.02	0.42	0.06
290	1	2117.138	7285.053	–455	0.26	0.02	0.43	0.05
	2				0.31	0.02	0.42	0.06
390	1	2115.307	7314.997	–485	0.26	0.01	0.37	0.04
410	1	2117.138	7285.053	–485	0.26	0.01	0.37	0.04

[1] 1: "ordinary rock unit"; 2: "deformation zone unit"

[2] The values of σ_H are related to the depth level of each cube

Table 7-17. Rock mass strength for the cubes with confidence level 1.

		Centrum co-ordinates (m)			σ_{cm} (MPa)		c_m (MPa)		ϕ_{rm} (°)	
Cube ID	Rock unit type[1]	X	Y	Z	Mean	Std Dev.	Mean	Std Dev.	Mean	Std Dev.
4	1	1933.811	7333.952	–395	78.4	29.5	19	6.5	38.9	4.7
	2				47.4	17.6	11.8	4.1	36.8	4.4
5	1	1963.755	7335.784	–395	78.4	29.5	19	6.5	38.9	4.7
	2				47.4	17.6	11.8	4.1	36.8	4.4
50	1	2117.138	7285.053	–395	63.9	27.8	14.9	6.5	40.3	4.5
	2				56.1	20.4	13.4	4.7	38.9	4.4
105	1	1972.912	7186.063	–395	54.7	18.4	12.1	4.2	42.4	4.3
170	1	2117.138	7285.053	–425	82.9	32.6	19.8	7.2	38.9	4.5
	2				56.1	20.4	13.4	4.7	38.9	4.4
270	1	2115.307	7314.997	–455	70.7	22.9	15.9	5.3	41.5	4.3
	2				56.1	20.4	13.4	4.7	38.9	4.4
290	1	2117.138	7285.053	–455	70.7	22.9	15.9	5.3	41.5	4.3
	2				56.1	20.4	13.4	4.7	38.9	4.4
390	1	2115.307	7314.997	–485	73.3	16.4	16.4	3.3	41.4	3.8
410	1	2117.138	7285.053	–485	73.3	16.4	16.4	3.3	41.4	3.8

[1] 1: “ordinary rock unit”; 2: “deformation zone unit”

7.4.2 Predictions for cubes of confidence level 3

All the other cubes have been assigned confidence level 3. The rock type distribution is then considered the same in all “ordinary rock units”, see Table 7-10 and Figure 7-5, and the rock type distribution in “deformation zone units” is the same as presented in Table 7-11. As a consequence, the properties are the same for all blocks of the same “rock unit” type on a same depth level (influence on in situ and confining stresses).

The results of the deformation properties of the different cubes with confidence level 3 are presented in Table 7-18 and Table 7-19. The results of the strength properties are shown in Table 7-20.

Table 7-18. Young’s modulus for the cubes with confidence level 3.

		E_m (GPa)			
		σ_H [2]		$\sigma_{H/4}$	
Cube ID	Rock unit Type[1]	Mean	Std Dev.	Mean	Std Dev.
Cubes without zones	1				
Depth level 1 (–395 m)	1	40.3	4.57	18.8	5.7
Depth level 2 (–425 m)	1	41	4.82	23.3	5.9
Depth level 3 (–455 m)	1	41.7	5	27.6	6.3
Depth level 4 (–485 m)	1	42.5	5.08	31.6	6.66
Cubes with zone EW-1	2	13	1.56	6.8	1.43
Cubes with zone NE-1	2	4.5	0.4	2.4	0.5
Cubes with zone NE-2	2	35.4	4.35	24.5	5.15

[1] 1: “ordinary rock unit”; 2: “deformation zone unit”

[2] The values of σ_H are related to the depth level of each cube

Table 7-19. Poisson's ratio for the cubes with confidence level 3.

		ν_m			
		σ_H [2]		$\sigma_{H/4}$	
Cube ID	Rock unit Type[1]	Mean	Std Dev.	Mean	Std Dev.
Cubes without zones	1				
Depth level 1 (–395 m)	1	0.27	0.02	0.57	0.08
Depth level 2 (–425 m)	1	0.26	0.02	0.51	0.07
Depth level 3 (–455 m)	1	0.06	0.02	0.44	0.06
Depth level 4 (–485 m)	1	0.25	0.02	0.38	0.05
Cubes with zone EW-1	2	0.35	0.03	0.58	0.08
Cubes with zone NE-1	2	0.1	0.01	0.3	0.03
Cubes with zone NE-2	2	0.31	0.02	0.42	0.06

[1] 1: "ordinary rock unit"; 2: "deformation zone unit"

[2] The values of σ_H are related to the depth level of each cube

Table 7-20. Rock mass strength for the cubes with confidence level 3.

		σ_{cm} (MPa)		c_m (MPa)		ϕ_{rm} (°)	
Cube ID	Rock unit Type[1]	Mean	Std Dev.	Mean	Std Dev.	Mean	Std Dev.
Cubes without zones	1						
Depth level 1 (–395 m)	1	67.17	28.21	15.81	6.62	40.11	4.78
Depth level 2 (–425 m)	1	73.65	29.43	17.1	6.6	40.2	6.5
Depth level 3 (–455 m)	1	80.36	31.3	18.6	7.11	40.4	4.6
Depth level 4 (–485 m)	1	86.9	32.57	20.2	7.3	39.7	4.5
Cubes with zone EW-1	2	47.4	17.31	11.8	4.14	36.8	4.42
Cubes with zone NE-1	2	0.5	0.2	0.2	0.07	24.5	3
Cubes with zone NE-2	2	56.1	20.44	13.41	4.7	38.9	4.37

[1] 1: "ordinary rock unit"; 2: "deformation zone unit"

The results of the theoretical approach are discussed and compared to two empirical approaches, one developed on the same restricted set of input data, and one using all available data in the model volume /Hudson (ed.), 2002/.

8 Discussion

8.1 Input parameters

8.1.1 Deformation zones and fracture pattern

The DFN model provided for the Test Case was developed for other applications, and might not be the best suited for the Test Case. Fracture data for this model were collected on the Zedex tunnel, and defines the local fracturing in the surrounding of the tunnel.

In this model no special attention was paid to deformation zones. However, five major deformation zones are going through the models, and the "deformation zone units" they define must be considered separately. Indeed, fracture frequency and fracture orientation might be different in the core of the deformation zones, and in the volume surrounding these zones. Therefore the provided DFN model can not be used to simulate the fracturing in the deformation zones.

In order to simulate the fracture pattern in the deformation zones for the Test Case, some assumptions based on qualitative descriptions were made to define simplified fracture networks in the zones.

8.1.2 Mechanical properties for intact rock and fractures

The characterisation of the properties of the intact rock is not complete because tests were not provided for all rock types. Moreover, the samples were located in a relatively confined volume compared to the model volume. The spatial variability might then be underestimated.

Different results were provided in two different reports for the same laboratory test on the same rock type. In order to define input parameters for the simulations, the appropriate values were chosen on the basis of engineering expertise on rock mass properties.

8.2 Methodology

The numerical code used is not optimal for the methodology. The automatic block generation in UDEC removes fractures ending in the rock mass, and a lot of manual work needed to be done on the input data in order to create the appropriate rock block model. Special work was particularly required for the assignment of different mechanical properties to different sets of fractures.

8.3 Results

The validity of the estimations of the rock mass mechanical properties produced by the theoretical model is discussed in Hudson ed. 2002, where both theoretical and empirical models are analysed.

9 Conclusions and further recommendations

For future modelling work the following conclusions can be drawn from the tests presented in this report:

Regarding input data

- All laboratory and field-testing must be done according to standards or methods recommended by SKB and done by laboratories accepted by SKB.
- The samples for testing must be spread over the volume to get an estimation of the spatial variability of the parameters.
- Special DFN models must be set up for the deformation zones.
- The spatial variability (especially versus depth) must be studied for each parameter to see if it is necessary to divide the rock units from the geometrical model.

Regarding developing of the methodology

- In order to assure the quality and reliability of the developed methodology and of the modelling output comparisons should be made with other modelling codes that can simulate the behaviour of fractured rock masses.
- The automatic block generation procedure in UDEC must be developed further to include all fracture traces even fractures ending inside blocks.
- The procedure for assigning material properties to specific fractures or fracture sets must be further developed in UDEC.
- Further comparisons with 3D modelling are recommended.
- The stress dependency with depth of the mechanical properties, especially the deformation modulus for the rock mass, could be further studied.
- Complementary methods, such as kriging, could be studied to evaluate data uncertainty and spatial variability.
- The methodology has been applied on one specific type of rock mass. In order to test the domain of applicability of the methodology, other combinations of DFN models, rock types and mechanical properties should be studied and compared to empirical experiences.

10 References

Andersson J, Almén K-E, Ericsson L O, Fredriksson A, Karlsson F, Stranfors R, Ström A, 1998. Parameters of importance to determine during geoscientific site investigation. SKB Technical Report TR-98-02, Stockholm, Sweden.

Andersson J, Ström A, Svemar C, Almén K-E, Ericsson L O, 2000. What requirements does the KBS-3 repository make on the host rock? Geoscientific suitability indicators and criteria for siting and site evaluation. SKB Technical Report TR 00-12, Stockholm, Sweden.

Andersson J, Christiansson R, Hudson J A, 2002. Site Investigations. Strategy for Development of a Desriptive Rock Mechanics Model, SKB Technical Report TR 02-01, Stockholm, Sweden.

Bandis S C, Barton N R, Christianson M, 1985. Application of a New Numerical Model of Joint Behaviour to Rock Mechanics Problems, in Fundamentals of Rock Joints. Proceedings of the International Symposium on Fundamentals of Rock Joints, Björkliden, September 1985, pp. 345–356. Luleå, Sweden: Centek Publishers.

Barton N, Lien R, Lunde J, 1974. Engineering classification of rock masses for the design of tunnel support. Rock Mech., 6(4), pp.189–239.

Barton N, 1982. Modelling Rock Joint Behaviour from In-Situ Block Tests: Implications for Nuclear Waste Repository Design, ONWI-308, September.

Bieniawski Z T, 1989. Engineering rock mass classification. New York, Wiley sciences.

Cundall P A, Hart R D, 1984. Analysis of Block Test No.1 Inelastic Rock Masshavior: Phase 2 – A Characterization of Joint behaviour. Itasca Consulting Group Report, Rockwell Hanford Operations, Subcontract SA-957.

Dershowitz W S, Herda H, 1992. Interpretation of fracture spacing and intensity. Proceedings, 32nd US Rock Mechanics Symposium, Santa Fe, New Mexico.

Dershowitz W S, Lee G, Geier J, Foxford T, LaPointe P, Thomas A, 1998. FracMan Version2.6 Interactive Discrete Feature data Analysis, Geometric Modeling, and Exploration Simulation, user documentation, Report 923-1089, Golder Associates Inc, Seattle, Washington.

Gupta A S, Rao K S, 2001. Weathering indices and their applicability for crystalline rocks. Bulletin of Engineering Geology and the Environment, vol 60, no 3 aug 2001.

Hakami E, Hakami H, Cosgrove J, 2002. Strategy for Development of a Desriptive Rock Mechanics Model, Development and testing of an Approach to modelling the State of Stress. SKB Report R 02-03, Stockholm, Sweden.

Hermansson J, Stiggson M, Wei L, 1998. A Discrete Fracture Network model of the Äspö Zedex tunnel section. SKB Progress Report PR-HRL-98-29, Stockholm, Sweden.

Hoek E, Kaiser P K, Bawden W F, 1995. Support of Underground Excavations in Hard Rock. Balkema, Rotterdam.

Hoek E, Brown E T, 1997. Practical estimates of rock mass strength. International Journal of Rock Mechanics and Mining Sciences, Vol 34, No 8, pp. 1165–1186.

Hudson J A (ed.), 2002. Strategy for Development of a Desriptive Rock Mechanics Model. A Test Case based on data from Äspö HRL. SKB Report R 02-04, Stockholm, Sweden.

ISRM, 1983. International Society for Rock Mechanics. Commission on standardization of Laboratory and Field Testing. Suggested method for determining the strength of rock materials in triaxial compression: revised version. Int. J. of Rock Mechanics and Mining Sciences & Geomech. Abstracts. Vol 20 No. 6 pp. 283–290, 1983.

ISRM, 1999. International Society for Rock Mechanics. Commission on Testing Methods. Draft ISRM suggested method for the complete stress – strain curve for intact rock in uniaxial compression. Int. J. of Rock Mechanics and Mining Sciences. 36 (1999) 279–289.

Lanaro F, 2001. Determination of the normal and shear stiffness of rock joints: geometry, normal and shear stiffness. SKB, Technical report, under publication, Stockholm, Sweden.

Makurat A, Löset F, Wold Hagen A, Tunbridge L, Kveldsvik V, Grimstad E, 2002. Äspö HRL – A Descriptive Rock Mechanics Model for the 380-500 m level. SKB Report R-02-11, Stockholm, Sweden.

Marinos P, Hoek E, 2000. GSI: A geologically friendly tool for rock mass strength estimation. GeoEng. 2000. An Int. Conf. on geotechnical and geological engineering, Melbourne, Nov. 2000, Proc. Vol.1, pp.1422–1440.

Martin D R, Christiansson R, Söderhäll J, 2001. Rock stability considerations for Siting and Constructing a KBS-3, Repository: Based on experiences from Äspö HRL, AECL´s URL, tunneling and mining. SKB Technical Report TR-01-38, Stockholm, Sweden.

Munier R, 1995. Studies of geological structures at Äspö. Comprehensive summary of results. SKB, Progress Report 25-95-21, Stockholm, Sweden.

Nisca D H, 1988. Geophysical laboratory measurements on core samples from KLX01, Laxemar and KAS02, Äspö. SKB Progress Report PR 25-88-06, Stockholm, Sweden.

Nordlund E, Li C, Larsson B, 1999. Mechanical properties of the diorite in the prototype repository at Äspö HRL. SKB, International Progress Report IPR-99-25, Stockholm, Sweden.

Röshoff K, Lanaro F, Jing L, 2002. Strategy for Development of a Desriptive Rock Mechanics Model, Development and testing of the Empirical Approach. SKB Report R 02-01, Stockholm, Sweden.

SKB, 2000. Äspö Hard Rock Laboratory, Annual report 1999, SKB Technical Report TR-00-10, Stockholm, Sweden.

SKB, 2001a. Site Investigations. Investigation methods and general execution programme, SKB Technical Report TR-01-29, Stockholm, Sweden.

SKB, 2001b. Platsundersökningar – Undersökningsmetoder och generellt genomförandeprogram. SKB Report R-01-10, januari 2001, Stockholm, Sweden.

Stille H, Olsson P, 1989. First evaluation of rock mechanics. SKB, Progress Report 25-89-07, Stockholm, Sweden.

Sundberg J, Gabrielsson A, 1999. Äspö Hard Rock Laboratory – Laboratory and field measurements of thermal properties of the rocks in the prototype repository at Äspö HRL. SKB International Progress Report IPR-99-17, Stockholm, Sweden.

Tirén S A, Beckholmen M, 1987. Structural analysis of contoured maps Äspö and Ävrö, Simpevarp area, Southeastern Sweden. SKB Progress Report 25-87-22, Stockholm, Sweden.

UDEC, 2000a. Universal Distinct Element Code. Theory and Background. Itasca Consulting Group, Inc. Minneapolis.

UDEC, 2000b. Universal Distinct Element Code. Special Features. Itasca Consulting Group, Inc. Minneapolis.

Appendix A

Models for the Geometry of Fractures

Introduction to Discrete Fracture Network

Isabelle Staub

Golder Associates AB

May 2002

Contents

1 Introduction

Two terms are mainly used in the reviewed literature: fractures and joints. According to the technical terminology, the English term “fracture” is a general word used to define mechanical breaks in a rock mass, which implies any kind of discontinuity such as joints, fissures, faults and cracks. Nevertheless, the term does not refer in any way to the mode of rupture. On the other hand, the term “joints” is used to describe a discontinuity in the rock mass along which there had been no visible movement parallel to the plane.

According to the aforementioned definitions, the term “fracture(s)” would be the most appropriate as all natural fractures must be considered to build a model of the fractured rock mass. Anyhow, the term “joints” has been kept in some specific cases when quoting authors that used the same term.

Moreover, using the term fractures is in accordance to the SKB’s classification that has been developed in order to get unambiguous terminology during site investigation. This specific classification and naming of fractures has been based on the length and width of the fractures /Andersson et al, 2000/. One might then talk of regional fracture zone, local major fracture zone, local minor fracture zones or fractures.

The term “fracture” as used in this report and in the SKB’s classification is a general description of a structural feature. Further information on fracture zones and fractures are needed to understand the structural context and build the model.

1.1 Background

Geometric and mechanical characteristics of rock fractures are the basis for most of the work of engineering geologists. However, the complete description of fractures is difficult because of their 3-D nature and their limited, most often 2D, exposure in outcrops, boreholes and tunnels. An ideal characterization of the fracturation network would involve the specific description of each fracture in the rock mass, exactly defining its geometric and mechanic properties /Dershowitz and Einstein, 1988/. This is not possible for a number of reasons: 1) the visible part of fractures are limited, for instance to fracture traces only; 2) fractures at a distance from the exposed rock surfaces cannot be observed directly; 3) direct and indirect measurements have local accuracy. For that reasons fractures in a rock mass are usually described as an assemblage rather than individually.

1.2 Properties of fractures – a short review

The geometric characteristic of fractures that are necessary to describe the rock mass can be divided into primary and secondary characteristics /Dershowitz, 1984/:

Primary Geometric Fracture Characteristics

- Fracture shape and planarity
- Fracture size
- Fracture location and spacing
- Fracture orientation (attitude)
- Aperture

Secondary Geometric Fracture Characteristics

- Fracture termination
- Autocorrelation and correlation

The primary characteristics completely define the fracture system. The secondary characteristics are not necessary for the system identification but provide a better idea of correlation between the primary characteristics.

1.3 Characterisation of the fractures in the rock mass

Two major approaches have been tried in order to describe the assemblage of geometric fracture characteristics in a rock mass: the traditional disaggregate characterisation and the more recent aggregate characterisation /Dershowitz and Einstein, 1988/. In the former, each fracture characteristic is described separately, for instance through orientation distributions, spacing distributions and others. In the latter the interdependence of fracture characteristics is captured through the formulation of fracture system models. A particular fracture system model represents a typical geometry. The individual characteristics are still stochastic but their interdependence is specified.

1.3.1 Disaggregate characterisation

This is the traditional procedure developed by structural and engineering geologists and involves the application of statistical procedures to characterise fracture orientations. This approach is meant to define distribution forms of the geometric parameters, as listed above, in order to fit them with the observation and measurement data. In this way, it constitutes a basis for the further development of rock fracture system models. A short review of the distribution forms for use is presented.

Fracture shape

This parameter is most often assumed to be constant within a model. Anyhow, /Veneziano, 1978/ presented a model with stochastic distribution of fracture shape (the form of the distribution is not known, only the moments are).

Fracture size

The determination of fracture size is the result of an interpolation of 2D observation data to 3D data. Three main distribution forms have been identified and developed /Dershowitz, 1984/:

- Exponential form for trace length distribution (insert equations)
- Lognormal distribution
- Hyperbolically shaped distributional form

Fracture location

Results in 3D are extrapolated from 2D data. Three stochastic processes have been proposed:

- The most commonly accepted is the Poisson process, in which the fracture network is simulated by a uniform distribution. This process will produce an exponential distribution of fractures along a sampling line in any direction.
- The second process is based on a distribution of fracture centers such that fracture spacings along a sampling line follow a lognormal distribution.
- The third process is a stationary correlated stochastic process; the location of fractures is correlated to the location of other fractures, but the distribution in space is homogeneous and the process is considered independent along x, y and z.

Fracture orientation

This parameter is represented by the dip and dip angle. According to studies carried out by /Dershowitz, 1979/, no distribution form fit the data at a confidence of 95%. Nevertheless, distributions such as Fisher, Bingham, bivariate Fisher and bivariate Bingham can be used to represent fracture orientation.

The most commom for use is the Fisher distribution because it is the analog of the normal distribution for fracture data, and because of the ease to derive parameters from field data.

This approach, which “disaggregates” the rock mass and studies each geometric characteristic apart of the other, can not account for a good determination of autocorrelation and correlation for the different characteristics. However, the distributional forms provided can be used in conjunction with assumption on fracture geometry and spatial structure to develop rock fracture systems.

1.3.2 Aggregate characterization / Fracture system models

The aggregate characterization of rock fracture geometry through fracture system models is an attempt to describe primary and secondary fracture characteristics as an entity. The use of this approach is more a complement to the previous one than a substitute /Dershowitz, 1984/.

Since there are so many geometric fracture characteristics and thus a seemingly infinite number of combinations, one could produce a corresponding number of fracture system models. On the other hand, reality shows a relatively limited number of predominant rock mass geometries /Pollard and Aydin, 1988/.

Mainly three ”classes” are developed to compare the geometry of fracture systems, which are persistence, connectivity and block size /Dershowitz, 1984/.

- Persistence: it specifies the intensity of fracturing, i.e. the quantity of fractures within a given rock mass. This parameter is interesting to compare the amount of fracturing in different rock masses.

- Connectivity: it quantifies intersection between fractures within a given rock mass, and identifies the resulting networks. This is specifically of importance for hydrogeological applications.

- Block size: it defines the size of the blocks of intact rock defined by the fracture system. This parameter is preferred than fracture intensity for slope stability assessments.

The differences between conceptual models is accounted for the different models and/or combination of models chosen for parameters: model for fracture shape, model for location of sets, termination mode (does it exist, and what type of mode), model for fracture size (bounded or unbounded).

The aggregate measures can be developed and implemented for every rock fracture system model, and so, for different combinations of fracture system geometric characteristics.

2 Discrete Fracture Network (DFN) models

2.1 Fracture network models

Mainly three approaches have been developed to simulate fracture network geometry and transport. These are the Discrete Fracture Network (DFN) Model, the Stochastic Continuum (SC) Model and the Channel Network (CN) Model. The choice of an appropriate conceptual model depends on the phenomena of interest. Amongst the different approaches developed to characterize fracture networks, studies show that the discrete fracture network (DFN) model is the most appropriate to simulate realistic geological representation than other models /Dershowitz et al, 1996/. The SC and CN models are more suited for the modelling of groundwater flow and transport in fractured rocks. Therefore this review focused on the different conceptual models developed for simulation of Discrete Fracture Network.

2.2 Development of the DFN models

Various conceptual models have been used to provide the geometry of discrete fracture networks. The first comment is that the different models have first been developed to simulate a specified fracture network and hence their utilization might be restricted to rock masses showing the same pattern. However, some generalizations of the primary models have been performed in order to simulate different pattern schemes.

The classification of the conceptual models that have been developed is not so trivial. Indeed, few models are well recognized and identified in the literature, and the consistency of the data is sometimes difficult to assess. This review is an attempt to make a synoptic chart flow of the conceptual models that might be of use for the development of a rock mechanic model for the repository.

3 Presentation of the main used DFN models

/Dershowitz and Einstein, 1988/ reviewed the main used and known conceptual DFN models (Table 3-1). The development of each model is based on specific relationships between characteristics such as location of fracture sets, termination, and fracture shape. Each model consists of a particular combination of the rock system characteristics. By capturing the relationships of fracture characteristics, "joint system models" can represent rock mass geometry as an entity.

Table 3-1. "Joint system models" /Dershowitz and Einstein, 1988/.

Model	Joint characteristics considered in model				
	Joint Shape	Joint Size	Termination at intersection	Co-planarity	Orientation of sets
Orthogonal	Rectangle	Bounded Unbounded Unbounded	No yes no	– yes yes	Parallel Parallel Parallel
Baecher	Circle Ellipse	Bounded	no	no	Stochastic
Veneziano	Polygon	Bounded	In joint planes only	yes	Stochastic
Dershowitz	Polygon	Bounded	yes	yes	Stochastic
Mosaic Tessellation	Polygon	Bounded	yes	yes	Regular Stochastic

Note: For all models, fractures are planar, and any location or autocorrelation process is possible. Joint locations are usually stochastic. Bounding of fractures implies that fractures smaller than the region under consideration can be represented. –Joint sizes are usually stochastic either specified directly or indirectly through stochastic location or orientation. Any component characteristic specified as being stochastic may also be deterministic.

Beside these, some other interesting conceptual models can be accounted for the modelling of fractures' geometry, such as geostatistical models and fractal models. A short review of the main assumptions, statistical approaches and applicability of these models is presented in the following. The joint system model's table (Table 3-1) has been implemented by adding these conceptual models and reviewing the main fracture characteristics considered in the models (Table 3-2).

Table 3-2. Main features of the fracture system models.

Model	Stationarity	Fracture characteristics considered in model					
		Fracture Shape	Fracture Size	Termination at intersection	Co-planarity	Orientation of sets	Location of sets
Orthogonal	Stationary	Rectangle Rectangle Rectangle	Bounded Unbounded Unbounded	no yes no	- yes yes	Parallel Parallel Parallel	Deterministic / Stochastic (Poisson location model)
Disk Baecher	Stationary	Circle	Bounded	no	no	Regular / Stochastic	Deterministic / Stochastic (Poisson location model)
Veneziano	Stationary	Polygon	Bounded	In joint planes only	yes	Stochastic	Uniform distribution (Poisson planes and lines)
Dershowitz	Stationary	Polygon	Bounded	yes	yes	Stochastic (specified distribution)	Uniform distribution (Poisson planes)
Mosaic Tessellation	Stationary	Polygon	Bounded	yes	yes	Regular Stochastic	Tessellation models (based on Poisson models)
Enhanced Baecher	Stationary	Polygon	Bounded	yes	no	Stochastic	Uniform distribution
BART	Non-stationary	Polygon	Bounded	yes	no	Stochastic	model
Poisson Rectangle	Stationary	Rectangle	Bounded	yes	no	Stochastic	Uniform distribution
Box Fractal model	Non-stationary	Polygon	Bounded	yes	no	Stochastic (random)	Fractal location model
Geostatistical	Non-stationary	Polygon	Bounded	yes	no	Stochastic	Geostatistic (variogram)
War Zone	Non-stationary	Polygon	Bounded	yes	no	Stochastic	Binary models
Non-Planar Zone	Non-stationary	Polygon	Bounded	yes	yes	Binary	Binary models
Levy-Lee Fractal	Non-stationary	Polygon	Bounded	yes	no	Stochastic	Fractal location model
Nearest-neighbor	Non-stationary	Polygon	Bounded	yes	no	Stochastic	Probabilistic
Fractal POCS model	Non-stationary	Polygon	Bounded	yes	no	Stochastic	Fractal location model

3.1 Orthogonal model

The earliest model developed to represent fracture systems were based upon the assumption that all fractures can be defined by three sets of unbounded orthogonal fractures /Dershowitz and Einstein, 1988/. The distinguishing feature is the assumption that the fractures are contained in two or three mutually orthogonal set of parallel fractures (Figure 3-1).

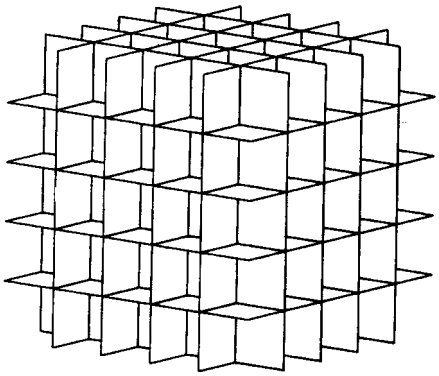

Figure 3-1. *Three-dimensional orthogonal model /Dershowitz and Einstein, 1988/.*

The basic model defined by /Snow, 1965/ consists of orthogonal sets of parallel unbounded fractures, with a constant spacing between the fractures within each set. In that way, the model is completely defined by only one parameter, the mean spacing between fractures in each set. The assumption of constant fracture spacing S_j can be relaxed, and replaced by an assumption for fracture location. The most common assumption is that fractures in each set are located by a Poisson process. In this case, the location of fractures can still be described by the distance between fractures in each set, defined by spacing S_j, with S_j now a random variable. For a Poisson process with intensity parameter λ, the spacing between fractures is exponential:

$$f\left(S_j\right) = \lambda e^{-\lambda S_j} \tag{3.1}$$

Orthogonal fracture models may also be defined by bounded fractures (Figure 3-2). /Müller, 1963/ introduced a version of the orthogonal fracture model for rock mechanics applications in which fractures are defined as coplanar on fracture planes.When fractures are bounded, it is necessary to define fracture shapes, sizes and termination processes.

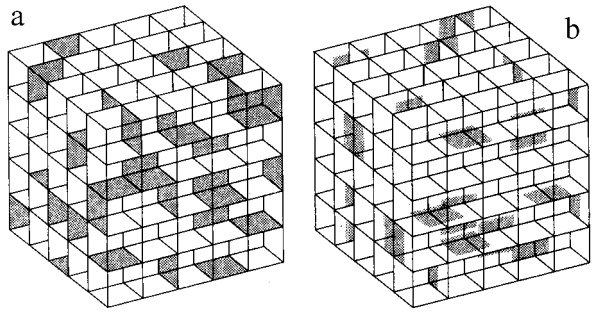

Figure 3-2. *"Definition of bounded fractures in orthogonal system models. (a) Joint defined by joint plane intersections; (b) Joints defined without respect to joint plane intersections" /Dershowitz and Einstein, 1988/.*

Applicability: The most fundamental assumption of the orthogonal model is that it consists of three mutually perpendicular sets of parallel fractures. As a consequence of this assumption, rock blocks are all rectangular prisms. Natural fracture network patterns involve substantial scatter in fracture orientation, and the orthogonal model does not seem to be the best suited to model them. However, simulations performed by /Weiss, 1972/ provided a reasonable approximation for many fracture networks in which most blocks can be approximated by rectangular prisms.

By definition of the orthogonal fracture system model, only very minor variations in fracture orientation are permissible. As a result, this model is only appropriate where fracture formation processes are sufficiently regular as to produce subparallel jointing. Complicated mechanisms such as complex folding, subsequent shearing, or superposition of other fracture sets could introduce sufficient dispersion so as to make the orthogonal fracture system model inappropriate. The planar fracture assumption is also a significant limitation of the model.

3.2 Baecher disk model

This model has been developed by /Baecher et al, 1978/ and simultaneously by /Barton, 1978/, and was one of the first well-characterised discrete fracture models. The appropriate geometric parameters used to describe the fracture network are therefore the density of the fractures (number of fractures per unit volume), the orientation distribution of these fractures, the size and shape of the fractures, and the equivalent hydraulic apertures /Long and Billaux, 1987/.

Any combination of fracture size, location, and orientation assumptions are possible.

The fundamental feature of the ordinary model is the assumption of circular fracture shapes.

In the ordinary Baecher model, the fracture centres are located uniformly in space, using a Poisson process and the fractures are generated as disks with a given radius and orientation.

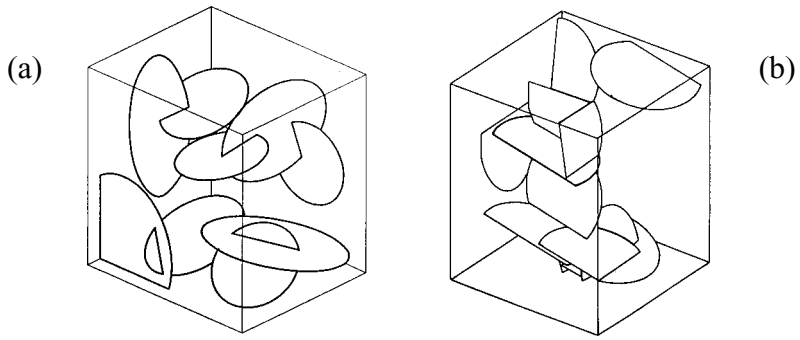

Figure 3-3. *Comparison of (a) the general Baecher model with (b) the Enhanced Baecher model /Geier et al, 1989/.*

The size of circular fractures are defined completely by one parameter, the fracture radius R_j. Fracture radius may be defined deterministically, as a constant for all fractures, or stochastically by a distribution of radii $f_r(R_j)$. Since fracture radii distributions have not been distributed in situ, the selection of a distribution form is primarily a matter of convenience. Appropriate distribution forms include the exponential and lognormal distributions of fracture trace length.

Fracture location may be defined by a regular (deterministic) pattern or a stochastic process. The simplest stochastic assumption is a Poisson process, in which fracture centres are located by a uniform distribution in space. Fracture orientations may also be defined by any orientation distribution, or by a constant orientation /Dershowitz and Einstein, 1988/. As a result of the fracture location, shape and size process of the model, fractures terminate in intact rock and intersect each other as shown on the Figure 3-3a.

Applicability: Such circular fracture shapes have been observed and many documented cases exist and can be explained from a fracture mechanics' point of view. Anyhow, disk shaped fractures can only form blocks if they are large compared to the region under consideration. Thus the often observed blocky appearance of rock masses implies either that the fractures are not disk shaped or, if they are disks, that they are greater than the visible part of the rock mass. Another restriction is the fact that fractures have to be planar.

3.3 Enhanced Baecher model

The ordinary Baecher model has been further on developed to account for fracture terminations at intersections with pre-existing fractures and for more general fracture shapes /Geier et al, 1989/. The fracture shapes are generally initiated as polygons with three to six sides. The requirements for orientation' and size statistics are the same as for the ordinary Baecher model. Termination is specified, as termination probability accounted for a fracture set is the probability that a fracture of that set will terminate when it intersects a fracture of an earlier set. Figure 3-3b depicts the features obtained using this model, showing termination of polygonal fractures at intersections with pre-existing fractures.

Applicability: the Enhanced Baecher model is more appropriate to simulate the connectivity of natural fracture populations. Indeed, results of simulations /Geier et al, 1989/ indicate that for fracture systems in which fractures terminate at intersections, the

ordinary Baecher model will produce networks with erroneously low connectivity measures, if the parameters of the Baecher model are adjusted to match trace length. Anyhow, a limitation of this model is that in case of termination at intersection, the algorithm may cause distorsion in the size distribution for that fracture set.

3.4 BART (Baecher Algorithm, Revised Terminations)

This model is a generalisation of the Enhanced Baecher model, which result in non-uniform fracture locations. These models differ primarily from the precedent in the algorithm used for fracture termination modes /Dershowitz et al, 1998b/. Termination is assigned by termination percentage. This implementation provides a better correlation to field data. Indeed, the percentage of fractures that terminate at intersections with other fractures matches the termination percentage calculated from field data. Because in this model the locations of secondary fractures are controlled by the locations of the primary fractures, the resulting fracture populations exhibit spatial correlation and tend to occur in clusters or chains /Axelsson et al, 1990/. The 3D geometrical model produced using this algorithm is presented in Figure 3-4.

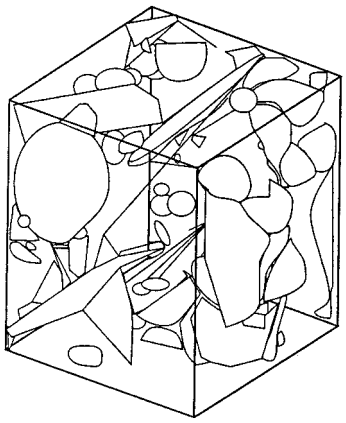

Figure 3-4. *3D BART geometric model /Dershowitz et al, 1998b/.*

Applicability: The termination mode assigned speed up the model because there is no need to calculate fracture intersections. It is also significantly more heterogeneous, because fracture locations of terminating fractures are correlated to the location of pre-existing fractures /Dershowitz et al, 1998b/. This characteristic can be expected to produce simulated fracture populations that are more well-connected than fractures simulated with the ordinary Baecher model.

3.5 Veneziano model

/Priest and Hudson, 1976/ illustrated that model of fractures simulated by Poisson planes and lines show a good similarity with geometry of fractures observed in the field. However, the simple Poisson plane fracture model is based on the assumption of infinite extent of fractures, which is not so appropriate to represent rock geometry. Therefore /Veneziano, 1978/ introduced a method for adaptation of the concept of Poisson plane fractures to bounded fractures.

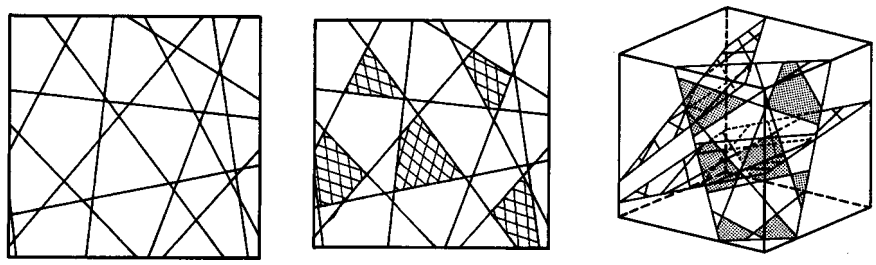

Figure 3-5. *"Generation of Veneziano joint system model" /Einstein, 1993/.*

The model requires three consecutive stochastic processes /Dershowitz and Einstein, 1988/. First, fracture planes are generated as Poisson planes (Figure 3-5). These fracture planes are located in space by a uniform distribution, but may have any desired distribution of orientation. Second, a Poisson line process on each fracture plane divides fracture planes into polygonal regions. Finally, a portion of these polygons is randomly marked as jointed, while the remainder is defined as intact rock. With this model, fracture shapes are polygonal, and fracture sizes are defined by the intensity of the Poisson line process and the proportion of polygons marked as fractures. In a 2D trace plane, this models resembles the Baecher model, except that fractures are represented by coplanar line segments or fibres rather than independent fibres. In addition, Veneziano demonstrated that his model leads to an exponential distribution of fracture trace lengths rather than lognormal distribution found with the Baecher model /Dershowitz, 1984/.

"With regard to fracture termination, in the Veneziano model, fractures in each joint plane are defined by an independent Poisson line process. Therefore, the definition of fractures on each joint plane is independent of plane intersections" /Dershowitz et al, 1988/.

Applicability: polygonal shapes as defined by this model can often be observed in nature. This model is more appropriate than the orthogonal model for most cases, particularly if the fractures are coplanar.

Despite the adaptation of the Poisson plane model to represent bounded fractures, the model usually fails to construct rock blocks unless they are 100% persistent and unbounded.

This model has been applied to slope stability problems by /Einstein et al, 1983/, and to the hydrology of fractured rock masses by /Rouleau, 1984/. Both of these applications utilized the Veneziano model in a 2D trace plane only, since the geometry of this model is quite complex in 3D.

3.6 Dershowitz model

/Dershowitz, 1984/ remedied the disadvantage of the Veneziano model that fracture intersections and fracture edges do not coincide.

Like the Veneziano model this model is based upon a system of Poisson planes representing fracture planes, but two stochastic processes (instead of three) are required to generate the model. The first process is the definition of fracture planes by a Poisson plane process of uniformly distributed locations, and by orientations following a specified distribution (Figure 3-6). The intersections between these planes define a

process of lines on each fracture plane, which divides each plane into polygons. The second process is the marking of a persistent portion of polygons on each plane as fractures, and the remainder as intact rock. As in the Veneziano model, this is done by a stochastic process in which each potential fracture has an equal probability of being marked as an open fracture. Thus fracture edges are defined by fracture plane intersections, and as a result all fracture intersections occur at fracture edges. Also, fractures correspond directly to the faces of the polyhedra defined by fracture planes. As a result, polyhedra faces are either completely intact or completely jointed and rock blocks can be modelled relatively easily.

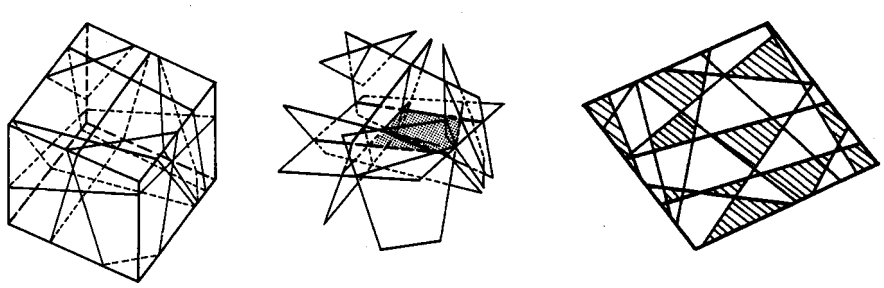

Figure 3-6. *"Generation of Dershowitz joint system model" /Einstein, 1993/.*

Applicability: since fracture edges correspond to fracture intersections, distinct rock blocks can be defined at any scale, regardless of the proportion of each fracture plane which is defined as jointed. This model has the advantages of the orthogonal model for definition of distinct rock blocks, but has the additional advantage of flexible orientation distributions, such that a variety of polygonal fracture shapes and polyhedral block shapes can be modelled. This model is a more accurate representation of a system that exhibits distinct rock blocks, bounded polygonal fractures, and orientation dispersion /Dershowitz and Einstein, 1988/.

Difficulties are caused by the fact that polygon (block face) sizes are controlled by the intensity of intersecting fracture plane processes. If fractures are defined as a constant percentage of each plane, the increases in plane process intensity results in a larger number of smaller polygons.

The model is not accurate for models with bounded, non co-planar fractures. However, by a reduction in the proportion of each fracture, which is defined as jointed, the effect of co-planarity can be reduced, and the model can be used as an approximation. But the model has then the same weaknesses as the ordinary Baecher model.

3.7 3D Hierarchical Fracture Model (Ivanova)

/Ivanova, 1995, 1998/ developed a 3D model specially aimed for reproducing geologic fracture systems. The construction of the fracture system geometry is based on Poisson plane and line processes, and is therefore related to the Veneziano's and Dershowitz's models developed earlier (see sections 3.5 and 3.6).

Based on field data and geological history, fracture sets are identified. Primary fractures that originate in the intact rock or do not have any relation with other sets in previously fractured rocks are set as independent. Secondary, tertiary,…, fracture identify dependent sets.

Fractures are modelled as convex polygons that are randomly oriented and randomly located in space. Three major stochastic processes are required to develop the model. First, a Poisson plane process models the stress field that creates fractures along planes of maximum shear and tension in rocks. The second process is a Poisson line tessellation and polygon marking, which will divide fracture planes into intact and fractured regions. The tertiary process is a random polygon translation and rotation, which is accounted for the representation of the local stress field variations. This process controls the co-planarity of fractures and deviations of fracture orientations from the regional directions due to local geologic structures.

These processes are used to model the independent fracture sets, as well as the dependent ones. Anyhow, dependence relations, based for example on a termination function, must be implemented. /Ivanova, 1998/ describes several algorithms that can be accounted for the representation of rock fracture systems in the major geologic environments, such as folds, faults, remote tension, thermal contraction and central structures.

Applicability: the stochastic processes of the model enable the representation of relationship between fracture geometry and underlying mechanisms. Such processes generate fracture clusters that reflect the natural development of smaller fracture along specific geologic structures. This model has been applied by /Ivanova, 1998/ for representation of the fracture system in the oil-producing sedimentary rocks, Yates field, Texas. Other potential engineering applications include risk assessment during undergroung construction, study of flow and transport.

Some limitations of the model are related to the data acquisition in the field (1D or 2D data are used to infer the 3D geometrical characteristics). Moreover, implementations in the tool to model relationships between underlying mechanisms and fracture system geometry are needed.

3.8 Nearest Neighbour model

The Nearest Neighbour model is identical to the Enhanced Baecher model as described above except for its assumptions about the spatial distribution of fractures /Geier et al, 1989/.

This is a semi-stochastic, pattern-based model which simulates the tendency of fractures to be clustered around major points and faults by preferentially producing new fractures in the vicinity of earlier fractures /Dershowitz et al, 1998b/. In order to reproduce this feature, the fractures are organised into primary, secondary and tertiary groups, and are generated in this sequence, with fractures in the primary groups dominating the generation of fractures in succeeding groups (Figure 3-7). The probability of a fracture at a point x in three-dimensional space is given by:

$$P_x(x) = CL^{-b} \tag{3.2}$$

where L is the distance from point x to the nearest fracture of a previous, dominant group, and b and C are empirical constants /Geier et al, 1989/.

The model requires the same data as the Enhanced Baecher model, plus information on the spatial interrelationship of the fractures, and accounts for fracture terminations in terms of the termination probability.

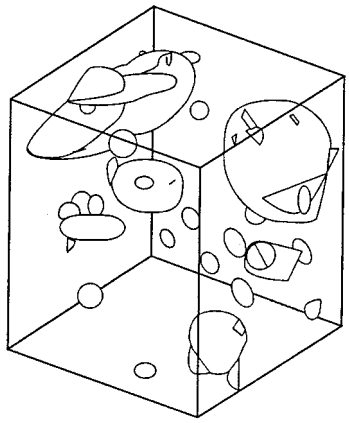

Figure 3-7. *3D geometric nearest-neighbor model /Dershowitz et al, 1998b/.*

Applicability: According to the simulation algorithm (fractures clustered around the first group of fractures), this model tends to provide more well-connected fracture populations than the ones produced by the ordinary Baecher model. The definition of the fracture groups allows more explicit representation of geological observations than is allowed in the Levy-Lee model, for cases in which the fractures can be classified into different groups in correspondence with a theory of fracture genesis.

3.9 "War Zone" model

The War Zone model is based upon the internal geometry of shear zones, such as those described by /Segal and Pollard, 1983/, which have high fracture intensities due to the formation of conjugate shear fractures between subparallel faults. In the War Zone model, the regions lying between pairs of neighbouring, subparallel pairs of primary fractures, are identified (Figure 3-8a). These regions, referred to as "war zones", are assigned a higher probability density function /Geier et al, 1989/:

$$P_x\left(x_w\right) = k_w P_x\left(x_0\right), \qquad k_w>1 \tag{3.3}$$

where $P_x(x_w)$ is the probability of a fracture occurring at any point x_w inside of a war zone, $P_x(x_0)$ is the probability of a fracture occurring at any point x_0 outside of all war zones, and k_w is the empirically determined war zone intensity factor, which is the ratio of fracture intensity inside war zones to the fracture intensity outside war zones.

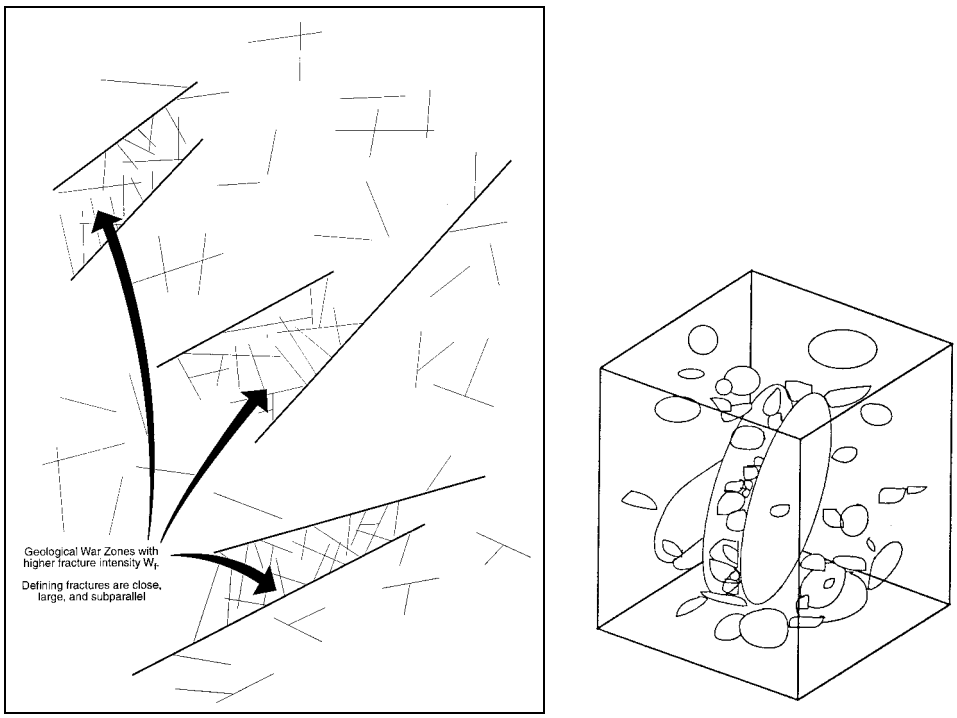

(a) (b)

Figure 3-8. *(a) War-Zone geologic conceptual model, and (b) 3-D geometric conceptual model /Dershowitz et al, 1998b/.*

Pairs of fractures forming “war zones” are identified from among the primary set of fractures on the basis of three dimensionless qualities “parallelness”, “largeness” and “closeness” (definitions of these parameters are found in /Geier et al, 1989; Dershowitz et al, 1998b/), and higher fracture densities are assigned in these “war zones” (Figure 3-8b).

This model is identical to the Enhanced Baecher model except for its assumptions about the spatial distribution of fractures, and requires the same data, plus the war zone intensity factor and the war zone selection parameters. These are determined statistically from field data, but in some cases the locations of major fracture zones can even be defined deterministically, by means of remote sensing, hydraulic testing and fracture mapping.

Applicability: the validity of this model is supported by observations of major fracture zones made at the Stripa site and elsewhere. Moreover the probabilistic War Zone model has been validated with sets of fractures identified in the TSE drift /Geier et al, 1989/. This simulation demonstrates that the combination of the three war zones parameters as defined above can be used to define fracture zones. However, more accurate results would likely be obtained by putting an effort in the optimisation of war zone selection parameters.

3.10 Non-Planar Zone model

This is a semi-stochastic model which generates fractures with location and orientation varying according to a user defined non-planar surface /Dershowitz et al, 1998b/.

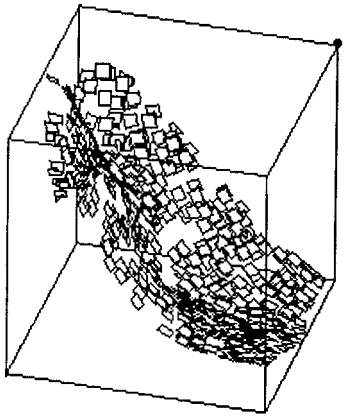

Figure 3-9. *3D geometric non-planar model /Dershowitz et al, 1998b/.*

3.11 Geostatistical "models"

The geostatistical approach was developed to describe the spatial behaviour of regionalised variables of the fracture network, and thus of the underlying random process /Gervais et al, 1995/.

It is based on the assumption that the location on fractures and their other geometrical and hydromechanical attributes have spatial correlation /La Pointe, 1993/. Spatial correlation implies that the properties of a specific fracture and group of fractures are similar to neighbouring fractures and less similar to distant ones, and that this similarity decreases as the relative distance between fracture increases.

The variogram function is the basic tool for geostatistics, but in practice the theoretical variogram function is estimated using the following approximation /La Pointe, 1993/:

$$\gamma(h) = \frac{1}{2} n(h) \sum_{i=1}^{n(h)} \left(X(z_i) - X(z_i + h) \right)^2 \qquad (3.4)$$

where n(h) is the number of pairs separated by a relative distance h, and z_i is the *i*th fracture.

It describes the spatial behaviour of a regionalised variable and, hence, of the underlying random process. Different tools such as the variogram of cumulated length of fracture traces per m^2, the variogram of number of fracture trace centres per m^2 and the variogram of fracture direction can be calculated to determine spatial correlation between different geometrical fracture properties.

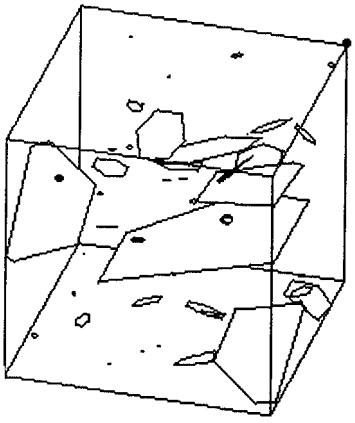

Figure 3-10. *3D geometric geostatistical model /Dershowitz et al, 1998b/.*

There are in practice several options for incorporating spatial correlation properties into the simulation, such as Turning Band methods and Indicator Kriging. The Turning Bands algorithm, which is the one developed in FracMan, can generate simulations with non-fractal correlation properties (Figure 3-10), which makes it a useful complement to the 3D Box Fractal and Fractal POCS algorithms /Dershowitz et al, 1998b/.

Applicability: Geostatistical models are rarely used in engineering design, but may be fruitful for portrayal of rock mass fracture networks. One limitation of this model is that a wide sampling area is required to collect confident geostatistical data. A limitation of the model developed in FracMan is that the algorithm will work only if the population values distribution approximate a Gaussian distribution /Dershowitz et al, 1998a/. However, this distribution law is badly suited for phenomena that do not have a high degree of continuity /La Pointe, 1993/.

3.12 Fractal models

Fractal geometry is a useful mathematical model when the histogram of the quantity is declining power law and when the spatial relation between objects of different size exhibit regularities that transcend the scale of observation /La Pointe, 1993/. The attractiveness of fractal geometry is mainly that this approach is independent of the scale of observation. The fractal description combines heterogeneity and connectivity at all scales, such that the observation at one scale can be interpreted at a different scale of interest /Dershowitz et al, 1992/.

Applicability: the application of the fractal models to the engineering design is largely untested, and there is no verification to prove that fractals produce model input that predict behaviour better than other method /La Pointe, 1993/.

3.12.1 Levy-Lee model

The key feature of the Levy-Lee conceptual model is that fracture centres are created sequentially by a Levy flight process in 3D, and that the size of a fracture is related to its distance from previous fracture /Geier et al, 1989/, see Figure 3-11.

The Levy Flight process is a type of random walk, for which the length L' of each step is given by the probability function:

$$P_L\left(L' > L\right) = L^{-D} \tag{3.5}$$

where D is the fractal dimension of the point field formed by the fracture centres. Only the centres of fractures are fractal –the networks themselves may not be fractal.

The effect of the correlation of fracture size to step length is to produce clusters of smaller fractures around more widely scattered, larger fractures /Geier et al, 1989/.

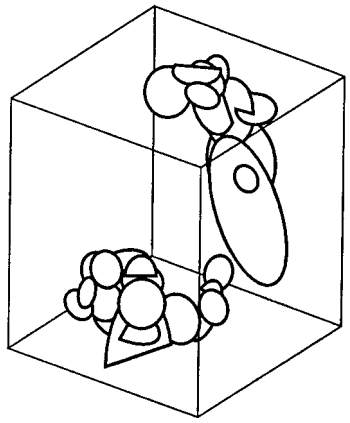

Figure 3-11. *3D geometric Levy-Lee fractal model /Dershowitz et al, 1998b/.*

Applicability: One very attractive feature of that model is its ability to generate a non-stationary fracture system, using a set of parameters that remain constant throughout the generation region /Geier et al, 1989/.

This model requires the same data as the Enhanced Baecher model, plus data describing the spatial structure of fracture population, such as correlation between fracture spacing and size, correlation between fracture spacing and orientation, fractal dimension of the point field defined by fracture centres. Field validation of the determination of the fractal dimension has been carried out and the fit to the data for all clusters gave a coefficient correlation of 0.9969, indicating that the clusters are well characterised. Nevertheless, further work is needed to validate the other features of the Levy-Lee model, namely the correlation between fracture size and spacing, and the correlation between fracture orientation and spacing /Geier et al, 1989/.

Numerical simulations have been carried out on the basis of this model /Dershowitz et al, 1992/, and the results showed that fractal dimension can be a useful index for fracture connectivity and block formation, and an index for site comparison. However, further study will be required to determine which values of fractal dimension are preferable for repository location in particular geologic environments.

This model has been combined with geostatistical analysis of data to develop a Hierarchical Fracture Trace Model that have been used to describe fracture trace patterns on outcrops /Gervais et al, 1995/. This accounts for the chronology of fracture formation. The sequential generation and correlation of fracture sets is intended to correspond to what happens in nature. A major limitation of this model as presented in /Gervais et al, 1995/, is to be two-dimensional.

3.12.2 Box Fractal Model

This model is used to simulate a self-similar three-dimensional discrete fracture network. The generation region is divided into an assemblage of grid cells, with each grid cell assumed to be a cube with an edge length equal to 1/64 of the generation region edge length /Dershowitz et al, 1998b/. From the user specified "Box fractal dimension" D_b, the number of boxes that contain one or more fractures is computed from the relation:

$$N(\delta) = \delta^{-D_b} \tag{3.6}$$

where δ is the edge length, D_b is the box fractal dimension and $N(\delta)$ is the number of boxes of edge length d that contain one or more fractures.

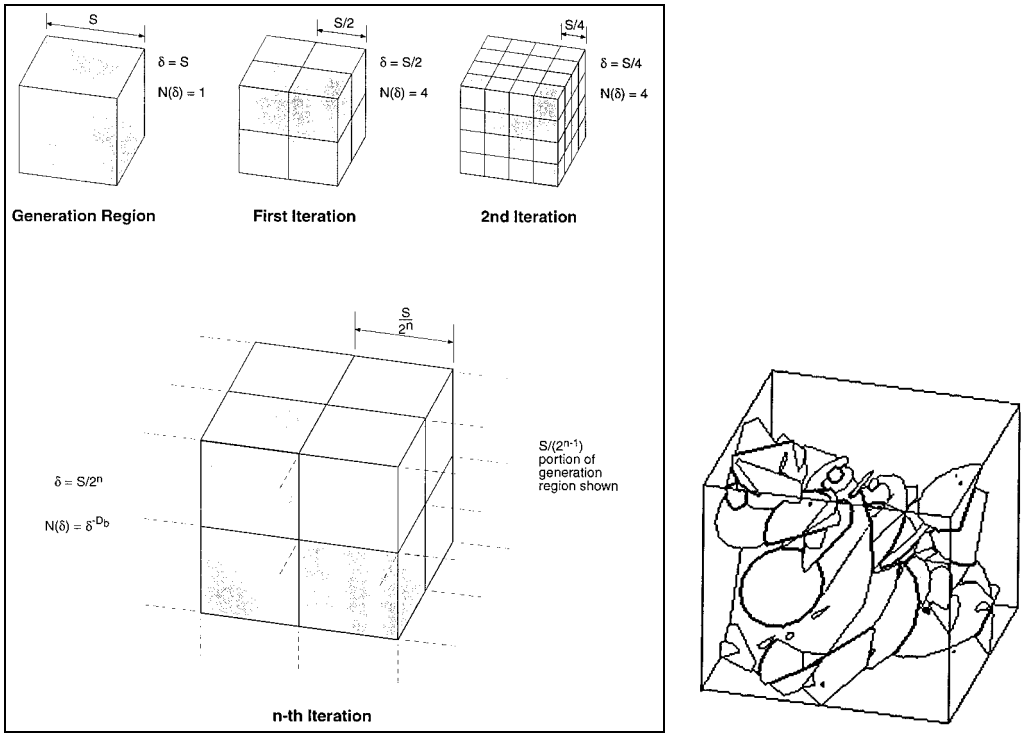

(a) (b)

Figure 3-12. *(a) 3-D fractal Box algorithm, and (b) 3-D geometric model /Dershowitz et al, 1998b/.*

As the size of grid cells become smaller, the number of filled boxes increases (Figure 3-12a). Because of the recursive nature of the algorithm, the location of filled boxes is not random, and the number of filled boxes at any level of aggregation conforms to equation and is fractal. An illustration of the 3-D geometric model generated is provided in Figure 3-12b.

3.12.3 Fractal POCS Model

The POCS algorithm (Projection on Convex Sets) is a general procedure of generation of stochastic fields according to constraints such as spatial correlation which can be represented mathematically as convex sets /Malinverno and Rossi, 1994/. In FracMan

for example, five constraints are imposed in the generation of POCS stochastic fields of fracture centres or surface points /Dershowitz et al, 1998b/. These are shortly resumed: 1) Known data is honoured; 2) Self-affine spatial correlation is honoured; 3) The mean data of the value is preserved; 4) The values of the data set are bounded; 5) The energy of the data is preserved.

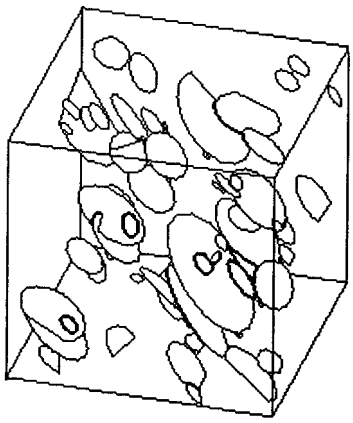

Figure 3-13. *3D geometric fractal POCS model /Dershowitz et al, 1998b/.*

This model will then generate a random field of fracture initiation points (a) consistent with a user specified fractal dimension, (b) consistent with a user specified variogram, and (c) conditioned to intensities at specified locations /Dershowitz et al, 1998b/. The 3-D geometric conceptual model is illustrated in Figure 3-13.

3.13 Poisson Rectangle model

This is a simple version of the Enhanced Baecher model, in which fractures are represented by rectangles with prescribed length and width, rather than as polygonal disks with an "effective radius". Location and termination are treated in the same way as in the Enhanced Baecher model.

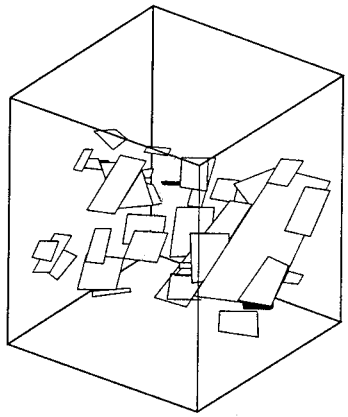

Figure 3-14. *3D geometric Poisson rectangle model /Dershowitz et al, 1998b/.*

3.14 Mosaic Block Tessellation Models

"Mosaic Block Tessellation" refers to a tessellation process that is based upon the definition of blocks containing the space rather than upon the definition of fractures which incidentally divide space into blocks. Space may be divided into regions by regular or stochastic grids of interlocking polyhedra where the polyhedra faces do not have to be on fracture planes /Dershowitz and Einstein, 1988/.

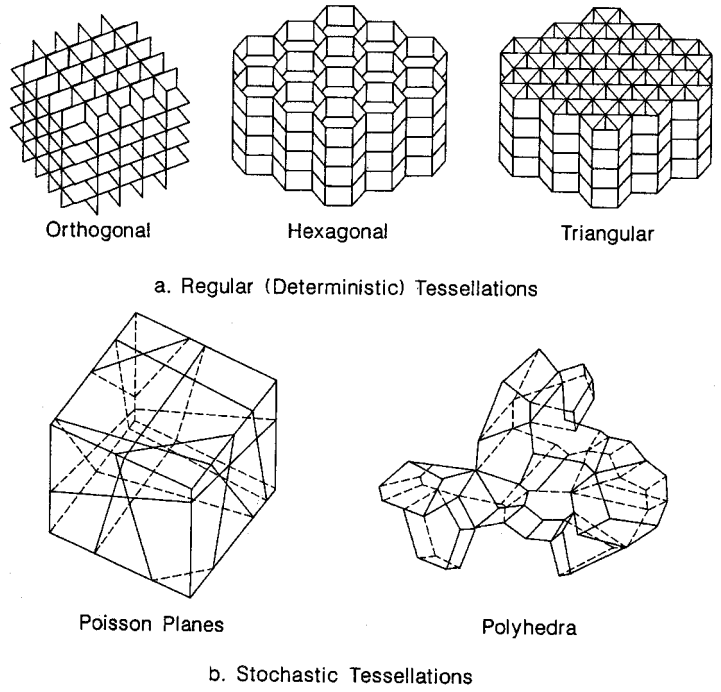

Figure 3-15. *Three-dimensional mosaic tessellations /Dershowitz and Einstein, 1988/.*

These models can be deterministic (regular geometry) or stochastic (fracture and block shapes may vary according to a distribution), see Figure 3-15. Stochastic tessellations are generally based upon a process of defining block centres or vertices, the "seeds". There are a wide variety of combinations of stochastic and deterministic seed points and block processes, which can be used to define a stochastic tessellation in 2-D.

In rock fracture system model based upon the mosaic block tessellation, not all block faces need be defined as fractures.

Applicability: This model offers the capability to model fractures, which are not coplanar. This is a new level of flexibility in fracture system modelling. Another interesting but somewhat problematic feature is the generation of block first, followed by rock fractures derived from the faces of the blocks. Fracture sizes, shapes, locations and orientations are modelled indirectly, and it is therefore not possible to directly use sampled distributions of fracture characteristics to construct a particular block tessellation model. To obtain a specific distribution of fracture shapes, an appropriate combination of processes for location of the seeds and for block growth must be determined.

This model is appropriate for fracture systems which are actually the result of a process of block formation in a rock mass (for ex, jointing in columnar basalts).

This may not be appropriate for cases, which do not display polyhedral blocks, and polygonal fractures.

4 What model(s) to use?

As the project is aimed to develop a Descriptive Rock Mechanic Model, and for the reasons mentioned in the introduction, focus has been made on Discrete Fracture Network (DFN) models, and no valuable information regarding continuum models have been introduced.

4.1 Sum-up and discussion about the described models

Several DFN conceptual models have been reviewed, that differ mainly by the way fracture characteristics are handled (see Table 3-2, section 3). Some general comments can be made:

- Some fracture characteristics are defined in the same way in most of the models presented. These are the fracture shape, most often considered as polygon, the fracture size (generally bounded) and the termination at intersection (yes). This implies that the specifications of the models mostly rely on the distribution laws utilised to simulate fracture orientation and fracture location.
- A differentiation can be made between quite generic conceptual models, such as mosaic block tessellation models, geostatistical models, polygonal models, and more specific and restrictive models like War Zone models and orthogonal models.
- Considering the relation between different fracture sets, two groups of models can be identified: stationary models and non-stationary models. Those provide tools to simulate spatial correlation between fracture sets. The non-stationarity can be determined by stochastic distribution laws (e.g. nearest neighbour) and/or they might be user-defined (binary models, e.g. War Zone model).
- Specific models have generally been developed from generic models to simulate specific fracture networks in rock masses. Therefore, the examination of field data is a key to determine what models is the most appropriate according to their applicability, advantages and limitations. Table 4-1 is a synthesis other these considerations for the DFN conceptual models that have been reviewed in this study.

4.2 Recommendations

4.2.1 Choice of the model

The choice of the DFN model is mostly related to the assumptions that can reasonably be made from field data and geological observations. As discussed in section 4.1, some models are specific in the way fractures are generated.

In a general case, the Enhanced Baecher model (and in some extent the BART model as well) provide an appropriate model. Any combination of the different fracture characteristics can be used.

As a support for the decision, Table 4-1 highlights the DFN conceptual models, as regards to their applicability, advantages and limitations.

Table 4-1. Main review of the DFN model, as regard to their applicability, advantages and limitations.

Model	Concept	Applicability	Advantages	Limitations
Orthogonal	Fracture network simulated from 3 sets of unbounded orthogonal joints	rock masses with completely defined rectangular rock blocks / mostly to hydrology	Simple geometry and treatment of data	Planar assumption, limitation in the variation of fracture orientation
Baecher disk	Generate fracture network from fracture centres that are distributed uniformly in space	Homogeneous rocks	Few field data available / Accurate in rock mechanics and hydraulics when a little is known	Do not simulate terminations of fractures, fractures must be planar / Do not account for complex features of fracture populations
Enhanced Baecher	Generate fractures from fracture centres located at random points in space. Intersections are calculated with pre-existing fractures	Fractured rock masses in which joint terminations are observed	Suited for simulation of connectivity of natural fracture population / Multiple intersections per fracture are possible	Fracture size distribution is not preserved; joints must be planar
BART	Same principle as for the Enhanced Baecher model, except that the centre of fracture terminating at intersections is generated from point on fracture intersection	Fractured rock masses in which fracture terminations are observed	Quick simulation / Fracture size distribution is preserved; spatial correlation in the simulated fracture population	fractures must be planar
Veneziano	Fracture network generated in 3 stochastic processes based on Poisson plane and Poisson lines	Suited for 100% persistent and unbounded fractures	Polygonal shapes are often observed in nature. More appropriate than orthogonal model for most cases, specially in case of coplanarity	Often fail to construct blocks / Intersections of fractures do not often match joint edges / Complex 3-D model
Dershowitz	Fracture network generated from 2 stochastic processes based on Poisson plane	Accurate for systems which exhibit distinct rock blocks, bounded polygonal fractures, and orientation dispersion	Model distinct rock blocks of various shape, flexibility in the distribution of fracture orientations / Joint intersection at joint edges	Can generate a large number of smaller polygons / Not so well fitted for coplanar fractures

Mosaic Tessellation	Deterministic and/or stochastic generation of the blocks, then definition of the fracture planes	Fracture systems resulting from a process of block formation (jointing in columnar basalts)	Manage non co-planarity, creation of the blocks first	Not so accurate in cases that do not display polyhedral blocks and polygonal fractures; blocks created first; indirect modelling of location, orientation and shape of fractures
Poisson Rectangle	Same concept as Enhanced Baecher except that fractures are rectangular	Same as Enhanced Baecher	Same as Enhanced Baecher	Specific conceptual model / Require a good knowledge of the rock mass geometry
Geostatistical	Generate fractures according to a specified variogram	Describe the spatial behaviour of regionalised variables of the fracture network	Account for a good spatial correlation	The size of the sampling area must be consequent compared to the study area
War Zone	Simulate higher densities of fractures between two major subparallel fractures	Simulation of fracture network in shear zones and in the surrounding rock mass	Binary model / identify "fracture zone" and "non-fracture zone"	Specific conceptual model / Require a good knowledge of the rock mass geometry
Non-Planar Zone	Generate fractures along a non-planar user defined surface	Simulation of fracture network along specific features (deformation zones,...)	Enhance rock zones with specific geometrical properties / binary model	Require a good knowledge of the rock mass geometry
Levy-Lee Fractal	Generate clusters of smaller fractures around wider fractures	In combination with geostatistical analysis: Hierarchical Fracture Trace Model	Accounts for the chronology of fracture formation / Ability to generate a non-stationary fracture system with a set of parameters that remain constant throughout the generation system	Do not consider the size and shape of the blocks delimited by the simulated fractures / Definition of the most appropriate fractal dimension
Nearest-neighbour	Fractures are organised into primary, secondary and tertiary groups, and are generated in this sequence	Can account for the generation of fracture network according to the theory of fracture genesis	Generate clusters of fractures around the primary group / More explicit than Levy-Lee model if fractures can be classified	Must have enough data to assess the different groups and chronology

4.2.2 Input parameters required

Despite some variations between the different models, the basic input data are related to the distributional form of the primary characteristics of the fractures, and include fracture shape, fracture size distribution, fracture orientation, and fracture density for each set of fractures. As an example, Table 4-2 is an illustration of the typical input data used for the generation of a BART model. The raw data collected in the field have been analysed to characterise statistically 3 fracture sets.

Table 4-2. Presentation of parameters used to define a DFN model.

Parameter	***Used data***			***Data from***	***Reference***
Orientation K1=3.96 K2=10.53 K3=9.32	Set	Strike(*)	Dip(*)	Pilot and Exploratory holes.	Prototype Repository DFN Model 2
	1	212.8	83.7		
	2	126.9	86.8		
	3	17.9	7.5		
FracMan: Size	Set	Mean	Std dev	TBM tunnel.	LaPointe TR95-15
	1	2	2		
	2	8	2		
	3	5	4		
Spatial model	BART model (fracture termination probability of 37%).			TBM tunnel.	SKB R-99-43, p. 32 SKB ICR-96-05
FracMan: Natural Fracture intensity P_{32n}	Set		P_{32c}	From 1m and 3m section pump tests in exploratory holes.	Prototype Repository DFN model 2
	1		0.26		
	2		0.85		
	3		0.18		

5 Conclusions

Discrete Fracture Network approach is used to generate 3D models of the geometry of fractures in rock masses. Different conceptual models are available that are developed upon combinations of the geometrical characteristics of the fractures. The fracture characteristics that constitute the fundaments of these models are: fracture shape, fracture size dsitribution, termination at intersection, co-planarity, location and orientation of fracture sets.

Most of the conceptual models are stochastic, and several assume a uniform distribution of the location of fracture sets. The distributional forms are derived from the processing of raw data. Most of the models generate bounded fractures, for which termination at intersections is accounted for.

As for the set to consider the relation between different fracture sets, the conceptual models can be divided in two groups: stationary and non-stationary models. The specificity of the non-stationary models is the consideration of spatial and temporal relation between different set of fractures; the generation of the secondary, tertiary,… sets are subjected to the primary set. This is often useful to simulate fracture clusters that develop in the vicinity and in relation to fracture and deformation zones. Nevertheless, these models require a good knowledge of the geological and geomechanical history at place.

The stationary models are also accounted for relation between the different fracture sets through the estimation and representation of termination. The Enhanced Baecher model is one current used stationary model for different applications.

6 References

Andersson J, Ström A, Svemar C, Almén K-E, Ericsson L, 2000. What requirements does the KBS-3 repository make on the host rock? Geoscientific suitability indicators and criteria for siting and site evaluation. SKB Technical Report TR-00-12, Stockholm, Sweden.

Axelsson C-L, Jonsson E-K, Geier J, Dershowitz W, 1990. Discrete Fracture Modelling. SKB Progress Report 25-89-21, Stockholm, Sweden.

Barton C M, 1978. Analysis of joint traces. Proceedings of the 19th U.S. Symposium on Rock Mechanics, American Institute of Mining Engineers, 39–40.

Baecher G B, Lanney N A, Einstein H H, 1978. Statistical description of rock properties and sampling. Proceedings of the 18th U.S. Symposium on Rock Mechanics, 5C1-8.

Dershowitz W S, 1979. A probabilistic model for the deformability of jointed rock masses. M. S. Thesis, Massachusetts Institute of Technology, Cambridge, Massachusetts.

Dershowitz W S, 1984. Rock joint systems. Ph.D. Thesis, MIT, Cambridge, MA.

Dershowitz W S, Einstein H H, 1988. Characterizing rock joint geometry with joint system models. Rock Mech. and Rock Eng., vol.21, n1, pp.21-51.

Dershowitz W S, Redus K, Wallmann P, LaPointe P, Axelsson C L, 1992. The implication of fractal dimension in hydrology and rock mechanics. SKB Technical Report TR 92-17, Stockholm, Sweden.

Dershowitz W S, Wallmann P, Shuttle D, Follin S, 1996. Canister and far-field demonstration of the discrete fracture analysis approach for performance assessment. SKB Progress Report U-96-41, Stockholm, Sweden.

Dershowitz W S, Foxford T, Doe T, 1998a. Fractured Reservoir Discrete Feature Network Technologies. Research report, Fracture Data Analysis Technology, BDM-Oklahoma, U.S. Department of Energy. Prepared by Golder Associates Inc. Redmond, Washington, 1998.

Dershowitz W S, Lee G, Geier J, Foxford T, LaPointe P, Thomas A, 1998b. FracMan Version2.6 Interactive Discrete Feature data Analysis, Geometric Modeling, and Exploration Simulation, user documentation, Report 923-1089, Golder Associates Inc, Seattle, Washington.

Einstein H H, Veneziano D, Baecher G B, O'Reilly K J, 1983. The effect of discontinuity persistence on rock slope stability. Int. J. Rock Mechanics and Mining Sciences, 20, n.5, p.227–236.

Einstein H H, 1993. Modern developments in Discontinuity Analysis – The persistence-Connectivity problem. In Comprehensive Rock Engineering, Vol3 – Rock testing and site characterization, pp.193–213.

Geier J E, Lee K, Dershowitz W S, 1989. Field Validation of Conceptual Models for Fracture Geometry. Submitted to Rock Mechanics and Rock Engineering.

Gervais F, Gentier S, Chiles J P, 1995. Geostatistical analysis and hierarchical modelling of a fracture network in a stratified rock mass. In Fractured and Jointed Rock Masses, Myer, Cook, Goodman and Tsang (eds), Balkena, Rotterdam, 1995.

Ivanova V, 1995. Three-dimensional stochastic modeling of rock fracture systems. S.M. Thesis, Massachusetts Institute of Technology, Cambridge, MA.

Ivanova V, 1998. 3-D hierarchical fracture model – Fracture Reservoir Discrete Feature Network Technologies. A project of Fundamental Geoscience Research and Development, BDM-Oklahoma, U.S. department of Energy, National Oil and Related Programs. Research Report, Golder Associates, Cambridge, Massachusetts.

LaPointe P R, 1993. Pattern analysis and Simulation of Joints for Rock Engineering. In Comprehensive Rock Engineering, Vol3 – Rock testing and site characterization, pp.215–239.

Long J C S, Billaux D M, 1987. From field data to fracture network modeling: an example incorporating spatial structure. Water Reour. Res 23, 1201–1216.

Pollard D D, Aydin A, 1988. Progress in understanding jointing over the past century. Geological Society of American Bulletin, v.100, p.1181–1204.

Malinverno A, Rossi D J, 1993. Applications of Projection Onto Convex Sets to Stochastic Inversion. SPE 25659, Middle East Oil Show, Bahrain, April.

Müller L, 1963. Der Felsbau, Ferdinand Enke, Stuttgart.

Priest S D, Hudson J A, 1976. Discontinuity spacings in rock. Int. J. Rock Mech. and Min. Sc., vol.13, pp.135–148.

Rouleau A, Gale JE, 1985. Statistical characterisation of the fracture system in the Stripa Granite, Sweden. Int. Jl of Rock Mech. and Mining Sci. and Geomech. Abstracts, vol. 22, pp.353–367.

Segall P, Pollard D D, 1983. Nucleation and growth of strike slip faults in granite. Journal of Geophysical Research, 8, p.555–568.

Snow D T, 1965. A parallel plate model of fractured permeable media. Ph. D. dissertation, University of California, Berkeley.

Veneziano D, 1978. Probabilistic model of joints in rock. Unpublished manuscript, Massachusetts Institute of Technology, Cambridge, Massachusetts.

Weiss L E, 1972. The minor structures of deformed rocks. A photographic atlas. Springer-Verlag, New York.

Appendix B

Models for the Modelling of Fractured Rock Masses

Introduction to numerical codes for Finite Element and Discrete Element Methods

Isabelle Staub

Golder Associates AB

May 2002

Contents

1 Introduction

The mechanical properties of fractured rock masses are strongly dependent on the properties and geometry of fractures. Fractured rock masses are usually weaker and more deformable and are highly anisotropic when compared with intact rocks. Constitutive modelling of fractured rock masses has long been a subject of interest and numerous models have been developed in attempt to simulate their mechanical responses. This report constitutes an attempt to review the main constitutive models for use to simulate mechanical behaviour of fractured rock masses.

Two different approaches for the numerical modelling of fractured rock masses are used today /Jing, 1990/, that are the Continuum Analysis Techniques and the Discontinuum Analysis techniques. As the designation of these approaches implies, the main feature lies in the way of considering and modelling the fractured rock mass, and the deformation that can take place in it. We have reviewed the different models developed under each analysis technique and highlighted their applicability, advantages and limitations.

Even if some mathematical formulations are presented in this report, this general review does not focus or account for the presentation of mathematical/physical laws or equation resolutions, which are embedded in the different methods. It focuses on the concepts that have been undertaken to tackle the problematic of modelling fractured rock masses. Special attention has been given to the assumptions made to develop the different methods, their applicability and their main advantages/limitations.

Along this report both terms “fractures” and “joints” are used. The term “fractures” is the used in the meaning of the definition given in section 1, appendix A. The terms “joints” is used when referring to the model equations and developments, as it is the term generally employed by the authors.

2 Continuum analysis techniques

2.1 Introduction

The Rock Mass is taken as a continuum and infinitesimal deformation is usually assumed. A matrix equation is written for the entire body considered as homogeneous, including the constraints at the boundaries. The unknowns of the system are then obtained by solving the matrix equation. Rigid motion of the body is usually not included in the formulation.

Mainly two different approaches account for solving problems at the contacts or boundaries. These include basically the Finite Element Method (FEM) and the Boundary Element Method (BEM).

Regarding FEM, the whole region is discretised and approximations are made throughout the whole region.

Following the BEM, only the boundary is divided in elements, and approximations occur only on the boundary.

The fractures are modelled either by using specially formulated joint elements in FEM /Goodman, 1976/, or displacement discontinuity in BEM /Crouch and Starfield, 1983/, or other equivalent models of the fractured rock mass.

2.2 Review of the continuum methods

2.2.1 The Finite Element Method (FEM)

The basis of the finite element method is the definition of a problem domain surrounding an excavation, and division of the domain into an assembly of discrete, interacting elements /Brady and Brown, 1999/. The domain is divided into a set of triangular or curvilinear quadrilateral elements (Figure 2-1b). A representative element of the set is presented in Figure 2-1c, with the points i, j and k defining the nodes of the element. The problem is to determine the state of total stresses, and the excavation-induced displacements, throughout the assembly of finite elements.

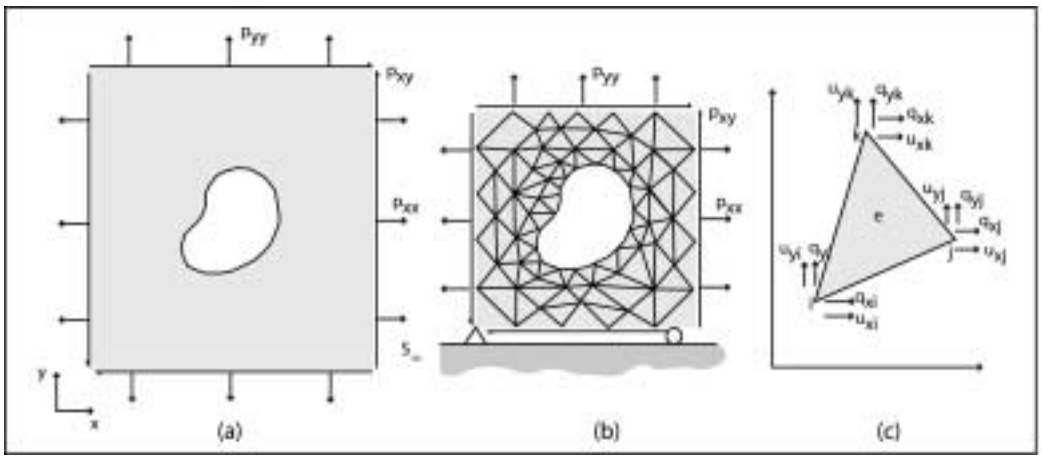

Figure 2-1. *Development of a finite element model of a continuum problem /from Brady and Brown, 1999/.*

Basic concept of the method

The method is an application of the direct stiffness method of structural analysis. The main steps are to divide the structure into nodal points and elements, define the structural stiffness matrix of the structure, which will connect nodal displacements and forces at nodal points, then introduce forces and write equations of equilibrium /Goodman, 1974/.

The first step is then to divide the structure in finite elements. The simplest element is a triangle defined by 3 nodal points (Figure 2-1c) and derived assuming a constant state of strain throughout the element.

Then, a set of functions, which define the displacement components at any point within a finite element, must be written in terms of the nodal displacements. By defining the displacement field in an element in terms of the nodal displacements $-u_{xi}$, u_{yi} (Figure 2-1c), the interpolation procedure ensures continuity of the displacements both across an element interface with an adjacent element, and within the element itself /Brady and Brown, 1999/.

The assumption in the finite element method is that transmission of internal forces between the edges of adjacent elements can be represented by interactions at the node of the elements, and the strains are related to nodal displacements.

According to these assumptions, the stiffness matrix, [K], of an element is expressed as followed /Goodman, 1974/:

$$[K] = a[L_0]^T [C] L_0 \tag{2.1}$$

where a is the area of the triangle, $[L_0]^T$ is the matrix accounting for the relationship between strains and nodal displacements, and [C] is the matrix derived from the stress strain relationship. The general expression of $[L_0]$ is:

$$\{\varepsilon\} = [L_0]\{u\} \tag{2.2}$$

where $\{\varepsilon\}$ represents the strains, and $\{u\}$ the nodal displacements.

The general expression of [C] is the following:

$$\{\sigma\} = [C]\{\varepsilon\} \tag{2.3}$$

Expressions of [C] are dependent of the behaviour of the rock masses, and are related to the values of the Young's modulus and the Poisson's ratio.

Since strains are constant throughout a triangle and are related to nodal displacements, and according to equation (2.2), stresses are related to nodal displacements by the following expression:

$$\{\sigma\} = [C][L_0]\{u\} \tag{2.4}$$

Hence, these induced strains and the elastic properties of the medium together determine the induced stresses in an element.

Representation of the joint system

However, isotropic rock masses are quite uncommon and joints must be input in the models. Joints are inserted in the previous discretised model as described above by special elements consisting of 2 lines of nodal points that link the "rock" structural elements, or triangles (Figure 2-2). As for the intact isotropic rock mass, strains are related to nodal displacements in terms of the relative displacements and rotation of the 2 walls as measured at the joint centre. The strain displacement matrix can be expressed as followed /Goodman, 1976/:

$$\{\varepsilon_j\} = [L_0]\{u\}_{s,n} \tag{2.5}$$

where $\{\varepsilon_j\}$ is the strain quantity along joints, and $\{u\}_{s,n}$ represents the nodal displacements at points I, J, K and L in the local directions s, n.

Joint "stresses" and "strains" can then be expressed as followed:

$$\{\Delta\sigma_j\} = [C_j]\{\varepsilon_j\} \tag{2.6}$$

where $[C_j]$ is the joint stiffness matrix in local co-ordinates.

An expression of the stiffness matrix of the joint element is then derived with regard to the global co-ordinates, and a possible expression is the following /Goodman, 1976/:

$$\{\Delta F\}_{x,y} = [K_{x,y}]\{u\}_{x,y} \tag{2.7}$$

where $\{\Delta F\}_{x,y}$ represents the increment of external forces, $[K_{x,y}]$ the joint stiffness matrix, and $\{u\}_{x,y}$ the nodal displacements matrix, all expressed in global co-ordinates.

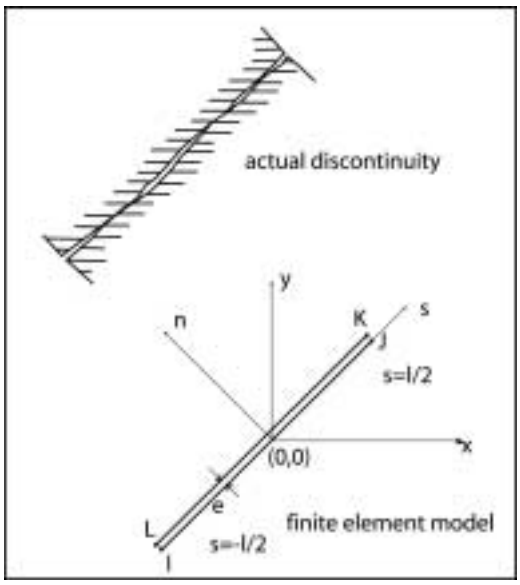

Figure 2-2. *Representation of a "joint" element /after Goodman, 1976/.*

The next step is to introduce applied forces and write the equations of equilibrium. Different equations of the residual stress forces are then provided according to the origin of the applied forces. The solving of these equations provide the solution.

2.2.2 Other continuum models, derived from FEM

Different approaches have been conducted to attempt modelling, with the continuous analysis technique, the influence of joints in a rock mass.

Anisotropic continuum model /Singh, 1973/

/Singh, 1973/ developed an anisotropic continuum model in which the average influence of joints, bedding planes and similar planar features are considered. Discontinuous, but parallel, system of joints may be considered, each having the same normal and shear stiffness. The intact rock is homogeneous but may be anisotropic. Knowing the average fracture frequency n_1 and the average compliance of the joints, the compliance matrix of the rock mass [M] can be expressed as:

$$[M] = [M_r] + n_1 \left[K_{jl}\right]^{-1} \left[B_{jl}\right] \tag{2.8}$$

where $[M_r]$ is the compliance of the rock, $\left[K_{jl}\right]^{-1}$ is the block matrix expressing the stiffness of the joint set, and $\left[B_{jl}\right]$ is the matrix expressing the stress concentration factors along the joint. The same formulation as equation (2.8) can be written for a system of joints that is orthogonal to the first one. The model can be generalised to account for system of joints that may express random variations of stiffness and spacing.

The results of this model proved to be accurate, when compared to the finite element joint model, in regions of lower stress gradients.

Compliant joint model /Labreche, 1985/

/Labreche, 1985/ presents a compliant joint model developed from a continuum approach, which is based on a distribution of the joints throughout the model and which monitored apertures of joints. To account for the presence of joints, the deformability of the rock mass is expressed in terms of equivalent elastic moduli. However, the model did not provide a realistic response of the rock mass when compared to the experimental data.

Constitutive model of jointed rock masses /Cai and Horii, 1991/

/Cai and Horii, 1991/ developed a implementation constitutive model that accounts for connection and interaction effect, density and orientation of joints, as well as for the mechanical properties of the joints themselves. The interaction and connection terms refer to the impact of the presence of joints and their stiffness to the stress distribution in the rock mass. The key-point in this model of jointed rock masses is the fact that the stress acting on the joint is different from the overall stress of the Representative Volume Element (RVE). The stress carried by the joint depends on the stiffness of its surroundings, which is affected by other joints and the connection of joints. To represent the relation between the average incremental stresses over the joint and the average incremental stresses over the RVE, they introduced the joint stress concentration tensor (JSCT).

In their model, /Cai and Horii, 1991/ assumed that the behaviour of the intact rock is elastic and the equations are derived from the formulations presented in the precedent paragraph. The constitutive laws describing the behaviour of the joints are based on the plasticity theory.

Their estimation of the joint stress concentration tensor is based on the decomposition of the original problem into sub-problems (Figure 2-3). Then the equations describing the relationships between strains and displacements are written in terms of the system stiffness:

$$\begin{aligned} d\bar{\sigma} &= \bar{K}^{n} d\bar{\upsilon} \\ d\bar{\tau}_{s} &= \bar{K}^{s} d\bar{u}_{s} \\ d\bar{\tau}_{t} &= \bar{K}^{t} d\bar{u}_{t} \end{aligned} \qquad (2.9)$$

The expressions of $\bar{K}^{n}, \bar{K}^{s}$ and $\bar{K}^{t}$ are dependent of the properties of the joints, as well as the effect of joint interaction and connection.

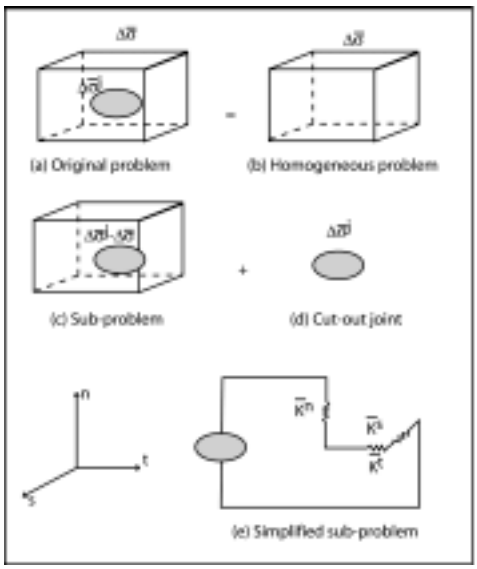

Figure 2-3. *Representation of the presence of a joint /from Cai and Horii, 1993/.*

Applicability

The main applications of the method are relating to civil engineering in rock masses, and especially large-scale underground excavations. /Cai and Horii, 1993/ have applied their model to a plate-loading test of a diorite with 2 sets of joints, and showed that this is quite appropriate. Nevertheless, some problems, such as formation of the joints, remain to be solved. This is an important issue, as evolution of joint aperture and density will influence the behaviour of the jointed rock mass along the test.

The extent of the discretised space must be large enough to avoid that the conditions imposed on the outer boundary influence the solution near the cavity. The elements near the outer boundary may be rather large as deformation and displacement may not vary much at large distances from the cavity. However, the "transition mesh" between inner and outer boundaries must be sufficiently smooth to avoid gradients in the solutions /Crouch and Starfield, 1983/. Another limitation is that most of the models developed and implemented with the finite element method are time-independent and do not reflect the evolution of properties of the rock masses with time.

2.2.3 The Boundary Element Method (BEM)

This method is particularly useful where linear elastic behaviour can be assumed for a rock mass, or where elastic domains are separated by continuous planes of weakness.

General formulation of the model

The essence of the method is definition and solution of a problem entirely in terms of surface values of traction and displacement. For semi-infinite and infinite body problems, the application of the principle of superposition makes the solution most applicable to elastic media. The principle of superposition is based on the assumption that a specific problem can be defined as the superposition of two problems (Figure 2-4). The impact of an excavation in an infinite, elastic medium, can be treated as the superposition of a) a continuous, uniformly stressed body (Figure 2-4b), and b) the surface subject to excavation-induced surface tractions and displacements (Figure 2-4c).

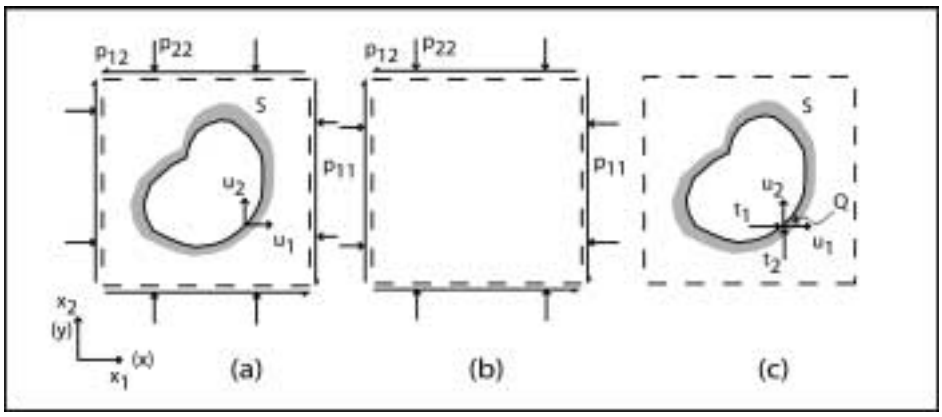

Figure 2-4. *Problem definition for Boundary Element Analysis /from Brady, 1987/.*

Hence, solutions must be found at the boundary. The procedure is to divide the boundary or surface S into N elements. Adopting a physical (and more or less indirect) approach, a system of N singular equations is set at the midpoints of each element. These equations account for the conditions required for each element, and the unknowns are the strengths. Once solutions are defined at singularities, they are computed to match the rest of the boundary or surface. On the other hand, the mathematical (and more direct) approach is based on a system of algebraic equations that relate the unknown boundary parameters to specified parameters at each element of the contour /Crouch and Starfield, 1983/.

The boundary can be approximated by a set of linear elements, or by different shape functions (Figure 2-5). In the case of linear isoparametric elements (Figure 2-5b), formulations of variations of tractions and displacements are as followed /Brady, 1987/:

$$t_i(\xi) = t_i^1 N^1(\xi) + t_i^2 N^2(\xi) = t_i^p N^p(\xi) \tag{2.10}$$

$$u_i(\xi) = u_i^1 N^1(\xi) + u_i^2 N^2(\xi) = u_i^p N^p(\xi) \tag{2.11}$$

where $t_i(\xi)$ and $u_i(\xi)$ are the variations of tractions and displacements of the intrinsic element ξ, and $N^p(\xi)$ are the linear shape functions.

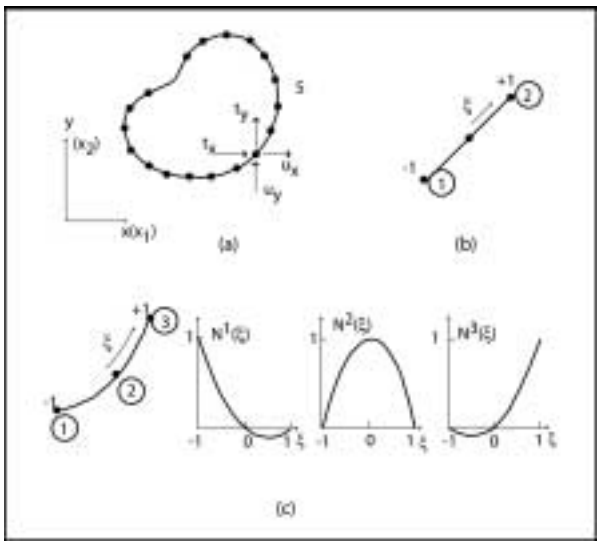

Figure 2-5. *(a) Discretisation of a boundary surface into elements defined by surface nodes, (b) linear boundary element, (c) element geometry and shape functions for a quadratic boundary element /after Brady, 1987/.*

In the case of quadratic isoparametric elements (Figure 2-5c), the nodal displacements are expressed in local co-ordinates:

$$u_i(\xi) = u_i^p \bar{N}^p(\xi) \qquad p=1, 2, 3, \qquad -1 \le \xi \le 1 \tag{2.12}$$

In order to maintain compatibility between displacement and traction, the three-noded has to be considered in two sections, with local co-ordinates ♀, ☨ for each section /Yeung and Brady, 1982/:

$$\begin{aligned} t_i(\alpha) &= t_i^1 N^1(\alpha) + t_i^2 N^2(\alpha) = t_i^p N^p(\alpha) \quad -1 \le \alpha < 0 \\ t_i(\beta) &= t_i^2 N^1(\beta) + t_i^3 N^2(\beta) = t_i^{p+1} N^p(\beta) \quad 0 \le \beta \le 1 \end{aligned} \tag{2.13}$$

BEM for a non-homogeneous medium and dominant discontinuities

The concept has been developed to account for heterogeneous media and planes of weakness. In case of non-homogeneous medium and dominant discontinuities (Figure 2-6), the conditions to be satisfied for the problem are the governing equations for elastostatics in each subregion, continuity of traction and displacement at the interfaces between subregions, and the criteria defining slip and separation on the joint surfaces /Brady, 1987/. Equations developed for the homogeneous system are implemented adding a boundary constraint between homogeneous subregions. The complete set of equations for interfaced subregions and excavations within them are constructed and then explicit boundary conditions are needed for excavation surfaces only. Stresses and displacements within any subregion can be calculated from the boundary element equation for the subregion, using the appropriate surface and interface tractions and displacements.

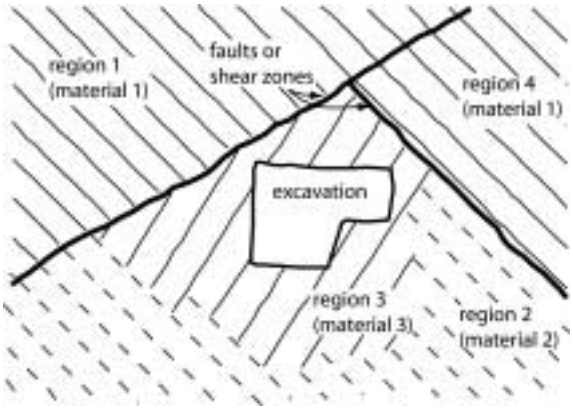

Figure 2-6. *Problem definition for boundary element analysis of a heterogeneous medium and continuous planes of weakness /from Brady, 1987/.*

Joints are assumed to follow elastic response to applied loads, and the system is represented by a set of two springs accounting for the normal and tangential stiffness. Equations of tractions are implemented according to the conceptual models of joints.

The equation yielding the system is dependent on blocks of the displacement and traction matrices, as well as blocks of the joint stiffness matrix. The formulations involve that direct solutions representing joint elastic and subregion behaviour can be provided, and then iterative procedure determine the equilibrium stresses and displacements at the joint nodes.

Applicability

The boundary element method can be used to solve both dynamic – such as transient heat flow, linear visco-elasticity or dynamic elasticity –, and static problems – such as equilibrium problems in linear elasticity.

This method has mostly been used and developed to solve problems in excavation design, which usually involves evaluation of a range of design options or iterating to establish the optimum design for a structure in rock /e.g. Crotty and Wardle, 1985/. /Brady and Brown, 1981/ also applied the method in determining mine local stiffness, which is seen as a part of the broader problem of mine global stability.

/Andersson and Dverstorp, 1987/ present an application of the boundary element method to the simulation of fluid flow in a 3-D discrete fracture network. The flow is discretised at each disk and boundary conditions are set at the boundary of the disk and inside the disk.

2.3 Computer Programs for Modelling Continuous Systems

Many computer programs based upon a continuum mechanics formulation (e.g. finite element and Lagrangian finite-difference programs) can simulate the variability in material types and non-linear constitutive behaviour typically associated with a rock mass, but the representation of discontinuities requires a discontinuum-based formulation. There are several finite element-, boundary element- and finite difference

programs available, which have interface elements, or “slide lines” that enable them to model a discontinuous material to some extent.

A program called JETTY, based on the finite element method, has been developed by St. John (presented in /Goodman, 1976/). This program can be identified to a “basic” development that requires further improvements and enlargements.

One can refer to the code BITEMJ, described by /Crotty, 1983/, that is based on the boundary element method and implements non-linear joint features. This code should be particularly useful for analysis of the stability of pillars containing planes of weakness /Brady, 1987/.

/Larsson et al, 1985/ developed a theoretical model that has been implemented in a finite element program in order to determine the reaction of the joints and bolts (in term of displacement and stresses) during the excavation. The model is based on a continuum approach of a bolt-reinforced rock mass, *i.e.* intact rock, joints and bolts are assigned continuous properties. The equations relating to the different structural components have been derived from the assumed behaviour laws. The results of the numerical model were in good agreement with the experimental tests especially for the initial part of the shearing.

However, their formulation is usually restricted in one or more of the following ways. First, the logic may break down when many intersecting interfaces are used; second, there may not be an automatic scheme for recognising new contacts; and, third, the formulation may be limited to small displacements and/or rotation. For these reasons, continuum codes with interface elements are restrictive in their applicability for analysis of underground excavations in fractured rock /UDEC, 2000/.

3 Discontinuum analysis techniques

3.1 General definition of the approach

A discontinuous medium is distinguished from a continuous one by the existence of contacts or interfaces between the discrete bodies that comprise the system. Hence, in the discontinuum analysis approach, the object material is taken as an assemblage of discrete bodies interfaced by joints in the case of fractured rock masses, or regularly-shaped particles in the case of granular materials. The bodies act as entities and communicate with their neighbours via contact forces at boundaries.

This approach is more appropriate than the continuous one to model fractured rock masses. The presence of joints influences the behaviour of the rock mass, and the properties are lower than that of the intact rock. In this case, the elasticity assumption made on the intact rock mass by the continuous approach may not be appropriate and a rigid behaviour may be assigned to the rock mass.

The finite translational and rotational displacements of discrete bodies, including complete detachment, are permitted and the contacts among the discrete bodies considered can be identified and updated automatically during the course of calculation. This permits a more efficient treatment of non-linearity of the mechanical behaviour of the joints, such as sliding, opening or closing. Both dynamic and static problems can be treated using an appropriate viscous damping scheme /Jing, 1990/.

The approaches developed upon the assumptions aforementioned are grouped under the expression “Discrete Element Method”. These methods can be categorised both by the way they represent contacts and by the way they represent the discrete bodies in the numerical formulation /UDEC, 2000/. Two main approaches are highlighted that are the Distinct Element Method (DEM) and the Discontinuous Deformation Analysis Method (DDA); other “minor” approaches that are the modal method and the momentum-exchange method can also be mentioned.

3.2 Concept and problematic

The conceptual and numerical model must account for two types of mechanical behaviour in a discontinuous system: (1) behaviour of the discontinuities, and (2) behaviour of the solid material /UDEC, 2000/.

3.2.1 Behaviour of the discontinuities

First, the model must recognise the existence of contacts or interfaces between the discrete bodies that comprise the system. Numerical methods are divided into two groups by the way in which they treat behaviour in the normal direction of motion at contacts:

- Soft-contact approach; a finite normal stiffness is taken to represent the measurable stiffness that exists at a contact or joint.

- Hard-contact approach; interpenetration is regarded as non-physical, and algorithms are used to prevent any interpenetration of the two bodies that form a contact.

3.2.2 Behaviour of the solid material

According to the type of structural model adopted, the solid material constitutes the particles or blocks in the discontinuous system. There are two main divisions in this representation: the material may be assumed rigid or deformable. The assumption of material rigidity is a good one when most of the deformation in a physical system is accounted for by movement on discontinuities. This condition applies, for example, in an unconfined assembly of rock blocks at a low stress level, such as a shallow slope in well-fractured rock. The movements consist mainly of sliding and rotation of blocks and of opening and interlocking of interfaces. If the deformation of the solid material cannot be neglected, two main methods can be used to include deformability. In the direct method of introducing deformability, the body is divided into internal elements or boundary elements in order to increase the number of degrees-of-freedom. The possible complexity of deformation depends on the number of elements into which the body is divided. For example, the discrete element code UDEC (Itasca) automatically discretises any block into triangular, constant-strain zones, which in case of elastic properties, have the same formulation to that of constant-strain finite elements (see section 2.2.1). The zones may also follow an arbitrary, non-linear constitutive law. The disadvantage of the method is that a body of complex shape must necessarily be divided into any zones, even if only a simple deformation pattern is required.

3.3 Review of the main codes for Discrete Element methods

According to /Cundall and Hart, 1985/, the name “discrete element” applies to a computer program only if it:

(a) Allows finite displacements and rotations of discrete bodies, including complete detachment; and

(b) Recognises new contacts automatically as the calculation progresses.

A discrete element code typically will embody an efficient algorithm for detecting and classifying contacts. It will maintain a data structure and memory allocation scheme that can handle many hundreds or thousands of discontinuities. /Cundall and Hart, 1985/ identify the following four main classes of codes that conform to the definition of a discrete element method:

- Distinct element programs.
- Modal methods.
- Discontinuous deformation analysis.
- Momentum-exchange methods.
- Alternative codes (“Limit equilibrium methods”).

3.3.1 The Distinct Element Method

The distinct element method described by /Cundall, 1971/ was the first to treat discontinuous rock mass as an assembly of quasi-rigid blocks interacting through deformable joints of definable stiffness /Brady and Brown, 1999/. It has been first developed to model the progressive failure of slopes /Cundall, 1971/.

The rock mass is treated as an assemblage of blocks interfaced by a joint network (i.e. the discontinuity is treated as a boundary condition). Movements result from the propagation through the block system of disturbances caused by applied loads or body forces. This is a dynamic process in which the speed of propagation depends on the physical properties of the discrete system /UDEC, 2000/.

The essential numerical problems that must be solved are the following /Jing, 1990/:

- Representation of the block geometry.
- Representation of internal deformation of blocks.
- Representation of the block contacts, both kinematically and mechanically.
- Integration of equations of motions.

Representation of the block geometry

Blocks are presented as polyhedra in 3D with each face a planar polygon having any number of rectilinear edges, or, in 2D, as polygons with straight edges /Jing, 1990/. An example of 2D representation is illustrated in Figure 3-1a.

Representation of internal deformation of blocks

The intern deformation of distinct blocks is modelled by internal discretisation of a finite number of finite difference triangular elements (Figure 3-1b). The complexity of the resulting system depends on the number of elements created. The sum of the net nodal forces is 0 if the body is at equilibrium, or in steady-state (e.g. plastic flow). Otherwise, the nodes will be accelerated according to the finite different form of Newton's second law of motion. Strains and rotations are related to nodal displacements at each timestep, so that strain in each zone is known after each timestep. Hence, stresses must be determined to proceed the next timestep from the stress-strain relations.

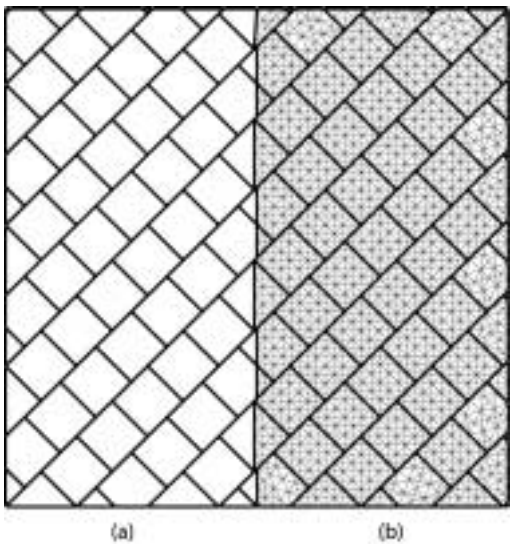

Figure 3-1. *Zoning within a model containing a system of continuous and discontinuous joints: (a) distinct element blocks, (b) zoning within blocks /UDEC, 2000/.*

Rock joint representation

As stated in section 3.1, the numerical model of discrete element must recognise the behaviour of discontinuities. First of all, the existence of contact surface between blocks, *i.e.* the existence of rock joints, must be recognised.

A rock joint is defined as a contact surface, composed of individual contact points that form between two block edges. Contacts are identified when a pair of blocks do touch, or if the distance (or gap) between the blocks is minimal. In case of rigid block assumptions, the deformability of the assemblage is conferred by the deformability of the joints. Mainly two types of approaches can be used (see section 3.1). According to the soft approach, a linear stress-displacement relation is assumed in the normal direction, and is written as followed:

$$\Delta\sigma_n = -K_n \Delta u_n \tag{3.1}$$

where $\Delta\sigma_n$ is the effective normal stress increment, K_n is the joint stiffness, and Δu_n is the normal displacement increment. The overlap between touching blocks is a convenient way of measuring relative normal displacement (Figure 3-2b).

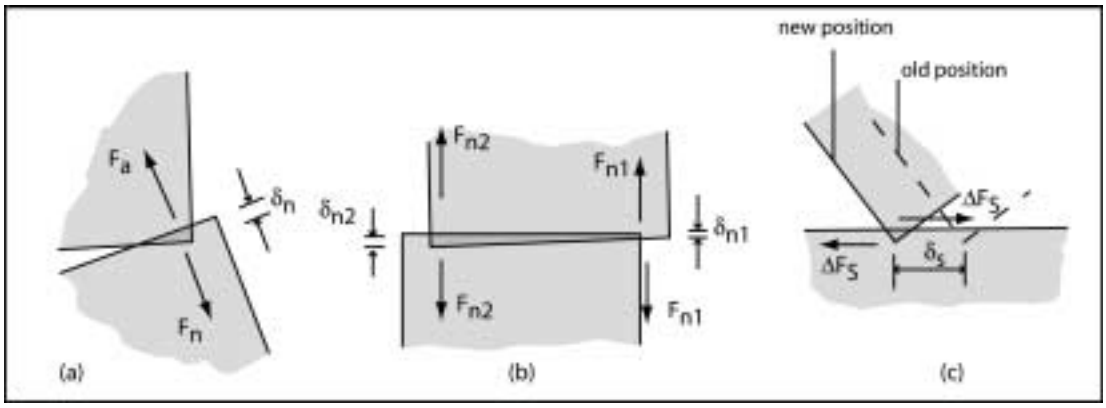

Figure 3-2. *Normal and shear modes of interaction between distinct elements /Brady and Brown, 1999/.*

Note: δ_n, δ_s are respectively similar to Δu_n and Δus as presented in equation (3.1), and F_i and δ_t are related by the expression: $\sigma_i = F_i / l$.

The normal stress is determined by the relative spatial position of the two blocks. However, the shear stress depends at any stage on the deformation path to which the contacts have been subjected. For an increment of shear displacement Δu_s, the increment of shear stress is expressed as followed:

$$\Delta\sigma_s = K_s \Delta u_s \tag{3.2}$$

where $\Delta\sigma_s$ is the increment shear stress, K_s is the shear contact stiffnesss, and Δu_s the shear displacement increment (Figure 3-2c).

The increment displacements of the contacts are dependent of the behaviour of the joints, and hence, of the constitutive models chosen (for description of the models the reader is referred to sections 3.1.2 and 3.1.3 in the main report).

The deformation equations (3.1) and (3.2) account for elastic, reversible processes. However, when separation occurs, contacts vanish and these relations are not appropriate. To represent this behaviour, the total shear force must be computed at any stage. If the total shear force exceeds the maximum frictional resistance ($F_n \tan\phi$), slip will occur /Brady and Brown, 1999/.

Integration of equations of motions

The calculations performed in the distinct element method alternate between application of a force-displacement law at all contacts (presented in section 3.3.1) and Newton's second law at all blocks. The force-displacement law is used to find contact forces from known (and fixed) displacements. Newton's second law gives the motion of the blocks resulting from the known (and fixed) forces acting on them. If the blocks are deformable, motion is calculated at the gridpoints of the triangular finite-strain elements within the blocks. Then, the application of the block material constitutive relations gives new stresses within the elements.

The Newton's law of motion is used to obtain velocities and displacements from unbalanced forces, which occur when elements are not in perfect equilibrium with their neighbours. The task is to find a set of displacements that will bring elements at equilibrium, or, if not possible, indicate the mode of failure. Different numerical solution schemes can be used /Cundall, 1987/:

- Direct resolution of a system of equations by a standard matrix method. This approach can account for non-linearity but is not well suited for frequent changes of connectivity.

- Relaxation scheme. A common form of relaxation scheme is one where displacements are adjusted in such a way as to reduce the unbalanced forces at nodes. The approach proposed by /Otter et al, 1966/ is more appropriate for taking into account large displacement increments, partly due to the use of velocity-proportional damping. This allows reaching a force equilibrium state as quickly as possible.

However, the use of velocity-proportional damping involves three main difficulties (listed by /Brady, 1987/), such as the application of a single damping constant for the whole model. Alternative forms of velocity-proportional damping can be used, such as viscous damping for quasi-static analysis or adaptative damping /Cundall, 1987/.

The reader is referred to the UDEC user manual /UDEC, 2000/ for detailed description of calculations for the Distinct Element Method (regarding equations of motions, equations for conservation of momentum and energy in the DEM).

Applicability

The essential feature and asset of the method is to model the motion of each block with respect to any other. These methods have been applied to both civil and mining engineering problems, and are appropriate to assess stability of discontinuous rock slopes. The Distinct Element method has become a powerful numerical technique for general geomechanical problems. Specific formulations have been developed to account for local and spatially extensive reinforcement /Brady and Lorig, 1988/.

/Lemos et al, 1985/ present different applications of the distinct element method as implemented in UDEC (numerical code described in section 3.4.1): collapse of an excavation roof modelled with both rigid and deformable blocks, the potential earthquake generation of "en echelon" faults, modelling of joint displacement during an earthquake.

3.3.2 Modal Methods

This code was first developed from the Distinct Element Method for improving solutions to calculate element deformations /Williams and Mustoe, 1987/.

General concept of the modal method

As mentioned above, this method is an implementation of the Distinct Element method. The representation of blocks and the identification of contacts are made following the same assumptions. Specially designed regularly-shaped blocks are required for this

method to avoid large errors. Rigid and deformable bodies are handled and modelled by this method. The method is similar to the DEM in the case of rigid blocks but differ for deformable bodies. The main characteristics of the approach are described in the following section.

Representation of internal deformation of blocks

Superposition of block deformation is used instead of internal discretisation of blocks used in DEM. The novelty of this method is in the decoupling of the rigid body and strain deformation equations for each element /Hocking et al, 1985/. The deformability of an element can be written in terms of its eigenvectors, as a superposition of its natural modes. The zero frequency modes yield the rigid body motion, and the non-zero modes provide the deformational behaviour.

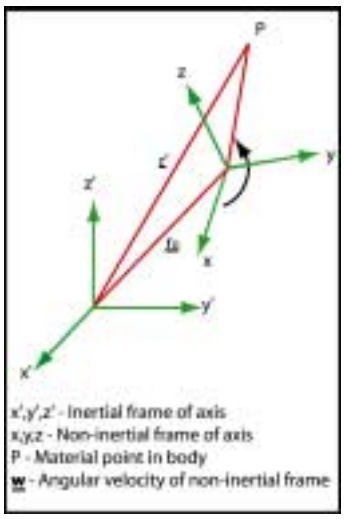

Figure 3-3. *Inertial and non-inertial axes /from Hocking et al, 1985/.*

In theory, the motion is decomposed into a mean rigid body motion and a relative motion. The rigid body defines a non-inertial dynamic reference frame, whereas the "deformations" define an inertial frame. Transfer and transformations are done according to the relationships between both frames (Figure 3-3), and deformations are addressed with respect to that non-inertial frame /Hocking et al, 1985/. As a result, three equations of motion, relative to the non-inertial reference frame, are written. They define the translational motion of the centre of mass, the rotational motion of the body around the centre of mass, and the internal deformation of the body. Hence, decoupled equations are derived for each natural mode of vibration of the element.

In case of a structure discretised into many finite element bodies, the equation of motion can be solved by defining modes for the whole structure, and a solution is achieved by the modal superposition method /Bathe and Wilson, 1976/. In this way, the structure, as described above, is resolved to a single complex element whose properties are provided by the modes. To reflect internal deformation, the flexibility of the structure to the modes must be determined.

Applicability

A typical code, CICE, has been developed by /Hocking et al, 1985/ and applied to some ice mechanics problems, such as ride-up and pile-up. This code provides the potential to analyse discontinuous media undergoing fracturing, with parts of the media undergoing large motion relative to the other parts. If the Stress State exceeds a specific yield limit, then the elements may fracture resulting in additional nodes and elements being automatically generated. The connectivity of the elements is also automatically updated regarding the amount of displacement of an element or an assemblage of elements. The same process is applied in case of large displacements.

This method appears to be better suited for loosely-packed discontinua, and may not be well suited for geomechanical problems in which the deformation gradient inside one block has very ununiform distribution /Jing, 1990/.

3.3.3 Discontinuous Deformation Analysis (DDA)

This method is a "back-analysis" scheme used to solve inverse problems, that means for example identifying the mechanisms of displacement measured in a rock slope. This is especially useful when the mechanisms involved is a combination of different modes and the sets of data obtained by field survey are not so obvious.

General concept of the method

Blocks are a) in 2D polygons with straight edges and any number of edges, and b) in 3D polyhedra with faces represented as planar polygons with any number of edges. Both convex and concave blocks are allowed.

As for the aforementioned discrete element methods, the bodies may be rigid or deformable. The main novelty is that displacements are considered in terms of formulations of the difference between predicted and measured displacements. This method is described by /Shi and Goodman, 1985/ and shortly reviewed in the following section.

Formulation of block displacements

The displacements (u,v) of a point (x,y) are formulated according to parallel translation, rotation, and the expression of normal and shear strain. The cumulative displacements of a point in a rigid block is expressed as followed /Shi and Goodman, 1985/:

$$\begin{aligned} u &= \varepsilon_x (x - x_0) + (\Gamma_{xy} - \omega)(y - y_0) + u_0 \\ v &= (\Gamma_{xy} + \omega)(x - x_0) + \varepsilon_y (y - y_0) + v_0 \end{aligned} \tag{3.3}$$

where $\varepsilon_x, \varepsilon_y$ represent the strains, Γ_{xy} defines an irrational shear strain, ω expresses the rotation, (u_0, v_0) determine the displacement of a point (x_0, y_0).

Having formulated predicted displacements, the square difference between predicted and measured displacements Φ_a is expressed as:

$$\Phi_a = (m_1 - u)^2 + (m_2 - v)^2 \tag{3.4}$$

where m_1 and m_2 are the measured displacement components of the point (x,y).

Displacements along contacts (or between blocks) are formulated as displacements of two points P_1 and P_2 belonging two neighboring blocks, i and j (Figure 3-4a). A fictitious line E_b is drawn between these two points and the displacements of these points are projected on the line. Then, the expressions are combined to produce a formulation for the square of the difference between the calculated and measured extension along line E_b between P_1 and P_2:

$$\chi_b = \left[m + p^i - p^j \right]^2 \tag{3.5}$$

where p^i and p^j are the projection at displacements at P_1 and P_2 along line E_b.

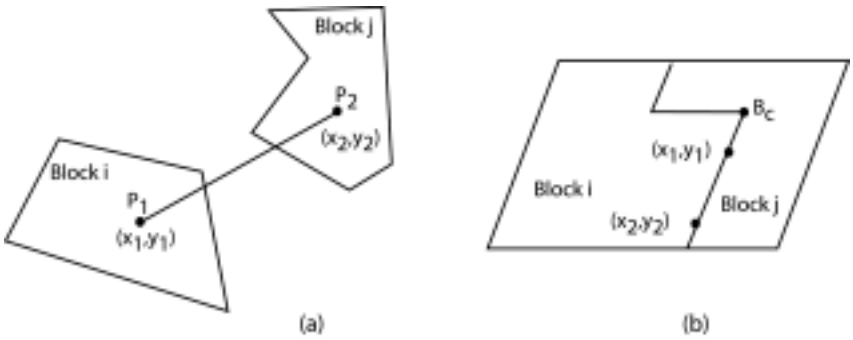

Figure 3-4. *(a) Problem definition for block displacements, and (b) for non-closing of joints.*

Assuming an end point of a segment on a boundary between two blocks (Figure 3-4b), the contacts between the blocks are considered regarding the unit vector normal to the boundary. The equations of normal displacements of both blocks at this end point B_c are written, and the relative displacement is the sum of the displacement of both blocks. The segment is opening when this sum is positive, and is closing is it is negative. In order to avoid closing and overlapping or "interpenetration" of blocks, a "punishment" factor is introduced /Shi and Goodman, 1985/. The square of relative deformation across the boundary, ψ_c, is expressed as:

$$\psi_c = P\left(e^i + e^j\right)^2 \tag{3.6}$$

where e^i and e^j represent the displacement component for block i and j, P is the "punishment factor.

Integration of equations of motions

Relationships (3.3), (3.4) and (3.5) here presented as simplified expressions define the system, with the assumption that joint opening is preferred to joint closing. The solution is gained through a differentiation of the functions to each deformation displacement at each block.

The equilibrium of the block is attained by minimisation of a potential energy functional and a first order approximation of the displacements are used under the assumption that at each time step, block displacement and deformation are small. Both static and dynamic analysis with large translational and rotational displacements can be handled easily by this method. Constant strain is calculated for each block.

Applicability

This method has been previously developed to provide an attempt to analyse deformation data /Shi and Goodman, 1985/. One advantage of the method is to provide both forward and backward simulation capacities. The method has been extended by improving the contact algorithm, adding block fracturing and sub-blocking capacities /Lin et al, 1996/. The further development of the DDA extended its range of applicability to the study of rock fall, slope stability and underground excavation problems. The new algorithms turn the DDA to a useful tool for modelling fracture propagation in already fractured rock masses.

However, the constant strain logic for the entire block, currently used in this code, may not be very well suited for some geomechanical problems in which the deformation and stresses inside one distinct block are not uniform /Jing, 1990; Lin et al, 1996/. Another limitation is that the formulation of the DDA is based on the minimisation of the potential energy of the system, and is a displacement method.

Limitations are also related to the lack of possibilities for modelling reinforcement systems, and for modelling load changes as a function of time. Moreover, the joint constitutive model can not encompass sequential or cyclic loading.

3.3.4 Momentum-exchange methods

This method assumes both the contacts and bodies to be rigid; momentum is exchanged between two contacting bodies during an instantaneous collision. Friction sliding can be represented /UDEC, 2000/.

This method has been mostly used in the 1980s, and developed for particle and impact mechanics. The range of application of this method is not under the scope of this study, and no further review has been done.

3.3.5 Limit equilibrium methods

Another class of codes, defined as limit equilibrium methods, can also model multiple intersecting discontinuities but does not satisfy the requirements for a discrete element code /UDEC, 2000/. These codes use vector analysis to establish whether it is kinematically possible for any block in a blocky system to move and become detached from the system. The "key-block" or block theory developed by /Goodman and Shi, 1985/ and the vector stability analysis approach by /Warburton, 1981/ are examples of the Limit Equilibrium method.

General concept of the "block theory" method

Block theory may be called a geometric approach; it considers the creation of an excavation as the introduction of a geometric space in a rock mass, and evaluates the possibilities for the rock mass to invade this space /Goodman, 1995/. This method pertains primarily to blocky rocks. The following definition of blocky rock is given by /Goodman, 1995/: "blocky rock has three or more persistent joint sets clearly developed (…), and includes rock masses which are regularly cut by extensive joint sets in highly determined orientations, and rock masses which are variably and randomly cut by non-

extensive joint sets in statistically dispersed sets of orientations, as well as all intermediate structural conditions".

The system of joints identified in the rock mass is modelled according to the data set and using different statistic distribution laws. However, the simplified trace map simulation technique developed by /Shi et al, 1985/ proved to be more appropriate to generate joint systems in large volumes and determine the key-blocks.

All blocks are assumed to be rigid. This approach does not examine subsequent behaviour of the system of blocks or redistribution of loads.

The approach is based on the identification of a "key-block", term which identifies any block that would become unstable when intersected by an excavation. The analysis of vector equations and inequalities is handled using stereographic projection. From graphical analysis of the projections and taking into account the friction angle of joint faces, safe and unsafe areas can be determined, as well as the mode of sliding. /Shi and Goodman, 1989/ introduced the graphical representation of loops for friction angles that identified what friction angle is required for equilibrium.

The recent formulation of the block theory can handle sliding and rotational modes of key-blocks.

Applicability

/Goodman and Shi, 1985/ present application and development of block theory for surficial excavations, underground chambers, and for tunnels and shafts. /Goodman, 1995/ focuses on the application of the method to the identification and analysis of blocks in foundations, and especially on the assessment of the safety of a dam.

Rather than determining strains, stresses and displacements, this method directly identifies dangerous or potentially dangerous blocks in an open slope or under an excavation. It may be considered as a first step by identifying the blocks to analyse. Moreover, this is a three-dimensional, easy-to-handle method, in which solution is mostly found with graphical techniques.

3.4 Computer Programs for Modelling Discontinuous Systems

A well-known and use numerical code for Distinct element methods is the two-dimensional program called UDEC /Cundall, 1980; Lemos et al, 1985/. This program was first developed in 1980 to combine, into one code, formulations to represent both rigid and deformable bodies (blocks) separated by discontinuities. This code can perform either static or dynamic analyses. Since the first developments, the code has been implemented to account for fluid flow, different non-elastic behaviours of the rock mass or the joints /Lemos et al, 1985/.

The following section includes a short description of the computational solutions adopted in UDEC to model the behaviour of fractured rock masses. This section refers to the UDEC's user manual /UDEC, 2000/.

3.4.1 UDEC

The code is based on a dynamic (time domain) algorithm that solves the equation of motion of the blocks system by an explicit finite difference method. The motion laws and joint constitutive relations are applied at each time step. Hence, displacements, new contacts and new positions are updated after each time step.

An important feature in this code is the contact detection, identification, and updating. In general, for each pair of blocks that touch (or is separated by a small enough gap), data elements are created to represent point contacts. In UDEC, adjacent blocks can touch along a common edge segment or at discrete points where a corner meets an edge or another corner. For rigid blocks, a contact is created at each corner interacting with a corner or edge of an opposing block. If the blocks are deformable, point contacts are created at all gridpoints located on the block edge in contact. Thus, the number of contact points can be increased as a function of the internal zoning of the adjacent blocks.

A specific problem with contact schemes is the unrealistic response that can result when block interaction occurs close to or at two opposing block corners. In reality, crushing of the corners would occur as a result of a stress concentration. In UDEC, a realistic representation is achieved by rounding the corners.

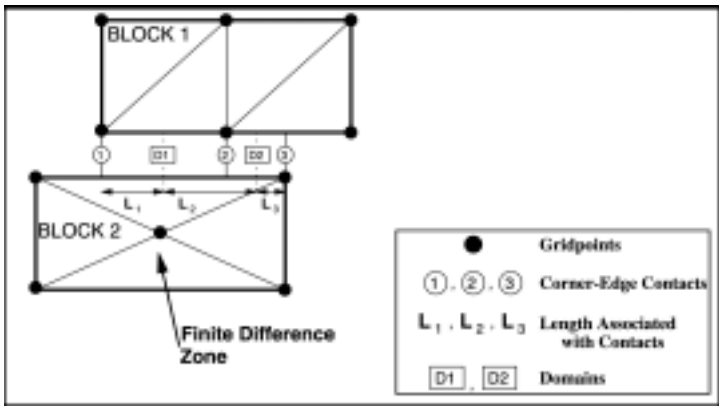

Figure 3-5. *Contacts and domains between two deformable blocks /UDEC, 2000/.*

Contact points are updated automatically as block motion occurs, that means that a high number of contacts may be deleted and created in case of dynamic systems. The computational code takes advantage of a network of “domains” to determine contacts between blocks (Figure 3-5). New contacts can only be created within a domain. Update is proceeded when the fictitious displacement exceeds a certain tolerance. An alternative solution is the so-called “cell mapping”. The system is divided into a rectangular gridcell, and the mapping of the blocks (and their envelops in space) is proceeded into the cells. Accurate results depend on an appropriate definition of the cells’ size. The cells are re-mapped after each timestep to take into account motion.

An advantage of this program is to mix rigid, simply-deformable and fully-deformable blocks in one simulation. Hence, a better description of the problem can be modelled. Moreover, linked boundary element-distinct element schemes (see section 4) are accounted for in this numerical code.

3.4.2 Implementation in 3-D: 3DEC

The two-dimensional code has been implemented in a computer program called 3DEC, which also accounts for block deformability and failure of intact material /Hart et al, 1988/. Specific care must then be paid for the generation of the joint systems. A module inserted in the program enables to generate a blocky structure by modelling of several joint sets. However, there are some limitations in the capability of the code to handle a high number of joint sets, as well as to compute joint that are terminating in the rock mass.

The concept of the code is the same as the one applied in UDEC.

Some applications of 3DEC are reported in the literature. /Shen and Stephansson, 1990/ applied the numerical code for the mechanical analysis of the effects of glaciation in order to assess the safety of a nuclear waste repository. The impact of thermal loading related to the repository of canisters has also been modelled using the implementation of 3DEC developed by /Mack and Hart, 1989/.

4 Linked computational schemes

According to /Brady, 1987/, the regions that really need to be model using the Finite Element Method or the Distinct Element Method are usually small and localised, so that only these zones require the analytical versality conferred by finite elements or distinct elements. He suggests linkage of algorithms to represent the key components of rock mass response, and provide conceptually valid and computationally efficient schemes for the design of excavation.

4.1 Concept of the coupled models

Some engineering problems – e.g. relatively dense fracture systems compared to the size of the excavation – can be solved using a boundary element-distinct element scheme. By representing the rock which will constitute the near-field of an excavation with distinct elements, and the far-field with boundary elements, the conceptual advantages of the distinct element are retained, and rigour in relation to far-field boundary conditions is preserved /Brady, 1987/. Linkage of both schemes is performed by satisfying the conditions of displacement continuity and force or traction equilibrium at the interface between the two solution domains. The components produced to solve the problems are presented in Figure 4-1. The adequacy of the analytical procedure has been demonstrated by /Lorig, 1984/ on a circular hole in a hydrostatic stress field, and by /Lorig and Brady, 1983/ in a design problem posed by an excavation in a stratified rock.

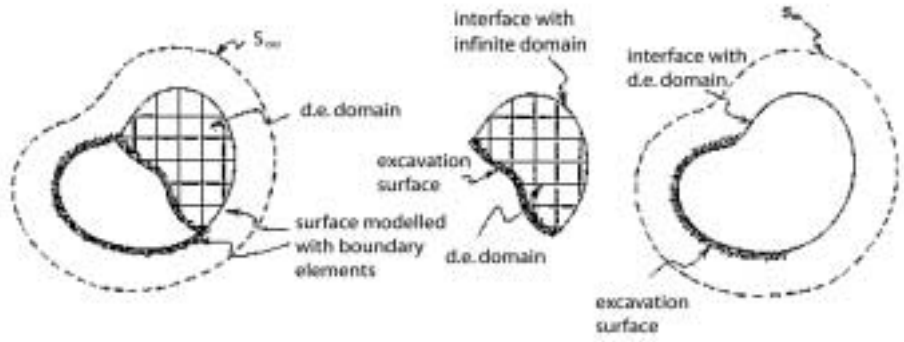

Figure 4-1. *Resolution of a distinct element-boundary element problem into component problem /Brady, 1987/.*

In the same way, a linked boundary element-finite element scheme can be developed for analysis of engineering works in rock masses presenting a high density of jointing. A finite element code modelling elastoplastic or similar constitutive behaviour may be needed to model the near-field randomly jointed or fracture rock round an excavation. The schematic representation is the one presented in Figure 4-1, but with finite elements replacing the distinct elements. Excavations may be bounded by boundary elements or finite elements, on which the specified boundary conditions must be satisfied. At the

interface between the finite element domain and the boundary element domain, the equilibrium and continuity conditions for traction and displacement must be satisfied.

4.2 Applicability

/Elsworth, 1985/ developed a coupled finite element-boundary element scheme for modelling non-linear potential flow. The non-linear portion of the domain is discretised by quadrilateral finite elements, and the linear behaviour is formulated with a direct boundary element method. The model developed provided adequate simulation of turbulent flows.

The advantage of the linked boundary element-distinct element scheme is that it can be easily linked to a structural element method of analysis, which provides a method for detailed analysis of the interaction between rock around excavation and support installed within the opening.

5 What model(s) to use?

5.1 Sum-up and discussion

Different methods have been presented that are of use for modelling fractured rock masses and that answer for two main analysis techniques, continuum and discontinuum. An alternative method, the limit equilibrium, has also been reviewed. According to the assumptions and mathematical laws derived, two methods – one in each analysis technique (continuum and discontinuum) – can be considered as the basis for the development of the approach; these are the finite element method in continuum approach and the distinct element method in discontinuum approach. Other methods have generally been developed from these methods.

- Block theory and other limit equilibrium methods assume that failure occurs along predefined failure surfaces with a perfectly plastic shear force law. Stability is usually considered as the comparison of forces (driving/resisting) for a particular failure mode. Therefore, the methods pertain good solutions for simple and identifiable failure mode /Lorig et al, 1991/, and is particularly useful for the analysis of open slopes. Hence the method could be inappropriate for problems in which the failure mode is not clearly identifiable, or in which displacements have to be known. Moreover, all blocks are assumed to be rigid, and internal deformation is not accounted for.

- The continuum analysis methods account for the fractured rock mass by an equivalent continuum representation. Hence it cannot give an appropriate estimation of the displacement (such as sliding, separation and rotation) that can occur along discontinuities. Even if implementations to the conceptual models have been made /Cai and Horii, 1993/, and numerical codes developed to overcome part of these weaknesses, these methods are still limited by several factors such as the representation of the system of joints (number of joints and intersection) and the amount of displacement that is considered. Modelling of large displacement along joints or large rotations of blocks is difficult using this approach.

- The discrete element methods account for the fractured rock mass by a discontinuous geometry in which contacts between blocks are joints. The main advantages of the different numerical models are that the system can undergo large displacements and rotations, interaction forces between blocks arise from changes in their relative geometrical configuration, and the solution is explicit in time /Lorig et al, 1991/. The different methods available are most often based on the theory developed by /Cundall, 1971/, and provide implementations to model and analyse specific engineering problems (impact mechanics by the momentum-exchange method, ice pile-up by the modal method).

5.2 Recommendations

5.2.1 Choice of the model

There is no clear-cut that enables to define what model should be used for what problem. Anyhow, some reflections about the problem that is to be solved, the general geological and mechanical context can support the choice of a model.

First, the analysis technique that should be used for this study must be defined, and then the method or numerical code that is the most appropriate for this approach must be motivated.

Choice of the analysis technique

The scale of the studied area must be considered, in itself and in relation to the fracture network system in the rock mass, and to the excavation in case of engineering design problem. /Brady, 1987/ proposed four conceptual models of rock structure and their rock response to excavation. The suitability of the method depends on the size of the engineering works relative to the average spacing of joints.

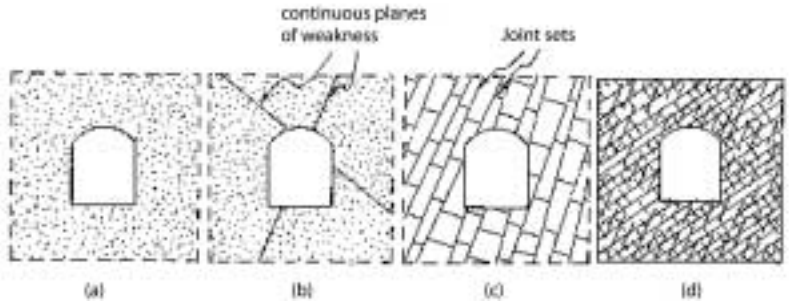

Figure 5-1. *Conceptual models relating rock structure and rock response to excavation /Brady, 1987/.*

The rock mass is intended to behave as a continuum in case of intact or sparsely fractured rock mass with relatively large size of excavations, therefore the FEM and BEM methods will be more appropriate (Figure 5-1a, b). On the other side, DEM and DDA will be more appropriate in cases where the averages spacing of the joints is of a similar order of magnitude as the size of the excavation (Figure 5-1c, d). According to /Brady, 1987/, problems representations illustrated in Figure 5-1c, d are suitably modelled by linked distinct element-boundary element (Figure 5-1c), and a linked finite element-boundary element scheme (Figure 5-1d).

Then, the choices of assumptions that have to be made for the analysis are guided by the purpose of the analysis and the type of media investigated. Assumptions are related to the geometry of the blocks, the type of contacts, the deformability of the blocks, and the equations of motions. Another important issue is the evolution of parameters in time. Amongst the methods reviewed, several are time-independent and do not account for the modification of mechanical behaviours of fractured rock masses, as a result of e.g. loading-unloading cycles. An overview of the concept and assessment of the different methods for use is provided in Table 5-1.

According to the main purpose of the Descriptive Rock Mechanical Model that will be developed in this project, a continuous approach does not seem to be appropriate. Indeed, a realistic representation of the fracture system is required, and this is best provided by continuous analysis techniques.

Table 5-1. Overview of the continuum and discontinuum analysis techniques.

			Assessment of the method		
		Concept	Applicability	Advantages	Limitations
Continuum	Finite Element Method (FEM)	Divide the structure into finite elements that are assigned a constant state of strain. Strains are expressed in terms of nodal displacements	Civil engineering in rock masses, and especially large-scale underground excavations.	Best suited for the computation of homogeneous material properties and linear material behaviour	Time-independent / Not so accurate modelling of joint influence / Definition of the extent of the mesh
	Boundary Element Method (BEM)	Discretisation of the boundary (or surface) of the problem / Formulation in terms of surface values of traction and displacement	Elastic rock mass or heterogeneous media with major discontinuities/ problems in excavation design	Resumes the FEM approach by limiting the formulation at the surface	The problem definition for heterogeneous medium does not enable modelling of highly fractured rock mass
	Distinct Element Method (DEM)	Discretisation of the deformable blocks in finite difference elements	Static and dynamic problems: stability of rock slopes, study of stress distribution in rock masses, modelling of joint displacement	Time-dependent / Rigid and deformable blocks can be combined	The formulation can be highly complicated in case of discretisation of deformable blocks in numerous elements
Discontinuum	Modal method	Deformability of blocks is considered through a superposition or decoupling approach	Ice mechanic problems (ride-up and pile-up)	Suitable for modelling media undergoing large displacements and fracturing, specially for loosely-packed media	Not well suited for high deformation gradient inside block
	Discontinuous Deformation Analysis (DDA)	Reverse analysis for the displacements of blocks	Determine the mechanism(s) that cause(s) displacements and deformations, rock falls, fracture propagation	Specially appropriate when the mechanisms involved are a combination of different modes	Joint opening assumption / Rigid blocks
	Momentum-exchange		Particle and impact mechanics	Momentum is exchanged between 2 contacting bodies during a collision	Rigid blocks only
Limit equilibrium	Block Theory	Identify the blocks that will become immediately unstable when cutting a slope, or opening an excavation	Assessment of slope stability, safety of dam foundation	3-D / Most appropriate when the failure mode is known	Static approach: do not account for displacements between the blocks / assume a perfectly plastic shear force law for failure

Choice of the conceptual model / numerical code

/Cundall and Hart, 1985/ summarise the attributes of the various discrete element and limit equilibrium methods (Figure 5-2). This is based on the different assumptions used for the development of the codes and determine the type of material behaviour that can be model.

The assumptions made on some methods are highly restrictive and hence, the choices of these methods should be made carefully. On the other hand, both the DEM and modal methods integrate possibilities for modelling different material behaviours. In that way, their range of applicability is wider.

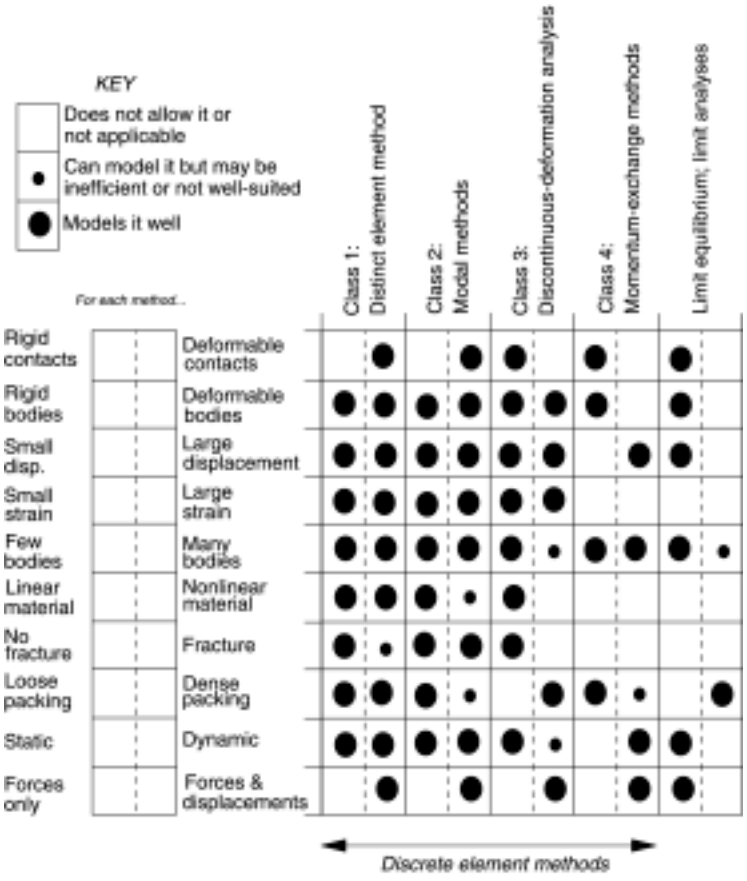

Figure 5-2. *Attributes for the four classes of the discrete element method, and the limit equilibrium method /Cundall and Hart, 1985/.*

5.2.2 Input parameters required

The parameters required are related to the geometrical and mechanical characteristics of the jointed rock mass. A typical program of input parameters used in UDEC includes:

- the definition of the model size,
- the definition of the fracture geometry (this can include the importation of a Discrete Fracture Network generated in a previous step),
- the mesh generation,

- the definition of the in-situ stresses and the definition of the boundary stresses,
- the materials properties, as considered separately for the intact rock and for the joints (a review of the models for use is presented in sections 3.1.2 and 3.1.3 in the main report),
- the definition of the history of displacement and the definition of the deformation profiles,
- the number of cycles of damping is determined,
- the results that are presented in some result files.

6 Conclusions

This report presents a review of the principal models for use for modelling fractured rock masses. There are basically two types of analysis techniques in use, the continuum and discontinuum analysis techniques. Under each approach, different conceptual models have been developed and implemented in order to solve static and dynamic problems.

The continuum analysis techniques assume that the jointed fractured rock mass is a continuous medium. The Finite Element method and the Boundary Element method are two models developed using this approach.

The discontinuum analysis considers the jointed rock mass as a discontinuous medium, accounting for the geometry and mechanical properties of fractures. The Distinct Element method represents the main model with this approach. Several models have been developed from this one to account for specific engineering or dynamic problems.

The suitability of the model is mostly defined by the size of the engineering works in relation to the geometry of the fractured rock mass, and specially the fracture system. Highly fractured rock masses will be better represented by a discontinuum approach with special emphasis on how contacts are handled, whereas homogeneous media or media sparsely jointed can be modelled as continuous. The DEM is particularly suited for study of large displacements between blocks and for reproducing block movements (translation and rotation).

There is no chart to define what type of approach to use, and what conceptual model or numerical code. Anyhow, choices may be supported by a synthetic table such as Table 5-1. The general concept of the method as well as applications, advantages and limitations are summarised and shortly presented.

7 References

Andersson J, Dverstorp B, 1987. Conditional simulations of fluid in Three-Dimensional networks of discrete fractures. Water Resources Research, vol.23, n.10, p.1876–1886.

Bathe K, Wilson E L, 1976. Numerical methods in Finite Element Analysis. Prentice-Hall, New Jersey.

Brady B H G, Brown E T, 1981. Energy changes and stability in underground mining: design applications of boundary element methods. Trans. Instn Min. Metall., vol. 90, A61-8.

Brady B H G, 1987. Boundary element and linked methods for underground excavation design. In Brown, E.T. (Ed.), Analytical and Computational Methods in Engineering Rocks Mechanics, chap.5. Allen & Unwin, London, pp.164–204.

Brady B H G, Lorig L, 1988. Analysis of rock reinforcement using finite difference methods. Computers and Geotechnics, vol.5, nr.2, pp.123–149.

Brady B H G, Brown E T, 1999. Rock mechanics for underground mining. 2nd edition. Chapman & Hall.

Cai M, Horii H A, 1991. A constitutive model of highly jointed rock masses. Applied Mech. Group, Dept of Civil Engng, University of Tokyo, Report 91-9.

Cai M, Horii H A, 1993. A constitutive model and FEM Analysis of jointed rock masses. Int. J. Rock. Mech. Min. Sci. & Geomech. Vol.30, No.4, pp.351–359.

Crotty J M, 1983. User's manual for BITEMJ – two-dimensional stress analysis for piecewise homogeneous solids with structural discontinuities. Melbourne: CSIRO (Australia), Division of geomechanics.

Crotty J M, Wardle L J, 1985. Boundary integral analysis of piecewise homogeneous media with structural discontinuities. Int. J. Rock Mech. Min. Sci. & Geomech. Abstr., vol. 22, pp.419–427.

Crouch S L, Starfield A M, 1983. Boundary element methods in solid mechanics. George Allen & Unwin, London.

Cundall P A, 1971. A computer model for simulating progressive large scale movements in block rock systems. Proc. Symp. Int. Society of Rock Mechanics, Nancy, France, Vol.1, Paper n II-8.

Cundall P A, 1980. UDEC-a generalized distinct element program for modelling jointed rock, Rept PCAR-1-80, Peter Cundall Associates Report, European Research Office, U.S. Army.

Cundall P A, Hart R D, 1985. Development of a 2-D and 3-D Distinct Element Programs for Modeling Jointed Rock. Itasca Consulting Group Report to U.S. Army Engineering Waterways Experiment Station, May 1983; published as Misc. Paper SL-85-, U.S: Army Corps of Engineers.

Cundall P A, 1987. Distinct element models of rock and soil structure. In Brown, E.T. (Ed.), Analytical and Computational Methods in Engineering Rocks Mechanics, chap.4. Allen & Unwin, London, pp.129–163.

Elsworth D, 1985. Coupled finite element/boundary element analysis for nonlinear fluid flow in rock fissures and fissure networks. 26th US Symp. On Rock Mech., Rapid City, SD, 26-28 June 1985, vol.1, pp.633–641.

Goodman R E, 1974. Introductory lecture on finite element analysis for jointed rocks. In Rock Mechanics, Ed. By L.Myller, pp.112–129.

Goodman R E, 1976. Methods of Geological Engineering in Discontinuous Rocks. West, St Paul, MN.

Goodman R E, Shi G H, 1985. Block theory and its application to Rock Engineering. Prentice-Hall, Englewood Cliffs, NJ.

Goodman R E, 1995. Block theory and its application. Géotechnique 45, No.3, pp.383–423.

Hart R D, Cundall P A, Lemos J, 1988. Formulation of a 3-D distinct element model – Part II: Mechanical calculations for motion and interaction of a system composed of many polyhedral blocks. Int. J. Rock Mech. Min. Sci. and Geomech. Abstr., vol 25 n.3, pp.117–126.

Hocking G, Mustoe G G W, Williams J R, 1985. Validation of the CICE discrete element code for ice ride up and ice ridge cone interaction. Proc. ARCTIC'85 Conf., ASCE, San Francisco.

Jing L, 1990. Numerical Modelling of Jointed Rock Masses by Distinct Element Method for Two, and Three-Dimensional Problems. Ph.D thesis, Luleå University of Technology, Sweden.

Labreche D A, 1985. Calculation of laboratory stress-strain behavior using a compliant joint model. 26th U.S. Symp. On Rock Mechanics, pp.515–522.

Larsson H, Olofsson T, Stephansson O, 1985. Reinforcement of jointed rock mass – a non-linear continuum approach. In Proceedings of the International Symposium on Fundamentals of Rock Joints, Bjärkliden, 15-20 September 1985, pp.567–577.

Lemos J V, Hart R D, Cundall P A, 1985. A generalized distinct element program for modelling jointed rock masses – a keynote lecture. Proc. Int. Symp. on Fundamentals of Rock Joints, Björkliden, pp.335–343.

Lin C T, Amadei B, Jung J, Dwyer J, 1996. Extensions of Discontinuous Deformation Analysis for jointed rock masses. Int. J. Rock Mech. Min. Sci. & Geomech. Abstr., Vol.33, N.7, pp.671–694.

Lorig L J, Brady B H G, 1983. An improved procedure for ecxavation design in stratified rock. In Rock Mechanics- theory- experiment- practice, Proc. 24th US Symp. Rock Mech., College Station, Texas, pp.577–585.

Lorig L J, 1984. A hybrid computational model for excavation and support design in jointed media. Ph.D. thesis, University of Minnesota.

Lorig L J, Hart R D, Cundall P A, 1991. Slope stability analysis of jointed rock using distinct element method. In Transportation Research Record 1330, pp.1–9.

Mack M, Hart R D, 1989. Verification of thermal logic in the three-dimensional distinct element code. Itasca Consulting Group, Inc. Minnesota 55414, U.S.A. Prepared for U.S. Nuclear Regulatory Commission.

Otter J R H, Cassell A C, Hobbs R E, 1966. Dynamic relaxation. Proc. Instn Civ. Engrs, 35, pp.633–656.

Shen B, 1990. Theoretical and numerical strudy of jointed rock mass behaviour. Licentiate Thesis, Technical University of Luleå, Sweden.

Shi G H, Goodman R E, 1985. Two dimensional discontinuous deformation analysis. International Journal for Numerical and Analytical Methods in Geomechanics, vol. 9, nr 6, pp. 541–556.

Shi G H, Goodman R E, Tinucci J P, 1985. Application of block theory to simulated joint trace maps. Proc. Int. Symp. On fundamentals of Rock Joints, Björkliden, pp.367–383. Rotterdam: Balkena.

Shi G H, Goodman R E, 1989. The key blocks of unrolled joint traces in developed maps of tunnel walls. Int. J. Numer. Analyt. Meth. Geomech., 13, pp.131–158.

Singh B, 1973. Continuum characterization of jointed rock mass. Int. J. Rock. Mech. Min. Sci. & Geomech. Abstr. 10, 311–349.

UDEC, 2000. UDEC Universal Distinct Element Code – Theory and Background. Itasca Consulting Group, Inc., Minneapolis, Minnesota.

Warburton P M, 1981. Vector stability analysis of an arbitrary polyhedral rock block with any number of free faces. Int. J. Rock Mech. Min. Sci. & Geomech. Abstr., vol. 18, pp.415–427.

Williams J R, Mustoe G G W, 1987. Modal Methods for the Analysis of Discrete Systems. Computers and Geotechnics, No 4, pp.1–19.

Yeung D, Brady B H G, 1982. A hybrid quadratic isoparametric finite element – boundary element code for underground excavation analysis. Issues in Rock Mechanics, Proceedings of the 23rd U.S. Symposium on Rock Mechanics, Berkeley, p.692–703.

Appendix C

Determination of Mechanical Properties of Intact Rocks and Rock Fractures at the Äspö Hard Rock Laboratory for the Test Case

Preparation of input parameters required in numerical modelling using udec code

Nader Fardin
Engineering Geology, Royal Institute of Technology

Isabelle Staub, Anders Fredriksson
Golder Associates AB, Stockholm

May 2002

Contents

1 Introduction

One of the most important parts of numerical modelling of fractured rock masses is the proper determination of mechanical properties of both intact rocks and rock fractures. Those properties are required as input parameters in pre-processing stage of analysis. The main objective of this work is to determine the mechanical properties of intact rocks and rock fractures at the Äspö Hard Rock Laboratory (HRL) using results obtained from laboratory tests. These tests were carried out on several samples of intact rocks and rock fractures by different groups and the obtained results of each experimental study are presented in different technical reports. In this report, the results obtained from these different groups are analysed and re-evaluated in order to obtain the complete parameters required in numerical modelling using UDEC code.

The available reports concerning mechanical properties of intact rocks and rock fractures at the Aspö HRL are listed below:

- /Stille and Olsson, 1989/. First evaluation of rock mechanics. SKB, Progress Report 25-89-07.
- /Stille and Olsson, 1990/. Evaluation of rock mechanics. SKB, Progress Report 25-90-08.
- /Nordlund et al, 1999/. Mechanical properties of the diorite in the prototype repository at Äspö HRL. SKB, International Progress Report IPR-99-25.
- /Lanaro, 2001/. Determination of the normal and shear stiffness of rock joints: geometry, normal and shear stiffness. SKB, Technical report (under publication).

/Nordlund et al, 1999/ present the mechanical properties of diorite samples obtained from boreholes KA3557G, KA3545G and KA3551G. The laboratory tests carried out on these samples are uniaxial and triaxial compression tests, Brazilian tests and three-bending points tests.

/Stille and Olsson, 1989, 1990/ summarise results from laboratory tests conducted on the four main rock types identified in the Äspö HRL – greenstone, fine-grained granite (aplite), diorite and granite-, and on rock fractures samples from two fracture sets, one steeply dipping and one gently dipping. All these samples are coming from borehole KAS02. The reports include results from: (1) uniaxial compression tests on intact rock samples; and (2) direct shear tests on rock fracture samples.

/Lanaro, 2001/ presents the results of laboratory tests conducted on rock fracture samples obtained from different boreholes in the Äspö HRL: (1) samples from a sub-vertical fracture set, obtained from boreholes KA3548A01, KA3573A, KA3600F, KG0021A01, KG0048A01; and (2) samples from a sub-horizontal fracture set, obtained from borehole KA3579G. The report includes results from normal and shear tests.

In these studies, different methods were used to evaluate mechanical properties of intact rocks and rock fractures, and none of these reports directly provide all the parameters required for the numerical modelling. As a consequence, a comprehensive analysis of all raw data available in these reports was carried out. The review of this analysis is presented in sections 2.1 and 2.2 for intact rocks, and in sections 3.2 and 3.3 for rock fractures. The input parameters required in numerical modelling using UDEC code are presented in section 2.3 for intact rocks and in section 3.4 for rock fractures.

2 Mechanical properties of the intact rock

As mentioned in section 1, different laboratory tests were carried out in order to determine the mechanical properties of different intact rocks in the Äspö region. All these tests were conducted according to the ISRM requirements.

The mechanical parameters that need to be determined for the modelling are uniaxial compressive strength, σ_c, tensile strength, σ_{ti}, deformation modulus, E, Poisson's ratio, ν, cohesion, c, and friction angle, ϕ.

Uniaxial compressive strength, σ_c, deformation modulus, E, and Poisson's ratio, ν, are determined from results of uniaxial and triaxial compression tests.

Tensile strength, σ_{ti}, is a parameter obtained from results of Brazilian tests.

Based on the results of the uniaxial, triaxial and Brazilian tests, the strength of the intact rock samples can be plotted in a σ_1-σ_3 diagram, see Figure 2-1. The strength envelope can be fitted either by the Hoek-Brown failure criterion, expressed as follows:

$$\sigma_1 = \sigma_3 + \sigma_c \cdot \left(m_b \cdot \sigma_3 / \sigma_c + s \right)^a \tag{2.1}$$

or by the Mohr-Coulomb failure criterion:

$$\sigma_1 = k\sigma_3 + \sigma_c \tag{2.2}$$

where

$$k = \frac{1+\sin\phi}{1-\sin\phi} \tag{2.3}$$

$$\sigma_c = 2c \cdot \frac{\cos\phi}{1-\sin\phi} \tag{2.4}$$

Using the H-B criterion, a fitting curve to the experimental results of triaxial tests can be obtained by selecting the appropriate value for the parameter m_b.

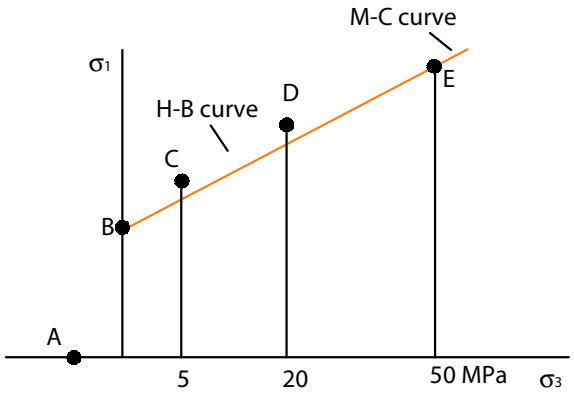

Figure 2-1. *The strength envelope of a rock sample. A – Brazil test; B – Uniaxial compression test; C, D and E – Triaxial compression test.*

According to the M-C criterion, the parameters k and σ_c are obtained by linear regression of the results of uniaxial and triaxial tests. The cohesion and friction angle of the intact rock are then calculated from equations (2.3) and (2.4).

The results obtained in two different studies are reviewed and compared in sections 2.1 and 2.2. Then, the input parameters required for the rock material model in UDEC are estimated and presented in section 2.3.

2.1 Mechanical properties of intact rocks according to /Stille and Olsson, 1989/

The intact rock samples are obtained from borehole KAS02, which co-ordinates are presented in Table 2-1.

Table 2-1. Co-ordinates* of borehole KAS02 (from Sicada, SKB).

Easting (m)	Northing (m)	Depth (m)	Bearing (°)	Inclination (°)	Length (m)
2125.32	7261.54	7.652	–19.91	–85.357	923.843

* Äspö-96 co-ordinate system

The intact rocks encountered in this borehole consist of four major rock types that are: greenstone, fine-grained granite (aplite), diorite and Småland granite, which are located at specific depths. The only laboratory test conducted on samples selected from this borehole was uniaxial compression test for determining the uniaxial compression strength, σ_c, Young's modulus, E, and Poisson's ratio, ν, of each rock type.

Depth of sampling, diameter of the samples, and rock type for each sample are available in /Stille and Olsson, 1989/. A summary of the mechanical properties of the four rock types determined from the laboratory tests carried out on these samples is presented in Table 2-2.

Table 2-2. Mechanical properties for the four intact rock types, estimated from uniaxial compression tests /from Stille and Olsson, 1989/.

Rock Type	Number of samples	σ_c (MPa)	E (GPa)	ν
Greenstone	4	118.8±39.5	52.4±17.3	0.22±0.03
Fine-grained granite	4	235.7±82	65.0±4.3	0.22±0
Diorite	4	175.1±8.8	59.8±5	0.22±0.03
Småland granite	4	188.7±49.1	62.3±0.5	0.24±0

As mentioned in section 1, no triaxial compression test has been carried out on those intact rock samples. Therefore, cohesion, c, and friction angle, ϕ, could not be defined for these samples. However, these parameters are required to estimate the shear strength of the rock from the failure criteria. An evaluation of these parameters is presented in section 2.3.

2.2 Mechanical properties of the diorite according to /Nordlund et al, 1999/

In /Nordlund et al, 1999/ the mechanical properties of intact rock samples of diorite were determined. The samples of diorite were selected from boreholes KA3545G, KA3551G and KA3557G. The co-ordinates of these boreholes are given in Table 2-3.

Table 2-3. Co-ordinates* of boreholes KA3545G, KA3551G and KA3557G (from Sicada, SKB).

Borehole	Northing (m)	Easting (m)	Depth (m)	Bearing (°)	Inclination (°)
KA3545G	7269.599	1921.281	–449.103	270	–81.1972
KA3551G	7270.39	1915.429	–448.933	269.3634	–79.6331
KA3557G	7271.259	1909.495	–448.847	271.1612	–81.4873

* Äspö-96 co-ordinate system

The laboratory tests conducted in this study are uniaxial and triaxial compression tests, Brazilian test and three-point bending tests. Different mechanical parameters were evaluated from these tests, and those of relevance for this study are listed below:

- From uniaxial compression tests: uniaxial compression strength, σ_c, deformation modulus, E, and Poisson's ratio, ν. It should be noted that both deformation modulus and Poisson's ratio were estimated at two different stages: (1) E_{ini} and ν_{ini} were defined at initial stage of compression; and (2) $E_{\%50}$ and $\nu_{\%50}$ were defined at a stress level equal to 50% of the initial uniaxial compression stress.
- From triaxial compression tests: uniaxial triaxial compression strength σ_{1c} under different confining stresses σ_3.
- From Brazilian tests: uniaxial tensile strength σ_{ti}.

The diameter and length of the samples are defined in accordance to the requirements of ISRM for the different laboratory tests. The identification of the tested intact rock samples (location, depth of sampling and geometry) is found in /Nordlund et al, 1999/.

A summary of the mechanical parameters evaluated from the different laboratory tests is presented in Table 2-4 to Table 2-6.

Table 2-4. Mechanical properties of the diorite, estimated from triaxial compression test /from Nordlund et al, 1999/.

σ_3 (MPa)	Number of samples	σ_{1c} (MPa)	
		Mean	Std Dev.
0	4	218.75	17.5
5	3	256.33	16.6
20	3	346.33	17.8
40	1	434	–
50	3	502	40.8

Table 2-5. Mechanical properties of the diorite, estimated from uniaxial compression tests /from Nordlund et al, 1999/.

Number of samples	E_{ini}, GPa		$E_{\%50}$, GPa		ν_{ini}		$\nu_{\%50}$	
	Mean	Std Dev.	Mean	Std Dev.	Mean	Std Dev.	Mean	Std Dev.
3	80	5.6	73.33	2.9	0.21	0.02	0.28	0.01

Table 2-6. Mechanical properties of the diorite, estimated from Brazilian tests /from Nordlund et al, 1999/.

Number of samples	σ_{ti} (MPa)	
	Mean	Std Dev.
5	14.7	1.6

Based on the results of the uniaxial, triaxial and Brazilian tests, the strength of the intact rock samples can be plotted in a σ_1-σ_3 diagram, see Figure 2-1. The strength envelope can be fitted either by the Hoek-Brown failure criterion (equation (2.1)), or by the Mohr-Coulomb failure criterion (equation (2.2)).

Fitting the results of compression and Brazilian results to the Hoek-Brown failure criterion leads to the determination of the constant m_b. Fitting the results of compression tests to the Mohr-Coulomb failure criterion leads to the evaluation of cohesion, c, and friction angle, ϕ, of the intact rock, see /Nordlund et al, 1999/.

A summary of the mechanical properties for the diorite determined in /Nordlund et al, 1999/ is presented in Table 2-7.

Table 2-7. The mechanical properties of the diorite in the Äspö HRL /Nordlund et al, 1999/.

Parameter	Mean value	Unit
Uniaxial Compressive Strength, σ_c	218.7	MPa
Tensile Strength, σ_{ti}	14.7	MPa
Initial Young's modulus, E_{ini}	80	GPa
Tangent Young's modulus, $E_{\%50}$	73	GPa
Initial Poisson's ratio, ν_{ini}	0.21	–
Tangent Poisson's ratio, $\nu_{\%50}$	0.28	–
Cohesion, c	49	MPa
Friction angle, ϕ	44	°
Hoek-Brown criterion parameter, m_b	15	°

2.3 Preparation of input mechanical parameters of intact rocks for modelling

In this project, the UDEC code (Itasca) was chosen to simulate the mechanical behaviour of fractured rock masses in the Äspö HRL region, see section 2.2 in the main report. The relevance and quality of numerical modelling is highly dependent onto the appropriate determination of input parameters for the material model of intact rock. Among the different material models available in UDEC, the Mohr-Coulomb plasticity model was selected for the intact rock in this project, see section 3.1.2 in the main report.

For the Mohr-Coulomb plasticity model, the required properties are: density, D, bulk modulus, K, shear modulus, G, friction angle, ϕ, cohesion, c, dilation angle, ψ, and tensile strength, σ_{ti}.

The average density, D, of the four intact rock types is determined according to /Rhén et al, 1997/, and the values for each rock type are presented in Table 2-8.

The bulk and shear moduli, as well as the dilation angle, are not provided in the reports analysed in sections 2.1 and 2.2. They were calculated on basis of the Elasticity theory, using the following equations:

$$K = \frac{E}{3(1-2\nu)} \tag{2.5}$$

$$G = \frac{E}{2(1+\nu)} \tag{2.6}$$

Cohesion, friction angle and tensile strength are provided only for diorite samples (see section 2.2), but are missing for other intact rock types. To evaluate cohesion and friction angle of the three other rock types –granite, greenstone and aplite-, the following assumptions were made. The friction angle, ϕ, of all rock types was considered to be equal to 45 degrees, with respect to the results obtained for the diorite in /Nordlund et al, 1999/. Then the cohesion, c, of each intact rock was back calculated according to equation (2.7):

$$c = \frac{\sigma_c \cdot (1-\sin\phi)}{2\cos\phi} \tag{2.7}$$

where σ_c is the uniaxial compression strength of the intact rock. Since the diameter of the selected samples was less than 50 mm, which is the standard diameter for testing suggested by ISRM, the uniaxial compression strength of each intact rock was improved before determining the c values using equation (2.8).

$$\sigma_c = \frac{\sigma_{cd}}{\left(50/d\right)^{0.18}} \qquad (2.8)$$

where σ_{cd} is the uniaxial compression strength of the intact rock sample having a diameter equal to d.

The tensile strength of intact rocks was only evaluated for the diorite (see section 2.2), but is a parameter that is missing for the three other rock types.

Usually, the tensile strength of intact rock samples is ten times smaller than their uniaxial compression strength, σ_c. Based on the values obtained on the diorite in the Äspö HRL /Nordlund et al, 1999/, a factor of 0.0678 was obtained for the ratio of tensile strength to uniaxial compression strength. Then, the tensile strength, σ_{ti}, of the three other rock types –granite, greenstone and aplite- was estimated by multiplying their uniaxial compression strength by this factor.

The dilation angle of all intact rocks was assumed to be equal to 0.

The mechanical properties for the four intact rock types are listed in Table 2-8. As can be seen in this table, results from these studies show high discrepancy in the mechanical properties obtained on diorite samples.

Also, the c and ϕ values of the diorite given in this table for /Nordlund et al, 1999/, differ from c and ϕ given in Table 2-7. The main reason is that, in /Nordlund et al, 1999/, the c and ϕ values of Mohr-Coulomb failure criterion were determined on basis of compression tests results only (see Figure 2-2). But in this work, the results of tensile strength were also taken into account to find the best fitting curve to the mentioned criterion, which is shown in Figure 2-3.

Table 2-8. Input mechanical parameters for the Mohr-Coulomb plasticity rock model, for the different rock types.

Report	Rock Type	σ_c [1] MPa	D [2] kg/m^3	K GPa	G GPa	c MPa	ϕ °	ψ °	σ_{ti} MPa
/Stille and Olsson, 1989/	Greenstone	115	2.96	31	21	23.82	45	0	8.0
	Aplite	228	2.67	38	26	47.22	45	0	15.0
	Diorite	169	2.75	35	24	35	45	0	12.0
	Granite	182	2.64	39	25	37.7	45	0	12.8
/Nordlund et al, 1999/	Diorite	214	2.75	52	28	31 [3]	49 [3]	0	14.8

[1] Values calculated for 50-mm samples
[2] /Rhén et al, 1997/
[3] These values have been re-evaluated from the values presented in /Nordlund et al, 1999/

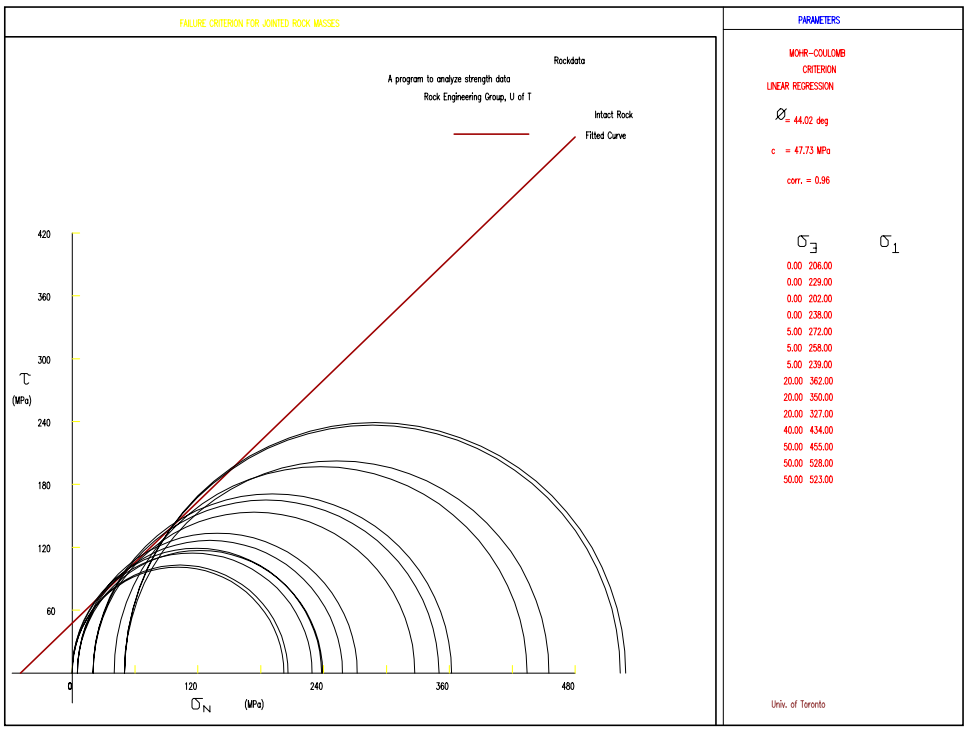

Figure 2-2. *The envelopes of Mohr-Coulomb failure criterion for diorite rock, obtained according to the compression tests only.*

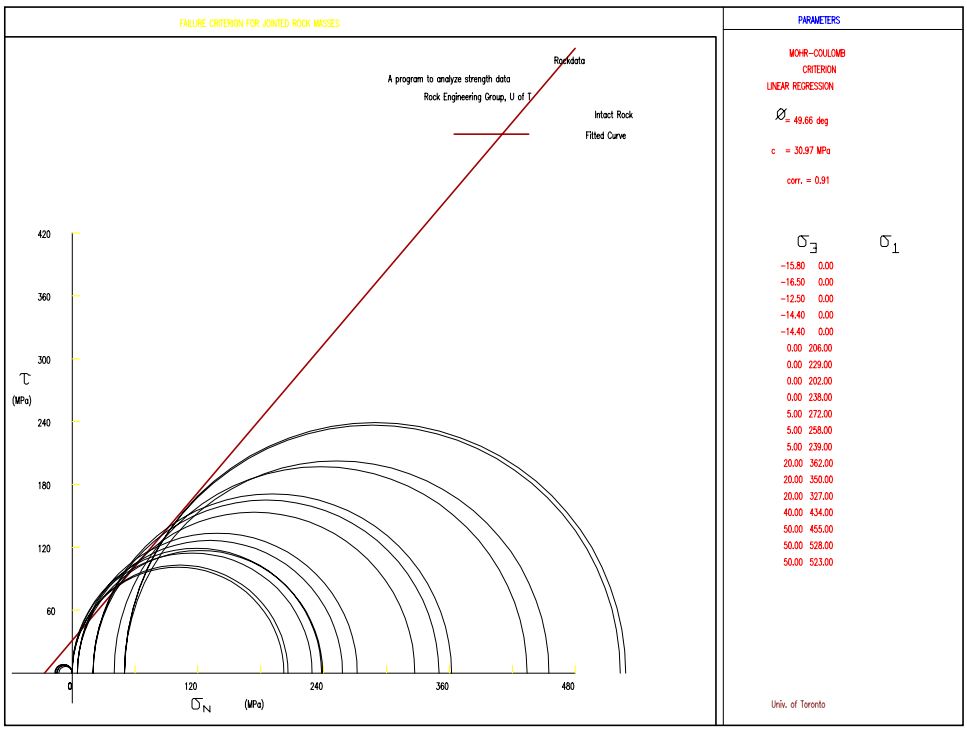

Figure 2-3. *The envelopes of Mohr-Coulomb failure criteria for diorite rock, obtained according to all tests.*

The data given in Table 2-8 can now directly be used as an input parameter for the Mohr-Coulomb plasticity model of the intact rock in UDEC.

3 Mechanical properties of rock fractures

The mechanical properties of different rock fractures in the Äspö region are provided in two studies. The results of laboratory tests conducted on several selected samples are presented in /Stille and Olsson, 1989; Lanaro, 2001/, see section 1.

The mechanical properties required for rock fractures are determined from the different following tests:

- Standard chart profiles: JRC.
- Tilt tests: JRC, basic friction angle, ϕ_b.
- Schmidt hammer test: Joint Compressive Strength, JCS, residual friction angle, ϕ_r.
- Direct shear tests: shear stiffness, K_s, normal stiffness, K_n, cohesion, c, and friction angle, ϕ, (Joint Roughness Coefficient, JRC).

In section 3.1 the process of determination of rock fracture properties from different field and laboratory tests is shortly presented. In sections 3.2 and 3.3, the results from both aforementioned studies are reviewed. Finally, in section 3.4 the required input parameters for numerical modelling are estimated with respect to the appropriate constitutive joint models available in UDEC code.

3.1 Determination of fracture parameters

3.1.1 Standard profiles

The parameter for roughness of fractures, JRC, can be determined by visual comparison of measured profile lines of a fracture surface to standard profiles, see Figure 3-1. This method is recommended by /ISRM, 1978/, with JRC values between 0 and 20 /Barton and Choubey, 1977/.

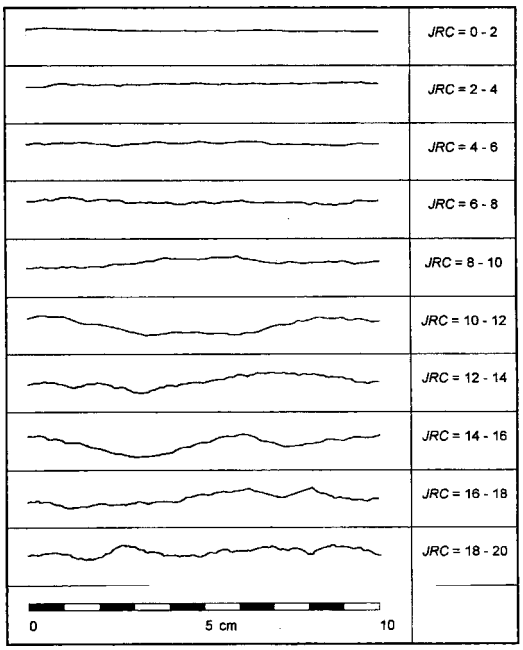

Figure 3-1. *Typical roughness profiles for JRC /Barton and Choubey, 1977/.*

3.1.2 Tilt tests

Simple tilt tests can be used to obtain the JRC values and basic friction angle of rock fracture samples. The tilt test is performed by placing a cored sample of the rock fracture on a flat surface and by tilting it until the top piece slide on the lower. The Joint Roughness Coefficient, JRC, is expressed by the following equation /Barton and Choubey, 1977/:

$$JRC = \frac{\alpha - \phi_r}{\log_{10}\left(JCS / \sigma_{n0}\right)} \tag{3.1}$$

where α is the tilt angle (°), ϕ_r is the residual friction angle (°), JCS is the Joint Compressive Strength (MPa), and σ_{n0} is the effective normal stress generated by gravitational force acting on the lower half part of the block (MPa).

The basic friction angle, ϕ_b, is estimated from residual tilt tests. This angle is the friction angle determined on dry unweathered sawn surfaces under low stress. Range of ϕ_b values for specific material are presented in Table 3-1.

Table 3-1. Measured basic friction angle, ϕ_b, for some materials /Barton, 1976/.

Rock type	Condition	Basic friction angle, ϕ_b [°]
Granite	Dry	31–35
	Wet	29–31
Gneiss	Dry	26–29
	Wet	23–26
Sandstone	Dry	26–35
	Wet	25–33

3.1.3 Schmidt hammer test

Parameters obtained from these tests are the Schmidt rebound on wet fracture surfaces, r, and the Schmidt rebound on dry unweathered sawn surfaces. These parameters can be used for calculating the Joint Compressive Strength, JCS, and the residual joint friction angle, ϕ_r.

/ISRM, 1978/ points out the Schmidt hammer test for evaluating the Joint wall Compressive Strength of rock fractures. The JCS can be expressed as follows /Barton and Choubey, 1977/:

$$\log_{10}(\mathrm{JCS}) = 0.00088 \cdot \gamma \cdot r + 1.01 \tag{3.2}$$

where γ is the unit weight of the rock and r is the mean Schmidt hammer rebound number on wet joint surfaces.

As stated by /Barton and Choubey, 1977/, the residual friction angle, ϕ_r, can be estimated from the basic friction angle, ϕ_b, according to the following empirical relation:

$$\phi_r = (\phi_b - 20) + 20(r/R) \tag{3.3}$$

where R is the mean Schmidt hammer rebound number on dry unweathered sawn surfaces, ϕ_b and ϕ_r are expressed in degrees.

3.1.4 Direct shear tests

Direct shear tests can be conducted under constant normal loading (CNL) or constant normal stiffness (CNS). Several tests are conducted for different values of normal stress, and the results of the different tests are plotted in τ-σ_n, τ-u_s/u_n, and u_s-u_n diagrams, where the shear strength, τ, the normal stress, σ_n, the shear, u_s, and normal displacements, u_n, are monitored during testing. These diagrams are analysed for determining cohesion and friction angle of rock fractures, with help of results from another tests, such as tilt tests. The results from direct shear tests can also be used to back-calculate the Joint Roughness Coefficient, JRC.

Shear strength of rock fractures

The simplest and in practice most used theoretical peak shear strength criterion for fractures was proposed by Coulomb, and has the following expressions for the peak shear strength, τ_p, of the rock fractures:

$$\tau_p = c_p + \sigma_n \cdot \tan\phi_p \tag{3.4}$$

The expression can also be used for the residual shear strength, τ_r, of the rock fractures:

$$\tau_r = c_r + \sigma_n \cdot \tan\phi_r \tag{3.5}$$

where c_p and c_r are the peak and residual cohesion, ϕ_p and ϕ_r are the peak and residual friction angles, σ_n is the normal stress.

This linear criterion can be adapted for both peak and residual cohesion and friction angle.

A more sophisticated and bilinear criterion was adapted from /Patton, 1966/ and proposed by /ISRM, 1981/. This criterion accounts for the curvature of the shear strength at low normal stress values. The graph is approximated by a line at low normal stresses smaller than a specific value σ_a, and by another line at higher normal stresses. Two sets of parameters are evaluated: (1) c_{pl} and ϕ_{pl} at low normal stresses; (2) c_{ph} and ϕ_{ph} at higher normal stresses.

The parameters determined at low normal stresses are considered the equivalent to peak cohesion and peak friction angle from the Coulomb criterion.

An empirical peak shear strength criterion has been developed by /Barton and Choubey, 1977/, which is expressed as follows:

$$\tau_p = \sigma_n \tan\left[JRC \log_{10}\left(\frac{JCS}{\sigma_n} \right) + \phi_r \right] \tag{3.6}$$

where JRC is evaluated from the chart profiles, see Figure 3-1, JCS is determined from results of Schmidt hammer tests, ϕ_r is the residual friction angle that can also be obtained by means of an equation proposed by /Barton and Choubey, 1977/.

Back-calculation of JRC

The Joint Roughness Coefficient, JRC, can be calculated from parameters obtained from direct shear tests under Constant Normal Load, CNL, according to the following equation:

$$JRC = \frac{\arctan\left(\tau_p / \sigma_n \right) - \phi_r}{\log_{10}\left(JCS / \sigma_n \right)} \tag{3.7}$$

where τ_p is the peak shear strength, JCS the Joint Compression Strength, σ_n the normal stress, and ϕ_r the residual friction angle of fractures.

These calculated JRC values can then be checked against the JRC values estimated from standard profiles, see section 3.1.1.

3.2 Mechanical properties of rock fractures according to /Stille and Olsson, 1989/

As mentioned in section 1, the tested rock fracture samples are obtained from borehole KAS02, which co-ordinates are given in Table 2-1.

Two different sets of fractures were distinguished in this borehole, which were defined as steeply dipping and gently dipping. Direct shear tests were conducted on each rock fracture sample under different normal stress levels. The mechanical parameters evaluated from these tests are: Joint Roughness Coefficient, JRC, shear stiffness, K_s, normal stiffness, K_n, cohesion, c, and friction angle, ϕ.

3.2.1 Determination of surface roughness of rock fracture samples

In /Stille and Olsson, 1989/, the surface roughness of rock fractures is evaluated from the standard chart profiles, see Figure 3-1. The JRC values obtained for both fracture sets are the following:

- JRC>8 (smooth undulating fractures) for steeply dipping fractures (ST1, ST2, ST3, ST5 and ST6)
- For gently dipping fractures (ST8, ST9, ST10, ST11 and ST12), the rock fracture samples can be divided in two groups: one with JRC≈3 (smooth planar joints) and one with JRC>8 (smooth undulating fractures). No information is provided on which value to assign for the different rock fracture samples.

3.2.2 Determination of strength of rock fracture samples

A summary of the strength mechanical properties obtained on the selected samples is listed in Table 3-2. As can be seen from Table 3-2, two different values were defined for both cohesion and friction angle. The test results could not fit a linear failure criterion. These two values were estimated with respect to the normal stress level, according to Patton's non-linear criterion, where the mechanical behaviour of rock fracture changes from dilation to shear. The values at low normal stress correspond to the dilation part of the deformation, and it can be noted that the cohesion of rock fractures is then almost equal to zero. The values at higher normal stress level belong to the shear part of the criterion.

Table 3-2. Mechanical properties of the rock fracture samples selected from borehole KAS02 /from Stille and Olsson, 1989/.

				Low normal stress		Higher normal stress	
Sample[(1)]	Level (m)	K_s (MPa/mm)	K_n (MPa/mm)	c_{pl} (MPa)	ϕ_{pl} (°)	c_{ph} (MPa)	ϕ_{ph} (°)
ST1	–397,81	8.4	4.7–22.7	0.1	47	0.4	43
ST2	–350,17	19.2	27.7	0.1	49	0.5	42
ST3	–327,44	7.2	10.4	0.8	63	2.4	29
ST5	–462,80	11.6	12.2	0.4	57	1.6	34
ST6	–500,18	7.4	9–26	0.3	47	1	36
ST8	–360,64	8.0	13.2	0.0	37	1.3	17
ST9	–394,52	7.6	12.5	0.2	38	1.0	29
ST10	–484,73	4.8	15.0	1.0	65	4.0	21
ST11	–281,40	8.9	11.6	0.5	54	1.7	38
ST12	–292,56	11.4	15.1	0.8	55	2.0	34

(1) ST1-ST6 belong to the steeply dipping fracture set, and ST8-ST12 belong to the gently dipping fracture set.

A summary of the results obtained for each fracture set is presented in Table 3-3 and Table 3-4. The cohesion and friction angle determined at low normal stresses can be considered closed to the peak cohesion and peak friction angle of the rock fractures. The cohesion and friction angle at high normal stresses are considered equal to residual cohesion and residual friction angle.

Table 3-3. Evaluated shear and normal stiffness for both fracture sets (from Table 3-2).

	Number of samples	K_s (MPa/mm)		K_n (MPa/mm)	
		Mean	Std Dev.	Mean	Std Dev.
Steeply dipping fractures [(1)]	5	10.8	5	12.8	8.8
				19.8	8
Gently dipping fractures	5	8.1	2.4	13.5	1.5

[(1)] The two mean values are calculated by combining the lowest and highest values given for K_n for two rock samples with other mean values

Table 3-4. Evaluated peak and residual cohesion and friction angle for both fracture sets (from Table 3-2).

	Number of samples	c_{pl} (MPa)		ϕ_{pl} (°)		c_{ph} (MPa)		ϕ_{ph} (°)	
		Mean	Std Dev.	Mean	Std Dev.	Mean	Std Dev.	Mean	Std Dev.
Steeply dipping fractures	5	0.34	0.3	52.6	7.1	1.16	0.85	36.8	5.8
Gently dipping fractures	5	0.5	0.4	49.8	12	2	1.18	27.8	8.8

It should be noted that the compression of the two blocks of rock fracture samples was not subtracted from the total measured compression when evaluating the normal stiffness, K_n.

3.3 Mechanical properties of rock fractures according to /Lanaro, 2001/

/Lanaro, 2001/ has comprehensively investigated the geometry (JRC and aperture), normal and shear stiffness as well as shear strength of two different fracture sets in the Äspö region. The rock fracture samples were selected from 6 different boreholes, which co-ordinates are given in Table 3-5.

Table 3-5. Co-ordinates* of boreholes KA3548A01, KA3573A, KA3600F, KG0021A01, KG0048A01 and KA3579G /from Sicada, SKB/.

Borehole	Northing (m)	Easting (m)	Depth (m)	Bearing (°)	Inclination (°)
KA3548A01	7267.473	1917.175	–446.576	188.3803	–3.0897
KA3573A	7270.896	1893.281	–446.068	188.4457	–1.9512
KA3600F	7275.456	1866.012	–445.583	248.2434	–1.8328
KG0021A01	7297.915	1941.001	–445.153	220.0787	17.5945
KG0048A01	7307.032	1915.444	–444.494	222.1866	14.1224
KA3579G	7274.422	1886.684	–448.366	296.5651	–89.3594

* Äspö-96 co-ordinate system

The two fracture sets encountered in the 6 mentioned boreholes were classified as sub-vertical fracture set (set 1) and sub-horizontal fracture set (set 2). General information on each rock fracture sample, including depth, type, mineral filling, roughness, surface and skin is provided in /Lanaro, 2001/.

3.3.1 Determination of JRC and aperture

For geometrical characterisation of selected samples, two surfaces of each rock fracture sample were scanned in the laboratory using a 3-D laser scanning technique. After obtaining the digitised replicas of each sample, surface roughness of both upper and lower parts of each rock fracture sample was characterised on basis of Barton's JRC (Joint roughness Coefficient) characterisation system, see section 3.1.1, Figure 3-1. The apertures of the selected sample were also determined using special technique /see Lanaro, 2001/. The range of values for JRC and aperture of the selected samples are given in Table 3-6.

Table 3-6. Range of values for JRC and aperture, estimated for both fracture sets (from Lanaro, 2001).

Fracture Set	JRC				Max. aperture Range of values	
	Upper surface		Lower surface			
	Min.	Max.	Min.	Max.		
Sub-vertical	3	15	3	15	1.17	9.61
Sub-horizontal	5	11	5	11	1.12	2.66

The JRC values for lower and upper surfaces are similar, which is reflected by a similar range of values, see Table 3-6. The range of JRC values obtained for a specific fracture set is extended, even highly heterogeneous for samples belonging to the sub-vertical fracture set. In the following, a unique value of JRC, determined from the values obtained on upper and lower surfaces, was applied to the samples.

A summary of the Joint Coefficient Roughness, JRC, and of the aperture for both sub-vertical and sub-horizontal fracture sets is given in Table 3-7.

Table 3-7. Geometrical characteristics of both sub-vertical and sub-horizontal fracture sets /Lanaro, 2001/.

Fracture Set	JRC		Aperture (mm)		
	Mean	Std Dev.	Mean max.[(1)]	Mean	Std Dev.
Sub-vertical	6	3.2	4.05	0.56	0.61
Sub-horizontal	8	2.3	1.76	0.18	0.14

[(1)] The maximum aperture value is the average maximum value calculated from all samples of a fracture set

3.3.2 Determination of normal and shear stiffness

To determine the normal stiffness, K_n, of the selected rock fracture samples, the deformability of the samples was measured under different normal loading conditions which consisted of three loading steps followed by three unloading-reloading cycles between the maximum and minimum stress at each step /see Lanaro, 2001/. It should be noted that the deformation of the intact rock sample, which had been determined by normal loading tests conducted on different intact rock samples, was subtracted from the deformation of the fracture. A summary of the normal loading tests on rock fracture samples is given in Table 3-8.

The shear stiffness, K_s, of the selected rock fracture samples was also determined using laboratory direct shear tests at four levels of normal stress: 0.5, 1, 5 and 10 MPa. The tests were carried out according to ISRM's suggested method and each sample was tested at three different normal stresses (0.5, 1 and 5, or 1, 5 and 10 MPa). The procedure of direct shear tests and method of data evaluation are given in /Lanaro, 2001/. A summary of the results obtained for shear stiffness of the selected rock fracture samples is given in Table 3-9.

The average normal and shear stiffness as well as their standard deviations are summarised in Table 3-10 and Table 3-11.

Table 3-8. Secant normal stiffness, K_n, during the virgin loading and reloading cycles, for different stress intervals /from Lanaro, 2001/.

Borehole	Fracture set	Depth (m)*	Secant normal stiffness, K_n (MPa/mm)										
			σ_n, during virgin normal loading cycle (MPa)								σ_n, during reloading (MPa)		
			Initial	0.5–5	0.5–10	0.5–15	0.5–30	5–10	5–15	10–15	0.5–5	0.5–10	0.5–15
KA3548A01	Sub-vertical fracture set	–446.87	40	78	151	155		312	278	218	144	200	207
		–447.51	22	61	84	86		91	106	101	72	67	74
KA3573A		–446.30	33	55	75	85		55	121	115	101	95	192
		–446.47											
		–446.81	300	71	124	139		92	200	184	101	101	179
KA3600F		–446.90											
		–446.90	138	106	134	117		177	93	93	142	141	189
		–446.91	24	59	81	92		110	126	126	77	77	98
KG0021A01		–432.84	57	83	136	138		199	141	141	137	167	139
KG0048A01		–442.68	66	161	326	453					440	699	565
		–437.87	41	89	143	174		105	277	299	206	146	165
		–433.37	85	69	92	116		150	183	182	101	112	125
		–433.26	68	55	54	61		54	78	78	120	123	124
KA3579G	Sub-horizontal fracture set	–457.80	118	185	279	363	535	514	853	949	280	385	681
		–459.10	37	73	130	191	357	457	1572	2023	174	279	735
		–459.62	31	72	132	193	352	525	1480	1669	222	424	1124
		–463.23	124	783	322	454	798	1027	2012	2700	818	1157	2432
		–467.81	124	274	500	738	1367	1972	7187	7702	578	1399	3170

* The depth of samples is absolute depth and has been re-calculated according to the co-ordinates of the boreholes.

Table 3-9. Shear stiffness, K_s, of the selected rock fracture samples for different normal stresses /from Lanaro, 2001/.

Borehole	Fracture set	Depth (m)*	Shear Stiffness, K_s (MPa/mm)											
			σ_n= 0.5 MPa			σ_n=1 MPa			σ_n=5 MPa			σ_n=10 MPa		
			Initial	Peak	Reload	Initial	Peak	Reload	Initial	Peak	Reload	Initial	Peak	Reload
KA3548A01	Sub-vertical fracture set	–446.87	5.6	3.3	7.9				17.5	11.4	27.6	35.5	14	37.7
		–447.51	1.9	2.1	4.4				7.9	6.2	35.1	25.1	12.8	46.6
KA3573A		–446.30	1.1	–	5.5				7.1	5.3	39.8	21.7	7.6	48.2
		–446.47												
		–446.81	1.5	1.2	7.9				20.1	16	27.7	35.1	13.6	45.1
KA3600F		–446.90												
		–446.90	3.9	3.7	5.3				22.9	8	36.8	43.4	11.5	30
		–446.91	4.2	0.2	3.8				1.5	1	45.3	28.1	15	52.3
KG0021A01		–432.84	0.8	0.6	–				4.7	4	40.4	25.7	5.4	40.2
KG0048A01		–442.68	4.6	2.2	27.1				11.8	7.5	–	27.2	8.1	–
		–437.87	0.9	–	5.8				19.3	13.6	28.3	27.1	9.3	67.9
		–433.37	2.3	2.1	6.1				13.1	9.2	27.9	32.2	14.9	37.9
		–433.26	15.4	4.5	6				–	13.5	17.6	32.7	6.3	45.7
KA3579G	Sub-horizontal fracutre set	–457.80	–	–	–	2.5	2.5	7.6	19.7	8.9	36.6	44.5	10.5	34.4
		–459.10	–	–	–	15.9	8.4	12.7	18.4	13.9	25.6	28.5	16.6	30.3
		–459.62	1.9	2.1	4.4	–	–	–	10.1	6.2	35.1	20.8	13	48.1
		–463.23	8.3	3.4	13.8	–	–	–	9.6	7.8	44.9	28.3	6.3	58.6
		–467.81	4.5	4.1	12.6	–	–	–	16.7	7.2	30.9	32.7	9.5	45.6

* The depth of samples is absolute depth and has been re-calculated according to the co-ordinates of the boreholes.

Table 3-10. The average and standard deviation of the Secant normal stiffness, K_n, during the virgin loading and reloading cycles, for different stress intervals /from Lanaro, 2001/.

Fracture set	Secant normal stiffness, K_n (MPa/mm)										
	σ_n, during virgin normal loading cycle (MPa)								σ_n, during reloading (MPa)		
	Initial	0.5–5	0.5–10	0.5–15	0.5–30	5–10	5–15*	10–15**,**	0.5–5	0.5–10	0.5–15***
Sub-vertical, Mean	57	81	127	147		135	160	154	149	175	187
Sub-vertical, Std Dev.	35	31.3	73	107		77.8	72	68	103	178	132
Sub-horizontal, Mean	87	157	273	388	682	899	2621	3009	414	729	1628
Sub-horizontal, Std Dev.	48	86	154	226	424	642	2586	2699	578	1399	3170

* 10–15; ** 10–30; *** 0.5–30 for sub-horizontal fracture set.

Table 3-11. The average and standard deviation of the shear stiffness, K_s, of the selected rock fracture samples, for different normal stresses /from Lanaro, 2001/.

	Shear Stiffness, K_s (MPa/mm)											
	σ_n= 0.5 MPa			σ_n=1 MPa			σ_n=5 MPa			σ_n=10 MPa		
Fracture set	Initial	Peak	Reload	Initial	Peak	Reload	Initial	Peak	Reload	Initial	Peak	Reload
Sub-vertical, Mean	3.8	2.2	8				12.6	8.7	32.6	30.4	10.8	45.2
Sub-vertical, Std Dev.	4.2	1.4	6.9				7.2	4.6	8.2	6.1	3.5	10.2
Sub-horizontal, Mean	4.9	3.2	10.3	9.2	5.4	10.2	14.9	8.8	34.6	30.9	11.2	43.4
Sub-horizontal, Std Dev.	3.2	1	5.1	9.5	4.2	3.6	4.7	3	7.2	8.7	3.9	11.3

It should be noted that the averages and standard deviations of both secant normal and shear stiffness, given in tables Table 3-10 and Table 3-11, were calculated using all data listed in Table 3-8 and Table 3-9. As can be seen from Table 3-10 and Table 3-11, some of the obtained values are out of range with respect to the average values and therefore, should not be taken into account in determining the average and standard deviation of each parameter.

3.3.3 Determination of shear strength

In his work, /Lanaro, 2001/ averaged the shear strength values for each normal stress level, and then carried out the comparison with the theoretical and empirical curves on the average values. The shear strength of both fracture sets was evaluated on the basis of both theoretical and empirical peak shear strength criteria, see section 3.1.4.

Shear strength fitted to theoretical shear strength criteria

The results of the sub-vertical fracture set were fitted to the Coulomb strength envelope. As this criterion was not suitable for describing the strength behaviour of the sub-horizontal fracture set at low stress level, /Lanaro, 2001/ used the bilinear failure criterion proposed by /Patton, 1966/ for determining the peak and residual parameters for normal stresses smaller and larger than 1 MPa. A summary of the results is presented in Table 3-12.

Table 3-12. Peak and residual cohesion and friction angle of rock fractures, estimated from theoretical shear failure criteria.

	Normal stresses < 1 MPa				Normal stresses > 1 MPa			
	c_p	ϕ_p	c_r	ϕ_r	c_p	ϕ_p	c_r	ϕ_r
Sub-horizontal		59.1		49.6	1.2	34.6	0.65	32
Sub-vertical	0.46	40.1	0.39	35.3	0.46	40.1	0.39	35.3

Shear strength fitted to empirical shear strength criterion

To determine the strength parameters of Barton and Choubey's failure criterion, the JRC values determined in section 3.3.1 are used. By forcing the relationship in equation (3.6) to fit the experimental data (mean strength for each level of normal stress), JCS and friction angle for peak and residual conditions were evaluated and the results are presented in Table 3-13.

Table 3-13. Peak and residual friction angle of rock fractures, estimated from empirical peak shear strength criterion.

	JRC	JCS (MPa)	ϕ_{bp} (°)	ϕ_{br} (°)
Sub-horizontal	8	80–82	32	27
Sub-vertical	6	82–85	36	32

3.4 Preparation of input mechanical parameters of rock fractures for modelling

The geometrical and mechanical parameters of the fracture sets, given in the previous sections, provide a great knowledge about the geometry, deformability, mechanical behaviour as well as shear strength of the fracture sets in the Äspö region under different normal and shear loading conditions. But, with respect to the fact that several specific fracture material properties are required in numerical modelling, further analyses have been conducted on the obtained data with respect to the constitutive joint model planned to be used.

As mentioned in section 2.3, the mechanical behaviour of fractured rock masses in the Äspö region will be determined and predicted using UDEC code. Among the different constitutive joint models available in UDEC, the Continuously Yielding joint model and the Barton-Bandis joint model seem to be more suitable to simulate the behaviour of rock fractures.

In the next sections of this chapter, the aforementioned joint models will be briefly described and the evaluation of input material properties for each model are explained in detail.

3.4.1 Preparation of input mechanical parameters of rock fractures for the Continuously Yielding joint model

Since the numerical modelling of practical problems usually take rock fractures through a complex load path, the empirical models, which where developed to fit laboratory tests by joint response to a simple loading condition are not suitable enough to model rock fracture behaviour under complex loading condition. One of the best models for the complex behaviour of rock fracture is the Continuously Yielding joint model, proposed by /Cundall and Hart, 1984/. The detailed description of this model is given in the UDEC user manual /UDEC, 2000a/ to which readers are referred for more information. The main structure of this model is briefly described below.

The non-linear behaviour of rock fractures, observed in the physical tests, is accounted for in the Continuously Yielding joint model. The model is described as follows:

The response to normal loading, $\Delta\sigma_n$, is expressed incrementally as:

$$\Delta\sigma_n = K_n \Delta u_n \tag{3.8}$$

where Δu_n is the normal displacement increment, and the normal stiffness, K_n, is expressed by:

$$K_n = a_n \sigma_n^{e_n} \quad (3.9)$$

which represents the observed increase of stiffness with normal stress, where a_n and e_n are model parameters. a_n is a constant and defines the initial rock fracture normal stiffness, and e_n the normal stiffness exponent. In this model, the tensile strength is assumed to be equal to zero.

The shear stress increment, $\Delta\tau$, is also calculated as follows:

$$\Delta\tau = FK_s \Delta u_s \quad (3.10)$$

where Δu_s is the shear displacement increment, F is a factor depending on the distance from the actual stress curve to the "bounding" stress curve (see section 3.1.3 in the main report), and the shear stiffness, K_s, is a function of the normal stress expressed as:

$$K_s = a_s \sigma_n^{e_s} \quad (3.11)$$

where a_s is a constant and defines the initial rock fracture shear stiffness, and e_s the shear stiffness exponent.

The model parameters associated with the Continuously Yielding model and that are required for modelling the behaviour of rock fractures under plain strain-loading conditions are summarised in Table 3-14. Among the parameters given in Table 3-14, four parameters: a_n, e_n, a_s and e_s have a major role on normal and shear behaviour of rock fractures, and are to be determined using available test data.

Table 3-14. Input parameters associated to the Continuously Yielding constitutive joint model.

Parameter	Description
a_n	initial joint normal stiffness (MPa/mm)
e_n	joint normal stiffness exponent
Max K_n	maximum value of joint normal stiffness (MPa/mm)
a_s	initial joint shear stiffness (MPa/mm)
e_s	joint shear stiffness exponent
Max K_s	maximum value of joint shear stiffness (MPa/mm)
jr	joint roughness parameter (m)
$\phi_m^{(i)}$	joint initial friction angle (°)
ϕ_i	joint intrinsic friction angle (°)

Analysis of data provided by /Stille and Olsson, 1989/

In Table 3-2, data as they are provided by /Stille and Olsson, 1989/ are presented. The stiffness values obtained from direct shear tests are a function of normal stress. Anyway, in this table, values of normal, K_n, and shear stiffness, K_s, are given without relationship to normal stress. Nevertheless, the values of K_n and K_s for different normal stress levels can be calculated by using laboratory raw data. The curves drawn from direct shear test results and presented in /Stille and Olsson, 1989/ can be used to determine the variation K_n and K_s with normal stresses. τ-σ_n curves were used to evaluate K_s for different values of σ_n according to equation (3.10). σ_n-Δu_n curves were

analysed to determine the values of K_n for range of values of σ_n, and according to equation (3.8). The calculated normal, K_n, and shear stiffness, K_s, of rock fracture samples ST1–ST12 are presented in Table 3-15.

Table 3-15. The normal and shear stiffness of rock fracture samples selected from borehole KAS02.

Sample*	Level (m)	K_s, MPa/mm								K_n, MPa/mm	
		σ_n	K_s	σ_n	K_s	σ_n	K_s	σ_n	K_s	Ini.	Peak
ST1	–397.81	0.87	3.5	1.75	3.9	2.62	7.9			4.7	31.25
ST2	–350.17	1.3	11.43	2.59	26.3	3.89	29.61			16.2	36.7
ST3	–327.44	1.21	6.52	2.41	7	3.62	6.4			8.65	11.11
ST5	–462.80	1.42	11.38	2.84	12.34	4.26	16.14	5.5	33	8.36	24
ST6	–500.18	1.16	7.05	2.26	6	3.47	12			6.6	29.5
ST8	–360.64	1.83	4.525	3.66	9	5.26	13.66			12	29.59
ST9	–394.52	1.81	5.87	3.61	9.47	5.19	11.98	7	19	10.15	45.14
ST10	–484.73	1.7	6.94	3.4	5.51	5.1	4.48	6.59	8.25	6.53	12.96
ST11	–281.40	1.82	7.05	3.63	10.42	5.45	9	7.04	8.54	9.94	29.88
ST12	–292.56	1.84	7.46	3.67	6.1	5.51	22.93	7.11	13.6	13.57	17.54

*ST1–ST6 belong to the Steeply dipping fracture set, and ST8–ST12 belong to the Gently dipping fracture set.

When the values of normal/shear stiffness as a function of normal stress are determined, they can be fitted to equations (3.9) and (3.11) to calculate the C-Y model's parameters. This is done by plotting normal/shear stiffness values against normal stresses, and by fitting a power law equation to the plotted data, see Figure 3-2 and Figure 3-3.

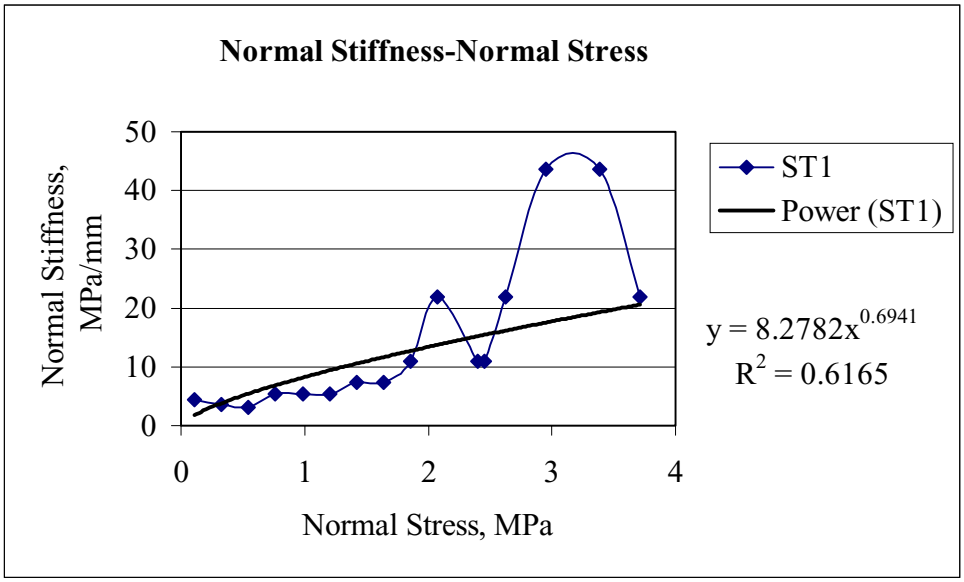

Figure 3-2. *The normal stiffness as a function of the normal stress and their power law relationship to determine a_n and e_n, sample ST1.*

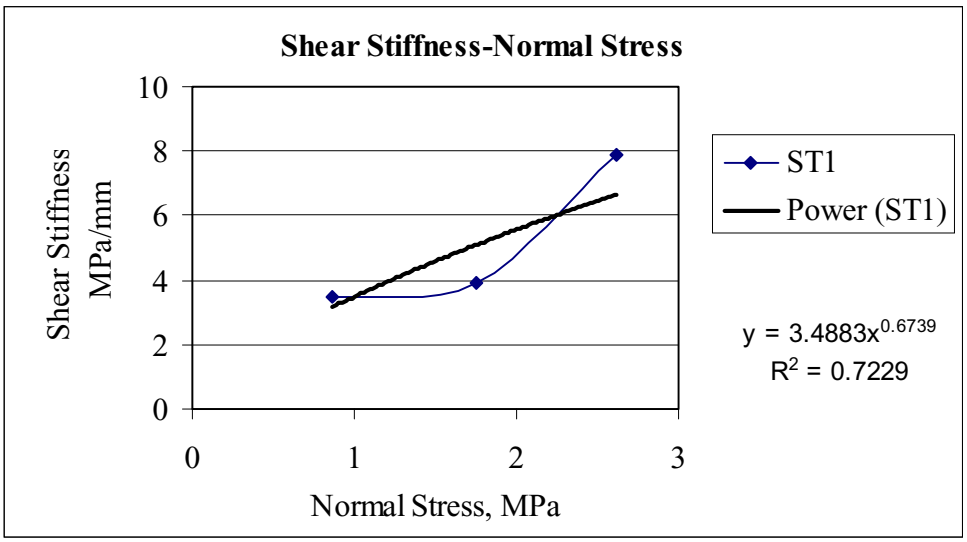

Figure 3-3. *The shear stiffness as a function of the normal stress and their power law relationship to determine a_s and e_s, sample ST1.*

The calculated parameters for normal, a_n and e_n, and shear stiffness, a_s and e_s, are presented in Table 3-16 for the steeply dipping set of fractures and in Table 3-17 for the gently dipping fracture set.

Table 3-16. Parameters for normal and shear stiffness fitted for the Continuously Yielding joint model, for rock fracture samples from the steeply dipping fracture set selected from borehole KAS02.

Sample	Level (m)	a_n MPa/mm	e_n	a_s MPa/mm	e_s
ST1	–397.81	8.2782	0.6941	3.4883	0.6739
ST2	–350.17	16.025	0.6936	9.5425	0.9045
ST3	–327.44	9.4939	0.2011	6.6573	–0.004
ST5	–462.80	10.755	0.4624	7.6824	0.6742
ST6	–500.18	6.6653	0.8068	5.8462	0.4223
Mean values		**10.24**	**0.57**	**6.64**	**0.53**
Standard deviation		3.57	0.24	2.24	0.34

Table 3-17. Parameters for normal and shear stiffness fitted for the Continuously Yielding joint model, for rock fracture samples from the gently dipping fracture set selected from borehole KAS02.

Sample	Level (m)	a_n MPa/mm	e_n	a_s MPa/mm	e_s
ST8	–360.64	13.632	0.2955	2.3951	1.0391
ST9	–394.52	11.339	0.4476	3.4412	0.8232
ST10	–484.73	8.8954	0.2978	6.2614	–0.016
ST11	–281.40	7.9031	0.4726	7.1249	0.1417
ST12	–292.56	11.055	0.2357	4.2493	0.6746
Mean values		**10.56**	**0.35**	**4.69**	**0.53**
Standard deviation		2.24	0.10	1.96	0.45

Analysis of data provided by /Lanaro, 2001/

The parameters a_n, e_n, a_s and e_s, need also to be calculated from the normal and shear stiffness data provided by /Lanaro, 2001/. In this case, the values of K_n and K_s were provided as a function of normal stresses, see Table 3-8 and Table 3-9.

As described in the previous section, the estimated values of K_n and K_s were plotted in two separate diagrams against normal stresses, and the values were fitted to a power law regression.

The calculated parameters are given in Table 3-18 for sub-vertical and sub-horizontal fracture sets.

Table 3-18. The Continuously Yielding joint model's parameters obtained for both sub-vertical and sub-horizontal fracture samples tested by /Lanaro, 2001/.

Borehole	Fracture set	Depth (m)*	a_n MPa/mm	e_n	a_s MPa/mm	e_s
KA3548A01	Sub-vertical fracture set	–446.87	52.884	0.7289	8.0808	0.5859
		–447.51	76.349	0.2201	3.0592	0.8006
KA3573A		–446.30	50.325	0.3772	1.9994	0.9488
		–446.47				
		–446.81	167.36	–0.037	3.2289	1.0712
KA3600F		–446.90				
		–446.90	122.95	0.0218	6.6911	0.7954
		–446.91	41.244	0.4903	3.8043	0.3628
KG0021A01		–432.84	71.74	0.4346	1.4708	1.0605
KG0048A01		–442.68	80.158	1.2713	6.3316	0.547
		–437.87	64.323	0.6869	2.1803	1.1855
		–433.37	66.302	0.3824	3.9792	0.8494
		–433.26	52.694	0.1002	6.4939	0.6156
KA3579G	Sub-horizontal fracture set	–457.80	114.64	0.7563	2.5248	1.2561
		–459.10	29.42	1.4612	15.126	0.2248
		–459.62	30.16	1.4812	3.187	0.7804
		–463.23	88.16	1.3046	9.2776	0.3225
		–467.81	130.45	1.412	6.7997	0.6388

* The depth of samples is absolute depth and has been re-calculated according to the coordinates of boreholes.

The mean values and standard deviations of the parameters obtained for sub-vertical and sub-horizontal fracture sets listed in Table 3-18 are given in Table 3-19 and Table 3-20.

Table 3-19. The mean values and standard deviations of the Continuously Yielding joint model's parameters obtained for sub-vertical fracture samples tested by /Lanaro, 2001/.

Sub-vertical fracture set	a_n MPa/mm	e_n	a_s MPa/mm	e_s
Mean value	76.939	0.4252	4.3018	0.8021
standard deviation	37.084	0.3754	2.2311	0.2549

Table 3-20. The mean values and standard deviations of the Continuously Yielding joint model's parameters obtained for sub-horizontal fracture samples tested by /Lanaro, 2001/.

Sub-horizontal fracture set	a_n MPa/mm	e_n	a_s MPa/mm	e_s
Mean value	78.566	1.2831	7.383	0.6445
standard deviation	47.021	0.3023	5.1257	0.41

Summary of values for input parameters

The values of the parameters have been presented in the previous sections. The roughness parameter, jr, for the C-Y model has been calculated according to equations (3.11) and (3.13) presented in the main report.

The input parameters for the Continuously Yielding model are presented in Table 3-21 for the sub-vertical fracture set and in Table 3-22 for the sub-horizontal fracture set.

Table 3-21. Summary of the values of input parameters for the Continuously Yielding joint model for the sub-vertical fracture set.

Sub-vertical fracture set	/Stille and Olsson, 1989/		/Lanaro, 2001/	
Parameter	Mean	Std Dev.	Mean	Std Dev.
a_n (MPa/mm)	10.24	3.57	76.9	37.1
e_n	0.57	0.24	0.4	0.37
Max K_n (MPa/mm)	Function of a_n and e_n, calculated for expected σ_n			
a_s (MPa/mm)	6.64	2.24	4.3	2.2
e_s	0.53	0.34	0.8	0.25
Max K_s (MPa/mm)	Function of a_s and e_s, calculated for expected σ_n			
jr (m)	0.002	–	0.002	–
$\phi_m^{(i)}$ (°)	40	–	40	–
ϕ_i (°)	35	–	35	–

Table 3-22. Summary of the values of input parameters for the Continuously Yielding joint model for the sub-horizontal fracture set.

Sub-horizontal fracture set	/Stille and Olsson, 1989/		/Lanaro, 2001/	
Parameter	Mean	Std Dev.	Mean	Std Dev.
a_n (MPa/mm)	10.56	2.24	78.6	47
e_n	0.35	0.10	1.3	0.3
Max K_n (MPa/mm)	Function of a_n and e_n, calculated for expected σ_n			
a_s (MPa/mm)	4.69	1.96	7.4	5.1
e_s	0.53	0.45	0.6	0.4
Max K_s (MPa/mm)	Function of a_s and e_s, calculated for expected σ_n			
Jr (m)	0.002	–	0.002	–
$\phi_m^{(i)}$ (°)	35	–	35	–
ϕ_i (°)	32	–	32	–

The evaluated values for normal, K_n, and shear, K_s, stiffness are significantly smaller when analysing results from /Stille and Olsson, 1989/. During this study, the compression of the two blocks of rock fracture samples was not substracted from the total measured compression when evaluating the normal stiffness. This could partly explain that their values are smaller than those evaluated from /Lanaro, 2001/.

Anyhow, values as evaluated from /Lanaro, 2001/ are far much higher than reference values found for rock fractures.

3.4.2 Preparation of input mechanical parameters of rock fractures for the Barton-Bandis joint model

The Barton-Bandis joint model, which has been implemented into UDEC, has been developed by Drs. Nick Barton and Stavros Bandis to describe the effects of surface roughness on discontinuity deformation and strength using series of empirical relations. A complete explanation of these relations can be obtained from /Barton, 1982/ and /Bandis et al, 1985/. The main feature of this model as well as its mathematical formulation is given in the UDEC user manual /UDEC, 2000b/.

The parameters required to model the behaviour of rock fractures by the Barton-Bandis joint model under plain strain-loading conditions are given in Table 3-23.

Table 3-23. Input parameters required by the Barton-Bandis joint model for plain strain loading test.

Property Keyword	Description
K_n	joint normal stiffness at expected normal loads (MPa/mm)
K_s	joint shear stiffness at expected normal loads (MPa/mm)
JRC_0	laboratory-scale joint roughness coefficient
JCS_0	laboratory-scale joint wall compressive (MPa)
L_0	laboratory-scale joint length (m)
ϕ_r	joint residual angle of friction (°)
σ_c	intact rock uniaxial compressive strength (MPa)
a_{jn}	joint aperture at zero normal stress (mm)

According to the Barton and Choubey's failure criterion (see equation (3.6)) JRC_0, JCS_0 and ϕ_r values will have a major effect on the shear strength of the rock mass.

Parameters evaluated from shear tests

In /Stille and Olsson, 1989/ the JRC value were given without any description about the method of estimation. Also, in /Lanaro, 2001/, the JRC_0 values of the fracture sets were considered constant with respect to the simple geometrical characterisation and the two other parameters (JCS_0 and ϕ_r) were back-calculated by forcing the relationship in equation (3.7) to fit the experimental data, see section 3.3.

In order to complete the study and precisely define the influence and interactivity of these 3 parameters, a sensitivity analysis has been carried out on the raw data obtained from direct shear tests under different normal stresses.

In the following, the application of this procedure on the sub-vertical fracture set tested by /Lanaro, 2001/ is described in detail and the summary of the results obtained for both fracture sets is given in Table 3-24 and Table 3-25. The results obtained for the rock fractures tested in /Stille and Olsson, 1989/ are presented in Table 3-26 to Table 3-31.

Results of direct shear tests from /Lanaro, 2001/ on both fracture sets were analysed in the same way. Available raw data for all samples of one fracture set were plotted in a τ-σ_n graph (see Figure 3-4). The samples represent rock fractures in diorite. The maximum uniaxial strength of diorite, σ_c, is equal to 214 MPa for 50-mm samples (see section 2.3). Therefore, it was assumed that the JCS_0 of the rock fracture samples can not take a value greater than the maximum uniaxial compressive strength of the intact rock, and its highest value was set to 210 MPa. The influence of JCS_0 was tested by decreasing this initial value by 10 MPa steps until a value of 100 MPa. The sensitivity analysis was conducted for the three different ϕ_r values of 28, 30 and 32 degrees. Then the JRC_0 values were determined by calculating the best fitting curve to the raw data, see Figure 3-4, according to equation (3.6) and using the ORIGIN software.

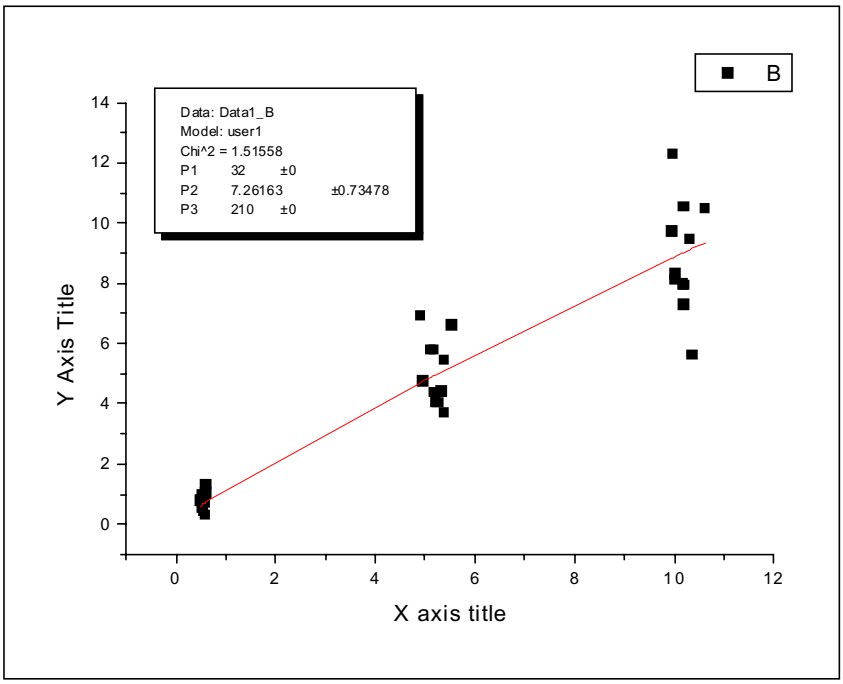

Figure 3-4. *An example of the best fitting curve to the raw laboratory test data of the sub-vertical fracture set, using OIGIN software (X axis is normal stress and Y axis is shear stress).*

The JRC_0 values calculated for the sub-vertical fracture set are presented in Table 3-24, and those calculated for the sub-horizontal fracture set in Table 3-25.

Table 3-24. The sensitivity analysis on the raw laboratory tests data of samples from sub-vertical fracture set for determining JRC_0, JCS_0 and ϕ_r values of Barton-Choubey's failure criterion.

JCS_0 (MPa)	JRC_0		
	ϕ_r=28°	ϕ_r=30°	ϕ_r=32°
210	10.115	8.69068	7.26163
200	10.2699	8.82456	7.37418
190	10.4378	8.96973	7.49626
180	10.6207	9.12789	7.62931
170	10.8209	9.30111	7.77509
160	11.0414	9.49198	7.93579
150	11.2858	9.70369	8.11416
140	11.5589	9.94046	8.3137
130	11.8668	10.2075	8.53896
120	12.2175	10.512	8.79598
110	12.6217	10.8634	9.09296
100	13.0945	11.2751	9.44134

Table 3-25. The sensitivity analysis on the raw laboratory tests data of samples from sub-horizontal fracture set for determining JRC_0, JCS_0 and ϕ_r values of Barton-Choubey's failure criterion.

JCS_0 (MPa)	JRC_0		
	ϕ_r=28°	ϕ_r=30°	ϕ_r=32°
210	8.75572	7.31466	5.86974
200	8.89301	7.43021	5.96334
190	9.04198	7.55564	6.06496
180	9.20439	7.69244	6.17584
170	9.3824	7.84244	6.29748
160	9.5787	8.00792	6.43175
150	9.79667	8.19178	6.58101
140	10.0406	8.39766	6.74826
130	10.3161	8.63037	6.93745
120	10.6307	8.89625	7.1538
110	10.9943	9.20394	7.40444
100	11.421	9.56555	7.69938

The data given in Table 3-24 and Table 3-25 can be used as a support for finding the most suitable parameters for the rock fractures in the Äspö region.

Data from /Stille and Olsson, 1989/ were analysed following the same procedure. The tested fracture samples belong to different rock types. Following rock types were found for the steeply dipping fracture set samples: greenstone for ST1, fine-grained granite for ST2 and ST6, and diorite for ST3 and ST5. The rock types of the gently dipping fracture set samples are: granite for ST8 and ST11, fine-grained granite for ST9 and ST10, and granite for ST12. The highest value set for JCS_0 was considered to be less or equal to the uniaxial compressive strength of each rock type and calculated for 50-mm samples, see Table 2-2.

To determine the strength parameters of Barton and Choubey's shear failure criterion for fracture samples tested in /Stille and Olsson, 1989/, the same procedure for sensitivity analysis was carried out using raw data obtained from laboratory direct shear

tests under different normal stress condition. The analysis was carried out for each fracture set, and separately for each rock type in a fracture set.

The summary of results obtained for fracture samples on the different rock types are presented in Table 3-26 to Table 3-31.

Table 3-26. The sensitivity analysis on the raw laboratory tests data of sample ST1 defined as greenstone and belonging to the steeply dipping fracture set, for determining JRC_0, JCS_0 and ϕ_r values of Barton-Choubey's failure criterion.

JCS_0 (MPa)	JRC_0		
	ϕ_r=28°	ϕ_r=30°	ϕ_r=32°
115	11.0182	9.87723	8.73417
105	11.272	10.1055	8.9366
95	11.565	10.3689	9.17027
85	11.9085	10.6779	9.44448
75	12.3199	11.048	9.77299
65	12.8256	11.5032	10.1772

Table 3-27. The sensitivity analysis on the raw laboratory tests data of sample ST2 and ST6 defined as fine-grained granite and belonging to the steeply dipping fracture set, for determining JRC_0, JCS_0 and ϕ_r values of Barton-Choubey's failure criterion.

JCS_0 (MPa)	JRC_0		
	ϕ_r=28°	ϕ_r=30°	ϕ_r=32°
230	9.94197	8.92908	7.91452
210	10.1454	9.1124	8.07751
190	10.3791	9.32274	8.26466
170	10.6514	9.56824	8.48294
150	10.9752	9.86004	8.74254
130	11.3698	10.2159	9.05925

Table 3-28. The sensitivity analysis on the raw laboratory tests data of sample ST3 and ST5 defined as diorite and belonging to the steeply dipping fracture set, for determining JRC_0, JCS_0 and ϕ_r values of Barton-Choubey's failure criterion.

JCS_0 (MPa)	JRC_0		
	ϕ_r=28°	ϕ_r=30°	ϕ_r=32°
170	12.7754	11.5488	10.3192
160	12.9892	11.7433	10.494
150	13.225	11.9577	10.687
140	13.4864	12.1956	10.9011
130	13.7787	12.4617	11.1406
120	14.1086	12.762	11.4111

Table 3-29. The sensitivity analysis on the raw laboratory tests data of sample ST8 and ST11 defined as granite and belonging to the gently dipping fracture set, for determining JRC_0, JCS_0 and ϕ_r values of Barton-Choubey's failure criterion.

JCS_0 (MPa)	JRC_0		
	ϕ_r=28°	ϕ_r=30°	ϕ_r=32°
180	9.11712	7.84347	6.5673
170	9.26185	7.9682	6.67186
160	9.42037	8.10484	6.78647
150	9.59509	8.25547	6.91282
140	9.78904	8.42269	7.05311
130	10.0061	8.60988	7.21018

Table 3-30. The sensitivity analysis on the raw laboratory tests data of sample ST9 and ST10 defined as fine-frained granite and belonging to the gently dipping fracture set, for determining JRC_0, JCS_0 and ϕ_r values of Barton-Choubey's failure criterion.

JCS_0 (MPa)	JRC_0		
	ϕ_r=28°	ϕ_r=30°	ϕ_r=32°
230	9.57184	8.3381	7.10251
210	9.81721	8.55325	7.28725
190	10.1021	8.80312	7.50191
170	10.43841	9.09825	7.75559
150	10.8442	9.45458	8.06208
130	11.3479	9.89715	8.44308

Table 3-31. The sensitivity analysis on the raw laboratory tests data of sample ST12 defined as greenstone and belonging to the gently dipping fracture set, for determining JRC_0, JCS_0 and ϕ_r values of Barton-Choubey's failure criterion.

JCS_0 (MPa)	JRC_0		
	ϕ_r=28°	ϕ_r=30°	ϕ_r=32°
115	14.0364	12.5277	11.0138
105	14.4717	12.9187	11.3599
95	14.9818	13.3773	11.7662
85	15.591	13.9254	12.2522
75	16.3361	14.5964	12.8479
65	17.2759	15.4441	13.6013

Parameters evaluated from tilt tests

Tilt tests have been performed on rock fracture samples collected along boreholes KAS02, KA2511a and KA2598a. The tests were carried out by NGI during 2001 /Makurat et al, 2002/ on rock fracture samples that had been collected at different depths. The results include all rock fracture samples, without distinction to fracture sets.

The parameters evaluated from these tests are ϕ_b, ϕ_r, JRC_{100} and JCS_{100}, see section 3.1.2. Table 3-32 to

Table 3-34 summarised the results of the tests for each borehole, and in Table 3-35 the statistical distribution of all tests is shown.

Table 3-32. Results of tilt tests in borehole KAS02.

Depth, m	Roughness amplitude a, mm	Basic friction angle ϕ_b,°	Rock Type	Residual friction angle ϕ_r, °	JRC_{100}	JCS_{100}, MPa
178.05	3.2	32.0	Granite	26.1	6.9	86.9
199.60	1.7	32.0	Granite	25.2	5.6	47.1
237.12	1.4	31.0	Granite	26.9	3.8	105.8
244.55	2.4	28.0	Granite	21.1	8.7	68.7
268.52	2.0	33.0	Amphibolite	28.3	4.4	61.4
305.74	2.5	32.0	Granite	29.9	6.9	89.6
329.44	1.7	35.0	Diorite	34.0	3.7	79.8
360.16	1.3	32.0	Granite	32.0	3.2	135.7
361.55	1.1	32.0	Granite	32.0	4.0	134.7
403.06	1.9	32.0	Diorite	27.0	3.9	68.0
406.39	1.1	36.0	Granite	31.4	5.0	57.9
414.50	2.2	35.0	Diorite	35.0	4.1	114.7
419.95	3.5	33.0	Diorite	30.5	5.2	102.6
455.06	3.1	33.0	Diorite	28.9	6.5	84.9
476.42	3.9	34.0	Granite	34.0	5.3	140.3
491.10	3.9	30.0	Diorite	30.0	6.0	151.5
513.05	1.7	34.0	Diorite	31.1	5.7	67.6
543.14	1.3	32.0	Diorite	25.9	6.4	67.2
543.87	0.8	32.0	Diorite	32.0	3.6	137.5
557.25	2.1	30.0	Diorite	27.9	4.6	89.3
565.18	1.2	34.5	Diorite	34.5	4.4	116.7
578.30	1.3	32.0	Diorite	31.0	5.6	134.8
609.77	2.1	33.5	Diorite	32.2	3.6	109.1
Mean	**2.1**	**32.5**		**29.9**	**5.1**	**97.9**
Std Dev.	0.9	1.8		3.4	1.4	31.0

Table 3-33. Results of tilt tests in borehole KA2511a.

Depth, m	Roughness amplitude a, mm	Basic friction angle ϕ_b, °	Rock Type	Residual friction angle ϕ_r, °	JRC_{100}	JCS_{100}, MPa
21.85	1.2	31.0	Diorite	28.1	4.4	109.3
42.05	0.9	34.0	Diorite	30.5	6.0	68.8
44.40	1.9	34.0	Diorite	28.3	5.8	67.8
49.75	1.3	32.0	Diorite	25.1	6.6	57.9
108.07	1.3	33.0	Diorite	33.0	4.7	164.0
111.59	2.7	32.5	Diorite	26.6	6.4	74.2
147.25	1.5	35.0	Diorite	33.3	3.8	91.0
150.00	1.6	33.0	Diorite	30.5	5.6	103.5
186.12	1.3	35.0	Diorite	30.1	6.1	67.6
186.70	1.4	31.0	Diorite	27.9	4.3	65.6
216.33	1.0	33.0	Diorite	30.4	3.8	102.3
242.58	0.5	30.5	Diorite	23.1	1.0	53.7
259.10	2.0	31.0	Diorite	26.4	5.2	101.8
268.30	1.7	28.0	Diorite	23.3	6.2	80.8
291.14	4.8	31.0	Diorite	24.3	5.7	57.3
Mean	**1.7**	**32.3**		**28.0**	**5.0**	**84.4**
Std Dev.	1.0	1.9		3.3	1.5	28.8

Table 3-34. Results of tilt tests in borehole KA2598A.

Depth, m	Roughness amplitude a, mm	Basic friction angle ϕ_b, °	Rock Type	Residual friction angle ϕ_r, °	JRC_{100}	JCS_{100}, MPa
14.45	1.9	33.0	Diorite	25.8	2.8	55.8
25.30	2.6	35.0	Diorite	33.0	3.6	81.1
34.08	2.3	35.5	Diorite	35.5	4.3	97.2
42.23	2.4	33.0	Diorite	31.8	6.1	124.3
56.30	2.2	31.0	Diorite	29.3	5.0	159.5
59.75	1.9	30.0	Granite	28.9	5.1	97.8
96.92	2.5	32.0	Granite	30.0	5.9	103.0
112.80	1.8	33.0	Diorite	30.8	4.7	112.7
124.72	1.1	34.0	Diorite	29.6	3.8	72.0
134.10	1.0	33.5	Diorite	26.9	3.9	50.2
145.05	1.3	34.5	Diorite	34.1	3.6	103.5
168.45	1.0	33.5	Diorite	28.6	3.5	73.0
172.07	1.6	33.0	Diorite	33.0	4.5	147.7
198.82	2.7	31.5	Diorite	31.5	4.9	133.5
212.65	2.9	33.0	Granite	31.5	5.5	106.7
219.32	3.1	33.5	Diorite	30.0	4.6	85.7
268.63	1.5	33.0	Diorite	25.8	6.5	54.8
270.00	0.8	35.0	Diorite	28.7	3.8	68.4
296.69	2.1	35.0	Diorite	26.2	7.7	47.8
296.82	2.3	25.0	Diorite	17.8	6.4	60.2
Mean	**2.0**	**32.9**		**29.4**	**4.8**	**91.7**
Std Dev.	0.7	2.3		3.8	1.2	32.7

Table 3-35. Results of all tilt tests.

	Roughness amplitude a, mm	Basic friction angle ϕ_b, °	Residual friction angle ϕ_r, °	JRC_{100}	JCS_{100}, MPa
Mean	1.9	32.6	29.2	5.0	92.3
Std Dev.	0.9	2.0	3.6	1.3	31.0

Values of input parameters for the Barton-Bandis joint model

The values used as input in the B-B model are presented in the previous sections. As described in the previous paragraph, there is no unique solution for fitting the Barton-Choubey's failure criterion (equation (3.6)). The choice of input parameters has been made on the results of the sensitivity analysis presented above.

L_0 is the size of the rock fracture sample that has been tested, and is provided in the technical reports /Lanaro, 2001; Stille and Olsson, 1989/.

The values for the input parameters required for modelling the behaviour of rock fractures with the Barton-Bandis joint model are presented in Table 3-36 for the sub-vertical fracture set and in Table 3-37 for the sub-horizontal fracture set.

Table 3-36. Values of the input for the Barton-Bandis joint model, sub-vertical fracture set.

Sub-vertical fracture set		
Parameter	Mean	Std Dev.
K_n (MPa/mm)	61.5	
K_s (MPa/mm)	35.5	
JRC_0	4/9.3/12/16	–
JCS_0 (MPa)	40/110/170	
L_0 (m)	5.51e–2	
ϕ_r (°)	29.2	3.6
σ_c	See Table 2-8	
a_{jn} (m)	0.56	–

Table 3-37. Values of the input for the Barton-Bandis joint model, sub-horizontal fracture set.

Sub-horizontal fracture set		
Parameter	Mean	Std Dev.
K_n (MPa/mm)	21.9	
K_s (MPa/mm)	15.7	
JRC_0	4/9.3/12/16	–
JCS_0 (MPa)	40/110/170	
L_0 (m)	6.1e–2	
ϕ_r (°)	29.2	3.6
σ_c	See Table 2-8	
a_{jn} (m)	0.2	–

4 References

Bandis S C, Barton N R, Christianson M, 1985. Application of a New Numerical Model of Joint Behaviour to Rock Mechanics Problems, in Fundamentals of Rock Joints. Proceedings of the International Symposium on Fundamentals of Rock Joints, Björkliden, September 1985, pp. 345–356. Luleå, Sweden: Centek Publishers.

Barton N, 1976. Rock Mechanics Review. The Shear Strength of Rock and Rock Joints. Int. J. Rock Mech. Min. Sci & Geomech. Abstr. Vol. 13. Pp. 255–279.

Barton N, 1982. Modelling Rock Joint Behaviour from In-Situ Block Tests: Implications for Nuclear Waste Repository Design, ONWI-308, September.

Barton N, Choubey, V, 1977. The Shear Strength of Rock Joints in Theory and Practice. Rock Mechanics 10. Pp 1–54.

Cundall P A, Hart R D, 1984. Analysis of Block Test No.1 Inelastic Rock Masshavior: Phase 2 – A Characterization of Joint behaviour. Itasca Consulting Group Report, Rockwell Hanford Operations, Subcontract SA-957.

ISRM, 1978. Suggested methods for the quantitative description of joints in rock masses. Int. J. Rock Mech. Min. Sci. & Geomech. Abstr. Vol 15, Pp. 319–368.

ISRM, 1981. Suggested methods for determining shear strength. In Rock characterization testing and monitoring, ISRM suggested methods, pp.129–140. Ed: E.T. Brown.

Nordlund E, Li C, Larsson B, 1999. Mechanical properties of the diorite in the prototype repository at Äspö HRL. SKB, International Progress Report IPR-99-25, Stockholm, Sweden.

Lanaro F, 2001. Determination of the normal and shear stiffness of rock joints: geometry, normal and shear stiffness. SKB, Technical report (under publication), Stockholm, Sweden.

Makurat A, Löset F, Wold Hagen A, Tunbridge L, Kveldsvik V, Grimstad E, 2002. Äspö HRL – A Descriptive Rock Mechanics Model for the 380-500 m level. SKB R-02-11, Stockholm, Sweden.

Patton F D, 1966. Multiple modes of shear failure in rock. Conference Proceedings "1st International Congress on Rock Mechanics", vol.I, pp.509–513.

Rhén I, Bäckbom G, Gustafson G, Stanfors R, Wikberg P, 1997. Äspö HRL – Geoscientific evaluation 1997/2. Results from pre-investigations and detailed site characterization. Summary report. SKB TR 97-03, Stockholm, Sweden.

Stille H, Olsson P, 1989. First evaluation of rock mechanics. SKB, Progress Report 25-89-07, Stockholm, Sweden.

Stille H, Olsson P, 1990. Evaluation of rock mechanics. SKB, Progress Report 25-90-08, Stockholm, Sweden.

UDEC, 2000a. Universal Distinct Element Code. Theory and Background. Itasca Consulting Group, Inc. Minneapolis.

UDEC, 2000b. Universal Distinct Element Code. Special Features. Itasca Consulting Group, Inc. Minneapolis.